August 2024

Modeling Eutrophication Processes in the Delaware River Estuary: Three-Dimensional Water Quality Model

Technical Report No. 2024-5

FINAL REPORT

Managing, Protecting and Improving
the Water Resources of the
Delaware River Basin since 1961

Delaware River Basin Commission
DELAWARE • NEW JERSEY
PENNSYLVANIA • NEW YORK
UNITED STATES OF AMERICA

Modeling Eutrophication Processes in the Delaware River Estuary: Three-Dimensional Water Quality Model

This report was prepared by the following staff with the Delaware River Basin Commission (DRBC) who performed the work described herein at the direction of Executive Director Steve Tambini.

Li Zheng, Ph.D. (primary author)	Senior Water Resource Modeler
Fanghui Chen, Ph.D., P.E.	Senior Water Resource Engineer
Jake Bransky	Senior Aquatic Biologist
Elaine Panuccio	Water Resource Scientist
Sarah Beganskas, Ph.D.	Senior Water Resource Scientist
Thomas Amidon, BCES	Manager, Water Resource Modeling
John Yagecic, P.E.	Manager, Water Quality Assessment
Namsoo Suk, Ph.D.	Director, Science and Water Quality Management
Kristen Bowman Kavanagh, P.E.	Deputy Executive Director

Suggested Citation

Zheng, L., Chen, F., Bransky, J., Panuccio, E., Beganskas, S., Amidon, T., Yagecic, J., Suk, N., & Kavanagh, K.B. (2024). *Modeling Eutrophication Processes in the Delaware River Estuary: Three-Dimensional Water Quality Model*. (DRBC Report No. 2024-5). Delaware River Basin Commission.

ACKNOWLEDGEMENTS AND DISCLAIMERS

This work was funded in part by generous grants from the United States Environmental Protection Agency, the New Jersey Department of Environmental Protection, the Pennsylvania Department of Environmental Protection, and the William Penn Foundation.

In addition, this work was funded in part by a grant from the U.S. Fish and Wildlife Service (FWS) through the National Fish and Wildlife Foundation (NFWF) Delaware Watershed Conservation Fund (DWCF), grant number 72417. The views and conclusions contained in this document are those of the authors and should not be interpreted as representing the opinions or policies of the U.S. Government or the National Fish and Wildlife Foundation and its funding sources. Mention of trade names or commercial products does not constitute their endorsement by the U.S. Government, or the National Fish and Wildlife Foundation or its funding sources.

Critical datasets, without which this work could not have been performed, were obtained from the National Oceanic and Atmospheric Administration's National Climatic Data Center as well as the United States Geological Survey (USGS).

The DRBC is grateful for the technical support and direction provided by its Model Expert Panel, composed of internationally renowned modelers: Dr. Steve Chapra, Dr. Carl Cerco, Dr. Bob Chant, and Tim Wool. Vince DePaul of USGS provided important technical support for this modeling project, in particular the estimation of boundary constituent concentrations for unmonitored tributaries and watersheds. DRBC also acknowledges with appreciation the invaluable guidance received from the day-to-day interactions with its modeling consultants, Dr. Victor Bierman and Scott Hinz of LimnoTech.

DRBC acknowledges the various National Pollutant Discharge Elimination System (NPDES) permit-holders within the tidal estuary that provided critical discharge data for this work. Water Quality Advisory Committee members provided technical reviews and comments on the draft report released in September 2022 that improved both the model and this report.

EXECUTIVE SUMMARY

The water quality model described herein is the culmination of a larger modeling study of the Delaware River Estuary, the goal of which was to develop and calibrate a water quality model of eutrophication processes in the Delaware River Estuary[1] ("the Estuary") from the head of the tide at Trenton, New Jersey, to the Atlantic Ocean. The purpose of the project is to provide the scientific basis for the Delaware River Basin Commission (DRBC) and others to evaluate management options for establishing water quality criteria for dissolved oxygen (DO) and nutrients as necessary to support higher aquatic life designated uses, and for establishing loading targets for point and non-point sources to achieve these criteria. This report documents the development, technical approach, and fitness of a three-dimensional water quality model that was deemed by an external Model Expert Panel[2] to be adequately calibrated for its intended purpose.

In order to supplement existing data necessary to estimate loads entering the Estuary (from tributaries, point sources, and direct runoff) as well as to characterize ambient conditions to develop and calibrate the water quality model, an intensive sampling effort was implemented by the DRBC and its partners, especially during the 2018-2019 period targeted for model calibration. The "Boat Run[3]" (a monthly sampling program dating back to 1967 that collects monthly samples at 22 locations in the Delaware River Estuary) and the continuous monitors maintained by the United States Geological Survey (USGS) and its partners comprised the foundation for model calibration data. Both programs were expanded significantly during the intensive monitoring period of 2018-2019: analytical parameters and sampling events were added to the Boat Run, while additional sensors were also added to the USGS monitors. To characterize loads from tributaries to the Estuary, DRBC also conducted a comprehensive sampling program in which 24 tributaries were sampled with varying degrees of frequency commensurate with their importance in terms of loading impacts. Data from preliminary sampling of 75 discharges to the Estuary from 2011-2015 were used to rank and prioritize point sources for the more intensive sampling period in 2018-2019. At the direction of DRBC, 32 of the point source discharges (designated Tiers 1 and 2) were monitored with various levels of frequency commensurate with loading impacts. Descriptions of and results from these and additional field sampling efforts related to this project are described in Section 2. The loading characterization shows that point source discharges contribute about 13 times more total ammonia

[1] The Delaware River Estuary includes the tidal Delaware River and the Delaware Bay.

[2] The Model Expert Panel was comprised of nationally recognized water resource scientists and engineers: Dr. Steve Chapra (Emeritus Professor and Berger Chair, Tufts University), Dr. Carl Cerco (Research Hydrologist, US Army Engineer Research and Development Center, ret.), Dr. Bob Chant (Professor, Rutgers University Institute of Marine Sciences), and Tim Wool (USEPA Region 4 Environmental Scientist, ret.).

[3] https://www.nj.gov/drbc/programs/quality/boat-run.html

nitrogen load than does the upstream Delaware River (at Trenton), the Schuylkill River, and all other monitored tributaries combined (Figure 2-8).

Modeling DO[4] in the Delaware River Estuary requires an understanding of complex interactions among many processes including: tidal dynamics and water circulation; temperature, salinity, and algal dynamics; nutrient cycling and transformation; and solute exchange across the air/water and sediment/water interfaces. The DRBC developed the water quality model using the Water Quality Analysis Simulation Program (WASP) to simulate important processes affecting dissolved oxygen over a range of hydrologic and loading conditions utilizing an appropriate level of complexity within the current state of the science and within the timeframe established by the Commission. The water quality model is linked to a hydrodynamic model that simulates transport information (water surface elevation, current velocity, salinity, and water temperature) required by the water quality model. The linked hydrodynamic model was developed by DRBC using the Environmental Fluid Dynamics Code (EFDC), and development and calibration of that model is documented in a separate report (Chen et al., 2024). The result is a spatially explicit, time-variable model of the entire estuary from the head of tide at Trenton to the mouth of the bay. Both the EFDC and WASP models are supported by the U.S. Environmental Protection Agency (EPA). DRBC led and executed this project through a rigorous process informed by a Model Expert Panel comprised of nationally recognized water resource scientists.

The water quality model in this study covers the same model domain and utilizes the same numerical grid as the linked hydrodynamic model (Chen et al., 2024), resulting in 11,490 computational cells in three dimensions extending from the mouth of the Delaware Bay to just upstream of the head of tide on the Delaware River in Trenton. WASP is a dynamic modeling program for aquatic systems that simultaneously solves mass balance equations for various constituents in each computational cell over time. The eutrophication model within WASP was utilized to simulate the major physical, chemical and biological processes that impact dissolved oxygen. Diagnostic model evaluations performed by the DRBC indicate that reaeration and photosynthesis are the major processes controlling dissolved oxygen production, while the major processes affecting dissolved oxygen consumption are nitrification, followed by sediment oxygen demand (SOD), carbonaceous biological oxygen demand (CBOD) oxidation, and algal respiration.

Three significant enhancements were made during this study to improve model accuracy and reliability:

1. <u>WASP and EFDC model integration:</u> Integration of three-dimensional and water quality models within a complex computations system was accomplished through a linkage file that stores information from EFDC (water volume, current velocity, flow rate, mixing coefficient, salinity,

[4] DO throughout much of this report is discussed in terms of water column concentration (mg/L). DO as a percent of saturation level, which is affected by water temperature and salinity, is certainly relevant for fish, which extract DO from the water column through their gills. DO percent saturation can be calculated as a function of DO concentration (simulated by the water quality model), water temperature and salinity (both of which are simulated by the underlying hydrodynamic model). Model predictions of DO can therefore easily be expressed as either concentration, percent saturation, or both.

water temperature, and turbulence dissipation rate) for use in by WASP simulating water column transport of constituents. Critical linkage factors were identified and adjusted to optimize the ability of WASP to reproduce conservative tracer transport by EFDC, maintaining mass balance in WASP, control WASP computation time, and maintain a manageable linkage file size.

2. Reaeration simulation: Reaeration is a process of dissolved gas exchange at the air–water interface and is an important process impacting dissolved oxygen in the Delaware River Estuary. Conventional options rely on empirical relationships that poorly capture the deep water and high energy environment prevalent in the Estuary. Reaeration simulation was enhanced by incorporating a more mechanistic formulation that accounts for the combined effects of current velocity, wind speed, and water temperature on reaeration.

3. Light extinction formulation: Light extinction in water refers to the loss of light in the water column due to absorption and scattering, and is the single most important process impacting phytoplankton growth in the Delaware River Estuary. A site-specific empirical submodel was developed specifically to predict light extinction in the Estuary as a function of location, salinity, dissolved organic carbon, and chlorophyll-a.

The Delaware River Estuary water quality model was calibrated for the 2018-2019 period to an intensive dataset obtained specifically for this purpose, encompassing a range of hydrologic and temperature conditions. In order to evaluate model performance during a drier period than was encountered in 2018-2019, the model was successfully corroborated against a 2012 hindcast based on available boundary data and forcing functions. The year 2012 was a historical period that resulted in the lowest DO encountered in more than 12 years and provided a useful benchmark. For each calendar year, time-variable boundary concentrations were assigned including: tributary and watershed inflow concentrations, point source concentrations, open tidal boundary concentrations (such as the ocean boundary), atmospheric loads, wind speed and solar radiation, and sediment oxygen demand and benthic nutrient fluxes.

During model calibration, kinetic coefficient values were adjusted within reasonable ranges to improve the agreement between model predictions and measured data, with special focus on periods of low dissolved oxygen in the urban estuary.[5] Overall model performance was evaluated both qualitatively and quantitatively to aid in calibration and to assess model fitness. Spatial, temporal, and statistical comparisons were made between model predictions and observed data from the Boat Run, USGS continuous monitors, and other data obtained by DRBC for this purpose.

[5] The urban estuary is loosely defined as the region from the Philadelphia, Pennsylvania and Camden, New Jersey area to Wilmington, Delaware.

An example spatial comparison of simulated model predictions (WASP output) versus measured data is shown in Figure ES-1 for dissolved oxygen concentration on July 9, 2018. River mile (RM) on the x-axis extends the full length of the model domain, from the ocean (RM 0) to RM 135, about two miles upstream of the head of tide at Trenton. Boat Run (labeled BR) sample results from this particular day are shown as red circles, while the daily range and median DO predictions are shown by the gray shaded region and blue dashed line, respectively.

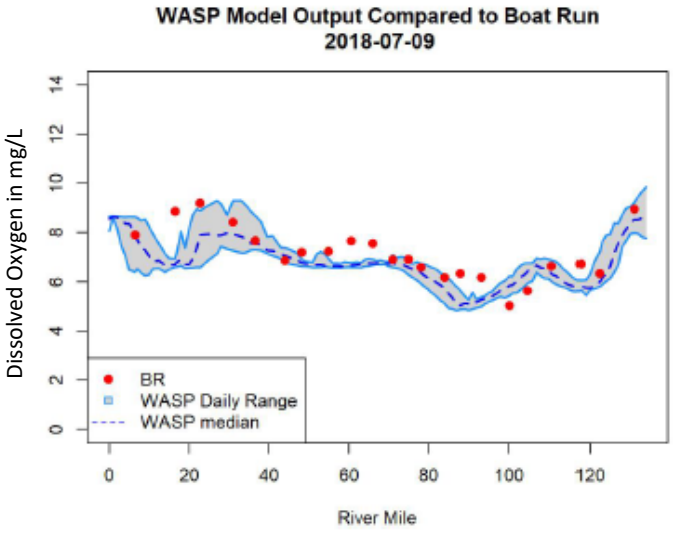

Figure ES-1: Example model to Boat Run data spatial comparison for dissolved oxygen concentration (mg/L)

Whereas the spatial comparison focuses on one particular day, the temporal comparison (Figure ES-2) focuses on one particular location over the entire 2018-2019 period, showing the following.

- A time series comparison is shown in the upper left frame, in which predicted (black line) and observed (red dots) DO values are plotted on the same graph with time over the 2-year period on the X-axis (the beginning of 2019 is labeled);
- A one-to-one comparison is shown in the upper right frame, in which pairs of predicted and observed DO values are plotted with predicted on the y-axis and observed on the x-axis. The blue line indicates a perfect fit whether each pair of predicted and observed values are identical.
- Cumulative frequency distributions are shown in the lower left frame, with the black line for predicted values and the red line for observed values. Each percentile indicates the proportion of total values over the 2-year period that are at or below a particular DO concentration.
- Finally, a map with relevant statistics is provided in the lower right frame showing the location of the temporal comparison and a few relevant statistics regarding the level of fitness between predicted and observed values.

The temporal comparison format can be used to compare with Boat Run samples, as shown, or continuous data from a particular location.

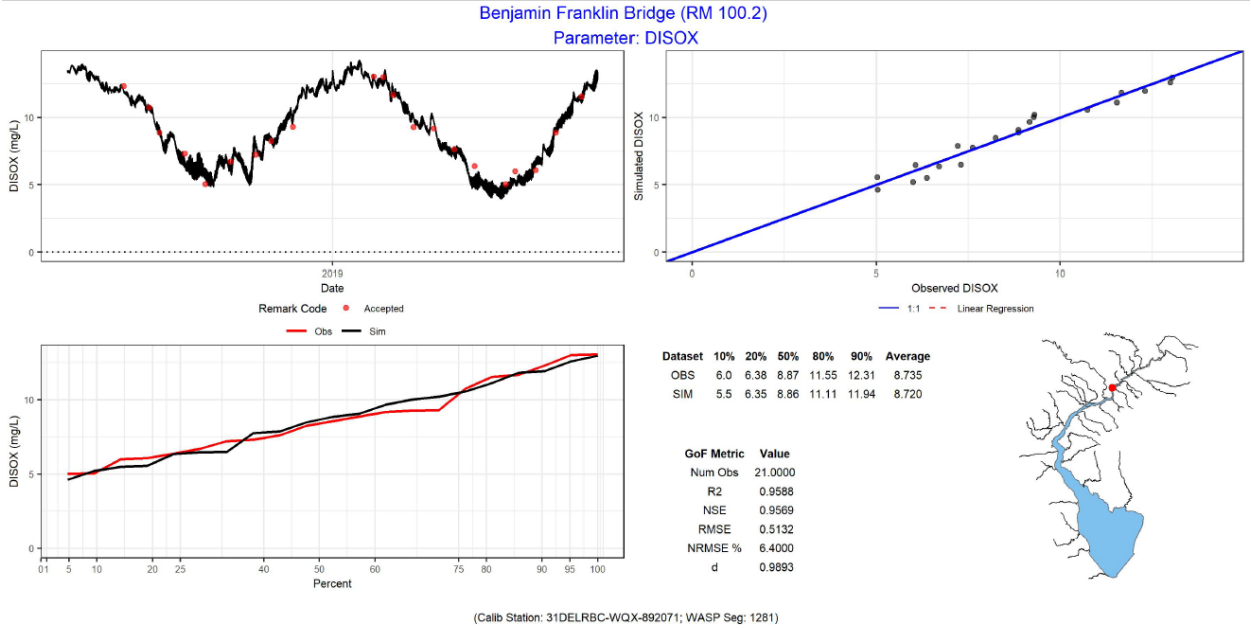

Figure ES-2: Example temporal comparison showing DO at Ben Franklin Bridge in Philadelphia

Figure ES-3 shows an example of one of the statistical analyses performed to evaluate model calibration, namely model skill (also called Index of Agreement; defined in Section 4.4.1). Model skill provides a measure of model error relative to natural variability; values range from 0 to 1, with 1 indicating a perfect fit of simulated and observed data, and a value of 0 indicating no agreement between them. The box and whisker plots show the distribution of model skill scores for all 22 Boat Run sampling locations during the 2018-2019 calibration period for dissolved oxygen, ammonia nitrogen, dissolved organic carbon, and phosphate (i.e., dissolved inorganic phosphorus). Median skill scores for dissolved oxygen, ammonia nitrogen, dissolved organic carbon, and phosphate were 0.980, 0.680, 0.815, and 0.813, respectively.

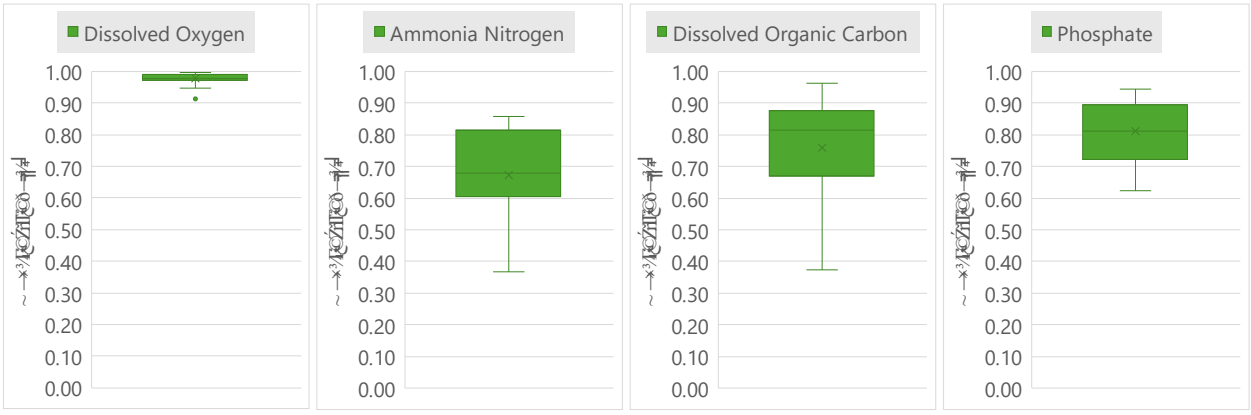

Figure ES-3: Model skill scores for dissolved oxygen, ammonia, DOC, and phosphate (Boat Run)

Particular attention was paid to model-to-data comparisons at locations with continuous data, primarily dissolved oxygen and phytoplankton chlorophyll-a. Six locations with continuous data were available

during the model calibration period: four long-term USGS gage stations and two buoys installed and maintained by the Philadelphia Water Department (PWD, see Figure ES-4 for locations of continuous monitors along with nearby Boat Run locations). These continuous monitors provided intensive data at six discrete locations: Pennypack Woods (RM 110.5), Ben Franklin Bridge (RM 100.1), Buoy B (RM 93.5), Chester (RM 83.6), Buoy P (RM 62.0), and Reedy Island (RM 54.1).

Figure ES-4: Continuous monitoring and Boat Run sampling locations

The continuous data from PWD were not made available until nearly the end of the model calibration process, so they provide especially valuable validation of model performance. In particular Buoy B near the Navy Yard boat run location, where the trough of the DO sag typically occurs, provides an excellent benchmark for model performance. As shown in Figure ES-5, the model simulates dissolved oxygen at this critical location extremely well. In fact, skill factors for all six continuous dissolved oxygen monitors from May 1 through October 15 in 2018-2019 (Table 4-7) range from 0.83 to 0.95 (0.93 at Buoy B).

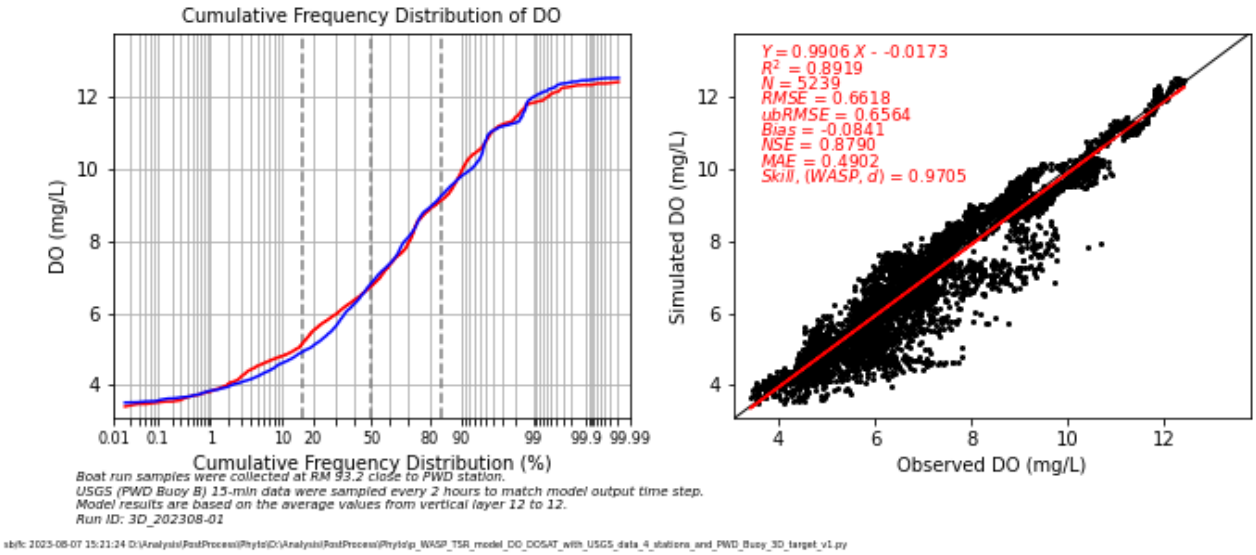

Figure ES-5: Model-to-data comparisons of dissolved oxygen during 2018-2019 at Buoy B

Continuous chlorophyll-a observations (a surrogate for phytoplankton, i.e., algae) were available at the Ben Franklin Bridge and Buoy B locations, derived from regressions between chlorophyll-a measurements and continuous fluorometric sensor data. Skill factors for chlorophyll-a during 2018-2019 were 0.55 at Ben Franklin Bridge and 0.62 at Buoy B; these, along with the chlorophyll-a grab data, show that the model does not fully capture the extent of bloom events that occur in the urban estuary. Several diagnostic analyses were performed and summarized in Section 4.5 to more fully understand why the model does not fully capture algal production and what is the impact of this limitation on simulated dissolved oxygen. For instance, an extreme diagnostic simulation was performed in which phytoplankton growth was completely suppressed. While the model underpredicts dissolved oxygen concentrations when phytoplankton blooms are not captured, this diagnostic simulation demonstrated that dissolved oxygen impacts were partly ameliorated through reaeration dynamics. The model also demonstrated that algal blooms impact the magnitude of dissolved oxygen peaks during blooms much more than the post-bloom decreases in dissolved oxygen. Therefore, the model limitations in simulating algae production were determined to be acceptable. Uncertainty analyses were also performed and discussed in the context of model limitations and applications.

In accordance with the established Quality Assurance Project Plan (DRBC, 2019) for this project, a "weight of evidence" approach for calibration was used in close coordination with the Model Expert Panel in order to judge the acceptability of the model for its intended purpose. The DRBC modeling team and the Model Expert Panel concluded[6] that the Delaware River Estuary water quality model is scientifically defensible

[6] The Model Expert Panel formalized these conclusions in a presentation to the Water Quality Advisory Committee meeting on April 27, 2022: https://www.nj.gov/drbc/library/documents/WQAC/042722/suk-amidon-bierman_modeling-update.pdf

over a wide range of environmental conditions and suitable for its intended use – to determine the improvement in dissolved oxygen condition that would result from specific reductions to point and nonpoint source loadings.

While the development and calibration of this water quality model represents a significant achievement and milestone, it is important to recognize that this model is not intended to be merely a useful reference. The model as described is fully adequate for its purpose, namely, to relate specific water and pollutant loading scenarios with dissolved oxygen outcomes in the Delaware River Estuary. However, the DRBC is continuing to develop modifications and improvements to the model both for its primary purpose and for related purposes as appropriate. Documenting model development and calibration within this report is of course necessary, but the model is not a static tool. The DRBC is using the tool to better understand estuary dynamics and will continuously improve the model consistent with its goals and resources.

TABLE OF CONTENTS

LIST OF APPENDICES

LIST OF TABLES

LIST OF FIGURES

LIST OF ACRONYMS/ABBREVIATIONS

2D	Two Dimensional
3D	Three Dimensional
Boat Run	DRBC's Delaware Estuary Water Quality Monitoring Program
BOD-5	5-day Biochemical Oxygen Demand
BOD-20	20-day Biochemical Oxygen Demand
CBOD	Carbonaceous Biochemical Oxygen Demand (CBODU indicates ultimate CBOD)
C&D Canal	Chesapeake and Delaware Canal
Chla	Chlorophyll-a
CSO	Combined Sewer Overflow
D-DIP	Inorganic Phosphate
DET-C	Detrital Carbon
DET-N	Detrital Nitrogen
DET-P	Detrital Phosphorus
DET-Si	Detrital Silica
DISOX	Dissolved Oxygen
DO	Dissolved Oxygen
DOC	Dissolved Organic Carbon
DON	Dissolved Organic Nitrogen
DOP	Dissolved Organic Phosphorus
DOSi	Dissolved Organic Silica
DOSAT	Dissolved Oxygen Saturation
DRB	Delaware River Basin
DRBC	Delaware River Basin Commission
DW	Dry Weight
EFDC	The Environmental Fluid Dynamics Code
EPA	U.S. Environmental Protection Agency
ETM	Estuary Turbidity Maxima
FNC	Federal Navigation Channel
FSS	Fixed Suspended Solids
Hr	Hour
IN-SI	Inorganic Silica

Ke	light extinction coefficient
LOADEST	Load Estimator
MDLs	Method Detection Limits
MEP	Model Expert Panel
MS4	Municipal Separate Storm Sewer System
NADP	National Atmospheric Deposition Program
NGO	Non-Governmental Organization
NH3-N	Ammonia Nitrogen, includes gaseous ammonia (NH3) and ionized ammonium (NH4+)
NH34	The state variable used by WASP to simulate ammonia nitrogen (NH3 and NH4+)
NO2-N	Nitrite Nitrogen
NO3-N	Nitrate Nitrogen
NO3O2	The state variable used by WASP to simulate nitrite (NO2) plus nitrate (NO#) nitrogen
NOAA	National Oceanic and Atmospheric Administration
NPS	Non-Point Source
NSE	Nash-Sutcliffe coefficients
NWQP	National Water Quality Portal
Org-N	Dissolved Organic Nitrogen
Org-P	Dissolved Organic Phosphorus
Org-Si	Dissolved Organic Silica
PAR	Photosynthetically Active Radiation
PWD	Philadelphia Water Department
R2	Coefficient of determination
RM	River Mile
SOD	Sediment Oxygen Demand
SPW	Special Protection Waters
SRP	Soluble Reactive Phosphorus
TDS	Total Dissolved Solids
TSS	Total Suspended Solids
TDN	Total Dissolved Nitrogen
TKN	Total Kjeldahl Nitrogen
TN	Total Nitrogen
TP	Total Phosphorus
TVS	Total Volatile Solids

ubRMSD	unbiased Root Mean Square Difference
USACE	U.S. Army Corps of Engineers
USGS	U.S. Geological Survey
UV	Ultraviolet
WASP	Water Quality Analysis Simulation Program
WQAC	Water Quality Advisory Committee
WRDB	Water Resources Database
WRTDS	Weighted Regressions on Time, Season, and Discharge Tool

1. INTRODUCTION

Dissolved oxygen (DO) is among the most critical environmental parameters directly affecting fish and aquatic habitats. When the Delaware River Basin Commission (DRBC or Commission) was created in 1961, little or no dissolved oxygen was present in a 38-mile section of the tidal Delaware River stretching from Wilmington, Delaware, to Philadelphia, Pennsylvania, for periods of up to six months each year, preventing the survival of resident fish and the passage of anadromous fish through these waters. The water quality and aquatic life uses of the Delaware River Estuary[7] ("the Estuary") have substantially improved since DRBC adopted designated uses and water quality criteria for these reaches in 1967, mainly due to new and upgraded wastewater treatment plants reducing the load of organic carbon discharged into the Estuary. Dissolved oxygen improvements over the years are illustrated in Figure 1-1 for a location in Philadelphia.

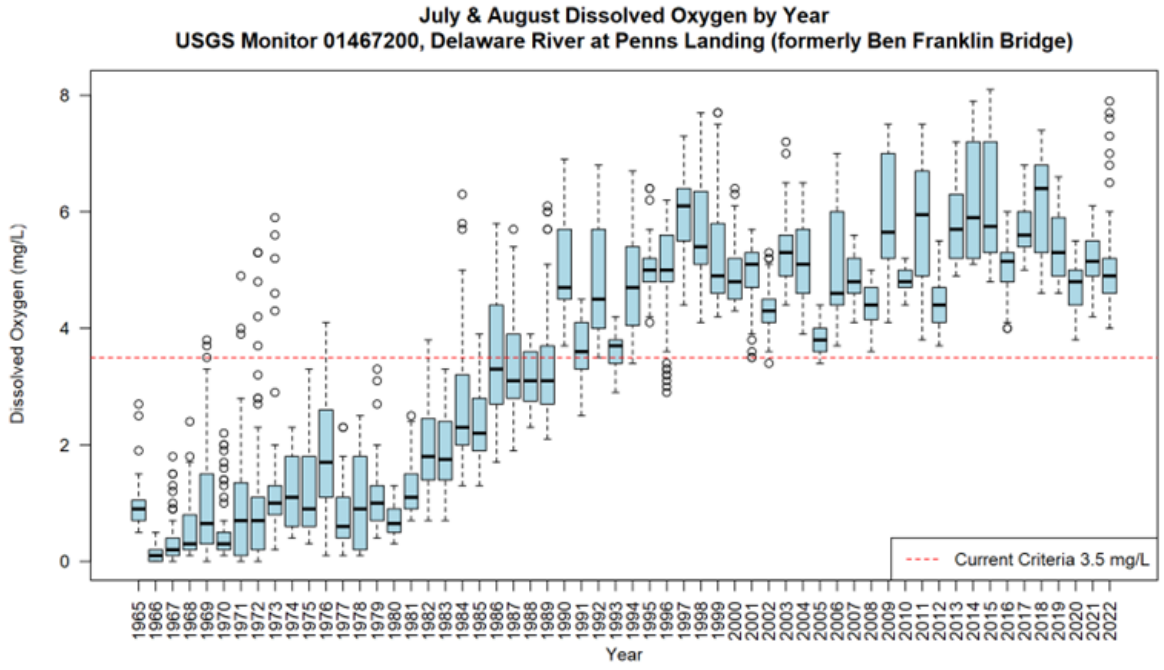

Figure 1-1: DO at Ben Franklin Bridge during July and August from 1965–2022

Nonetheless, DO in the more urban portion of the Estuary, comprising Zones 3, 4 and upper 5 and extending from River Mile (RM) 70 to 108, remains lower than in other areas of the Estuary. Viewed longitudinally from the head of tide at Trenton, New Jersey, to the mouth of the Delaware Bay (i.e., RM 0),

[7] The Delaware River Estuary includes the tidally-influenced Delaware River and the Delaware Bay.

the region of lower DO is referred to as a "sag," and is especially pronounced during summer periods (Figure 1-2).

The DRBC adopted Resolution No. 2017-4 on September 13, 2017, recognizing the significant water quality improvements in the Delaware River Estuary and the vital importance of determining the appropriate designated aquatic life uses and water quality criteria necessary to support these uses in the 38-mile section between Wilmington and Philadelphia[8]. The resolution specifically required the development and calibration of a eutrophication model for the Delaware River Estuary, as well as the formation of a Model Expert Panel to provide input and advice to the DRBC.

[8] The complete Resolution 2017-4 can be found online at https://www.nj.gov/drbc/library/documents/Res2017-04_EstuaryExistingUse.pdf.

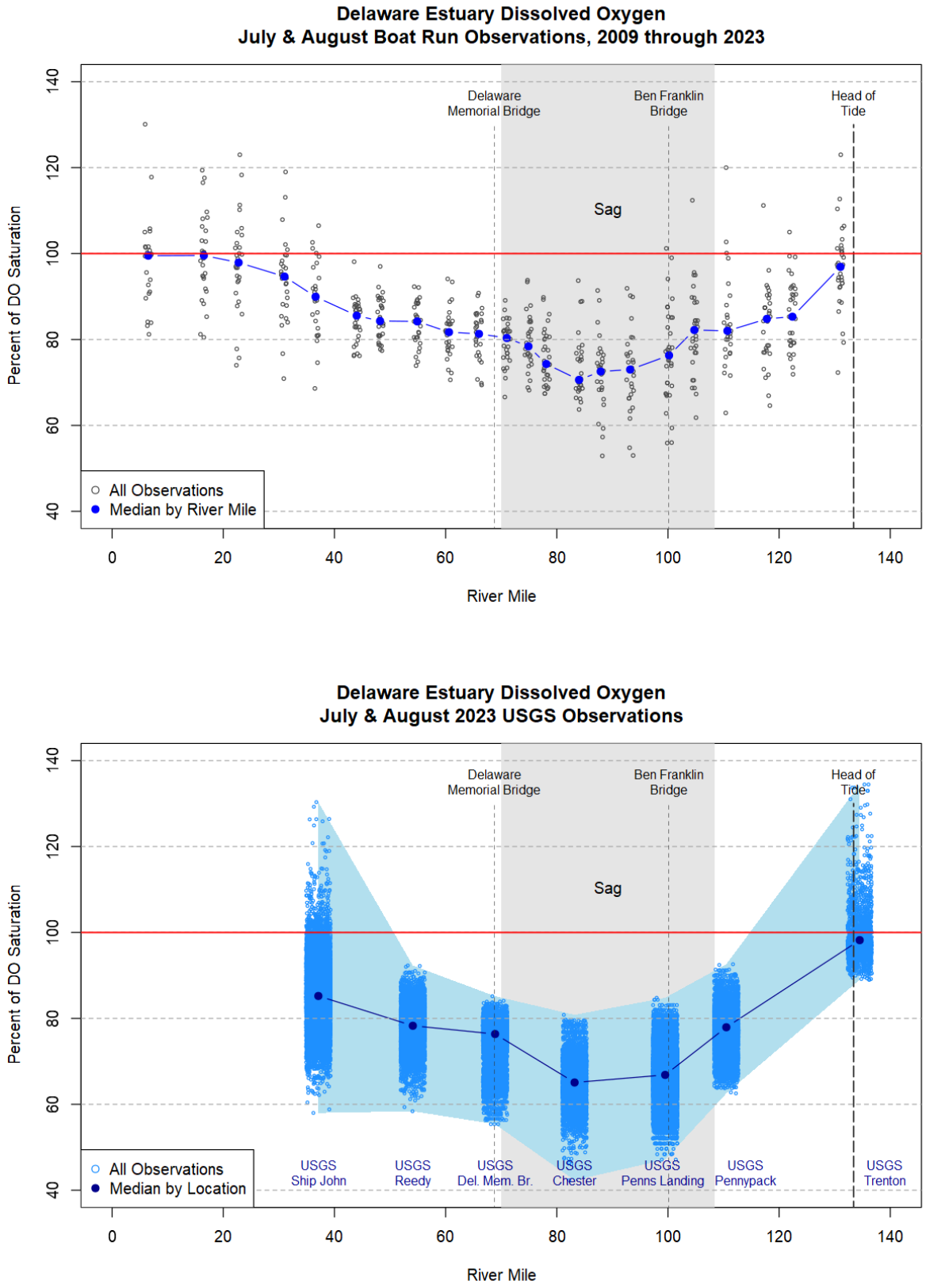

Figure 1-2: Dissolved Oxygen "sag" in the urban portion of the Delaware River Estuary

1.1 Purpose and Objectives of the Modeling Study

A three-dimensional water quality model was developed as one component of the larger eutrophication modeling study of the Delaware River Estuary, the goal of which is to develop and calibrate a technically sound model of eutrophication processes in the Delaware River Estuary from the head of the tide at Trenton, New Jersey, to the ocean utilizing an appropriate level of complexity within the current state of the science and within the timeframe established by the Commission. The eutrophication modeling study has improved our understanding of the impact of nutrient loads on dissolved oxygen conditions in the Delaware River Estuary, particularly in the 38-mile-long segment of the tidal river including Zone 3, Zone 4, and upper Zone 5 where a summertime DO sag (lower concentrations of dissolved oxygen than are observed elsewhere in the Estuary) is observed to occur every year. This effort included: 1) the convening of a Model Expert Panel, which has been actively engaged with this project since November 2016, to guide the development of the eutrophication model; 2) the completion of a two-year monitoring program in partnership with wastewater authorities in order to obtain data on nutrient loadings from point sources; 3) the completion of two years of intensive monitoring of key tributaries and ambient waters to develop loadings from key tributaries and to establish model calibration targets; 4) field studies on primary productivity in the lower Delaware River Estuary; and 5) development of linked hydrodynamic and water quality models. The three-dimensional hydrodynamic model that provides the foundation for the water quality model is documented in a separate report (Chen et al., 2024).

In accordance with DRBC Resolution No. 2017-4, which affirms the important goal of continued water quality improvement, the DRBC conducted a comprehensive scientific and engineering evaluation of water quality to provide the scientific basis for the DRBC to evaluate management options in establishing water quality criteria for dissolved oxygen and nutrients as necessary, and for establishing loading targets for point and non-point sources into the Delaware River Estuary to achieve these criteria. DRBC lead this groundbreaking effort through a collaborative process informed by a Model Expert Panel, comprised of nationally recognized water resource scientists and engineers, and in close consultation with its Water Quality Advisory Committee (WQAC), a stakeholder advisory group representing state and federal co-regulators, non-governmental organizations (NGOs), academic institutions, and municipal and industrial dischargers.

The eutrophication model developed by the DRBC will continue to enhance our understanding of the impact of carbon, nitrogen and phosphorus loads including nitrogenous and carbonaceous oxygen demand (CBOD) and effects from phytoplankton photosynthesis and respiration, on dissolved oxygen conditions in the Delaware River Estuary. The model also accounts for reaeration and sediment oxygen demand impacts to ensure processes affecting water column dissolved oxygen are adequately represented. Given the complexity of tidal dynamics and input loads, the spatial extent of the model includes the entire Delaware River Estuary. The model is designed to estimate ambient dissolved oxygen concentrations that can be expected to result from various levels of input load reductions using a dynamic (time-varying), long-term simulation of diurnal dissolved oxygen patterns.

1.2 Study Area

The study area encompasses the entire Delaware River drainage basin, while the Delaware River Estuary (the tidal Delaware River and Bay) defines the extent of the water quality model domain.

1.2.1 Delaware River Basin

The Delaware River extends 330 miles from Hancock, New York, in the Catskill Mountains to the mouth of the Delaware Bay where it enters the Atlantic Ocean between Cape May, New Jersey and Cape Henlopen, Delaware (Figure 1-3). It is the longest un-dammed river on the Atlantic coast of the United States. The entire Delaware River basin comprises 13,539 square miles in four states (New York, New Jersey, Pennsylvania, and Delaware), including the 782 square miles of the Delaware Bay itself.

The East and West Branches of the Delaware River combine at RM 330 at Hancock, New York, to form the mainstem Delaware River, which flows 197 miles south to the head of tide at Trenton, New Jersey (RM 133). Below Trenton, the river is tidally influenced for 133 miles down to the mouth of the Delaware Bay (RM 0). The drainage area at Trenton, New Jersey, is approximately 6,780 square miles. The total watershed downstream of Trenton to the mouth of the bay is 7,541 square miles. This includes the Schuylkill River (1,911 square miles) and Christina River (755 square miles) basins, the second and third largest tributaries (behind the Delaware River itself) in terms of freshwater flow contributed to the mainstem, and the Delaware Bay itself (782 mi^2). The hydrodynamic and water quality model domains extend from the head of tide at Trenton to the mouth of the bay into the Atlantic Ocean.

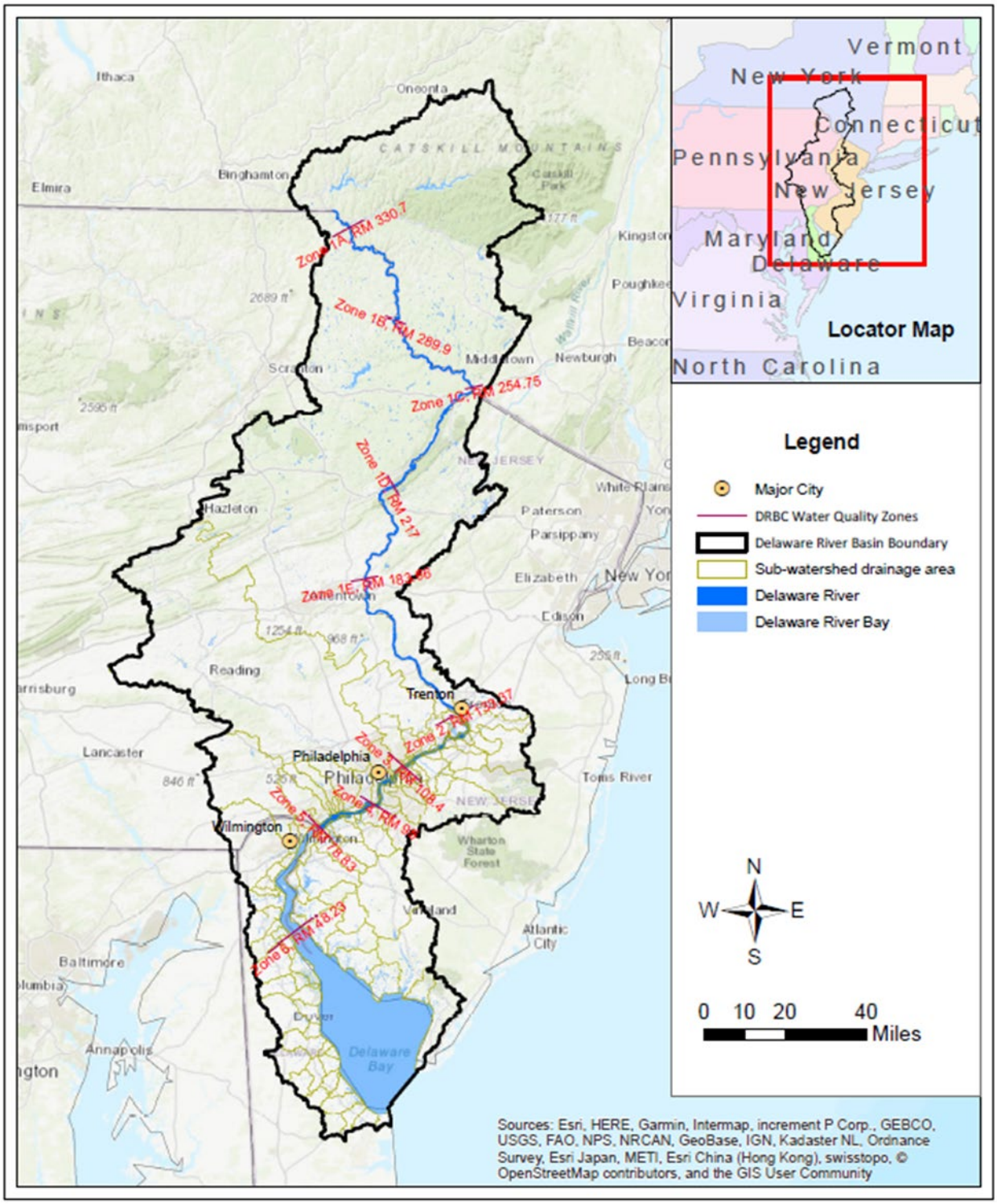

Figure 1-3: Delaware River Basin

The average annual water discharge at Trenton is approximately 12,055 cfs based on data from 1912 to 2023. The monthly statistics of river discharge show a clear flow seasonality, with the two highest monthly

mean flows in March and April (20,400 and 21,900 cfs, respectively) and the two lowest in July and August (6,420 and 6,680 cfs, respectively). The average annual water discharge in the Schuylkill River over the period 1932 to 2018 was approximately 2,850 cfs. According to a U.S. Geological Survey (USGS) study prepared for the Federal Emergency Management Agency (FEMA) in 2008, the flood frequencies of the Delaware River at Trenton, .New Jersey, are estimated as follows: 94,900 (2-year), 138,000 (5-year), 169,000 (10-year), 211,000 (25-year), 245,000 (50-year), and 280,000 (100-year) in units of cfs (Schopp and Firda, 2008).

Monitoring demonstrates that the dissolved oxygen concentrations and many other water quality constituents throughout the non-tidal Delaware River (upstream of Trenton) are generally better than standards (DRBC, 2023). A Special Protection Waters (SPW) Program, initially adopted by the DRBC in 1992 and expanded in 1994 and 2008 for the non-tidal portion of Delaware River, was designed to prevent degradation in streams and rivers where existing water quality is better than the established water quality standards. The program states that there will be no measurable change in existing water quality of SPW except towards natural conditions. Simply, the goal of SPW program is to keep the clean water clean.

1.2.2 Delaware River Estuary

The tidal portion of the Delaware River is a typical coastal plain estuary with a relatively homogeneous shallow depth of about 26 to 33 feet. Eighty percent of the estuary has a depth of less than 30 feet, except for the Federal Navigation Channel (FNC), which was deepened most recently in 2016 to a depth of 45 feet below Mean Lower Low Water (MLLW) level. The width of the Delaware Bay at its mouth is 11 miles, and the widest part of the bay is about 27 miles. Channel width decreases precipitously in the upstream direction: 2.4 miles wide in the reach from Delaware City just inland of the Chesapeake and Delaware Canal (C&D Canal) around RM 60; a half-mile wide in Philadelphia at the Ben Franklin Bridge (RM 100); about a quarter-mile wide at Burlington (RM 117.5); and less than 1,000 feet wide at Trenton (RM 134). Additional hydrophysical characterization of the Delaware River Estuary is found in the hydrodynamic model calibration report (Chen et al., 2024).

1.3 Processes Affecting Dissolved Oxygen

Dissolved oxygen is controlled by a series of complex physical, chemical, and biological processes, which are summarized in Figure 3-2 and represented in the water quality model framework as discussed in Section 3.3. Physical processes represented in the model include advection (movement with water), dispersion (mixing), reaeration, settling, and sorption. The model chemical processes consist of

ammonium[9] nitrification, organic carbon oxidation, sediment oxygen demand, dissolution, and mineralization. Lastly, the modeled biological processes involve photosynthesis, respiration, phytoplankton growth, death, and uptake of nutrients. Note that the distinctions among physical, chemical, and biological processes are somewhat arbitrary; for example, dissolution is both a physical and chemical process, while both nitrification and sediment oxygen demand are biologically mediated chemical processes. Of these processes, reaeration and photosynthesis contribute to the dissolved oxygen production; nitrification, sediment oxygen demand, CBOD oxidation, and respiration cause dissolved oxygen consumption. In addition, water temperature and salinity influence the levels (solubility) of dissolved oxygen in equilibrium with the atmosphere; warmer water contains less oxygen than colder water at saturation, while saltier water (higher salinity) carries less oxygen than fresh water.

1.4 Overview of Technical Approach

The DRBC's overall approach to developing the eutrophication model has been as follows.

- Develop three-dimensional hydrodynamic models of the system using the Environmental Fluid Dynamics Code (EFDC), which is supported by the U.S. Environmental Protection Agency (EPA).
- Develop a three-dimensional water quality model of the system that is linked to the hydrodynamic model using the Water Quality Analysis Simulation Program (WASP), which is also supported by EPA.
- Assess available nutrient and auxiliary environmental data as to the degree to which loads, ambient data, and kinetic rates are adequate for model development and calibration, and conduct additional monitoring of both source waters and ambient waters to fill data gaps as needed.
- Calibrate and validate the linked hydrodynamic and water quality models for the years 2018 to 2019 and 2012 to demonstrate fitness over a wide range of hydrologic conditions. The primary focus of the model calibrations was for the years 2018 and 2019 when water quality data were collected through DRBC's intensive eutrophication modeling study monitoring program. However, the 2012 year was added as a corroboration period to incorporate a year with drier hydrologic conditions than occurred in 2018 and 2019.

The primary technical objective of the study is to develop a linked and calibrated EFDC-WASP model that is appropriate for conducting forecast simulations to determine the input load reductions needed to

[9] Ammonia nitrogen consists of gaseous ammonia (NH_3) and ionized ammonium (NH_4^+), the latter of which is directly involved in nitrification. Due to hydrolysis in water, the two forms exist in equilibrium based on pH and temperature. Since ammonia nitrogen tests measure both forms, and since hydrolysis reactions are very fast maintaining equilibrium, the term "ammonia" is commonly used to mean both forms. Unless preceded by "gaseous," references to ammonia in this report refer to both forms together.

achieve varying magnitudes of ambient dissolved oxygen conditions in the Delaware River Estuary, and in particular the urban estuary.

This study used available data and information to the fullest extent possible, while acknowledging that data gaps exist in the present state of knowledge about the Delaware River Estuary study area and that all water quality models are numerical approximations of, and not exact replicas of, natural systems. Therefore, multiple lines of evidence were used to evaluate the reliability of the model during the calibration and corroboration process, since model fitness is impacted not just by the quality of the calibration but also by the quality of boundary and field data, neither of which are perfectly known. Model performance was evaluated for major water quality parameters, such as nitrogen and phosphorus species, phytoplankton, and dissolved oxygen through model to data comparisons.

2. SAMPLING PROGRAM AND RESULTS

The development of a spatially explicit eutrophication model for the entire Delaware River Estuary represents an ambitious undertaking that required a significant amount of data.

2.1 SAMPLING PROGRAM DESCRIPTION

The following monitoring programs were expanded and initiated in 2017 to support this study, and the corresponding sampling locations are shown in Figure 2-1:

- Delaware Estuary Water Quality Monitoring Program ("Boat Run");
- Tributary Monitoring including the Delaware River at Trenton and the Schuylkill River at Philadelphia;
- Additional sensors added to selected USGS continuous monitors;
- Additional wastewater treatment plant effluent monitoring for Tier 1 and 2 facilities from March 2018 to February 2020[10]; and
- For Tier 3 facilities, two-year effluent data collected from 2011 to 2015 and states' electronic Discharge Monitoring Reports were used to characterize effluent conditions for the model calibration period.

[10] Tier 1 facilities comprise 95% of the cumulative point discharge load for ammonia, total Kjeldahl nitrogen (TKN), and 5-day biological oxygen demand (BOD-5) based on the data sets collected between 2011 and 2015. Tier 2 facilities include facilities contributing to the 95% cumulative load for phosphorus, soluble reactive phosphorus (SRP,), nitrate, and total nitrogen (TN) that were not already included in Tier 1. Tier 3 facilities were those facilities not included in Tiers 1 or 2. More information is available online at https://www.nj.gov/drbc/library/documents/WQAC/082417/yagecic_point-source-monitoring.pdf.

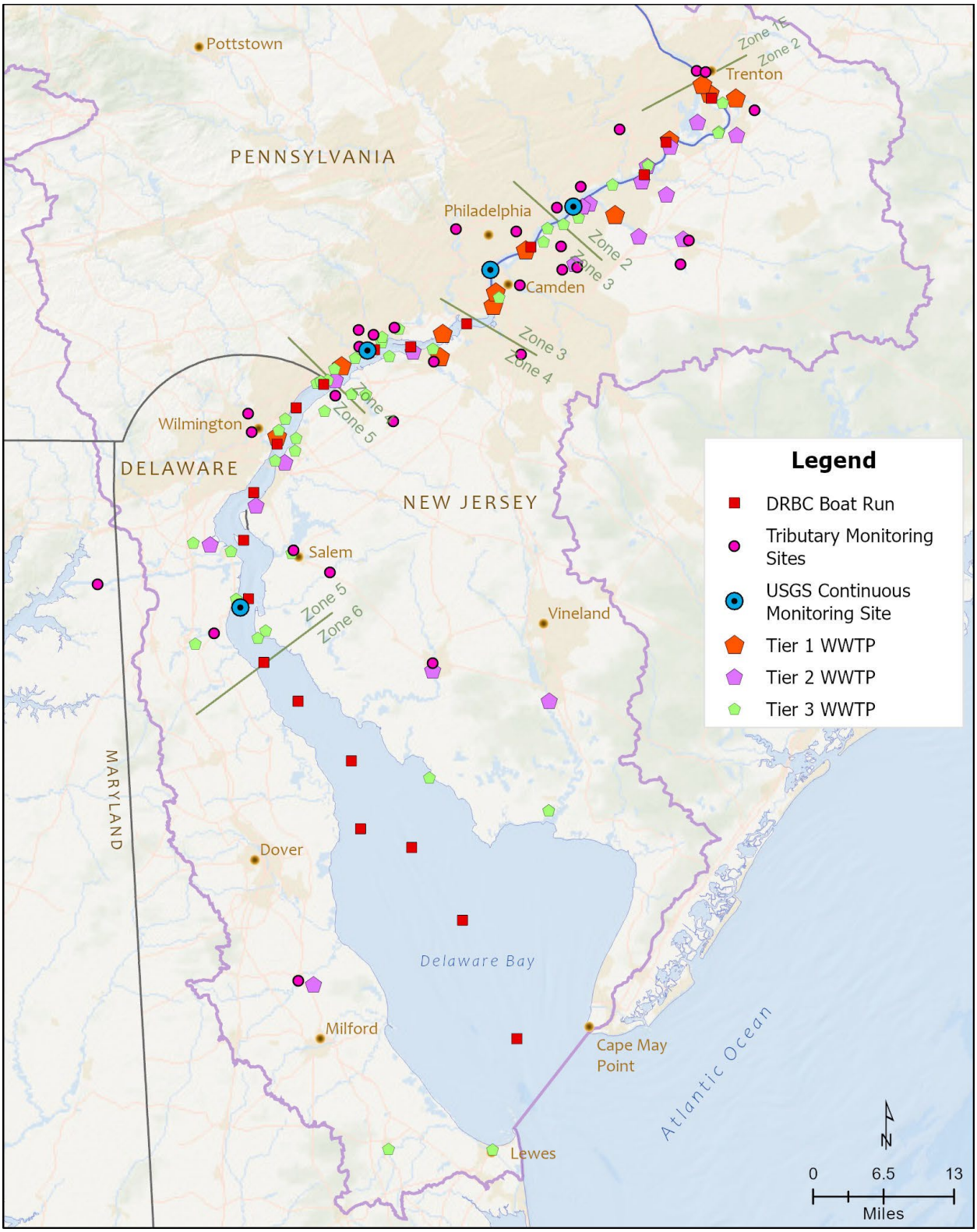

Figure 2-1 Overview of sampling locations by monitoring locations by monitoring program

2.1.1 Delaware River Estuary Water Quality Monitoring

Estuary water quality monitoring consisted of primarily event-based Delaware Estuary Water Quality Monitoring Program (Boat Run) monitoring and continuous monitoring at USGS fixed sites and PWD buoys, as shown in Figure 2-2. The DRBC Boat Run monitoring program was initiated in 1967 and involves the collection of discrete samples on specific sample collection days at 22 stations; samples were analyzed for an extended parameter list to support the water quality modeling effort. USGS monitors are deployed at four[11] fixed locations where they measure and report a shorter list of parameters on a continuous basis, and the Philadelphia Water Department (PWD) conducted water quality monitoring at two buoy locations. These ambient data were used as calibration targets by comparing with model outputs and to define initial conditions for the model.

[11] Since the model calibration period, two additional fixed monitoring locations in the Estuary have been added by USGS at Ship John Shoal and the Delaware Memorial Bridge.

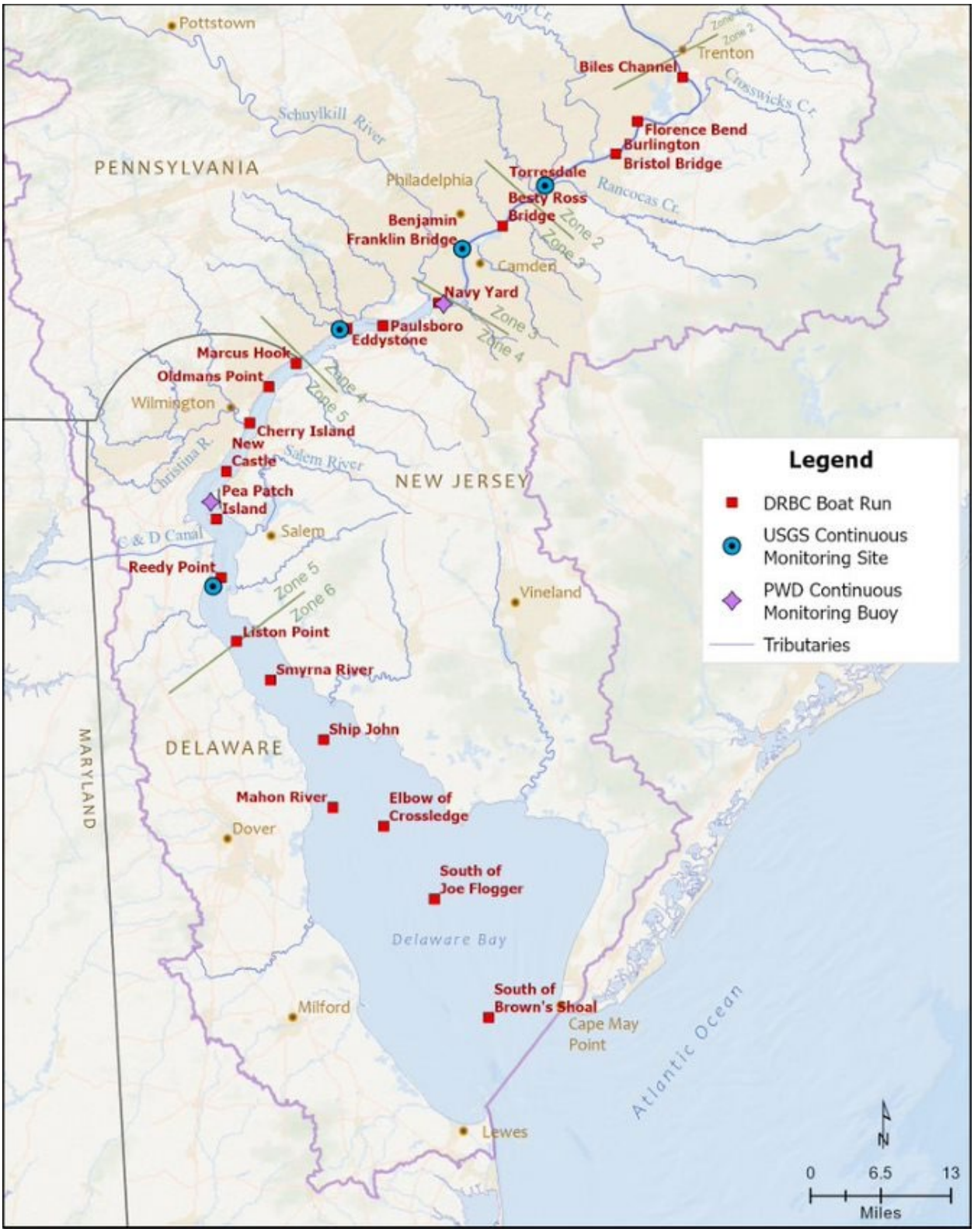

Figure 2-2: Boat Run sampling and continuous in-situ monitoring locations

2.1.1.1 DRBC BOAT RUN

Historically, Boat Run monitoring has been performed approximately monthly beginning in March or April and continuing through October. During the period from 2017 through 2020, the Boat Run was expanded to nearly year-round (weather permitting). From 2017 through 2020, Boat Run monitoring was performed on the dates shown in Table 2-1 below.

Table 2-1 Boat Run monitoring dates

CY2017	CY2018	CY2019	CY2020
18-Jan-17	--	26-Feb-19	--
6-Feb-17	--	11-Mar-19	24-Feb-20
13-Mar-17	19-Mar-18	25-Mar-19	9-Mar-20
10-Apr-17	23-Apr-18	22-Apr-19	--
22-May-17	7-May-18	20-May-19	--
12-Jun-17	11-Jun-18	17-Jun-19	--
10-Jul-17	9-Jul-18	15-Jul-19	--
7-Aug-17	13-Aug-18	27-Aug-19	24-Aug-20
26-Sep-17	17-Sep-18	9-Sep-19	14-Sep-20
9-Oct-17	8-Oct-18	7-Oct-19	5-Oct-20
6-Nov-17	7-Nov-18	4-Nov-19	--
18-Dec-17	--	9-Dec-19	--

The Boat Run program includes near-surface sample collection from 22 stations located in the center channel of the Delaware River Estuary from just below the head of tide near Trenton, New Jersey, to just above the mouth of the Bay. Sample locations are shown in Figure 2-2 and listed in Table 2-2 below.

Table 2-2 Boat Run sampling locations

Sample Location Description	River Mile (from Mouth of Bay)	Coordinates (Latitude and Longitude)
South Brown Shoal	6.5	38.932187, -75.103146
South Joe Flogger Shoal	15.5	39.068639, -75.177453
Elbow of Crossledge Shoal	22.75	39.144737, -75.239596
Mahon River	31	39.229606, -75.300302

Sample Location Description	River Mile (from Mouth of Bay)	Coordinates (Latitude and Longitude)
Ship John Light	36.6	39.296339, -75.375902
Smyrna River	44	39.380387, -75.472996
Liston Point	48.2	39.425987, -75.525838
Reedy Island	54.9	39.511917, -75.553137
Pea Patch Island	60.6	39.592357, -75.564242
New Castle	66	39.655110, -75.545412
Cherry Island	71	39.720878, -75.505794
Oldmans Point	74.9	39.774134, -75.467938
Marcus Hook	78.1	39.800655, -75.425245
Eddystone	84	39.844852, -75.342034
Paulsboro	87.9	39.848061, -75.267146
Navy Yard	93.2	39.881679, -75.180190
Benjamin Franklin Bridge	100.2	39.955502, -75.135818
Betsy Ross Bridge	104.75	39.984701, -75.066603
Torresdale	110.7	40.040199, -74.988048
Burlington Bristol Bridge	117.8	40.081067, -74.868852
Florence Bend	122.4	40.128025, -74.816028
Biles Channel	131.04	40.181566, -74.746191

Beginning in 2017 Boat Run samples were analyzed for an expanded list of analytical parameters related to the eutrophication study as summarized in Table 2-3 below.

Table 2-3 Boat Run parameters

Analytical Parameter	Units	Filtration	Sample Type
Specific Conductance	µS/cm	Unfiltered	in-situ surface water grab
Salinity	ppt	Unfiltered	near-surface water grab
Dissolved Oxygen	mg/L	Unfiltered	in-situ surface water grab
Dissolved Oxygen Saturation	% Saturation	Unfiltered	in-situ surface water grab

Analytical Parameter	Units	Filtration	Sample Type
pH, Field	1-14 S.U.	N/A	in-situ surface water grab
Secchi Depth	meters	N/A	in-situ surface water grab
Temperature, Water	ºC	N/A	in-situ surface water grab
Turbidity (Nephelometric)	NTU	Unfiltered	near-surface water grab
Light Attenuation	m^{-1}	N/A	in-situ ship level grab
Light Attenuation	m^{-1}	N/A	in-situ 1-meter depth grab
Color Dissolved Organic Material (CDOM)	RFU	Unfiltered	near-surface water grab
Chlorophyll-a	µg/L	0.70 µm filter	near-surface water grab
UV 254	cm^{-1}	Unfiltered	near-surface water grab
Alkalinity (titrimetric, pH 4.5)	mg/L	Unfiltered	near-surface water grab
Hardness as CaCO3	mg/L	Unfiltered	near-surface water grab
Chloride, Total	mg/L	Unfiltered	near-surface water grab
Sulfate	mg/L	0.45 µm filter	near-surface water grab
Dissolved Organic Carbon (DOC)	mg/L	0.45 µm filter	near-surface water grab
Particulate Organic Carbon (POC)	mg/L	0.45 µm filter	near-surface water grab
Silica, Dissolved	mg/L	0.45 µm filter	near-surface water grab
Silica, Total	mg/L	Unfiltered	near-surface water grab
Nitrogen, Total	mg/L	Unfiltered	near-surface water grab
Nitrogen, Total Dissolved	mg/L	0.45 µm filter	near-surface water grab
Nitrate as N, Dissolved	mg/L	0.45 µm filter	near-surface water grab
Nitrate/Nitrite as N, Dissolved	mg/L	0.45 µm filter	near-surface water grab
Nitrite as N, Dissolved	mg/L	0.45 µm filter	near-surface water grab
Nitrogen, Particulate	mg/L	0.45 µm filter	near-surface water grab
Ammonia Nitrogen (NH3-N)	mg/L	0.45 µm filter	near-surface water grab
Phosphorus, Particulate Organic	mg/L	0.45 µm filter	near-surface water grab
Phosphorus, Particulate Inorganic	mg/L	0.45 µm filter	near-surface water grab
Orthophosphorus, Soluble	mg/L	0.45 µm filter	near-surface water grab

Analytical Parameter	Units	Filtration	Sample Type
Phosphorus, Total	mg/L	Unfiltered	near-surface water grab
Phosphorus, Dissolved Total	mg/L	0.45 µm filter	near-surface water grab
Total Dissolved Solids (TDS)	mg/L	Unfiltered	near-surface water grab
Total Suspended Solids (TSS)	mg/L	Unfiltered	near-surface water grab
Fixed Suspended Solids (FSS)	mg/L	Unfiltered	near-surface water grab
Volatile Suspended Solids (VSS)	mg/L	Unfiltered	near-surface water grab

2.1.1.2 CONTINUOUS MONITORING DATA

Continuous monitoring data were available from four USGS water quality monitoring stations in the Delaware River Estuary: Pennypack Woods, Penn's Landing, Chester, and Reedy Island. Detailed information on the locations and analytical parameters measured at each station is provided in Table 2-4, while sampling locations are shown in Figure 2-2. Under an agreement between the DRBC and USGS beginning in May 2018, nitrite plus nitrate and dissolved organic carbon (DOC) were added to the list of analytical parameters at the USGS Chester station. Not all parameters were available at all stations for the full model calibration period. More information about each USGS monitoring station, as well as data retrieval, is available online[12].

The Philadelphia Water Department (PWD), with the support of Woods Hole Group, conducted a water quality measurement program in the Delaware River Estuary from 2017 through 2020.[13] Near-continuous water quality data were collected every 12 minutes at two stations: Buoy B near the Schuylkill River confluence with the Delaware River, and Buoy P at about 4 miles upstream of where the C&D Canal connects to the Delaware River. Station locations and measured parameters are summarized in Table 2-4.

[12] For more information, visit https://waterdata.usgs.gov/nwis.

[13] Data were transmitted to DRBC from the Woods Hole Group at the direction of PWD through a Memorandum from K. Lavallee to N. Suk on February 18, 2021.

Table 2-4: Continuous monitoring locations

Station ID	Name	Latitude Longitude	River Mile	Relevant Parameters
USGS/PWD 14670261	Delaware River at Pennypack Woods, PA	40°02'19" N –74°59'37" W	110.0	water temperature specific conductance dissolved oxygen dissolved oxygen % of saturation chlorophyll relative fluorescence turbidity
PWD Buoy B	Delaware River near Schuylkill River confluence	39° 52' 48'' N 75° 10' 14'' W	93.7	water temperature dissolved oxygen dissolved oxygen % of saturation chlorophyll relative fluorescence
USGS 1467200	Delaware River at Penn's Landing, Philadelphia, PA*	39°56'47" N –75°08'23" W	99.5 current 100.05 during calibration	water temperature specific conductance dissolved oxygen dissolved oxygen % of saturation chlorophyll relative fluorescence turbidity
USGS 1477050	Delaware River at Chester, PA**	39°50'44" N –75°21'03" W	83.6	water temperature specific conductance dissolved oxygen dissolved oxygen % of saturation turbidity nitrate plus nitrite dissolved organic carbon
PWD Buoy P	Delaware River at Pea Patch Island	39° 36' 49'' N 75° 34' 24'' W	62.2	water temperature dissolved oxygen dissolved oxygen % of saturation chlorophyll relative fluorescence
USGS 1482800	Delaware River at Reedy Island Jetty, DE	39°30'03" N –75°34'07" W	54.1	water temperature specific conductance dissolved oxygen turbidity

*During the model calibration period (prior to January 2020), the Penn's Landing gage was located RM 100.05 at the end of Pier 12 at a location about 150 ft upstream of the Ben Franklin Bridge (formerly called Ben Franklin Bridge Station). In January 2020 the gage was relocated to RM 99.5 and is now approximately 2,500 ft downstream from Ben Franklin Bridge, at Penn's Landing.

**Nitrite plus nitrate and dissolved organic carbon were added to the list of analytical parameters at the USGS Chester station in May 2018.

2.1.2 Point-Discharge Nutrient Monitoring

The DRBC adopted Resolution No. 2010-5 on July 14, 2010, which authorized DRBC to require point source dischargers to the Delaware River Estuary to perform monthly data collection for nutrients and related parameters for 24 months[14]. Starting in 2011, data were obtained over a two-year period from 75 facilities; this first round of point-discharge monitoring was conducted to allow ranking of facilities by nutrient loadings and assigning to tiers accordingly.

In March 2018, DRBC initiated a second round of point-discharge monitoring, a two-year intensive nutrient monitoring program to obtain model input data for the 2018-2019 calibration period based on a Resolution for the Minutes adopted on September 13, 2017[15]. Based on the first round of monitoring, facilities that contributed the top 95% of total load for ammonia nitrogen, TKN, or BOD-5 (Tier 1 facilities) were monitored weekly between 2018 and 2020, while facilities that contributed the top 95% of total load for total phosphorus (TP), SRP, Nitrate-N, or TN (Tier 2 facilities) were monitored monthly. For the 2018–2020 point-discharge nutrient monitoring period, 32 facilities monitored and submitted data to DRBC; twelve (12) Tier 1 facilities and twenty (20) Tier 2 facilities. The remaining 43 facilities are classified as Tier 3, for which the first round of monitoring data and states' electronic Discharge Monitoring Records were used for characterization. In addition to the submittal of results from an approved laboratory, facilities also submitted directly monitored effluent data, such as flow and temperature, during the intensive monitoring period. The discharge facilities are mapped by tier in Figure 2-3 and listed in Table 2-5 below.

[14] The complete Resolution 2010-5 can be found online at https://www.nj.gov/drbc/library/documents/Res2010-05EstuaryNutrientMonitoring.pdf.

[15] The complete Resolution for the Minutes can be found online at https://www.nj.gov/drbc/library/documents/ResforMinutes091317_nutrient-mon.pdf.

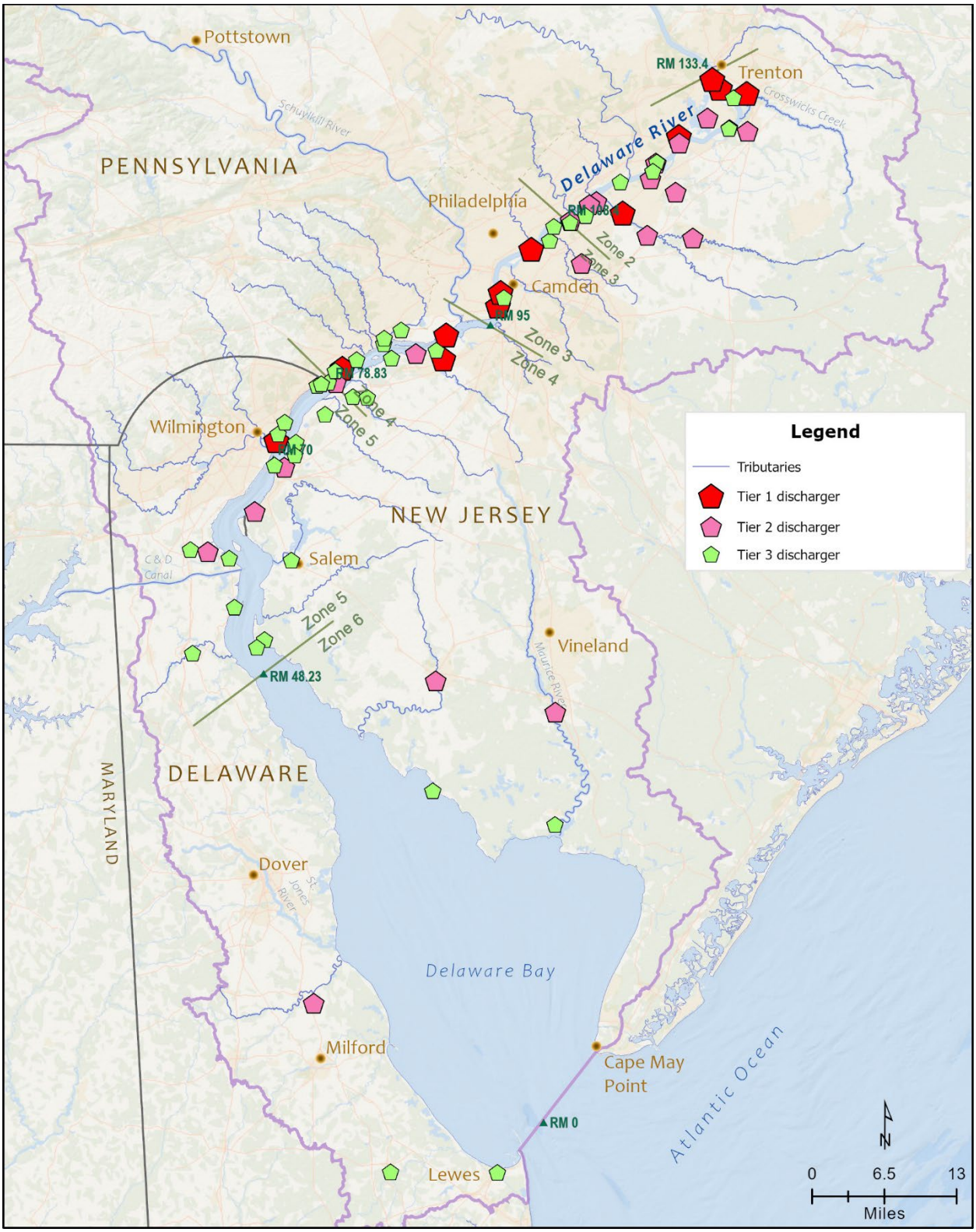

Figure 2-3: Monitored point source discharges by nutrient loading tier

Table 2-5 Monitored point source discharges

Facility Name	NPDES	Tier
Camden County Municipal Utilities Authority	NJ0026182-001A	Tier 1
City of Wilmington, Department of Public Works	DE0020320-001	Tier 1
DELCORA	PA0027103-001	Tier 1
Gloucester County Utilities Authority	NJ0024686-001A	Tier 1
Hamilton Township - Wastewater Utility	NJ0026301-001A	Tier 1
Lower Bucks County Joint Municipal Authority	PA0026468-001	Tier 1
Morrisville Borough Municipal Authority	PA0026701-201	Tier 1
Philadelphia Water Department Northeast	PA0026689-001	Tier 1
Philadelphia Water Department Southeast	PA0026662-001	Tier 1
Philadelphia Water Department Southwest	PA0026671-001	Tier 1
Trenton Sewer Utility	NJ0020923-001A	Tier 1
Willingboro Municipal Utilities Authority	NJ0023361-001A	Tier 1
Bordentown Sewerage Authority	NJ0024678-001A	Tier 2
Bristol Borough Water & Sewer Authority	PA0027294-001	Tier 2
Burlington City STP	NJ0024660-002A	Tier 2
Burlington Township Public Works	NJ0021709-002A	Tier 2
Chemours Chambers Works	NJ0005100-662A	Tier 2
Cinnaminson Sewerage Authority	NJ0024007-001A	Tier 2
City of Millville Sewage Treatment Authority	NJ0029467-001A	Tier 2
Cumberland County Utilities Authority	NJ0024651-001A	Tier 2
Delaware City Refining	DE0000256-601	Tier 2
Delran Sewerage Authority	NJ0023507-001A	Tier 2
Florence Township STP	NJ0023701-001A	Tier 2
GROWS Landfill, Waste Management	PA0043818-001	Tier 2
Kent County Department of Public Works	DE0020338-001	Tier 2
Moorestown Township WWTP	NJ0024996-001A	Tier 2
Mt. Holly Municipal Utilities Authority	NJ0024015-001A	Tier 2

Facility Name	NPDES	Tier
Mt. Laurel Municipal Utilities Authority	NJ0025178-001A	Tier 2
Paulsboro Refining Company	NJ0005029-001A	Tier 2
Pennsville Sewerage Authority	NJ0021598-001A	Tier 2
Riverside Water Reclamation Authority	NJ0022519-001A	Tier 2
Valtris Specialty Chemicals	NJ0005045-001A	Tier 2
Beverly Sewerage Authority	NJ0027481-001	Tier 3
Boeing	PA0013323-001	Tier 3
Bridgeport Disposal LLC	NJ0005240-001A	Tier 3
Calpine Mid-Atlantic Generation	DE0000558-016	Tier 3
Canton Village STP	NJ0062201-001A	Tier 3
Carneys Point STP	NJ0021601-001A	Tier 3
Chemours Company Repauno	NJ0004219-001	Tier 3
City of Lewes	DE0021512-001	Tier 3
Delaware City STP	DE0021555-001	Tier 3
DuPont Edgemoor	DE0000051-001	Tier 3
Evonik Degussa	PA0051713-001	Tier 3
Exelon Generating Company, Eddystone	PA0013714-107	Tier 3
Former BP Paulsboro Terminal No. 4555	NJ0005584-003A	Tier 3
Formosa Plastics	DE0000612-001	Tier 3
FPL Energy Marcus Hook	PA0244449-001	Tier 3
General Chemical	DE0000655-001	Tier 3
Hoeganaes Corporation	NJ0004375-001A	Tier 3
Hope Creek Generating Station	NJ0025411-461A	Tier 3
Logan Township MUA	NJ0027545-001A	Tier 3
MAFCO Worldwide Corp	NJ0004090-001A	Tier 3
Menu Food Inc	NJ0031216-001B	Tier 3
Mercer Generating Station	NJ0004995-441A	Tier 3
Mexichem Specialty Resins	NJ0004286-001	Tier 3

Facility Name	NPDES	Tier
Middletown-Odessa-Townsend	DE0050547-001	Tier 3
Milton STP	DE0021491-001	Tier 3
Monroe Energy	PA0012637-201	Tier 3
Occidental	DE0050911-001	Tier 3
Palmyra STP	NJ0024449-001A	Tier 3
Penns Grove Sewerage Authority	NJ0024023-001A	Tier 3
Port Penn STP	DE0021539-001	Tier 3
PSEG Fossil Burlington Generating Station	NJ0005002-WTPA	Tier 3
PSEG Nuclear Salem Generating Station	NJ0005622-048C	Tier 3
Riverton STP	NJ0021610-001A	Tier 3
Rohm & Haas Chemicals, Bristol	PA0012769-009	Tier 3
Salem City Wastewater Treatment Facility	NJ0024856-001A	Tier 3
Surfside Products LLC	NJ0004766-001A	Tier 3
Tinicum TWP	PA0028380-001A	Tier 3
US Steel, Fairless-103	PA0013463-103	Tier 3
US Steel, Fairless-203	PA0013463-203	Tier 3

The DRBC required facilities to monitor the analytical parameters listed in Table 2-6 below between March 2018 and February 2020. Parameters were monitored weekly at Tier 1 facilities and monthly at Tier 2 facilities. Based on the results obtained during the first round of sampling performed beginning in 2011, Tier 3 facilities were not required to monitor during the second round of sampling for this study (i.e., the 2018–2020 period).

Table 2-6 Effluent monitoring parameters

Analytical Parameter*	Units	Filtration	Sample Type
Total Phosphorus (TP)	mg/L as P	Unfiltered	24-hour composite
Total Kjeldahl Nitrogen (TKN)	mg/L as N	Unfiltered	24-hour composite
Nitrate Nitrogen (NO3-N)	mg/L as N	Unfiltered	24-hour composite
Nitrite Nitrogen (NO2-N)	mg/L as N	Unfiltered	24-hour composite
20-day Biochemical Oxygen Demand (BOD-20)	mg/L	Unfiltered	24-hour composite

Analytical Parameter*	Units	Filtration	Sample Type
5-day Carbonaceous Biochemical Oxygen Demand (CBOD-5)*	mg/L	Unfiltered	24-hour composite
Chemical Oxygen Demand (COD)	mg/L	Unfiltered	24-hour composite
Total Organic Carbon (TOC)	mg/L	Unfiltered	24-hour composite
Dissolved Organic Carbon (DOC)**	mg/L	0.45 µm filter	24-hour composite
Total Suspended Solids (TSS)	mg/L	Unfiltered	24-hour composite
Soluble Reactive Phosphorus (SRP)	mg/L as P	0.45 µm filter	24-hour composite
Ammonia Nitrogen (NH3-N)	mg/L as N	0.45 µm filter	24-hour composite
Discharge Flow	MGD	N/A	daily average
Water Temperature	°C	N/A	24-hour mean
Dissolved Oxygen	mg/L	N/A	24-hour mean
pH	1-14 S.U.	N/A	24-hour mean
Specific Conductance or TDS	µS/cm or mg/L	N/A	24-hour mean

*Note that unfiltered ammonia nitrogen, standard method 20-day Carbonaceous Biochemical Oxygen Demand (CBOD-20), and a DRBC-amended method of CBOD-20 were dropped from the parameter list in April 2019.
**Added in April 2019.

2.1.3 Tributary Nutrient Monitoring

Nutrient sampling at the head of tide of the Delaware River and its major tributaries within Zones 2 through 5 was conducted from 2018 through 2019 in order to develop tributary loading conditions. In 2018, DRBC sampled 24 tributaries and the C&D Canal once per month from April through November. In 2019, the same locations were monitored once per month from March through August, with two sampling events in September. Tributaries that are tidally influenced were monitored near low tide to minimize influence from the Delaware River Estuary. The Delaware River at Calhoun Street Bridge (Trenton, New Jersey) and the Schuylkill River at East Falls Bridge (Philadelphia, Pennsylvania) were monitored twice per month from January through December in both 2018 and 2019 as they are the largest freshwater inflows into the Delaware River Estuary. The tributary monitoring locations are shown in Figure 2-4 and listed in Table 2-7 below.

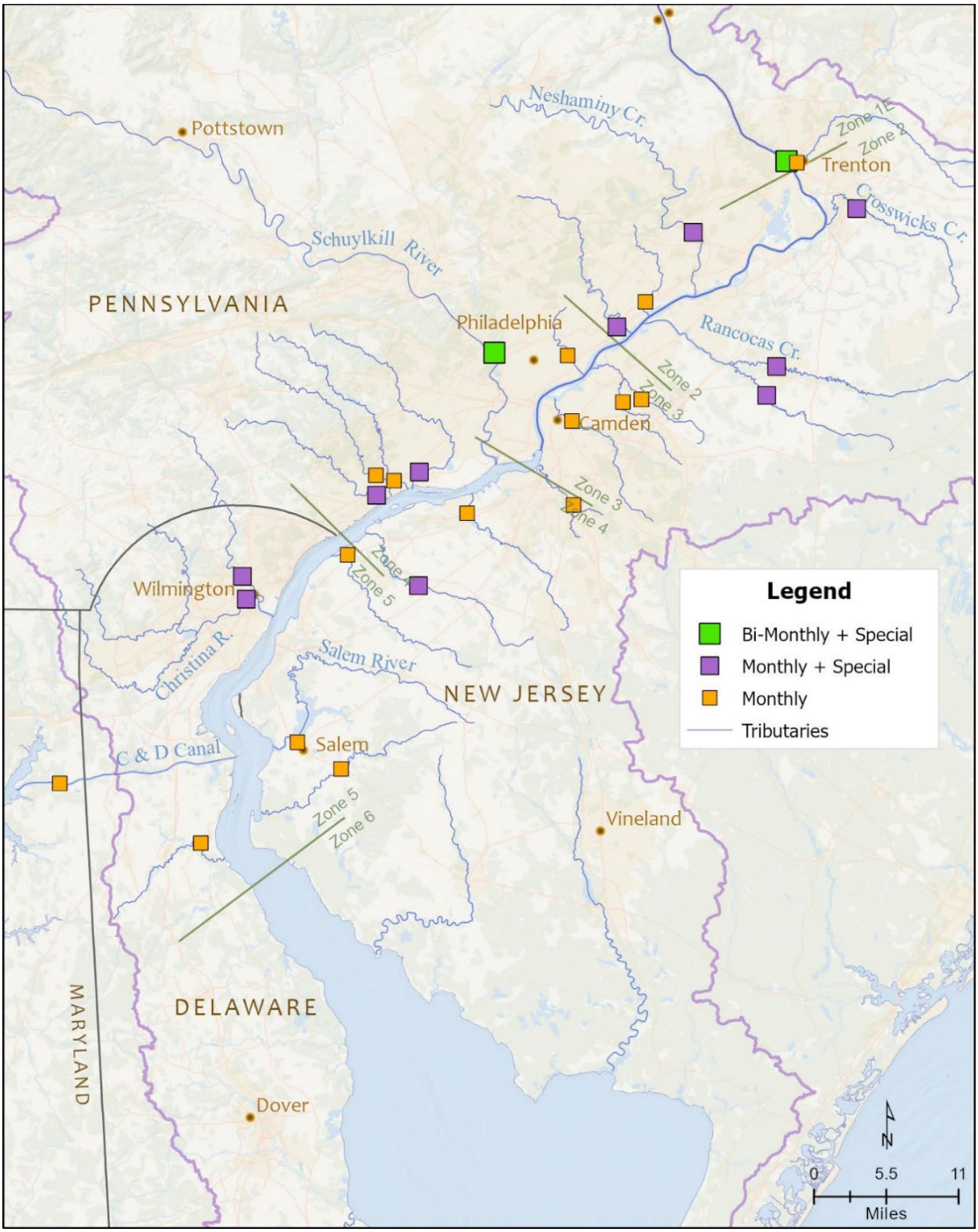

Figure 2-4: Tributary monitoring locations

Table 2-7 Tributary monitoring locations

Location	Site ID	DRBC Zone	State	Latitude	Longitude
Delaware River at Trenton	1343ICP	2	NJ	40.219819	-74.778107
Neshaminy Creek	NUTR-NESH	2	PA	40.141561	-74.912438
Rancocas South Branch	NUTR-RANS	2	NJ	39.961358	-74.807316
Rancocas North Branch	NUTR-RANN	2	NJ	39.993224	-74.792997
Crosswicks Creek	NUTR-CROS	2	NJ	40.167267	-74.677339
Pennypack Creek	NUTR-PNNY	2	PA	40.037176	-75.021786
Poquessing Creek	NUTR-POQU	2	PA	40.06486	-74.98098
Assunpink Creek	NUTR-ASSU	2	NJ	40.21826	-74.763063
Mantua Creek	NUTR-MANT	3	NJ	39.831246	-75.236045
Big Timber Creek	NUTR-BIGT	3	NJ	39.840497	-75.08392
Cooper River	NUTR-COOP	3	NJ	39.933259	-75.086351
Frankford Creek	NUTR-FRAN	3	PA	40.00545	-75.092486
Pennsauken North Branch	NUTR-PENO	3	NJ	39.957043	-74.986672
Pennsauken South Branch	NUTR-PESO	3	NJ	39.954196	-75.013308
Schuylkill River	DRBC-SCHU	4	PA	40.008405	-75.197454
Darby Creek	NUTR-DARB	4	PA	39.87655	-75.30453
Chester Creek	NUTR-CHES	4	PA	39.85073	-75.36554
Raccoon Creek	NUTR-RACC	4	NJ	39.751019	-75.3053
Ridley Creek	NUTR-RIDL	4	PA	39.87274	-75.366612
Crum Creek	NUTR-CRUM	4	PA	39.866919	-75.340823
Brandywine River	NUTR-BRAN	5	DE	39.76035	-75.556779
Christina River	NUTR-CHRI	5	DE	39.735236	-75.551033
Salem River	NUTR-SALE	5	NJ	39.57768	-75.47687
Oldmans Creek	NUTR-OLDS	5	NJ	39.784815	-75.406687
Alloway Creek	NUTR-ALLO	5	NJ	39.548457	-75.414473
C&D Canal	NUTR-CDCA	5	MD	39.530372	-75.815058
Appoquinimink River	NUTR-APPO	5	DE	39.465765	-75.613544

Parameters analyzed, shown in Table 2-8 below, include nutrients, solids, conventional parameters, and other parameters relevant to eutrophication processes and model development needs. Samples were collected by DRBC staff and analyzed by New Jersey Department of Health Environmental Chemical Laboratory Services. In addition to laboratory analyzed samples, dissolved oxygen, water temperature, specific conductance, and pH readings were collected by DRBC personnel at each location with a Eureka Manta multiprobe water quality meter, and turbidity was measured with a Hach Turbidimeter 2100Q.

Table 2-8 Tributary monitoring parameters

Analytical Parameter	Units	Filtration	Sample Type
Specific Conductance	µS/cm	Unfiltered	in-situ surface water grab
Dissolved Oxygen - Optical Electrode	mg/L	Unfiltered	in-situ surface water grab
Dissolved Oxygen	% Saturation	Unfiltered	in-situ surface water grab
pH, Field	1-14 S.U.	N/A	in-situ surface water grab
Turbidity (Nephelometric)	NTU	Unfiltered	near-surface water grab
Temperature, Water	ºC	N/A	in-situ surface water grab
Suspended Chlorophyll-a	µg/L	0.70 µm filter	near-surface water grab
Chemical Oxygen Demand	mg/L	Unfiltered	near-surface water grab
Chloride, Total	mg/L	Unfiltered	near-surface water grab
Ammonia as N, Dissolved	mg/L	0.45 µm filter	near-surface water grab
Nitrate + Nitrite as N, Dissolved	mg/L	0.45 µm filter	near-surface water grab
Total Kjeldahl Nitrogen (TKN)	mg/L	Unfiltered	near-surface water grab
Alkalinity (titrimetric, pH 4.5)	mg/L	Unfiltered	near-surface water grab
Total Suspended Solids (TSS)	mg/L	Unfiltered	near-surface water grab
Total Solids (TS)	mg/L	Unfiltered	near-surface water grab
Fixed Suspended Solids (FSS)	mg/L	Unfiltered	near-surface water grab
Total Volatile Solids (TVS)	mg/L	Unfiltered	near-surface water grab
Organic Carbon, Total	mg/L	Unfiltered	near-surface water grab
Organic Carbon, Dissolved	mg/L	0.45 µm filter	near-surface water grab
Organic Carbon, Particulate	mg/L	0.45 µm filter	near-surface water grab
Orthophosphate, Dissolved	mg/L	0.45 µm filter	near-surface water grab
Total Phosphorus as P, Total	mg/L	Unfiltered	near-surface water grab

Analytical Parameter	Units	Filtration	Sample Type
Total Phosphorus as P, Dissolved	mg/L	0.45 µm filter	near-surface water grab
Silica, Total	mg/L	Unfiltered	near-surface water grab
Silica, Dissolved	mg/L	0.45 µm filter	near-surface water grab
CBOD20, standard method	mg/L	Unfiltered	near-surface water grab
Acid-Hydrolyzable Phosphorus, Dissolved	mg/L	0.45 µm filter	near-surface water grab
Acid-Hydrolyzable Phosphorus, Total	mg/L	Unfiltered	near-surface water grab
Particulate Inorganic Phosphorus	mg/L	0.45 µm filter	near-surface water grab
Sulfate	mg/L	Unfiltered	near-surface water grab

2.2 Sampling Results

2.2.1 Long-Term Water Quality Monitoring Results

Two long-term water quality datasets were used for setting initial conditions in the model and for model calibration and corroboration. Data from DRBC's Boat Run Monitoring Program were accessed via the National Water Quality Portal (NWQP). Data from USGS continuous monitors in the Delaware River Estuary were accessed via the USGS National Water Information System (NWIS). Data from both datasets were downloaded using the Data Retrieval package in R. Figure 2-5 below shows box and whisker plots for the period 2010–2021 by river mile for a) ammonia nitrogen from the Boat Run and b) dissolved oxygen from USGS monitors. The box and whisker plot is a graphical illustration of numerical data to show the distribution of data through their quartiles (box) and data ranges (whiskers and circles). This report employed the standard box and whisker plot definition to summarize the data spread. The structure of each box indicates the following: bottom portion of the box = the first quartile (Q1 = 25th percentile); mid-point line on box = median (or 50th percentile); uppermost portion of the box = the third quartile (Q3 = 75th percentile); entirety of the box = interquartile range (IQR = the distance between the upper (Q3) and the lower quartiles (Q1); and the whiskers are based on the 1.5 IQR value. From above the upper quartile (Q3), a distance of 1.5 times the IQR is measured out and a whisker is drawn up to the largest observed data point from the dataset if that largest point falls within this distance. Similarly, a distance of 1.5 times the IQR is measured out below the lower quartile (Q1) and a whisker is drawn down to the lowest observed data point from the dataset if that lowest point falls within this distance. All other observed data points outside the boundary of the whiskers, if any, are plotted as symbols such as circles.

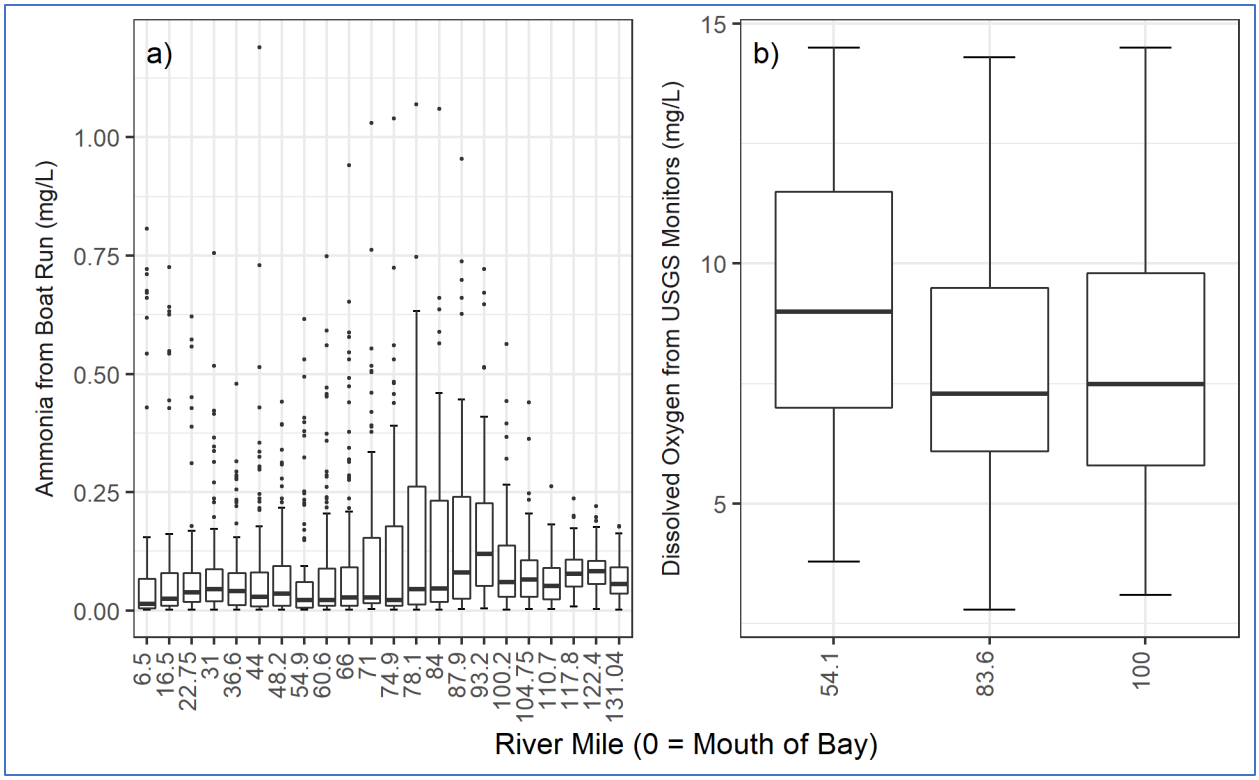

Figure 2-5 Long-term monitoring within the Estuary (example results)

2.2.2 Point-Discharge Monitoring Results

Point-discharge nutrient monitoring occurred over a two-year period from March 2018 through February 2020 (for Tier 1 facilities) and from April 2018 through March 2020 (for Tier 2 facilities). In order to properly represent point-discharge loadings in the model, substantial data are required for the calibration period (2018–2019). Tier 1 facilities monitored weekly, while Tier 2 facilities monitored once per month, with all facilities monitoring for the same suite of parameters (see Table 2-8). While time-variable discrete data were used in the model, mean concentrations of total phosphorus, total organic carbon, ammonia nitrogen, and total nitrogen (Total Kjeldahl Nitrogen as N [TKN] + Nitrate [NO3-N] + Nitrite [NO2-N]) are provided in Table 2-9 below, along with mean daily flows on the days sampled to show the magnitudes of key parameters.

Table 2-9 Mean point discharge concentrations of key nutrients

Facility	NPDES-Outfall	Total Phosphorus mg/L	Total Organic Carbon mg/L	Ammonia Nitrogen mg/L	Total Nitrogen mg/L	Effluent MGD
Philadelphia Water Dept NE	PA0026689-001	0.37	7.95	5.26	9.43	179.8

Facility	NPDES-Outfall	Total Phosphorus mg/L	Total Organic Carbon mg/L	Ammonia Nitrogen mg/L	Total Nitrogen mg/L	Effluent MGD
Philadelphia Water Dept SW	PA0026671-001	0.27	8.67	18.61	21.56	178.0
Philadelphia Water Dept SE	PA0026662-001	0.21	7.71	8.47	10.29	78.91
City of Wilmington DPW	DE0020320-001	0.87	12.97	11.54	18.39	71.03
Camden County MUA	NJ0026182-001A	1.79	11.97	16.85	21.99	53.03
DELCORA	PA0027103-001	1.51	14.26	7.83	15.76	34.80
Gloucester County UA	NJ0024686-001A	2.28	15.23	22.35	28.67	18.92
Kent County DPW	DE0020338-001	0.22	5.33	0.44	4.38	13.08
Trenton DWS	NJ0020923-001A	2.48	14.83	4.71	19.48	11.69
Delaware City Refining	DE0000256-601	0.97	11.64	0.33	33.54	10.15
Paulsboro Refining Company	NJ0005029-001	1.82	11.02	0.18	5.82	8.98
Hamilton Township Dept WPC	NJ0026301-001A	3.47	15.72	26.70	29.85	8.28
Lower Bucks County JMA	PA0026468-001	2.13	11.18	20.19	24.59	7.23
Chemours Chambers Works	NJ0005100-662A	0.51	6.74	0.16	6.79	5.79
Morrisville Borough MA	PA0026701-201	2.21	14.43	11.27	25.79	5.08
Mt. Laurel MUA	NJ0025178-001A	0.62	5.34	1.43	12.35	4.12
Willingboro MUA	NJ0023361-001A	1.50	13.66	3.39	21.00	3.77
Mt. Holly MUA	NJ0024015-001A	2.62	10.13	0.97	20.23	3.31
Cumberland County UA	NJ0024651-001A	1.41	11.03	6.90	14.35	3.26

Facility	NPDES-Outfall	Total Phosphorus mg/L	Total Organic Carbon mg/L	Ammonia Nitrogen mg/L	Total Nitrogen mg/L	Effluent MGD
Moorestown Township WWTP	NJ0024996-001	1.41	5.76	1.07	18.44	2.33
City of Millville DPW	NJ0029467-001A	2.94	12.35	26.76	26.67	2.28
Delran SA	NJ0023507-001A	2.44	5.08	0.15	15.88	2.07
Burlington City STP	NJ0024660-002A	2.37	11.60	0.99	17.97	2.02
Bordentown SA	NJ0024678-001A	4.31	5.15	0.21	29.37	1.67
Burlington Township DPW	NJ0021709-002A	1.59	5.54	0.38	2.96	1.52
Florence Township STP	NJ0023701-001A	0.99	14.15	3.25	15.25	1.48
Cinnaminson SA	NJ0024007-001A	2.81	11.81	17.87	22.75	1.45
Bristol Borough WSA	PA0027294-001	2.22	10.03	1.00	15.30	1.44
Pennsville SA	NJ0021598-001A	1.50	11.53	0.61	14.56	1.41
Valtris Specialty Chemicals	NJ0005045-001A	17.94	12.21	1.33	9.16	0.93
Riverside WRA	NJ0022519-001A	4.18	11.58	0.54	24.04	0.68
Waste Management - GROWS	PA0043818-001	0.31	61.83	0.25	231.39	0.15

The range of Total Phosphorus (TP) concentration data is non-detect to 64.0 mg/L (Method Detection Limits [MDLs] of non-detect results range from 0.007-0.1 mg/L); the mean TP concentration overall is 1.92 mg/L; and the median is 1.48 mg/L. The range of Total Nitrogen (TN) concentration data is 1.11-566.0 mg/L; the mean TN concentration overall is 22.6 mg/L; and the median is 19.7 mg/L. The range of Total Organic Carbon (TOC) concentration data is non-detect to 155.0 mg/L (MDLs of non-detect results range from 0.5-2.5 mg/L); the mean TOC concentration overall is 12.34 mg/L; and the median is 11.50 mg/L.

Point discharge ammonia concentrations range from non-detect to 37.8 mg/L (MDLs for non-detects range from 0.008-0.5 mg/L). The mean ammonia concentration overall is 10.7 mg/L, and the median is

8.47 mg/L. Ranked boxplots of point discharge ammonia nitrogen concentrations are provided in Figure 2-6. Detailed information on average flow rates and nutrient concentrations from point discharges for the period of 2018 – 2019 is summarized in Appendix A.

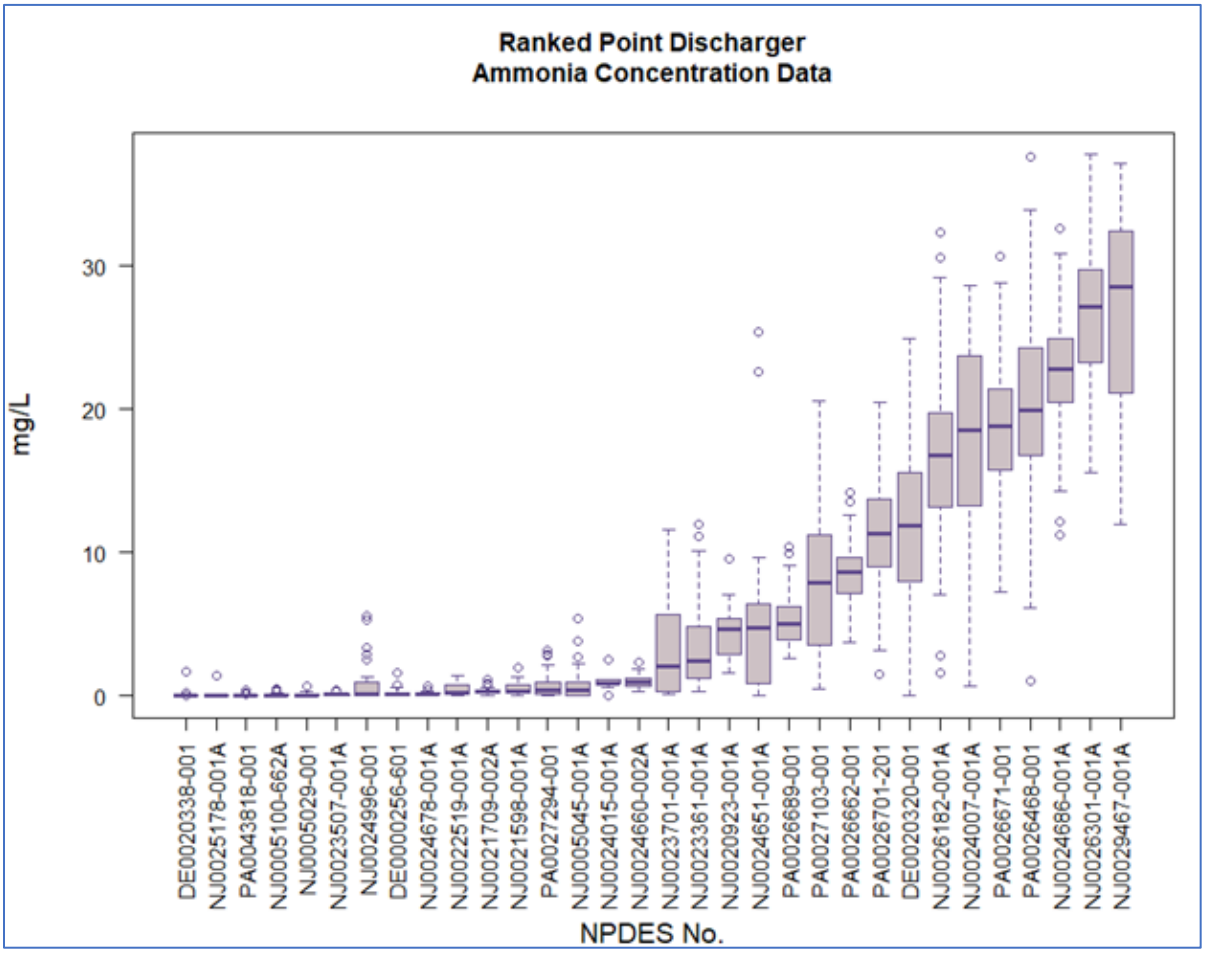

Figure 2-6 Point discharge ammonia concentrations – ranked boxplots

2.2.3 Tributary Nutrient Monitoring Results

Tributary nutrient monitoring occurred twice monthly for nearly a three-year period from January 2018 through December 2020 at the Delaware River at Trenton and Schuylkill River monitoring locations. For the 25 other tributary locations, including the C&D Canal that was monitored as a boundary condition for the model, monitoring occurred monthly for eight months in each of 2018 and 2019, and extra samples were collected August through October 2020. The same suite of parameters was collected from all sites (see the list in Section 2.1.3). For this section of the report, total phosphorus, total organic carbon, ammonia nitrogen, and total nitrogen (Total Kjeldahl Nitrogen as N + Nitrate (NO3-N) + Nitrite (NO2-N)) are examined. While time variable discrete data were used in the model, mean concentrations of these parameters are shown in Table 2-10 below.

Table 2-10 Mean concentrations of key nutrients at monitored tributaries

Tributary Monitoring Location	Total Phosphorus mg/L	Total Nitrogen mg/L	Ammonia Nitrogen mg/L	Total Organic Carbon mg/L	Discharge cfs
Alloway Creek	0.13	1.18	0.04	7.25	53.7
Appoquinimink River	0.16	1.44	0.06	4.14	58.2
Assunpink Creek	0.37	3.81	0.09	5.17	220
Big Timber Creek	0.15	0.94	0.09	4.42	52.6
Brandywine River*	0.05	3.07	0.02	2.48	756.6
Chester Creek*	0.15	4.06	0.03	2.73	150
Christina River*	0.07	1.93	0.04	4.73	569.8
Cooper River*	0.1	0.98	0.07	5.1	76.7
Crosswicks Creek	0.16	1.14	0.05	6.54	216.5
Crum Creek	0.03	1.72	0.04	2.99	72.9
Darby Creek*	0.09	2.01	0.14	3.63	163.7
Delaware River at Trenton	0.06	1.88	0.03	2.85	17,870
Frankford Creek*	0.09	2.31	0.13	3.2	54.7
Mantua Creek	0.13	1.55	0.09	4.09	85.8
Neshaminy Creek	0.13	2.12	0.05	3.89	525.9
Oldmans Creek	0.15	1.73	0.04	4.47	68.6
Pennsauken Creek, North Branch	0.08	1.04	0.16	5.11	37.5
Pennsauken Creek, South Branch	0.15	2.72	0.11	4.46	34.0
Pennypack Creek*	0.17	3.49	0.03	2.83	137.0
Poquessing Creek*	0.05	1.84	0.03	2.87	43.6
Raccoon Creek	0.17	1.99	0.08	4.57	65.8
Rancocas Creek, North Branch	0.14	1.09	0.16	11.05	259.5
Rancocas Creek, South Branch	0.19	1.35	0.09	12.8	294.2
Ridley Creek*	0.15	3.19	0.02	2.56	78.1
Salem River	0.15	1.49	0.07	4.24	144.8
Schuylkill River*	0.16	2.7	0.07	2.77	5,173

*Upstream combined sewer overflows (CSOs) may have influenced water quality under some conditions.

The range of TP concentration data is 0.014-0.96 mg/L; the mean TP concentration overall is 0.13 mg/L; and the median is 0.11 mg/L. The range of TN concentration data is 0.47-12.39 mg/L; the mean TN concentration overall is 2.08 mg/L; and the median is 1.74 mg/L. The range of TOC concentration data is 1.58-20.1 mg/L; the mean TOC concentration overall is 4.30 mg/L; and the median is 3.54 mg/L.

Tributary ammonia nitrogen concentrations range from non-detect to 0.76 mg/L (MDLs for non-detects range from 0.004-0.023 mg/L). The mean ammonia nitrogen concentration overall is 0.071 mg/L, and the median is 0.05 mg/L. Ranked boxplots of ammonia nitrogen concentrations at monitored tributaries are shown in Figure 2-7 below. Detailed information on average flow rates and nutrient concentrations from tributaries for the period of 2018 – 2020 is summarized in Appendix A.

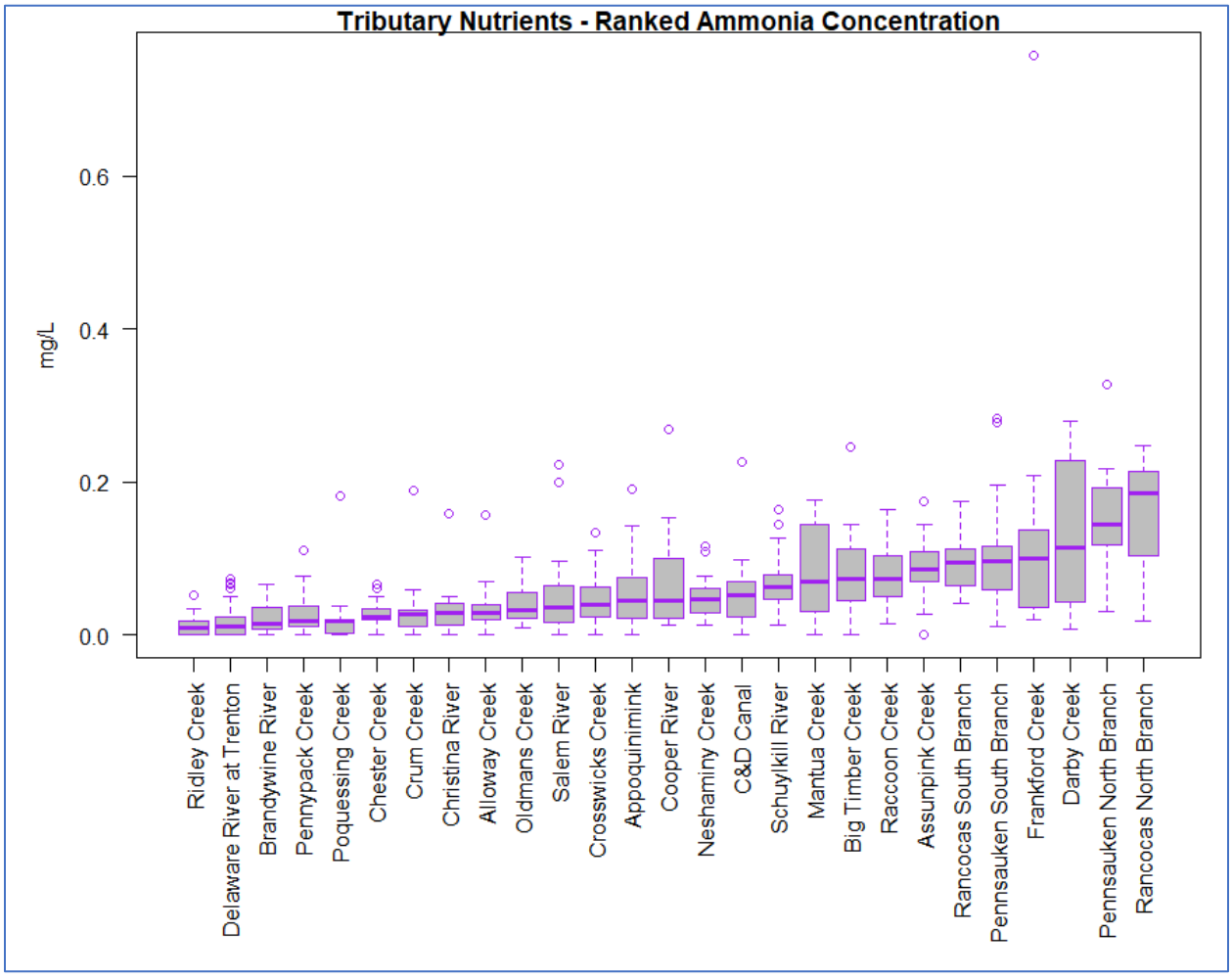

Figure 2-7 Tributary ammonia nitrogen concentrations - ranked boxplots

2.3 CHARACTERIZATION OF LOADS

In addition to water quality constituent concentration data, nutrient loadings were also assessed to evaluate relative loading contributions from point source discharges and monitored tributaries. To compute nutrient loadings from the Point-Discharge Nutrient Monitoring data, concentration data were multiplied by the effluent flow rate for each given sampling day for each facility and converted to kg/day. Similarly, to compute nutrient loading estimates from the Tributary Nutrient Monitoring dataset, concentration data were multiplied by the daily discharge flow rate for each given sampling day for each tributary site and converted to kg/day. Tributary discharge flows were taken from the hydrodynamic model (Chen et al., 2024) on which this study is based. The average of the estimated loads (kg/day) were calculated and multiplied by 365 (average days in a year) to obtain annual average loading estimates (kg/year).

Figure 2-8 shows the relative average daily ammonia nitrogen loads from monitored point discharges, the upstream Delaware River (at Trenton), the Schuylkill River, and all other monitored tributaries. Point discharges clearly comprise the largest category of ammonia nitrogen loads into the Delaware River Estuary. Note that this loading assessment reflects only the point sources and tributaries that were intensively monitored for this effort from 2018–2020.

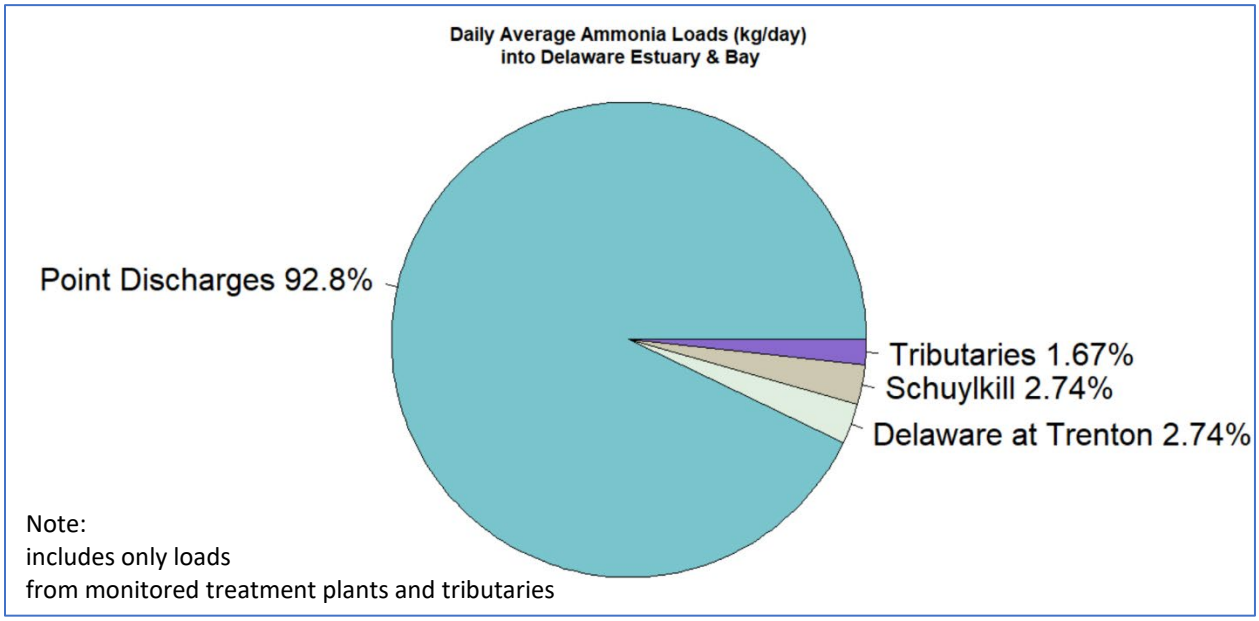

Figure 2-8: Ammonia nitrogen loads from monitored discharges and tributaries

Ranked ammonia nitrogen loading boxplots for monitored point source discharges and monitored tributaries, respectively, are shown in Figure 2-9 and Figure 2-10.

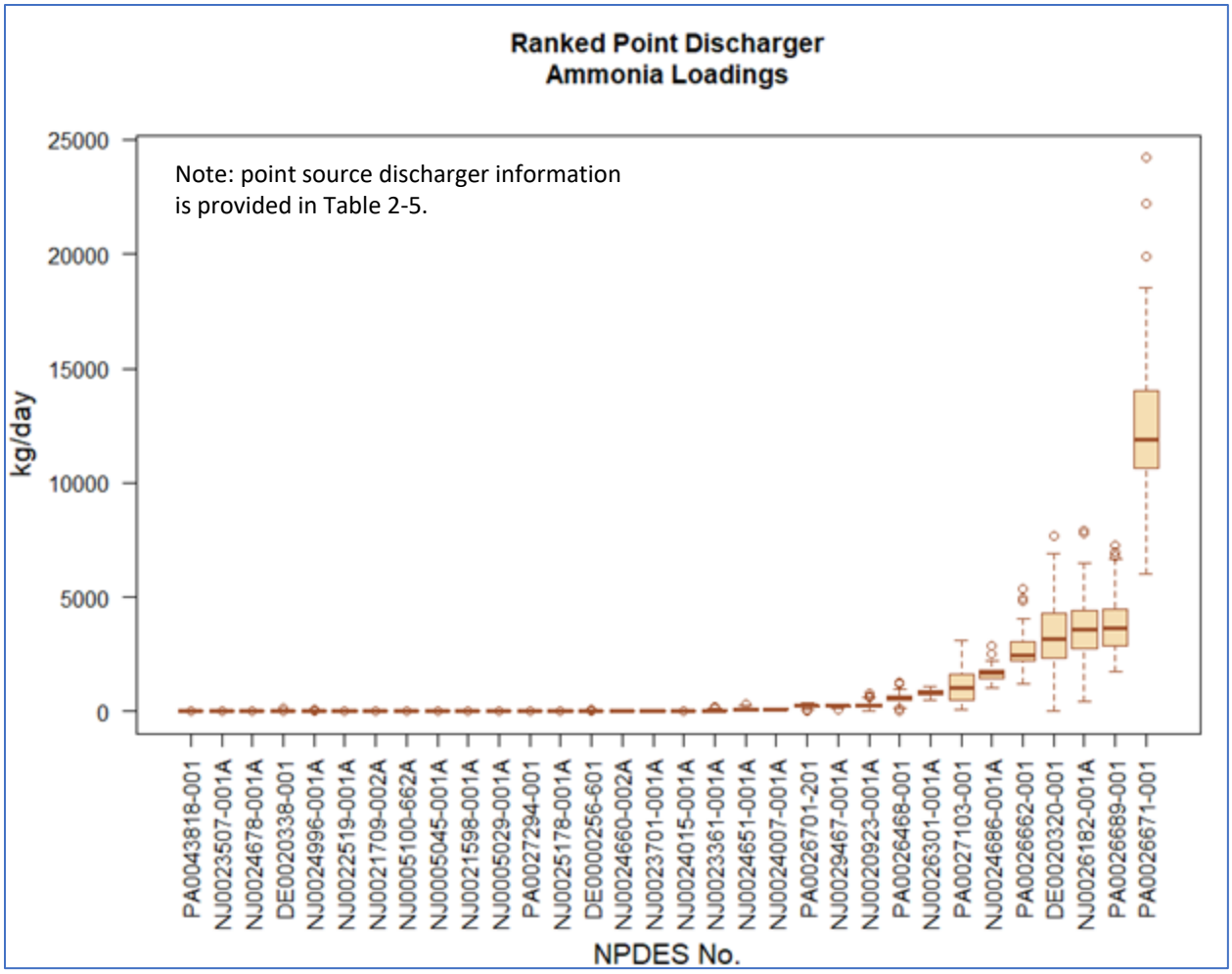

Figure 2-9: Point discharge ammonia nitrogen loads – ranked boxplots

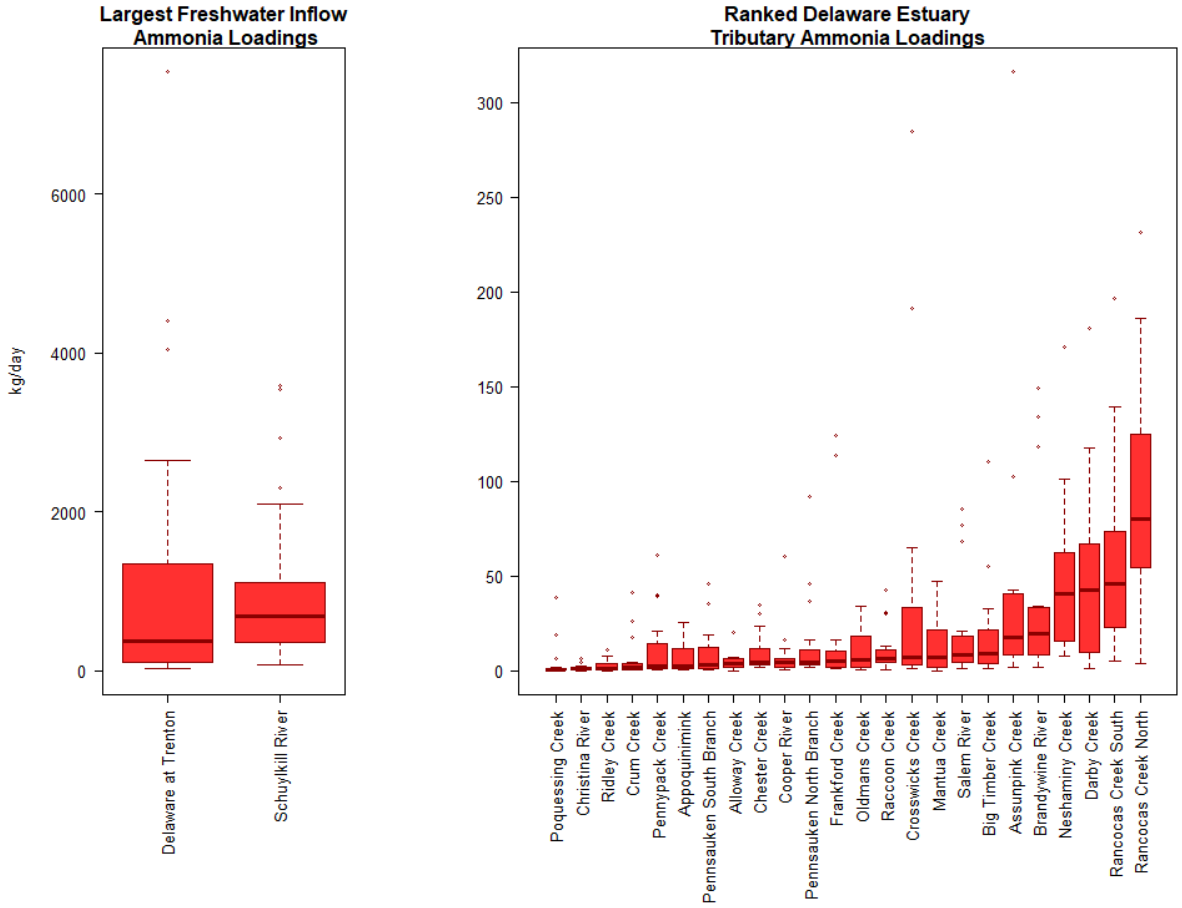

Figure 2-10: Tributary ammonia nitrogen loads – ranked boxplots

Average daily TP and TN estimated loadings (Figure 2-11 and Figure 2-12, respectively) indicate that the relative impacts are comparable among point sources, the Delaware River at Trenton, the Schuylkill River, and other tributaries. Note that the pie charts separate the tributary contributions into "Delaware at Trenton," "Schuylkill," and "Other Tributaries." By contrast, the Delaware River at Trenton contributes about 50% of TOC loads relative to the other sources assessed (Figure 2-13), while the point sources are estimated to contribute only 11% of the total assessed TOC load.

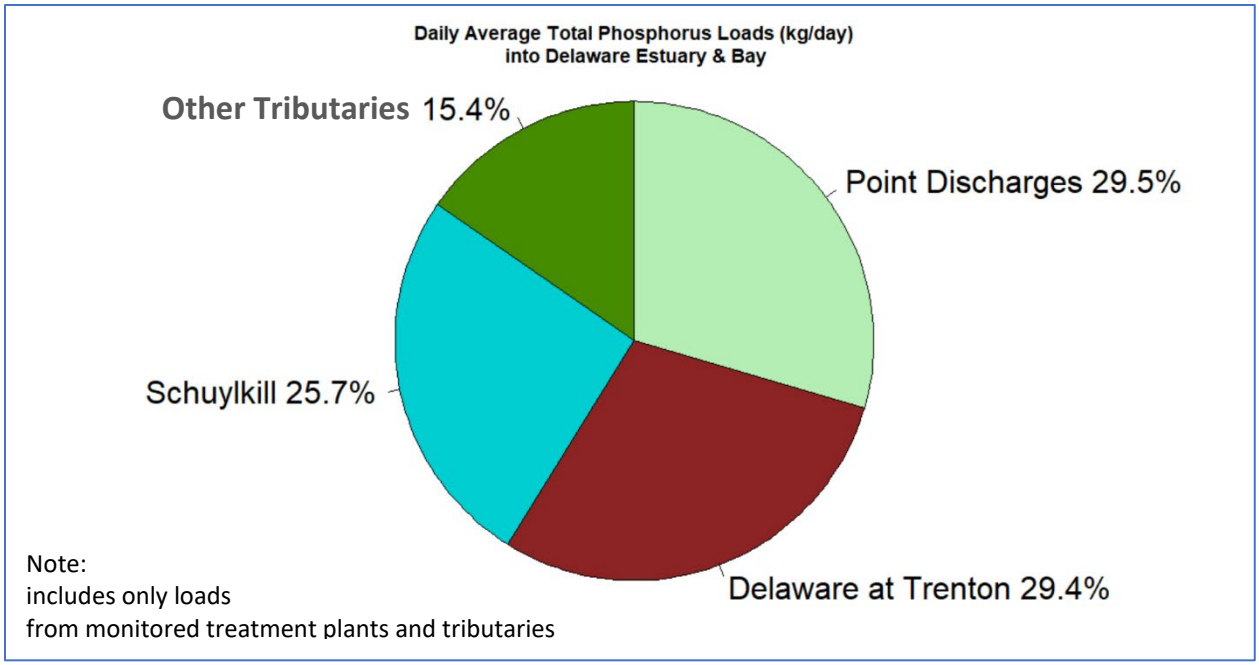

Figure 2-11: Total phosphorus from monitored point discharges and tributaries

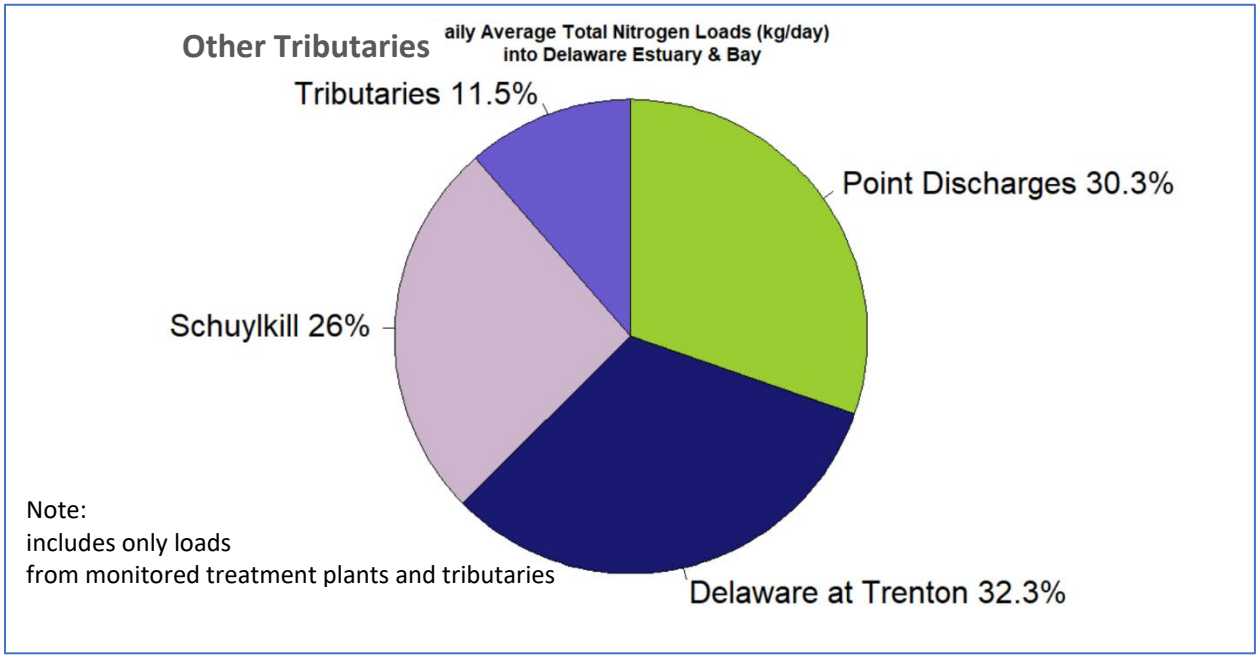

Figure 2-12: Total nitrogen from monitored point discharges and tributaries

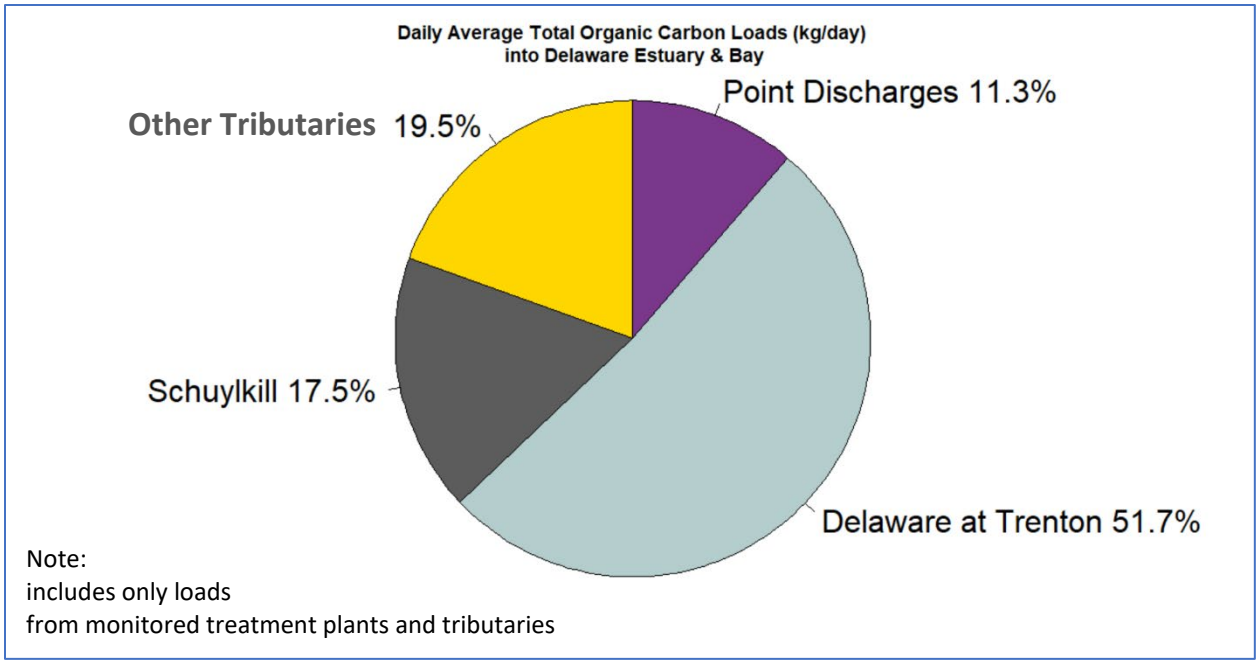

Figure 2-13: Total organic carbon from monitored point discharges and tributaries

Ranked boxplots of TP, TN, and TOC loads from monitored tributaries are shown in Figure 2-14, Figure 2-15, and Figure 2-16, respectively. Detailed information on loads from tributaries and point discharges for the period of 2018 – 2020 is summarized in Appendix A.

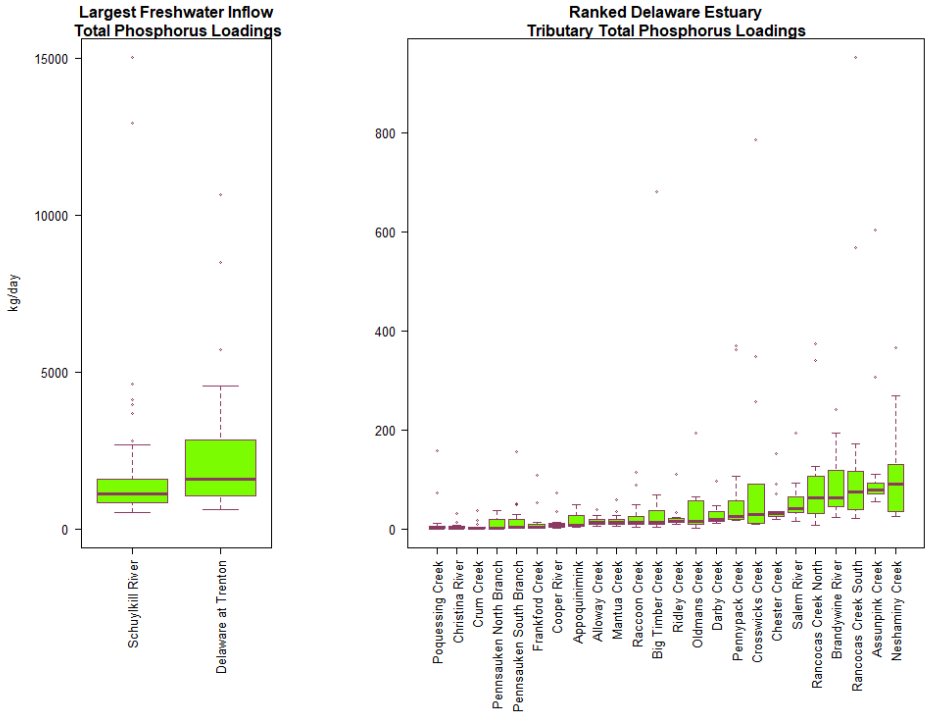

Figure 2-14: Tributary total phosphorus loads – ranked boxplots

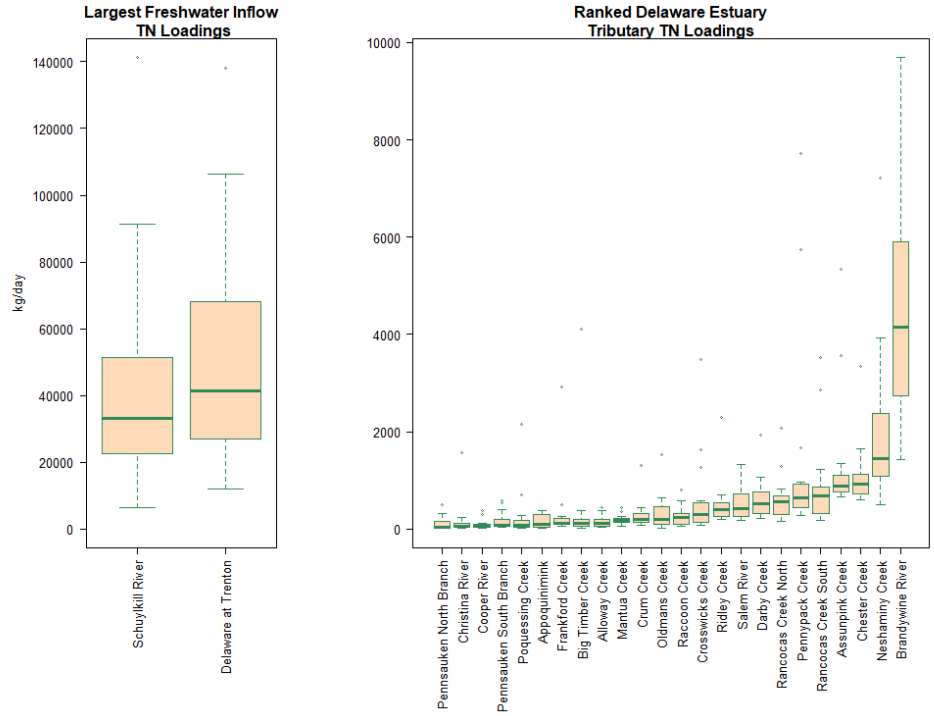

Figure 2-15: Tributary total nitrogen loads - ranked boxplots

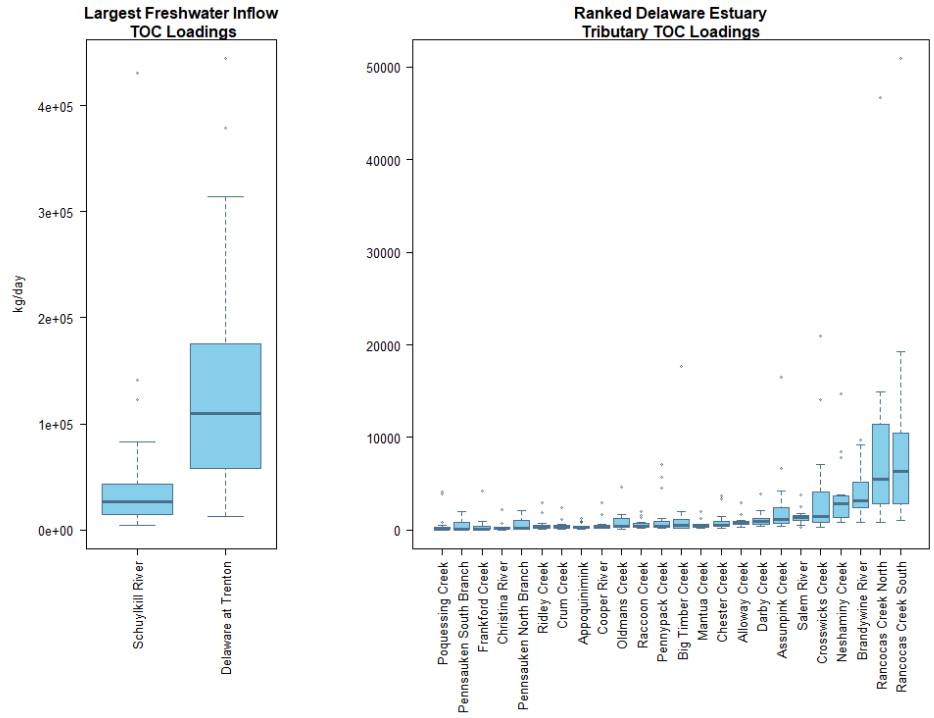

Figure 2-16: Tributary total organic carbon loads - ranked boxplots

2.4 Additional Field Data

Additional water quality data were compiled and used for the model input conditions. See Section 3.5 for characterization of nonpoint sources, atmospheric deposition, and Combined Sewer Overflows (CSOs).

2.4.1 Vertical Dissolved Oxygen Profiles

To assess the degree of dissolved oxygen stratification (vertical concentration gradients) in the Delaware River Estuary, vertical dissolved oxygen profiles were collected via boat on three occasions in Summer 2021 across two transects at Ben Franklin and Chester. The Ben Franklin transects were conducted just downstream of the Ben Franklin Bridge in Philadelphia, Pennsylvania; the Chester transects were conducted just downstream of Chester Island in Chester, Pennsylvania. At each location a series of five profiles was collected along a transect spanning the width of the river. At each profile collection point, a dissolved oxygen reading was taken at the surface and the bottom. If a difference of greater than 5% was seen between the two readings, additional readings were taken throughout the water column. At both transect locations, the navigational channel runs along the Pennsylvania side of the river. Additionally, at both transect locations, the easternmost point (i.e., the point closest to the New Jersey bank) occurred on a shallow shoal with depths less than 2 m. At these locations, only a surface reading was taken. In addition to dissolved oxygen, water temperature, specific conductance, and pH readings were collected at each location. All readings were taken with a Eureka Manta water quality meter.

Dissolved oxygen transect profiles were conducted at the Ben Franklin and Chester monitoring locations in May, July, and September 2021, spanning a range of conditions. May dissolved oxygen concentrations were high and ranged from 8.91–9.41 mg/L at Ben Franklin and 10.06–11.27 mg/L at Chester. July dissolved oxygen readings were lower and ranged from 5.92–6.27 mg/L at Ben Franklin and 4.50–6.09 mg/L at Chester. September dissolved oxygen readings ranged from 7.09–7.68 mg/L at Ben Franklin and 6.15–6.60 mg/L at Chester.

Dissolved oxygen stratification was not observed between bottom and surface readings collected in the Delaware River Estuary in Summer 2021 (Figure 2-17). The difference between top and bottom readings was always within 5% and almost always within the level of accuracy of the water

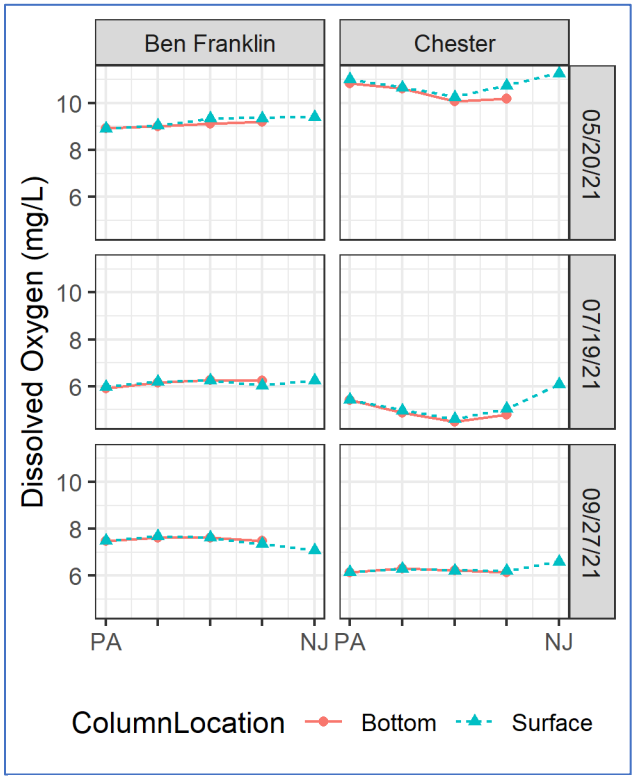

Figure 2-17: Dissolved oxygen profiles

quality meter (± 0.2 mg/L). On two instances the differences between top and bottom dissolved oxygen readings were greater than 0.2 mg/L. Both instances occurred at the Chester transect at the second station from the New Jersey bank where a large shallow shoal mixes with the main river channel. In both instances, dissolved oxygen concentrations at this shallow shoal were higher than those in the main channel and likely influenced the surface reading at this station. Both instances represented minor differences of approximately 5% from top to bottom.

USGS has conducted transect profile surveys at selected locations adjacent to USGS stations at Ben Franklin Bridge, Chester, and Reedy Island, where dissolved oxygen concentration, percent oxygen saturation, pH, conductivity, and water temperature were measured along the transects and at different depths. Profile data collected during the periods of model calibration and corroboration (Table 4-1) were used to evaluate model performance. Profile data collected in other years are presented in Appendix B. These profile data indicate that the Delaware River Estuary is weakly stratified, especially in the urban area.

2.4.2 Primary Productivity Estimates in the Delaware River Estuary

Field sampling studies to estimate primary productivity in the Delaware River Estuary were conducted in 2014, 2018, and 2019 (Fisher and Gustafson, 2015, 2019, and 2020). Sampling was conducted by boat on two dates each year, once in May and once in July. Sampling in 2014 focused on the Delaware Bay while sampling in 2018 and 2019 focused on the upper estuary. DRBC staff collected surface and bottom water samples along lateral transects at river miles 10, 25, and 40 in 2014 and at river miles 71, 86, 101, 116, and 131 in 2018 and 2019. In 2014, samples were collected at five sites on each lateral transect. In 2018 and 2019, samples were collected at three sites on each lateral transect.

More information on primary production including site mapping is available on the DRBC website at:

- https://www.nj.gov/drbc/library/documents/nutrients/nutrients-chlor-a_DelawareBay_UMd2015_rev012519.pdf
- https://www.nj.gov/drbc/library/documents/nutrients/nutrients-chlor-a_DelawareEstuary_UMd_feb2019.pdf
- https://www.nj.gov/drbc/library/documents/nutrients/nutrients-chlor-a_DelawareEstuary_UMd_sept2020.pdf

Field data were collected by DRBC personnel. Salinity, temperature, and dissolved oxygen data at the surface and bottom were obtained using a Eureka Manta water quality meter. Light extinction measurements were made using a LiCor LI-1400 data logger connected to a LI-190 surface PAR sensor and a LI-192 underwater sensor. These measurements were made *in situ* on the vessel when the water samples were taken for subsequent analysis of nutrients, respiration, and primary production in our

laboratory. Collected water samples were maintained at ambient bay or estuary water temperature at 60% light (surface samples) or in darkness (bottom water samples) while on the ship. At the dock the samples were transferred to staff from University of Maryland Center for Environmental Science (UMCES) for analysis.

Within 1.5 h of the ship's arrival at the dock, the samples were transferred to a BOD box at the Horn Point Laboratory maintained at 16.3°C in May and 25.7°C in July to approximate the median bay temperatures observed (range = 16.1-18.0°C in May, 25.5-27.0°C in July). Lights within the box simulated the appropriate day/night cycle for the month. Bottom samples were wrapped in black bags within the BOD box to maintain darkness and ambient temperature. On the morning following sample collection, aliquots of the samples were placed in incubation bottles for measurements of respiration (all samples) and 14°C-based primary production (surface samples only).

For this report, primary productivity is represented as an integrated rate of carbon fixation in the water column. Rates of primary production were averaged by river mile with sites in the bay collected in 2014 consisting of N=5 data points and sites in the upper estuary collected in 2018 and 2019 consisting of N=6 data points.

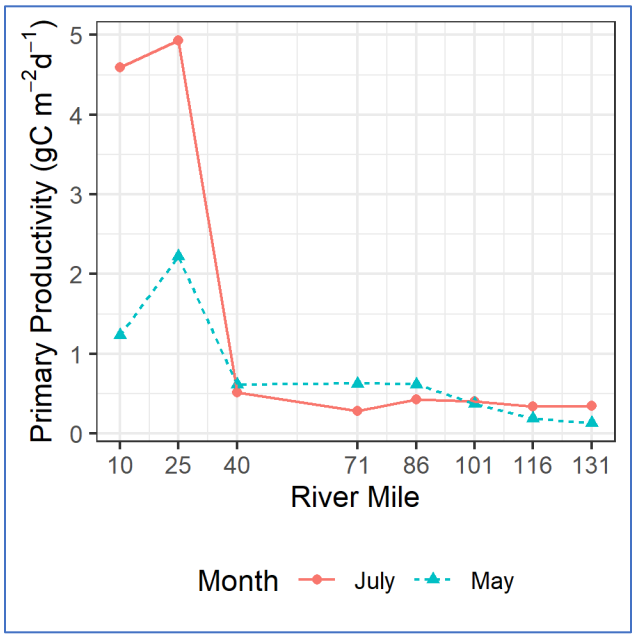

Figure 2-18: Primary production estimates

River mile-averaged primary productivity ranged from 0.13 – 4.93 gC/m²/d throughout the estuary (Figure 2-18). Samples downstream of river mile 40 were collected in 2014, and samples upstream of river mile 71 were collected in 2018 and 2019. Generally, rates of primary production were considerably higher downstream of river mile 25 than at upstream sites. Mean productivity was as high as 4.93 gC/m²/d at river mile 25 while mean productivity never exceeded 0.63 gC/m²/d at any site upstream of river mile 40. Mean primary productivity was variable between May and July samples. At sites in the bay collected in 2014, primary production was higher in July than May. At upstream sites collected in 2018 and 2019, primary production was similar in May and July.

For a more detailed analysis of primary productivity in the estuary along with estimates of nutrients, chlorophyl a, dissolved oxygen, and respiration rates from this sampling see reports from UMCES (Fisher and Gustafson 2015, 2019, and 2020).

3. WATER QUALITY MODEL DEVELOPMENT

The goal of this modeling project is to develop a technically sound eutrophication model for the Delaware River Estuary, from the head of the tide at Trenton, New Jersey, to the ocean, utilizing an appropriate level of complexity within the current state of the science and within the timeframe established by the Commission. This model will be used to address the impacts on dissolved oxygen from nutrients loads and carbonaceous oxygen demanding organic inputs.

DRBC is led and executed this effort through a collaborative process informed by a Model Expert Panel comprised of nationally recognized water resource scientists and engineers: Dr. Steve Chapra, Dr. Carl Cerco, Dr. Bob Chant, and Tim Wool. In addition to the Model Expert Panel, DRBC benefits from day-to-day interaction with modeling consultants, Dr. Victor Bierman and Scott Hinz.

3.1 MODEL DESCRIPTION

The water quality model used in this study is the Water Quality Analysis Simulation Program (WASP) with the Advanced Eutrophication sub-model. The WASP model was originally developed by HydroScience (Di Toro et al. 1983; Connolly and Winfield 1984) and has remained under continuous development and support by the U.S. Environmental Protection Agency (EPA). This model has been widely applied throughout the United States and worldwide to investigate water quality issues (Wool et al., 2003 and 2020; Ambrose et al., 2009; Petrus, 2015; Tetra Tech, 2015 and 2016; Defne et al., 2017; and Camacho et al., 2019). It has a user database with over 15,000 users. The specific version of the model used in this study, WASP8.32 (released April 2, 2019) is a recent version that has many upgrades to the user interface and to the model capabilities[16].

The three-dimensional mass-conservation equation used in WASP is given as:

$$\frac{\partial C}{\partial t} = -\frac{\partial}{\partial x}(U_x C) - \frac{\partial}{\partial y}(U_y C) - \frac{\partial}{\partial z}(U_z C) + \frac{\partial}{\partial x}\left(E_x \frac{\partial C}{\partial x}\right) + \frac{\partial}{\partial y}\left(E_y \frac{\partial C}{\partial y}\right) + \frac{\partial}{\partial z}\left(E_z \frac{\partial C}{\partial z}\right) \pm S_c \qquad (3\text{-}1)$$

where:

C = concentration of a particular water quality constituent;

t = time;

x, y, and z = spatial dimensions of fluid movement;

U_x, U_y, and U_z = lateral, longitudinal, and vertical advective velocities;

[16] WASP can be downloaded from the EPA user support site at http://epawasp.twool.com/. The specific version of the model used in this study is WASP Version 8.32 (WASP8). Throughout this report, WASP is used to refer both to the general model as well as to the specific version 8.32 used in this water quality study.

E_x, E_y, and E_z = lateral, longitudinal, and vertical diffusional coefficients; and

S_c = all sources and sinks of water quality constituent.

3.2 Model Domain and Numerical Grid

The water quality model in this study covers the same model domain and utilizes the same numerical grid as the linked hydrodynamic model (Chen et al., 2024). The model domain extends from the mouth of the Delaware Bay (River Mile [RM] 0) to just upstream of the head of tide on the Delaware River in Trenton (RM 135 [17]). The C&D Canal westward to the NOAA tide gage station at Chesapeake City is also included in the domain. Orthogonal curvilinear numerical grids were created to represent the geometry and shoreline of the river and estuary. Generally, the numerical grids for the water quality model are mapped one-to-one with those in the hydrodynamic model. The only exception is that two rows of grid cells at each of the two EFDC open boundaries (at the Atlantic Ocean and C&D Canal) were clipped out of the WASP domain in order to leverage flow predictions from within the EFDC grid. The resulting numerical grid consists of 1,876 horizontal cells and utilizes a generalized vertical coordinate (GVC) system, in which the number of active model layers is variable. The number of vertical layers ranges from a single layer at the upstream boundary at Trenton to 12 vertical layers near the mouth of the Bay, resulting in a total of 11,490 water-column cells (Figure 3-1). Grid cell resolution is greater in the tidal river than in the Bay, with average grid cell sizes in the river channel upstream of RM 70 of 580 m and 190 m in the longitudinal and lateral directions, respectively. The tidal river channel was generally delineated by 4 to 6 grid cells in the cross-channel direction, and the navigational channel was typically represented by one cell in the horizontal plane and 10 cells (layers) in the vertical. Grid cells in Zone 6 are much coarser, with average lengths in the longitudinal and lateral directions of 2,020 m and 1,900 m, respectively. Additional details regarding the model domain and numerical grid system are described in Section 2 of the hydrodynamic model calibration report (Chen et al., 2024).

[17] Note: While the exact head of tide at Trenton, New Jersey, is at RM 133, the model extends to RM 135 in order to capture the boundary flows at the USGS continuous gage #01463500 (Delaware River at Trenton).

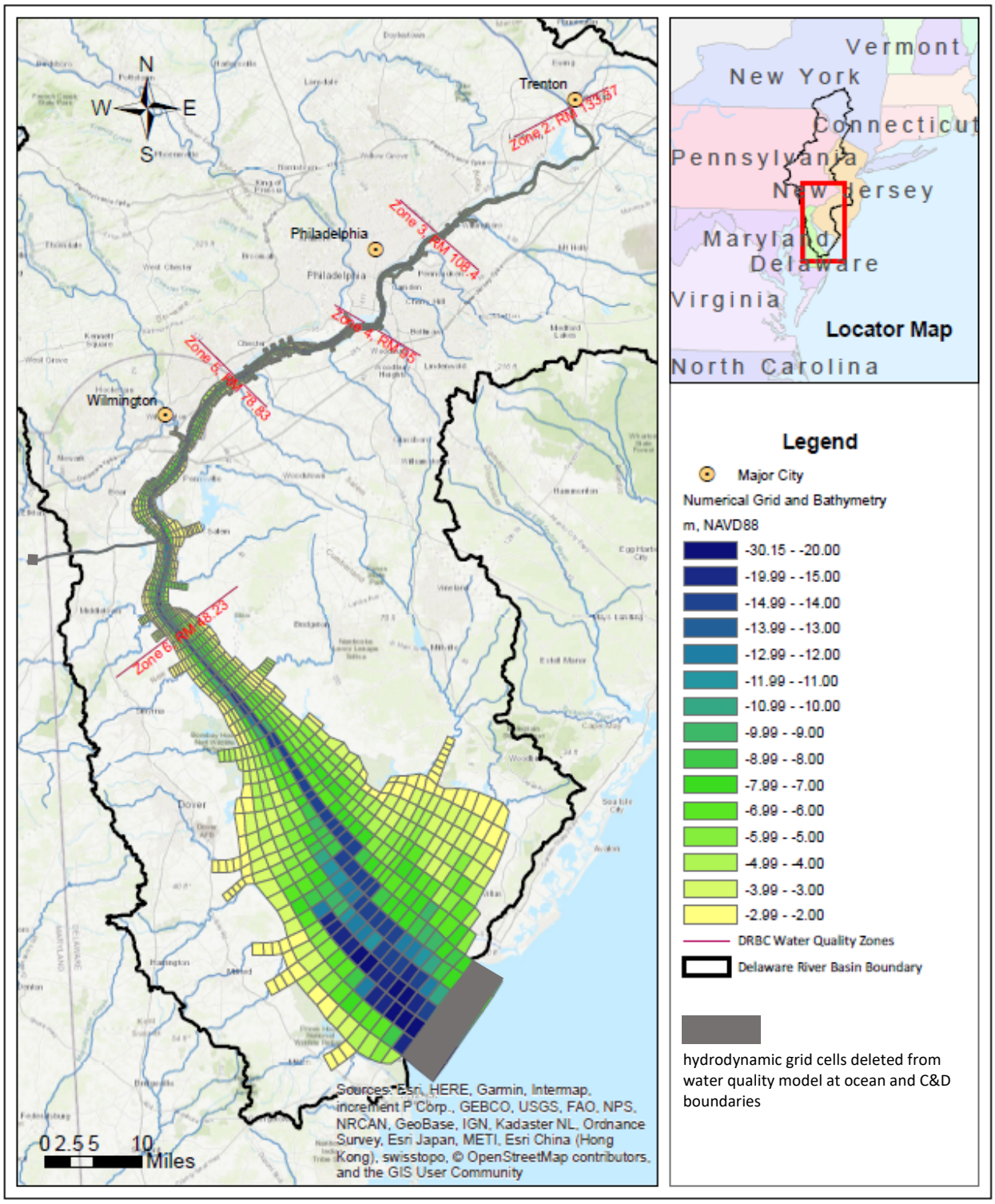

Figure 3-1: Numerical grid and projected bathymetry for water quality model

3.3 Model Kinetics

Figure 3-2 presents the major physical, chemical, and biological processes for nutrient cycling and dissolved oxygen in the WASP model for the Delaware River Estuary. These kinetic interactions provide sources and sinks in Equation (3-1). Principal kinetics are discussed below.

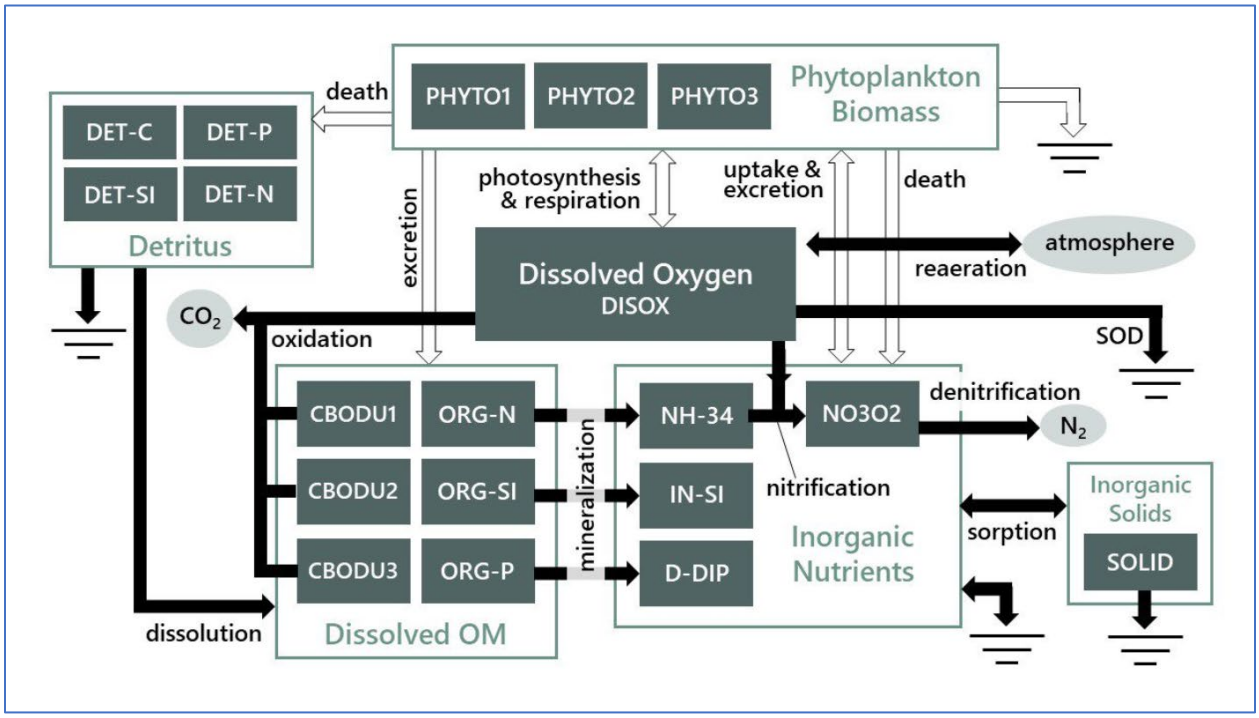

Figure 3-2: Water quality model kinetics

3.3.1 State Variables

The WASP model as applied to the Delaware River Estuary consists of 20 state variables (Table 3-1). The state variable is a water quality parameter for which the model simulates its mass (concentration) for each cell for each model calculation time step through physical, chemical, and biological processes.

Table 3-1: Water quality model state variables

Group	Symbol	Description	Unit
Dissolved: Gases	DISOX	Dissolved Oxygen	mg-O_2/L
Dissolved: Inorganic Nutrients	NH34	Ammonia Nitrogen	mg-N/L
	NO3O2	Nitrite + Nitrate Nitrogen	mg-N/L
	D-DIP	Inorganic Phosphate	mg-P/L

Group	Symbol	Description	Unit
	IN-SI	Inorganic Silica	mg-Si/L
Dissolved: Organic Nutrients	CBODU1	Ultimate CBOD from streams	mg-O_2/L
	CBODU2	Ultimate CBOD from point sources	mg-O_2/L
	CBODU3	Refractory CBOD	mg-O_2/L
	ORG-N	Dissolved Organic Nitrogen	mg-N/L
	ORG-P	Dissolved Organic Phosphorus	mg-P/L
	ORG-SI	Dissolved Organic Silica	mg-Si/L
Particulate: Phytoplankton Biomass	PHYTO1	Spring Marine Diatom Community	µg-Chla/L
	PHYTO2	Summer Freshwater Diatom Community	µg-Chla/L
	PHYTO3	Summer Marine Diatom Community	µg-Chla/L
Particulate: Detritus	DET-C	Detrital Carbon	mg-C/L
	DET-N	Detrital Nitrogen	mg-N/L
	DET-P	Detrital Phosphorus	mg-P/L
	DET-SI	Detrital Silica	mg-Si/L
Particulate: Other Solids	SOLID	Inorganic Solid	mg-DW/L
	TOTDE	Particulate Detrital Organic Material	mg-DW/L

Notes: "DW" represents Dry Weight, and "CBOD" represents Carbonaceous Biochemical Oxygen Demand.

3.3.2 Kinetic Processes

3.3.2.1 Carbonaceous Oxidation

The decomposition of carbonaceous matter consumes oxygen, which can be expressed as the carbonaceous biochemical oxygen demand (CBOD). Oxidation provides sinks to both CBOD and dissolved oxygen. A general chemical representation of carbonaceous oxidation is (Chapra, 1997):

$$C_6H_{12}O_6 + 6O_2 \rightarrow 6CO_2 + 6H_2O \quad (3\text{-}2)$$

Equation (3-2) indicates that six moles of oxygen are required to oxidate one mole of carbonaceous organic matter into carbon dioxide and water. This equation also provides a simplified expression of the life/death cycle, i.e., the reverse reaction represents photosynthesis and the forward reaction represents respiration and decomposition (Chapra, 1997).

The kinetic expression for carbonaceous oxidation in WASP contains three terms: a first-order rate constant, a temperature correction term, and a low-DO correction term (Wool et al., 2018 and 2006). The third term represents the decline of the aerobic oxidation rate as DO magnitudes approach 0. The user may specify the half-saturation constant that represents the DO concentration at which the oxidation rate is reduced by half.

$$S_{CBOD} = k_d \theta_d^{T-20} \left(\frac{C_{DO}}{K_{CBOD} + C_{DO}}\right) C_{CBOD} \quad (3\text{-}3)$$

where:

S_{CBOD} = *CBOD decay rate (mg-O_2/L-day);*

k_d = *CBOD decay rate constant at 20°C (1/day);*

θ_d = *CBOD decay rate temperature correction coefficient;*

T = *water temperature (°C);*

K_{CBOD} = *CBOD half saturation oxygen limit (mg-O_2/L);*

C_{DO} = *concentration of dissolved oxygen (mg/L); and*

C_{CBOD} = *concentration of CBOD (mg-O_2/L).*

3.3.2.2 NITRIFICATION

Nitrification is a process mediated by specialized groups of autotrophic bacteria that obtain energy through the oxidation of ammonium to nitrite and oxidation of nitrite to nitrate (Cerco and Noel, 2019). Thus, nitrification provides sinks to ammonium nitrogen and dissolved oxygen, and a source to nitrate nitrogen. A simplified expression for complete nitrification is (Cerco and Noel, 2019; Chapra et al., 2012; and Chapra, 1997):

$$NH_4^+ + 2O_2 \rightarrow NO_3^- + H_2O + 2H^+ \quad (3\text{-}4)$$

Equation (3-4) indicates that two moles of oxygen are required to nitrify one mole of ammonium into nitrate. Note that ammonium ($NH4^+$) and gaseous ammonia (NH3) exist in equilibrium in water due to hydrolysis reactions. Although the ammonium is the reactive form directly involved in nitrification, the equilibrium hydrolysis effectively involves both forms of ammonia nitrogen. Commonly and throughout this report, ammonia is used to denote both ionized ammonium and gaseous ammonia in equilibrium.

The kinetics of nitrification in WASP are modeled as a function of available ammonium, dissolved oxygen, and water temperature (Wool et al., 2018 and 2006):

$$S_{NIT} = k_{nitr}\theta_{nitr}^{T-20}\left(\frac{C_{DO}}{K_{NIT} + C_{DO}}\right)C_{NH4} \quad \text{when } T \geq T_{nitr} \tag{3-5}$$

$$S_{NIT} = 0 \quad \text{when T} < T_{nitr} \tag{3-6}$$

where:

S_{NIT} = *nitrification rate (mg-N/L-day);*

k_{nitr} = *nitrification rate constant at 20°C (1/day);*

θ_{nitr} = *nitrification temperature coefficient (dimensionless);*

K_{NIT} = *half saturation constant for nitrification oxygen limit (mg-O_2/L);*

C_{NH4} = *concentration of ammonium nitrogen (mg-N/L); and*

T_{nitr} = *minimum water temperature for nitrification reaction (°C).*

3.3.2.3 PHYTOPLANKTON PROCESSES

The theory and application of phytoplankton production and metabolism in WASP are provided by Wool et al (2004). A high-level summary is provided here.

Up to five groups of phytoplankton can be simulated in the current version of WASP, with three groups being used in this model to represent the diatom communities prevalent in the Delaware River Estuary, as explained in Appendix K. Phytoplankton kinetics are expressed as:

$$S_{k,i} = (G_{p,i} - R_{p,i} - D_{p,i} - k_{s,i})C_{alg,i} \tag{3-7}$$

where:

$S_{k,i}$ = *reaction term for phytoplankton group i (mg-C/L-day);*

$C_{alg,i}$ = *concentration of phytoplankton population group i (mg-C/L);*

$G_{p,i}$ = *specific growth rate constant (1/day);*

$R_{p,i}$ = *respiration rate constant (1/day);*

$D_{p,i}$ = *death rate constant (1/day); and*

$K_{s,i}$ = *settling rate constant (1/day).*

3.3.2.3.1 Phytoplankton growth due to photosynthesis

The specific growth rate constant, $G_{p,i}$, for group *i* is related to $k_{c,i}$, the maximum 20°C growth rate at optimum light and nutrients:

$$G_{p,i} = k_{c,i} X_{RT,i} X_{RI,i} X_{RN,i} \quad (3\text{-}8)$$

where:

$X_{RT,i}$ = *the temperature adjustment factor (dimensionless);*

$X_{RI,i}$ = *the light limitation factor (dimensionless); and*

$X_{RN,i}$ = *the nutrient limitation factor as a function of dissolved inorganic phosphorus, nitrogen, and silica (dimensionless).*

The temperature adjustment is based on the approach of Cerco and Cole (1994):

$$X_{RT,i} = e^{-\kappa_{1,i}(T-T_{opt,i})^2} \quad \text{when T} \leq T_{opt,i} \quad (3\text{-}9)$$

$$X_{RT,i} = e^{-\kappa_{2,i}(T-T_{opt,i})^2} \quad \text{when T} > T_{opt,i} \quad (3\text{-}10)$$

where:

$T_{opt,i}$ = *optimum temperature for phytoplankton group i growth (°C);*

$K_{1,i}$ = *effect of temperature below $T_{opt,i}$ on growth (°C^{-2}); and*

$K_{2,i}$ = *effect of temperature above $T_{opt,i}$ on growth (°C^{-2}).*

The light limitation is based on Steele light limitation function integrated over depth:

$$X_{RI,i} = \frac{ef}{K_e H}\left[exp\left\{-\frac{I_a}{I_{s,i}} exp(-K_e D)\right\} - exp\left\{-\frac{I_a}{I_{s,i}}\right\}\right] \quad (3\text{-}11)$$

where:

e = 2.718;

I_a = *light intensity at top of segment (W/m^2);*

$I_{s,i}$ = *saturating light intensity for the ith phytoplankton group (W/m^2);*

K_e = *segment light extinction coefficient (1/m). A site-specific light attenuation model was developed in this study. Details are provided in Section 3.4.3.*

f = fraction of day that is daylight (dimensionless); and

H = depth of water column or water segment (m).

The nutrient limitation factor is given below, based on Monod growth kinetics:

$$X_{RN,i} = Min\left(\frac{C_{DIN}}{K_{MN,i} + C_{DIN}}, \frac{C_{PO4}}{K_{MP,i} + C_{PO4}}, \frac{C_{SiO4}}{K_{MSi,i} + C_{SiO4}}\right) \quad (3\text{-}12)$$

where:

DIN, PO4, SiO4 represent inorganic nitrogen, phosphate, and silica, respectively;

DIN includes both ammonia and nitrate-nitrogen (the sum of the two concentrations); and

$K_{MN,i}$, $K_{MP,i}$, $K_{MSi,I}$ represent the half-saturation constants of phytoplankton group i for nitrogen, phosphorus, and silica uptake, respectively.

Phytoplankton growth provides sinks to dissolved inorganic nutrients through plant uptake. The kinetic processes are summarized in Equations (3-13) to (3-17) (Wool et al., 2018 and 2006). For notational simplicity, the transport terms are dropped in the equations below.

$$\frac{\partial C_{PO4}}{\partial t} = -\sum_{i=1}^{nalg} G_{p,i} C_{alg,i} a_{pc,i} \tag{3-13}$$

$$\frac{\partial C_{SiO4}}{\partial t} = -\sum_{i=1}^{nalg} G_{p,i} C_{alg,i} a_{sic,i} \tag{3-14}$$

$$\frac{\partial C_{NH4}}{\partial t} = -\sum_{i=1}^{nalg} G_{p,i} C_{alg,i} P_{NH4,i} a_{nc,i} \tag{3-15}$$

$$\frac{\partial C_{NO3}}{\partial t} = -\sum_{i=1}^{nalg} G_{p,i} C_{alg,i} (1 - P_{NH4,i}) a_{nc,i} \tag{3-16}$$

$$P_{NH4,i} = \frac{C_{NH4} C_{NO3}}{(K_{MN,i} + C_{NH4})(K_{MN,i} + C_{NO3})} + \frac{C_{NH4} K_{MN,i}}{(C_{NH4} + C_{NO3})(K_{MN,i} + C_{NO3})} \tag{3-17}$$

where:

$a_{pc,i}$ = phytoplankton phosphorous to carbon ratio of phytoplankton group i;

$a_{sic,i}$ = phytoplankton silica to carbon ratio of phytoplankton group i;

$a_{nc,i}$ = phytoplankton nitrogen to carbon ratio of phytoplankton group i;

P_{NH4} = preference for ammonia uptake term; and

nalg = number of phytoplankton groups.

Phytoplankton growth also provides a source to dissolved oxygen through photosynthesis, which is summarized in the sub-section entitled Dissolved Oxygen Processes.

3.3.2.3.2 Phytoplankton respiration

Phytoplankton respiration rate is temperature dependent and is determined by:

$$R_{p,i} = K_{R,i}\theta_{R,i}^{T-20} \tag{3-18}$$

where:

$K_{R,i}$ = *the endogenous respiration rate at 20 °C for phytoplankton group i (1/day); and*

$\theta_{R,i}$ = *temperature coefficient (dimensionless).*

Phytoplankton respiration provides sources to both inorganic and organic matter. The kinetic processes are summarized in Equations (3-19) to (3-21) (Wool et al., 2018 and 2006).

$$\frac{\partial C_{PO4}}{\partial t} = \sum_{i=1}^{nalg} R_{p,i}C_{alg,i}(1 - f_{OP,i})a_{pc,i}\,; \quad \frac{\partial C_{DOP}}{\partial t} = \sum_{i=1}^{nalg} R_{p,i}C_{alg,i}f_{OP,i}a_{pc,i} \tag{3-19}$$

$$\frac{\partial C_{SiO4}}{\partial t} = \sum_{i=1}^{nalg} R_{p,i}C_{alg,i}(1 - f_{OSi,i})a_{sic,i}\,; \quad \frac{\partial C_{DOSi}}{\partial t} = \sum_{i=1}^{nalg} R_{p,i}C_{alg,i}f_{OSi,i}a_{sic,i} \tag{3-20}$$

$$\frac{\partial C_{NH4}}{\partial t} = \sum_{i=1}^{nalg} R_{p,i}C_{alg,i}(1 - f_{ON,i})a_{nc,i}\,; \quad \frac{\partial C_{DON}}{\partial t} = \sum_{i=1}^{nalg} R_{p,i}C_{alg,i}f_{ON,i}a_{nc,i} \tag{3-21}$$

where:

DON, DOP, DOSi = dissolved organic nitrogen, phosphorus, and silica, respectively;

$f_{OP,i}$ = *fraction of respired phytoplankton group i recycled to the organic phosphorus pool;*

$f_{OSi,i}$ = *fraction of respired phytoplankton group i recycled to the organic silica pool; and*

$f_{ON,i}$ = *fraction of respired phytoplankton group i recycled to the organic nitrogen pool.*

Phytoplankton respiration also provides a sink to dissolved oxygen, which is summarized in Section 3.3.2.6 on Dissolved Oxygen Processes.

3.3.2.3.3 Phytoplankton death

Phytoplankton death consists of natural death, grazing by herbivorous zooplankton, salinity toxicity for freshwater diatom community, and freshwater toxicity for marine diatom community. The natural death term is represented by a first-order rate constant that is not temperature corrected. The death of

freshwater algae introduced to a saline environment is referred to as salinity toxicity, and freshwater toxicity refers to the death of saltwater algae introduced to a freshwater environment. In this study, death rates and threshold values due to salinity and freshwater toxicity were assigned to the appropriate phytoplankton class. The kinetic processes are summarized in Equations (3-22) to (3-26) (T. Wool, written communication, 2022).

$$D_{p,i} = K_{D,i} + K_{GZ,i} + K_{ST,i}X_{ST,i} + K_{FT,i}X_{FT,i} \quad (3\text{-}22)$$

$$X_{ST,i} = 1 - exp[Log_{10}(0.5) \times (\frac{Sal - Sal_{1,i}}{Sal_{1,i} - K_{H1,i}})^2] \quad \text{when } Sal > Sal_{1,i} \quad (3\text{-}23)$$

$$X_{ST,i} = 0 \quad \text{when } Sal \leq Sal_{1,i} \quad (3\text{-}24)$$

$$X_{FT,i} = 1 - exp[Log_{10}(0.5) \times (\frac{Sal_{2,i} - Sal}{Sal_{2,i} - K_{H2,i}})^2] \quad \text{when } Sal < Sal_{2,i} \quad (3\text{-}25)$$

$$X_{FT,i} = 0 \quad \text{when } Sal \geq Sal_{2,i} \quad (3\text{-}26)$$

where:

$D_{p,i}$ = *total death rate for phytoplankton group i (1/day);*

$K_{D,i}$ = *natural death rate for phytoplankton group i (1/day);*

$K_{GZ,i}$ = *loss rate due to grazing by zooplankton for phytoplankton group i (1/day);*

$K_{ST,i}$ = *mortality rate due to salinity toxicity for phytoplankton group i (1/day);*

$K_{FT,i}$ = *mortality rate due to freshwater toxicity for phytoplankton group i (1/day);*

Sal = *salinity (ppt);*

$Sal_{1,i}$ = *salinity mortality threshold (freshwater to saltwater) concentration for phytoplankton group i (ppt);*

$K_{H1,i}$ = *sustainable salinity level due to salinity toxicity for phytoplankton group i (ppt);*

$Sal_{2,i}$ = *salinity mortality threshold (saltwater to freshwater) concentration for phytoplankton group i (ppt); and*

$K_{H2,i}$ = *sustainable salinity level due to freshwater toxicity for phytoplankton group i (ppt).*

Phytoplankton death provides a source to the estuarine detrital pool. The kinetic processes are summarized in Equations (3-27) to (3-30) (Wool et al., 2018 and 2006).

$$\frac{\partial C_{detP}}{\partial t} = \sum_{i=1}^{nalg} D_{p,i} C_{alg,i} a_{pc,i} \quad (3\text{-}27)$$

$$\frac{\partial C_{detSi}}{\partial t} = \sum_{i=1}^{nalg} D_{p,i} C_{alg,i} a_{sic,i} \quad (3\text{-}28)$$

$$\frac{\partial C_{detN}}{\partial t} = \sum_{i=1}^{nalg} D_{p,i} C_{alg,i} a_{nc,i} \quad (3\text{-}29)$$

$$\frac{\partial C_{detC}}{\partial t} = \sum_{i=1}^{nalg} D_{p,i} C_{alg,i} \quad (3\text{-}30)$$

where:

detP, detSi, detN, detC = detrital phosphorus, silica, nitrogen, and carbon, respectively.

3.3.2.4 REAERATION

Reaeration is the transport of oxygen entering or leaving the system across the air-water interface. It provides a source or sink to the dissolved oxygen, depending on the dissolved oxygen deficit in the water column. Reaeration rate is a function of the difference between oxygen saturation and the interface oxygen concentration, mass transfer coefficient, and temperature (Chapra, 1997).

$$R_O = AK_L(C_{DO,sat} - C_{DO}) \quad (3\text{-}31)$$

where:

R_O = reaeration rate (mg-O_2/day);

A = surface area (m^2);

$C_{DO,sat}$ = oxygen saturation (mg-O_2/L);

C_{DO} = dissolved oxygen concentration at the air-water interface (mg-O_2/L); and

K_L = mass transfer coefficient of oxygen (m/day).

WASP provides several options for simulating reaeration, including hydraulic-driven reaeration in rivers and streams, wind-driven reaeration, and dam reaeration (Wool et al., 2018 and 2006). In this study, an enhancement in reaeration simulation was developed utilizing a turbulence dissipation rate near the air-water interface. Details on this enhancement are provided in Section 3.4.2.

3.3.2.5 Sediment Oxygen Demand (SOD) and Benthic Nutrient Fluxes

Oxygen demand by, and nutrient release from, sediment due to the mineralization (diagenesis) of organic matter affects surface water quality. WASP provides two options for representing sediment oxygen demand (SOD) and sediment nutrient releases (benthic nutrient fluxes): 1) externally specify (or prescribe) the rates, or 2) predict the rates (Martin and Wool, 2017). The latter option to predict the rates is accomplished in WASP via a sediment diagenesis model that was based on Di Toro's (2001) framework. The option to externally specify (or prescribe) the rates was used in this study based on the extensive measured SOD and benthic nutrient flux data available for 2012–2013 and 2016–2018 (see Section 3.5.6).

3.3.2.6 Dissolved Oxygen Processes

Dissolved oxygen processes include multiple kinetics discussed in the previous sub-sections. The kinetic expression for the dissolved oxygen process is given as (Wool et al., 2018 and 2006):

$$\frac{\partial C_{DO}}{\partial t} = \frac{K_L}{H}\left(C_{DO,sat} - C_{DO}\right) - S_{CBOD} - \frac{64}{14}S_{nitr} - \frac{SOD}{H}\theta_{SOD}^{T-20} \quad (3\text{-}32)$$

$$+\sum_{i=1}^{nalg} G_{p,i}\left[\frac{32}{12} + \left(\frac{3}{2}\times\frac{32}{14}\times a_{nc,i}\right)(1-P_{NH4})\right]C_{alg,i} - \sum_{i=1}^{nalg}\frac{32}{12}R_{p,i}C_{alg,i}$$

where the terms on the right-hand-side of Equation (3-32) represent: (1) dissolved oxygen (DO) gain from reaeration (where *H* is the water depth or segment depth); (2) DO loss due to carbonaceous oxidation; (3) DO loss resulting from nitrification; (4) DO loss caused by SOD; (5) DO gain from photosynthesis using NH_4 and NO_3, respectively; and (6) DO loss caused by respiration.

3.3.2.7 Denitrification

Under low dissolved oxygen conditions (i.e., hypoxic or anoxic), nitrate can be reduced to nitrite and nitrite converted to free nitrogen in gaseous form by denitrification (Chapra, 1997). This process also consumes dissolved organic carbon. Thus, the denitrification reaction provides sinks to both nitrate nitrogen and CBOD. A chemical representation of denitrification is (Chapra et al., 2012, and Wool et al., 2006):

$$5CH_2O + 4NO_3^- + 4H^+ \rightarrow 5CO_2 + 2N_2 + 7H_2O \quad (3\text{-}33)$$

Equation (3-33) indicates that for each milligram (mg) of nitrate-nitrogen reduced, 5/4 * (12/14) mg (or 15/14 mg) of carbon are consumed, which reduces CBOD by 5/4 * (12/14) * (32/12) mg (or 20/7 mg). Denitrification is not a significant loss in the water column but can be important when simulating anaerobic benthic conditions (Wool et al., 2006).

The kinetic expression for denitrification in WASP contains three terms: a first order rate constant (with appropriate stoichiometric ratios), a temperature correction term, and a DO correction term (Wool et al., 2018 and 2006). The third term represents the decline of the denitrification rate as DO magnitudes rise above 0. The user may specify the half-saturation constant, which represents the DO concentration at which the denitrification rate is reduced by half.

$$S_{DNIT} = k_{dnit}\theta_{dnit}^{T-20}\left(\frac{K_{NO3}}{K_{NO3} + C_{DO}}\right)C_{NO3} \quad (3\text{-}34)$$

where:

S_{DNIT} = *denitrification rate (mg-N/L-day);*

k_{dnit} = *denitrification rate constant at 20°C (1/day);*

θ_{dnit} = *denitrification temperature coefficient (dimensionless);*

K_{NO3} = *half saturation constant for denitrification oxygen limit (mg-O_2/L); and*

C_{NO3} = *concentration of nitrate-nitrogen (mg-N/L).*

The denitrification rate in Equation (3-34) is related to the concentration of nitrate-nitrogen. For CBOD, the loss due to denitrification is: (5/4) * (32/14) * S_{DNIT}.

3.3.2.8 Dissolution of Nutrients Associated with Particulate Organic Matter

Particulate organic matter (POM or simply detritus) is derived from algal death, but also from external (allochthonous) loads. This detrital matter transforms into dissolved organic matter through bacterial dissolution. Dissolved organic matter is further mineralized to inorganic forms, as discussed in the following section. Transformation of detrital carbon (including associated organic nitrogen, phosphorus, and silica) to dissolved forms in WASP follows a temperature-corrected first-order kinetic process. For algal nutrients these transformation terms are as follows:

$$S_{disP} = k_{disDet}\theta_{disDet}^{T-20}C_{DetP} \quad (3\text{-}35)$$

$$S_{disN} = k_{disDet}\theta_{disDet}^{T-20}C_{DetN} \quad (3\text{-}36)$$

$$S_{disSi} = k_{disDet}\theta_{minSi}^{T-20}C_{DetSi} \quad (3\text{-}37)$$

where:

S_{disP}, S_{disN}, *and* S_{disSi} = *dissolution rates of particulate organic matter (mg-P, N, Si/L-day);*

K_{disDet} = *dissolution rate constant at 20°C (1/day);*

Θ_{disDet} = *dissolution rate temperature correction coefficient (dimensionless); and*

C_{DetP}, C_{DetN}, C_{DetSi}, = *concentration of detrital P, N and Si (mg-P, N, Si /L).*

3.3.2.9 Mineralization of Dissolved Organic Nitrogen, Phosphorus, and Silica

Mineralization is a process whereby dissolved organic compounds are converted to dissolved inorganic products (Chapra, 1997; Cerco and Noel, 2019). Direct mineralization of particulate organic matter (detritus) does not occur, but this material does undergo a process of dissolution (see previous section) to dissolved organic forms which may then be mineralized. Thus, mineralization provides sinks to the dissolved organic matter and sources to the dissolved inorganic nutrients. The mineralization rates in WASP are related to a first order rate constant, a temperature correction term, and a phytoplankton concentration correction term. The third term slows the mineralization rate if the phytoplankton population is small but does not permit the rate to increase continuously as phytoplankton increase (Wool et al., 2018 and 2006).

$$S_{minP} = k_{minP}\theta_{minP}^{T-20}\frac{C_{algT}}{K_{mpc}+C_{algT}}C_{DOP} \quad (3\text{-}38)$$

$$S_{minN} = k_{minN}\theta_{minN}^{T-20}\frac{C_{algT}}{K_{mpc}+C_{algT}}C_{DON} \quad (3\text{-}39)$$

$$S_{minSi} = k_{minSi}\theta_{minSi}^{T-20}\frac{C_{algT}}{K_{mpc}+C_{algT}}C_{DOSi} \quad (3\text{-}40)$$

where:

S_{minP}, S_{minN}, *and* S_{minSi} = *mineralization rates of dissolved organic matter (mg-P, N, Si/L-day);*

k_{minP}, k_{minN}, *and* k_{minSi} = *mineralization rate constants at 20°C (1/day);*

θ_{minP}, θ_{minN}, *and* θ_{minSi} = *mineralization temperature coefficients (dimensionless);*

K_{mpc} = *algal half saturation constant for mineralization (mg-C/L); and*

C_{algT} = *concentration of total phytoplankton (mg-C/L).*

3.3.2.10 Sorption

There is an adsorption–desorption interaction between dissolved inorganic nutrients and suspended particulate matter in the water column. The subsequent settling of the suspended solids together with the sorbed inorganic nutrients can act as a loss mechanism in the water column and is a source of nutrients to the sediment (Wool et al., 2018 and 2006). Sorption kinetics is summarized below:

$$(NH_4^+, HPO_4^-, SiO_4^{3-}) + Solid \leftrightarrow (NH_4, HPO_4, SiO_4) - Particulate \quad (3\text{-}41)$$

$$K_d = \frac{C_p}{C_{solid} C_{dis}} \quad (3\text{-}42)$$

$$f_s = \frac{C_p}{C_{dis} + C_p} = \frac{K_d C_{solid}}{1 + K_d C_{solid}} \quad (3\text{-}43)$$

where:

K_d = *partition coefficient for inorganic nutrients (e.g., NH_4, PO_4, and SiO_4) (m^3/g);*

C_p = *particulate inorganic nutrient concentrations (g/m^3);*

C_{dis} = *dissolved inorganic nutrient concentrations (g/m^3);*

C_{solid} = *suspended solids concentration (g/m^3);*

f_s = *particulate fractions of inorganic nutrients (dimensionless).*

3.3.2.11 SETTLING

The settling rate in WASP is expressed as (Wool et al., 2018 and 2006):

$$k_s = \frac{v_s}{H} \quad (3\text{-}44)$$

where:

k_s = *settling rate (1/day);*

v_s = *net settling velocity associated with solids, phytoplankton, and detritus, respectively (m/day), where "net settling" represents gross settling minus gross resuspension; and*

H = *water depth or segment depth (m).*

Settling causes the loss of state variables from the system to the sediment. The loss term is expressed as: $-k_sC$, which includes the losses associated with 1) solid, $-k_sC_{solid}$; 2) detritus, $-k_sC_{detP}$, $-k_sC_{detSi}$, $-k_sC_{detN}$, and $-k_sC_{detC}$, respectively; 3) particulate inorganic matters, $-k_sf_{s,PO4}C_{PO4}$, $-k_sf_{s,SiO4}C_{SiO4}$, and $-k_sf_{s,NH4}C_{NH4}$; and 4) phytoplankton related, $-k_sa_{pc,i}C_{alg,i}$, $-k_sa_{sic,i}C_{alg,i}$, $-k_sa_{nc,i}C_{alg,i}$, and $-k_sC_{alg,i}$ for phytoplankton group *i*.

3.4 MODEL ENHANCEMENTS

Three enhancements were made during this study to improve the water quality model (WASP) accuracy and reliability: (1) a thorough investigation of WASP model integration with the hydrodynamic model EFDC, (2) reaeration simulation, and (3) light extinction formulation.

3.4.1 INTEGRATION WITH HYDRODYNAMIC MODEL

Application of a three-dimensional hydrodynamic model (EFDC) and a water quality model (WASP) to a complex system requires thorough examination of model integration. Information from EFDC, such as water volume, current velocity, flow rate, mixing coefficient, salinity, water temperature, and turbulence dissipation rate, is transferred to WASP via stored output (or linkage file) for use in simulating water column transport of constituents. The two models perform simulations on the same numerical grid, so spatial collapsing of EFDC output is not necessary. Temporally, WASP can use a larger time step than EFDC. Key parameters for preparing the linkage file include (1) the EFDC coupling interval (NTSMMT), i.e., the number of time steps for EFDC to average and output variables to the linkage file; and (2) the upper limit on the vertical mixing coefficient (ABMAX), aiming at capping larger vertical mixing coefficient values and maintaining numerical stability in WASP. Several factors were considered in determining these parameters: 1) the ability of WASP to reproduce conservative tracer transport by EFDC; 2) maintaining mass balance in WASP; 3) controlling WASP computation time; and 4) generating a manageable linkage file size.

The time step in the WASP model is related to the EFDC coupling interval, NTSMMT. Generally, a smaller NTSMMT results in a smaller time step in WASP and consequent longer computation time. A smaller NTSMMT also brings about better conservative tracer transport, improved mass balance, and a correspondingly larger linkage file. From a practical perspective, the chosen NTSMMT should be as large as possible, as long as the WASP model can maintain a good mass balance and reproduce the conservative tracer transport predicted by EFDC. A series of numerical tests suggested that NTSMMT = 30, combined with an adequate ABMAX value, would provide a good balance among the factors discussed above. Appendix C presents the results of conservative tracer transport and mass balance with NTSMMT = 30. This resulted in a time step for EFDC of 10 seconds (Chen et al., 2024), linkage output every 300 seconds (every 5 minutes), and a linkage file size of 45 Gigabyte for a one-year simulation. Results of the numerical tests using other NTSMMT values are not included in this report.

The WASP model honors the vertical mixing predicted by EFDC, subject to a maximum vertical mixing coefficient (ABMAX). However, the "Timestep Optimization" algorithm in WASP, without which computation time could double or triple, is sensitive to the ABMAX specification (i.e., a larger vertical mixing coefficient forces the algorithm to adopt a smaller time step in WASP to maintain numerical stability). For example, a WASP model with ABMAX = 0.01 m^2/s and NTSMMT = 30 takes about 100 hours for a one-year simulation with 20 state variables, whereas a WASP model with ABMAX = 0.001 m^2/s and NTSMMT = 30 takes about 32 hours for the same simulation. The ABMAX value of 0.01 m^2/s corresponds to about the 80^{th} percentile and up to 30^{th} percentile of the vertical mixing coefficients used in EFDC for the Bay and tidal river, respectively. Numerical tests presented in Appendix C indicate that a combination of NTSMMT = 30 and ABMAX = 0.01 m^2/s produces reasonable agreement in conservative tracer transport between EFDC and WASP, as well as adequate mass balance in WASP (e.g., 2% or lower yearly averaged error along the navigation channel, and 5% or lower instantaneous error in main stem cells), even though

this results in the ABMAX capping the top 70% of vertical mixing coefficient values in the tidal river at a maximum of 0.01 m^2/s. The reason is that a vertical mixing coefficient of 0.01 m^2/s is still sufficient to generate a well-mixed vertical profile in the tidal river under the model spatial and temporal scales.

An alternative combination with NTSMMT = 30 and ABMAX = 0.001 m^2/s generated comparable downstream transport, but less desirable upstream transport, compared to the first combination with ABMAX = 0.01 m^2/s (Appendix C). Though simulation times were three times faster, the ABMAX = 0.001 m^2/s simulations resulted in mass balance errors that were double those obtained using ABMAX = 0.01 m^2/s. However, the numerical results in Appendix C demonstrate that ABMAX = 0.01 and ABMAX = 0.001 m^2/s generate insignificant differences in simulated DO concentrations and identical results for all other parameters. Therefore, to balance mass transport accuracy and computation time during model calibration, the combination of NTSMMT = 30 and ABMAX = 0.001 m^2/s was used in the model calibration production runs. The combination of NTSMMT = 30 and ABMAX = 0.01 m^2/s was used for the final water quality model calibration results presented in this report.

3.4.2 REAERATION

Reaeration is a process of dissolved oxygen (DO) transfer at the air–water interface in both directions (air to water and water to air) depending on DO concentration gradients. DO component analysis (see Section 4.5.1) indicates that reaeration is an important contributor to DO gain in the tidal river. Conventional options for simulating reaeration in the WASP model, such as O'Connor-Dobbins (1958), categorize the reaeration process into (1) hydraulic-driven reaeration for streams or rivers where current effect is a predominant factor, and (2) wind-driven reaeration for lakes or bays where wind effect is dominant. Depth-averaged velocity and water column depth are used in the hydraulic-driven formulation for estimating the mass transfer coefficient, whereas wind speed is used in the wind-driven formulation. In both cases, DO concentrations are usually represented by the concentrations in the center of the surface grid cells. However, the Delaware River Estuary is a complex environment with deep water, high energy, flow reversals (tides), potential stratification, and geometry varying from relatively narrow river to relatively wide estuary, suggesting there was an opportunity for the representation of the surface DO concentration in the reaeration formulation to be improved. Furthermore, advancements in turbulence modeling in recent decades were believed to be able to help improve quantification of the mass transfer at the air–water interface. In this study, reaeration simulation was enhanced in two aspects: (1) extrapolating DO concentrations from the centers of the surface grid cells to the air–water interface for proper representation of gas transfer across the interface; and (2) utilizing the turbulence dissipation rate at the air–water interface for estimating the mass transfer coefficient (Zappa et al. 2007). Zappa's approach incorporates the comprehensive effects of current velocity, wind speed, and water temperature on reaeration into the key input parameters. Thus, users do not need to decide whether to use hydraulic- or wind-driven formulations. Details regarding the enhancement of the reaeration simulation, including comparisons between the Zappa and O'Connor-Dobbins' approaches, are discussed in Appendix D.

3.4.3 LIGHT EXTINCTION

Light extinction in water refers to the loss of light in the water column due to absorption and scattering. Light extinction in aquatic environments plays an important role in controlling water quality parameters such as temperature and dissolved oxygen (via photosynthesis). Understanding the dynamics of light extinction is essential to accurately modelling dissolved oxygen dynamics in the Delaware River Estuary. Water quality constituents that affect light extinction include suspended solids, phytoplankton, and detritus (Di Toro 1978). Ideally, all these parameters could be used to predict light extinction; however, to develop a dynamic light model for use within the eutrophication model, light extinction needed to be predicted using only model state variables. This limited the parameters available to model light extinction.

2018 and 2019 data from DRBC's Boat Run Monitoring Program were used to model light extinction in the Delaware River Estuary. The Boat Run provided a valuable dataset for this purpose, as it has broad spatial and temporal coverage of the Estuary and includes important parameters for modelling light extinction including photosynthetically active radiation (PAR, collected at the surface and 1 meter depth) along with several model state variables. Observed light extinction (K_e) was calculated from PAR data using the following equation (Chapra, 1997):

$$K_e = ln\left(\frac{PAR_{surface}}{PAR_{1\ meter}}\right) \quad (3\text{-}45)$$

The model state variables that were chosen to predict light extinction were chlorophyll-a, dissolved organic carbon, and salinity. Salinity, while not a direct driver of light extinction, acted as a surrogate for suspended solids for the purposes of the model. Suspended solids are the main driver of light extinction in the Delaware River Estuary and are also a model state variable; however they were unable to be used directly as an explanatory variable as several of the processes driving sediment dynamics in the Estuary are not incorporated in the model (e.g., erosion and resuspension of sediments). This leads to the underprediction of sediment loads in the model. Salinity was chosen as a surrogate for suspended solids because its gradient in the Estuary inversely resembles that of solids. Suspended solids are highest near the Estuarine Turbidity Maximum (ETM) zone, around river mile 55, and lowest at the mouth of the Bay. Salinity follows an inverse pattern showing highest concentrations at the mouth of the Bay and concentrations approaching zero at the upstream extent of the ETM. Therefore, an inverse relationship with salinity was able to be used as a surrogate for suspended solids up to the upper extent of the ETM. To accurately capture this dynamic, data from the mouth of the Bay to the lower end of the ETM (RM 36) were used to parametrize the salinity coefficient in the model. Since salinity values are near-zero upstream of the ETM, this parameter would have little to no influence on light extinction (K_e) predictions upstream of the ETM. Suspended solids are the dominant driver of light extinction near the ETM; however chlorophyll and dissolved organic carbon (DOC) are important drivers upstream and downstream of this reach. Because the effects of these secondary parameters are difficult to observe at the ETM, we

parametrized these variables using only data from upstream and downstream of the ETM (RM 0-36, 80-131). Finally, to capture light extinction dynamics more accurately throughout the Estuary, we calculated spatially variable intercepts for each Boat Run station. This allowed for a model that captures consistent large-scale spatial differences in K_e throughout the estuary (i.e., K_e is higher at the ETM than at the mouth or head of tide) while still retaining the dynamic capabilities of using modeled state variables to predict K_e. Additional information on developing the light extinction formulation is provided in Appendix J. The final predictive function for K_e is below:

$$K_e = Intercept + (0.345 * DOC) + (0.014 * Chlorophyll\ a) + (-0.097 * Salinity) \quad (3\text{-}46)$$

$$Intercept = 3.5944e^{-0.016 \times RM} + Max[0, (1.7549 - 0.069 \times |54.9 - RM|)] \quad (3\text{-}47)$$

3.5 Model Inputs

All flow, salinity, and water temperature inputs to the WASP water quality model are provided by the hydrodynamic model (Chen et al., 2021) through a linkage file. The water quality model also requires specification of input concentrations over the calibration and corroboration periods for all inflow boundaries and open boundaries for the water quality state variables listed in Table 3-1, as well as the assignment of loads/fluxes for certain source categories. The time-series model input files for each state variable are prepared based on the compiled monitoring data as presented in Section 2.2 and model input conditions described in this section. Methodologies used to develop the model input files are described for the following source categories.

- Tributary and watershed (municipal separate storm sewer systems (MS4s) and nonpoint source (NPS) runoff) inflow concentrations
- Wastewater treatment and CSO discharge concentrations
- Ocean and C&D Canal open boundary concentrations
- Atmospheric loads
- Meteorologic boundaries
- Sediment Oxygen Demand (SOD) and benthic nutrient fluxes

Procedures for calculating state variable concentrations from analytical parameters are described in Appendix E. The concentration values were used to specify the boundary conditions or calibration parameters. All boundary conditions were compiled into a Water Resources Database (WRDB) for use by the WASP model.

Initial model conditions and hydrologic conditions for the model calibration and corroboration periods are discussed in Sections 3.5.7 and 3.5.8, respectively.

3.5.1 Tributary and Watershed Inflow Concentrations

Concentrations for state variables must be assigned for freshwater inflows, including flows from upstream boundaries, tributaries (gaged and ungauged), non-point sources (NPS), and Municipal Separate Storm Sewer System (MS4) discharges. Groundwater/surface water interaction was not considered in this study.

The primary approach to assigning concentrations utilized the compilation and direct assignment of discrete or continuous observational data acquired from various agencies including the DRBC, USGS New Jersey, Pennsylvania, and Maryland Water Science Centers, Delaware Department of Natural Resources and Environmental Control (DNREC), New Jersey Department of Environmental Protection (NJDEP), Pennsylvania Department of Environmental Protection (PADEP), and U.S. Army Corps of Engineers (USACE). Discrete data were widely available during the 2018–2019 simulation period but less so during 2012. The frequency of data for each water quality parameter varied from monthly to quarterly, except for the Delaware River at Trenton, where data were collected on an approximate biweekly basis. Discrete measurements of DO were augmented with continuous DO collected at USGS gages located on selected tributaries (Delaware River at Trenton, Brandywine Creek, Christina River, Appoquinimink River, and Murderkill River). Additionally, sensory monitoring of chlorophyll-a at Trenton provided hourly input time series at the model upstream boundary.

At selected tributaries, the frequency of water quality data at the inflow boundaries were temporally enhanced using standard USGS regression techniques. Regression methods were implemented through two USGS-developed packages, Load Estimator (LOADEST) and the Weighted Regressions on Time, Season, and Discharge (WRTDS) tool. Both packages employ logarithms of daily discharge, decimal time, and sine and cosine transformations of decimal time (season) to estimate concentrations. The basic form of the LOADEST model consists of a seven-parameter model in which log-transformed daily concentrations are related to second-order polynomials of log-transformed daily flow, decimal time, and seasonal factors derived from transformations of decimal time (Cohn et al.,1989; Runkel et al., 2004). WRTDS resolves variations in constituent concentrations using five terms, excluding the squared terms that are used in LOADEST. A fundamental difference between the models is the manner in which coefficients are estimated. WRTDS estimates parameter coefficients for each estimation point (any given combination of discharge and time) using a unique weighted regression for each day of the estimation period, applying greater weight to observations closer in time, discharge, and season to the estimation point (Hirsch et al.,2010). In contrast, LOADEST estimates parameter coefficients once for the entire dataset. Both packages were combined into a single script, implemented using the R language, such that input requirements are common to both. Statistical models using both methods were run for NO2+NO3, NH3-N, TDN, DIP, TDP, DSI, TP, TN, DOC, TOC, and TSS for each tributary with a sufficient sample size (60+) and a representative range of hydrologic conditions. Model performance was assessed both graphically and statistically; if the model was deemed acceptable, the resulting regression data were used at the appropriate water-quality boundary.

In sparsely monitored or unmonitored portions of the watershed, environmental classification was used to transfer water quality information between measured and unmeasured sites. A hierarchical agglomerative cluster analysis was used to group sub-watersheds with similar physical and hydrologic attributes into general landscape regions, providing the basis for assigning water quality values to catchments lacking data. Hierarchical agglomerative clustering successively combines smaller clusters into larger ones while maintaining a minimal merge cost at each stage; similarity among clusters was determined using Ward's method of linkage with squared Euclidean distances.

The cluster analysis identified four general groups of watersheds: small to medium-sized urbanized basins with mixed geology, moderate slopes, and low base flow indices (BFI); medium-to-larger size, gently-sloped basins underlain by unconsolidated sand/silts with significant BFI; medium-to-larger size, steeper-sloped basins with forested uplands, underlain by consolidated bedrock; and small, low fluvial energy, coastal plain basins containing higher percentages of agricultural land use and wetlands.

Associated data from the control watersheds were composited into four matrices by season and streamflow condition and subsequently assigned to unmonitored watersheds on the basis of cluster membership. Time series for most state variables were compiled at a daily time step and applied to NPS and MS4 boundaries. Where a daily time series could not be prescribed, constant values, derived from averaging 2018–2019 tributary data, were used.

Additional information on developing the data time series for selected tributaries and watershed inflows using these methods is presented in Appendix I. Relevant information on developing watershed flows is described in the hydrodynamic model calibration report (Chen et al., 2024). Detailed information on flow rates, nutrient concentrations, and loads from tributaries, NPSs, and MS4s for the period of 2018 – 2019 is summarized in Appendix A.

3.5.2 Wastewater Treatment Plant Effluent Concentrations

Seventy-one (71) point discharge facilities (see Figure 2-3 and Table 2-5) are included in this study. Constituent concentrations from these point source discharges during the model calibration period of 2018–2019 were specified based on the second round of monitoring data described in Sections 2.1.2 and 2.2.2. If the concentration of a state variable was not measured directly, it was instead calculated based on other measured data following the procedures listed in Appendix E. The frequency of input data for Tier 1 and 2 facilities is weekly and monthly, respectively, consistent with the monitoring frequencies for the 2018-2019 period. The constituent concentrations from Tier 3 facilities are set to constant values for simplification, based on the medians of the collected data. For the model corroboration period of 2012, constituent concentrations from the point discharges were specified based on the first round of monitoring initiated in 2011 (see Section 2.1.2). The frequency of input data for 2012 is monthly for both Tier 1 and 2 facilities and less frequently for Tier 3 facilities due to less available data.

Data on CSOs during the model calibration and corroboration periods were provided to various degrees of resolution by four municipalities: Philadelphia Water Department (PWD), Camden County Municipal Utilities Authority (CCMUA), Delaware County Regional Water Quality Control Authority (DELCORA), and City of Wilmington (CoW). For simplification, all CSO outfalls were aggregated to 14 locations: five locations to represent all PWD CSOs; three locations to represent all CCMUA CSOs; three locations to represent all DELOCRA CSOs; and three locations to represent all CoW CSOs. CSO outfalls located upstream of tributary monitoring locations were excluded to avoid double-counting of flows and loads. All CSO discharges were assumed to have identical and constant constituent concentrations for each state variable as summarized in Table 3-2. These estimated values were based on limited CSO sampling data provided by DELCORA. These concentrations were also compared with PWD's CSO modeling methodology, and the estimated concentrations generally fall within the range PWD assumed for stormwater and wastewater.

Detailed information on flow rates, nutrient concentrations, and loads from point discharges and CSOs for the modeled periods is summarized in Appendix A.

Table 3-2: CSO constituent concentrations

State Variable	Estimated Concentration	Units
NH34	6.9	mg-N/L
NO3O2	0.5	mg-N/L
ORG-N	2.9	mg-N/L
DET-N	4.1	mg-N/L
D-DIP	0.8	mg-P/L
ORG-P	0.2	mg-P/L
DET-P	1.8	mg-P/L
STR-CBODU	0.0	mg-O_2/L
PS-CBODU	38.4	mg-O_2/L
CDOM	4.3	mg-O_2/L
DET-C	18.9	mg-C/L
DISOX	5.9	mg-O_2/L
PHYTO	0.0	ug-Chla/L
IN-SI	9.4	mg-Si/L
ORGSI	0.0	mg-Si/L
DETSI	1.9	mg-Si/L

State Variable	Estimated Concentration	Units
SOLID	57.0	mg-DW/L
TOTDE	0.0	mg-DW/L

3.5.3 Ocean and C&D Canal Boundary Concentrations

World Ocean Atlas 2018 (WOA18), published by NOAA National Centers for Environmental Information, provides a statistical analysis of long-term data collected since 1960 on a 1° grid resolution (Garcia et al., 2019). The monthly mean and depth-averaged concentrations of model state variables at the grid cell closest to the mouth of the Delaware River Estuary were chosen as the ocean boundary conditions (Figure 3-3a). These included concentrations of phosphate, nitrate, silicate, and dissolved oxygen (

Table ***3-3***). NJDEP grab samples collected at BMWM-3826A station (Figure 3-3b) provided supplemental information for characterizing phosphate and ammonia concentrations for the ocean boundary. Remaining state variable concentrations at the ocean boundary were specified based on the data collected by the DRBC Boat Run (see Section 2.1.1.1) at South Brown Shoal during the calibration and corroboration periods.

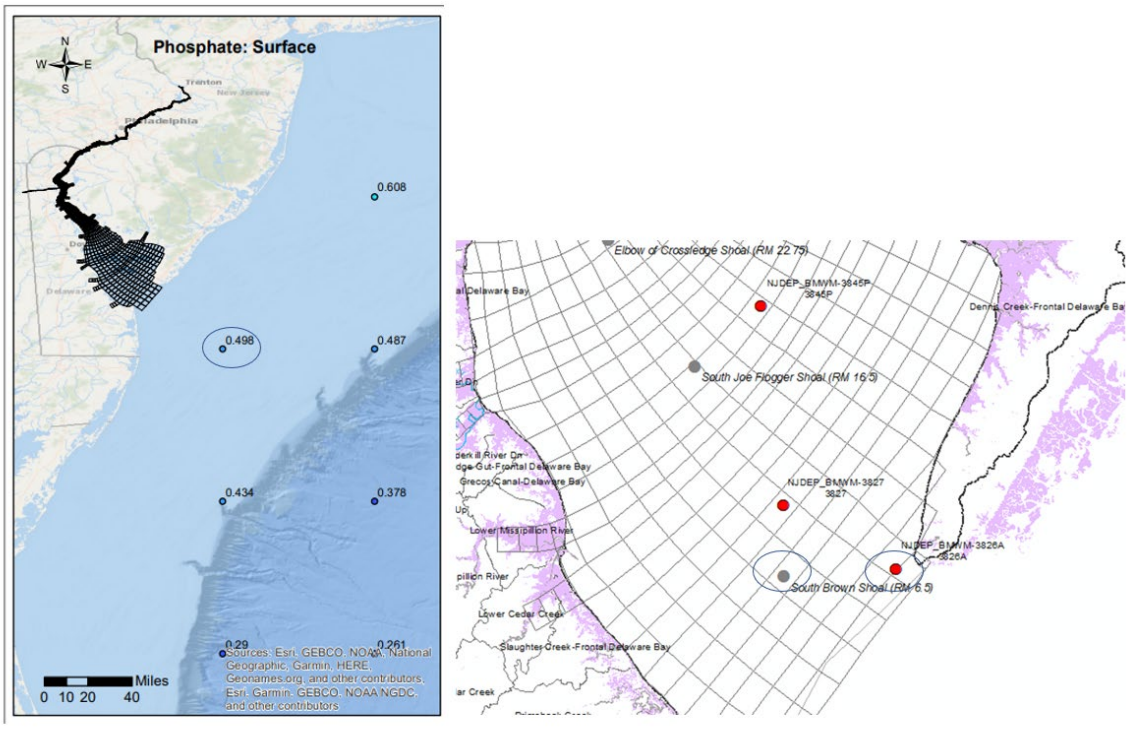

(a) (b)

Figure 3-3: Location maps of (a) WOA18 data on 1° grid; and (b) NJDEP and DRBC Boat Run monitoring stations near the mouth of the Estuary

Table 3-3: Concentrations of model state variables from WOA18 near mouth of Estuary

Month	Nitrate (mg-N/L)	Phosphate (mg-P/L)	Silicate (mg-Si/L)	Dissolved Oxygen (mg-O_2/L)
January	0.035	0.015	0.005	8.555
February	0.029	0.023	0.015	8.989
March	0.046	0.016	0.008	9.689
April	0.018	0.008	0.028	10.569
May	0.006	0.005	0.047	9.242
June	0.007	0.008	0.045	9.591
July	0.007	0.011	0.039	8.470
August	0.013	0.012	0.048	8.258
September	0.010	0.010	0.053	7.708
October	0.007	0.007	0.030	8.019
November	0.024	0.011	0.015	8.305
December	0.021	0.009	0.051	8.781

Source: The World Ocean Atlas (WOA) 2018

Concentrations of model state variables at the C&D Canal boundary were based on the data collected during the DRBC Tributary Nutrient Monitoring Program (Section 2.2.3), supplemented with data collected by the Maryland Department of Natural Resources and Delaware Department of Natural Resources and Environmental Control (DNREC).

3.5.4 Atmospheric Loads

Nutrient data collected by the National Atmospheric Deposition Program (NADP) from 2012 through 2019 provided the basis for estimating atmospheric nutrient loading to the tidal Delaware River Estuary. Wet deposition rates were calculated using precipitation and nutrient data (NH3-N, NO3O2) measured at Washington's Crossing, New Jersey, and Wye, Maryland, according to the methods of Ullman and others (2010). Dry deposition rates were estimated using NADP Total Deposition Maps (Schwede and Lear, 2014) in conjunction with wet deposition rates, whereby ratios of wet-to-dry deposition were estimated at each station. The ratios were then applied to the calculated wet deposition rates to estimate dry and ultimately total deposition rates. The rates are applied to all wet grid cells (water surface segments) of the model domain as a time-varying function (mg/m^2/d) throughout the 2012 and 2018–2019 simulation periods.

3.5.5 METEOROLOGICAL BOUNDARIES

As detailed in Section 2.4.4 of the hydrodynamic model calibration report (Chen et al., 2024), meteorological data, such as air temperature and pressure, dew point, cloud conditions, wind speed, wind direction, precipitation, and net shortwave solar radiation, were used in EFDC to calculate the heat flux at the water surface and water temperature in the water column. Although predicted water temperature values were transferred from the hydrodynamic model to the water quality model through the linkage file, some of the meteorological data (e.g., wind speed and solar radiation) are still required by WASP as direct inputs for use in calculating reaeration and photosynthetic active radiation (PAR). Similar to the hydrodynamic model, the meteorological inputs to WASP were provided from four weather stations as shown in Figure 3-4 and summarized in Table 3-4. Temporal variations in meteorological data for 2018 and 2019 were presented in the hydrodynamic model calibration report (Chen et al., 2024).

Table 3-4 NOAA National Climatic Data Center weather stations

Count	STATION	USAF	LAT	LON	Coverage
1	TRENTON MERCER AIRPORT	724095	40.277	-74.816	RM > 108.5
2	PHILADELPHIA INTERNATIONAL AIR	724080	39.873	-75.227	79 < RM < 108.5
3	NEW CASTLE COUNTY AIRPORT	724180	39.674	-75.606	48.5 < RM < 79
4	DOVER AFB AIRPORT	724088	39.133	-75.467	RM < 48.5

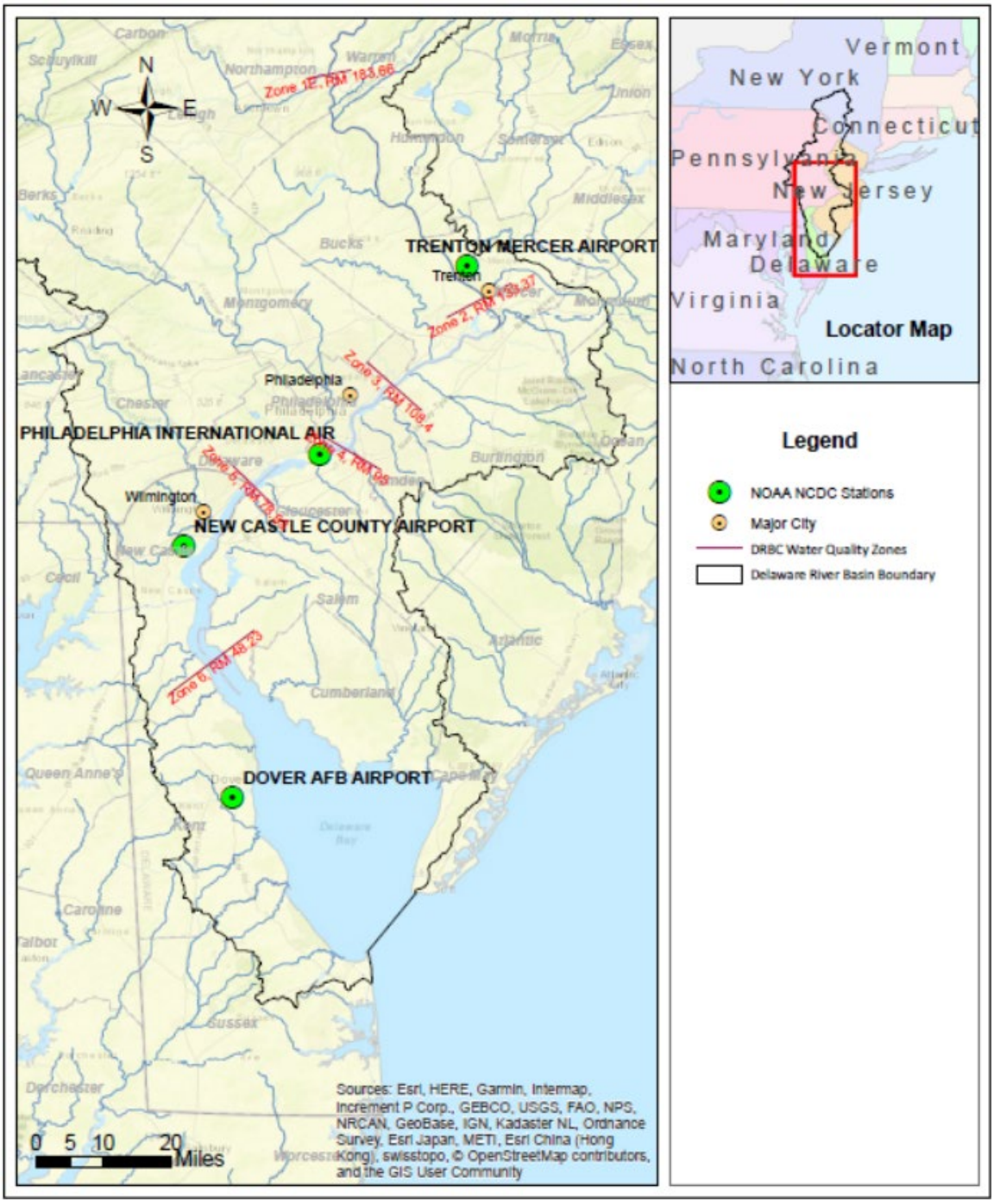

Figure 3-4: Weather stations used to characterize meterological boundary conditions

3.5.6 Sediment Oxygen Demand (SOD) and Benthic Nutrient Fluxes

A sediment diagenesis module with the capability of dynamically simulating sediment-water exchanges (see Section 3.3.2.5) was tested in this study. However, predicted SOD was substantially lower than indicated by the survey data, which may be attributable to under-prediction/specification of organic

carbon resulting in depletion of carbon in the sediment anaerobic layer. It is possible that the specification of organic carbon from tributaries and watersheds during heavy storm events is not being captured by the model, or that the model is not capturing organic carbon production from larger algal bloom events. Considering the timeframe and goals of the project, SOD and nutrient release rates from the sediment layer (benthic nutrient fluxes) for ammonia (NH3-N), nitrate (NO3-N), and phosphate (DIP) were externally specified as model inputs using available data rather than dynamically simulating sediment diagenesis. This project benefitted from an unusually large dataset of sediment measurements, as described below. Assigning SOD and benthic fluxes within the range of a significant number of observed values, from the standpoint of model certainty, might be considered advantageous compared to deriving a sediment boundary condition dynamically (e.g., better to use actual data for a boundary than a submodel). However, assigning static SOD and benthic flux inputs also imposes limitations, as discussed in Section 4.7. The decision to utilize an externally specified option for SOD and benthic flux assignments was based on the fact that it was not possible, given the current state of data and knowledge about the system and within the time and scope of this project, to dynamically simulate the degree of sediment diagenesis that both water quality and sediment data suggest is occurring in the system.

PWD, along with Woods Hole Group, Academy of Natural Sciences of Drexel University, and Chesapeake Biogeochemical Associates, designed and conducted a field data collection program to measure SOD and benthic nutrient fluxes between RM 63 and RM 128 of the Delaware River Estuary during 2012–2013 and 2016–2018. These data, which include 237 measurements of SOD and 158 measurements of benthic ammonia nitrogen, nitrite nitrogen + nitrate nitrogen, and inorganic phosphate fluxes (Figure 3-5), were provided to DRBC by the PWD modeling team; the methodology and partial results are documented by PWD (2015).

SOD raw data reflected in situ conditions and thus were converted to values at 20°C, as described in Section 3.3.2.5, using a temperature correction factor, Θ. Published literature provides a range of 1.04 to 1.13 for Θ, and a value of 1.065 is commonly employed (Zison et al., 1978; Bowie et al., 1985, and Chapra 1997). This same temperature correction of 1.065 was used in the WASP model calibration so that the temperature-normalized SOD at 20^{o}C values were adjusted based on the EFDC-simulated water temperatures which linked to WASP. Hereafter, the SOD data and model inputs are expressed as temperature-corrected values in this report. If a location contained replicate or triplicate samples during a single survey, the average value was used in the analysis.

The WASP model does not support temperature correction factors for benthic fluxes and allows only one time series function for the benthic fluxes. Given the limited data and model constraints, only data collected in August were used to estimate benthic fluxes. This approach focuses on the most critical summer period and also adds a degree of conservatism since the season with the highest observed flux values were used to bound the model calibration.

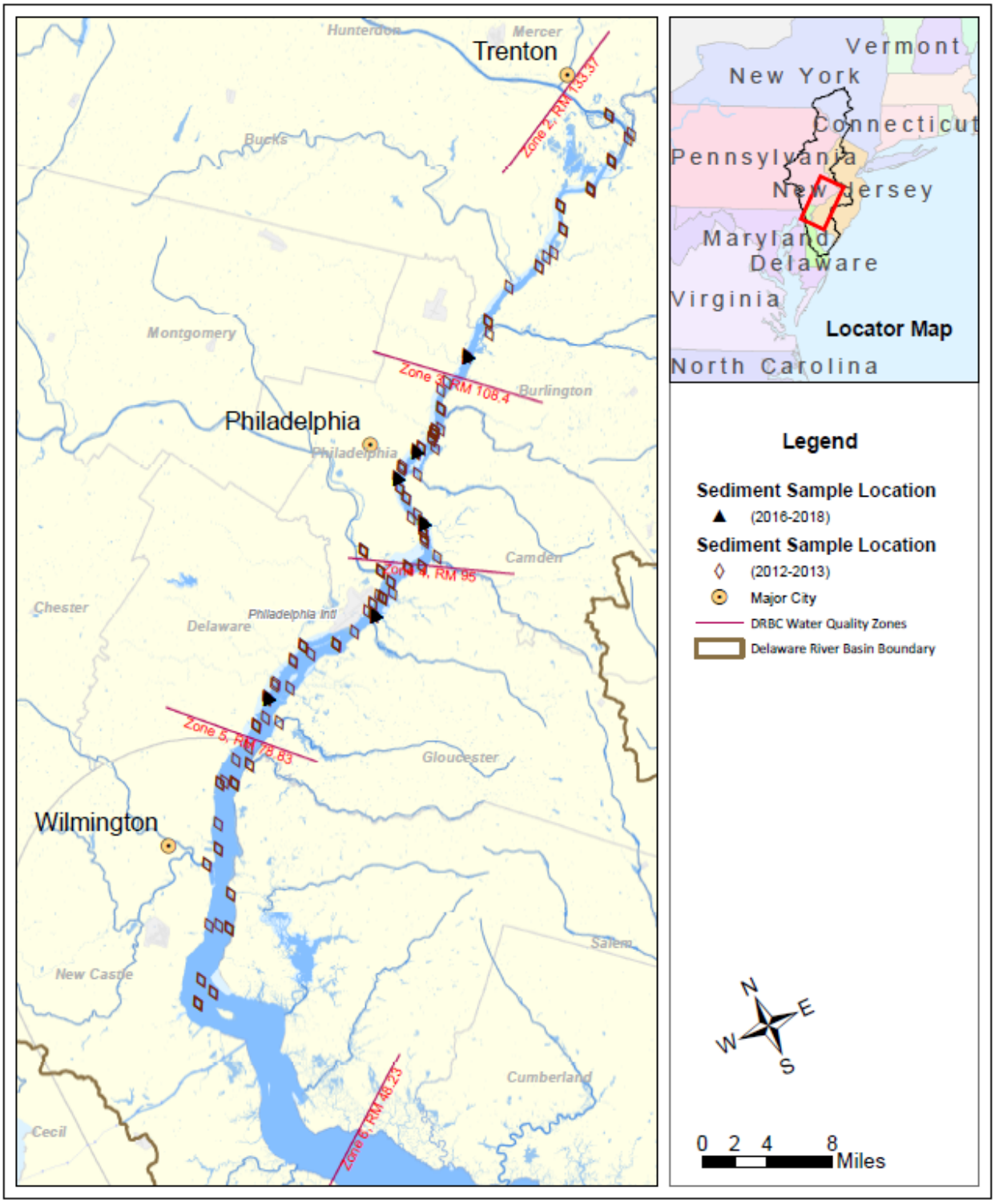

Figure 3-5: SOD and benthic flux survey locations

All benthic nutrient flux and SOD data are displayed by river mile on Figure 3-6. Comparing repeated SOD and benthic flux observations at five locations in 2012–2013 and 2016–2018, no apparent temporal trends

were observed (Figure 3-7 to Figure 3-10). Box plots display the minimum (bottom whisker), 25th percentile (bottom edge), median (middle line), 75th percentile (upper edge), and maximum (upper whisker) value among data collected at each location. For model SOD and benthic flux input assignments, data were grouped into relatively coarse bins (Figure 3-11). First, bins were delineated centered at each Boat Run station, then adjacent bins were combined so that each bin had at least five unique benthic flux measurements and at least 14 unique SOD measurements. Note that this methodology results in some differences between benthic flux bins and SOD bins. In the lower portion of Zone 5 (RM 48–63) and Zone 6 (RM < 48), where no measured data are available, SOD and initial SOD and benthic fluxes were assigned values from the adjacent bin (data collected from RM 63–73). While the basis for SOD and benthic flux assignments in Zone 6 and lower Zone 5 is limited, the impact of these assignments on the urban estuary, the critical area of concern, is negligible. Flux assignments were broadly benchmarked spatially by mapping average sediment organic carbon content and particle size, based on the assumption that higher SOC concentrations generally correspond to higher oxygen demand and nutrient release rates. Dotted lines on the benthic flux charts indicate the level at which net flux rate is zero; values above this line are positive fluxes into the water column, while values below the line are negative fluxes from the water column to the sediment.

SOD and benthic inputs were adjusted during calibration to improve model-data comparisons for water column DO and nutrient concentrations. SOD inputs were iteratively adjusted within the 10th and 90th percentiles of all available data, and a temperature adjustment was applied; benthic flux inputs were iteratively adjusted within the 10th and 90th percentiles of the August data, with no temperature adjustment applied. Final model inputs are shown as blue lines in Figure 3-11 and described broadly in Table 3-5. Data bins applied to benthic flux and SOD specifications are shown by alternate shading in Figure 3-11.

Table 3-5: SOD and benthic nutrient flux rates used in the water quality model based on survey data

Flux	Data included	Bay / Zone-6 (RM < 48)	ETM (RM 48–73)	Urban River (RM 73–115)	Upper River (RM > 115)
NH3-N	August	25 mg N/m^2/day	Median*	50–75th percentile*	75th percentile*
NO3-N	August	0 mg N/m^2/day	10th percentile*	10th percentile*	10th percentile*
DIP	August	6 mg P/m^2/day	Median*	25th percentile*	Median*
SOD	All	0.75 g O_2/m^2/day	75th percentile*	75–95th percentile*	90th percentile*

*Among measured values in each bin. Note these general regions are not bins. This table provides a high-level overview of the percentile ranges selected for individual bins.

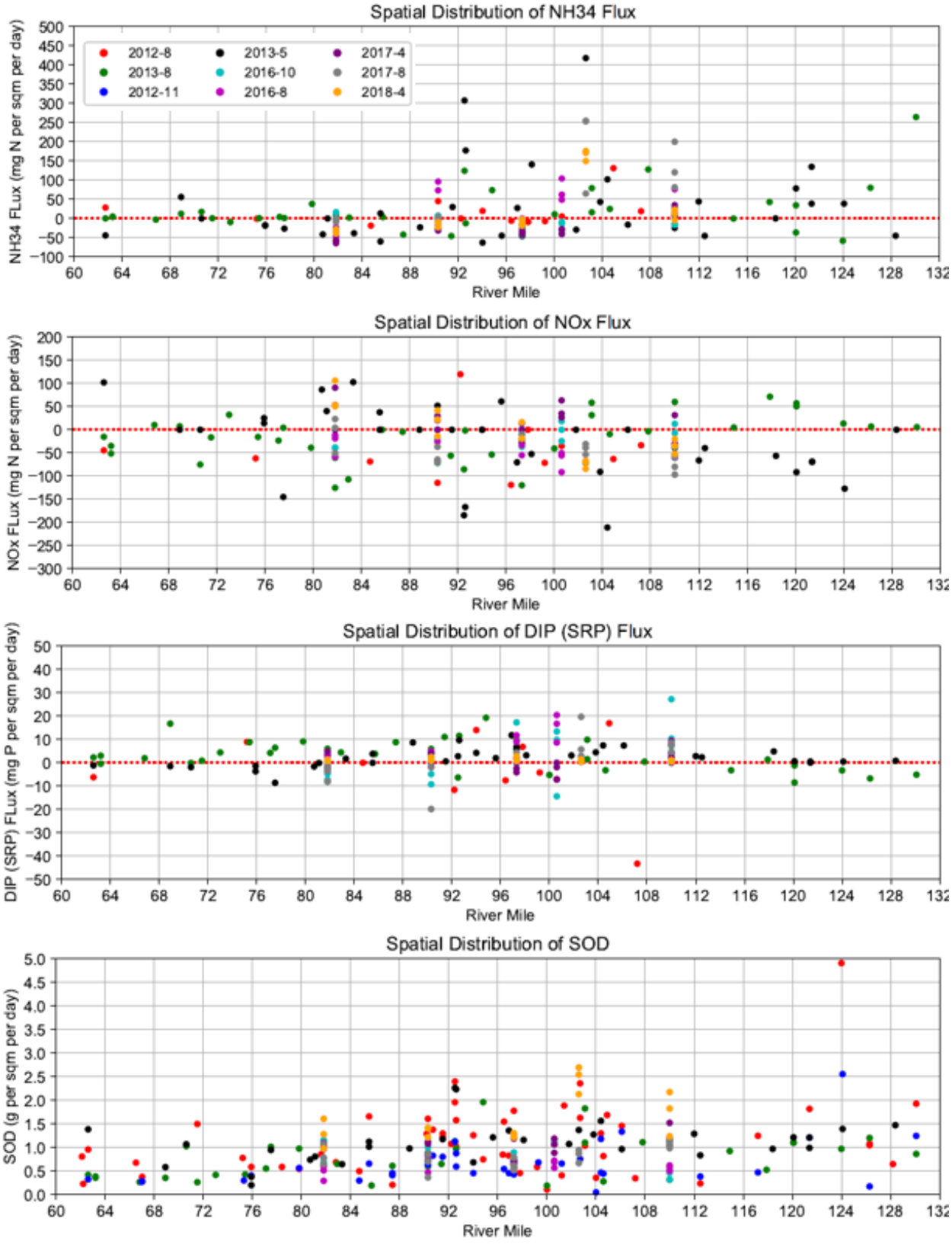

Figure 3-6: Spatial distribution of observed benthic nutrient flux and SOD data

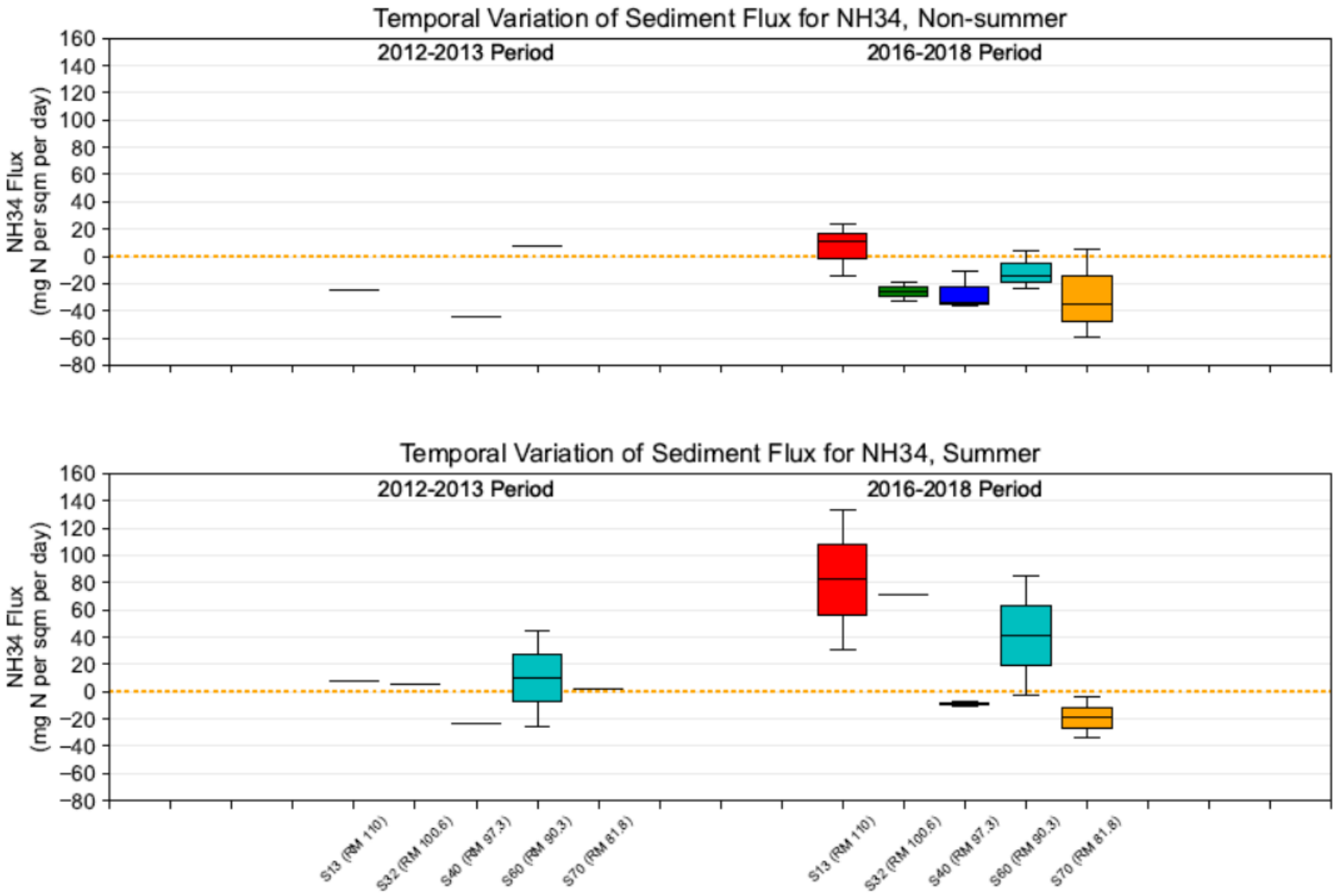

Figure 3-7: Temporal variation of sediment ammonia flux, summer vs. non-summer

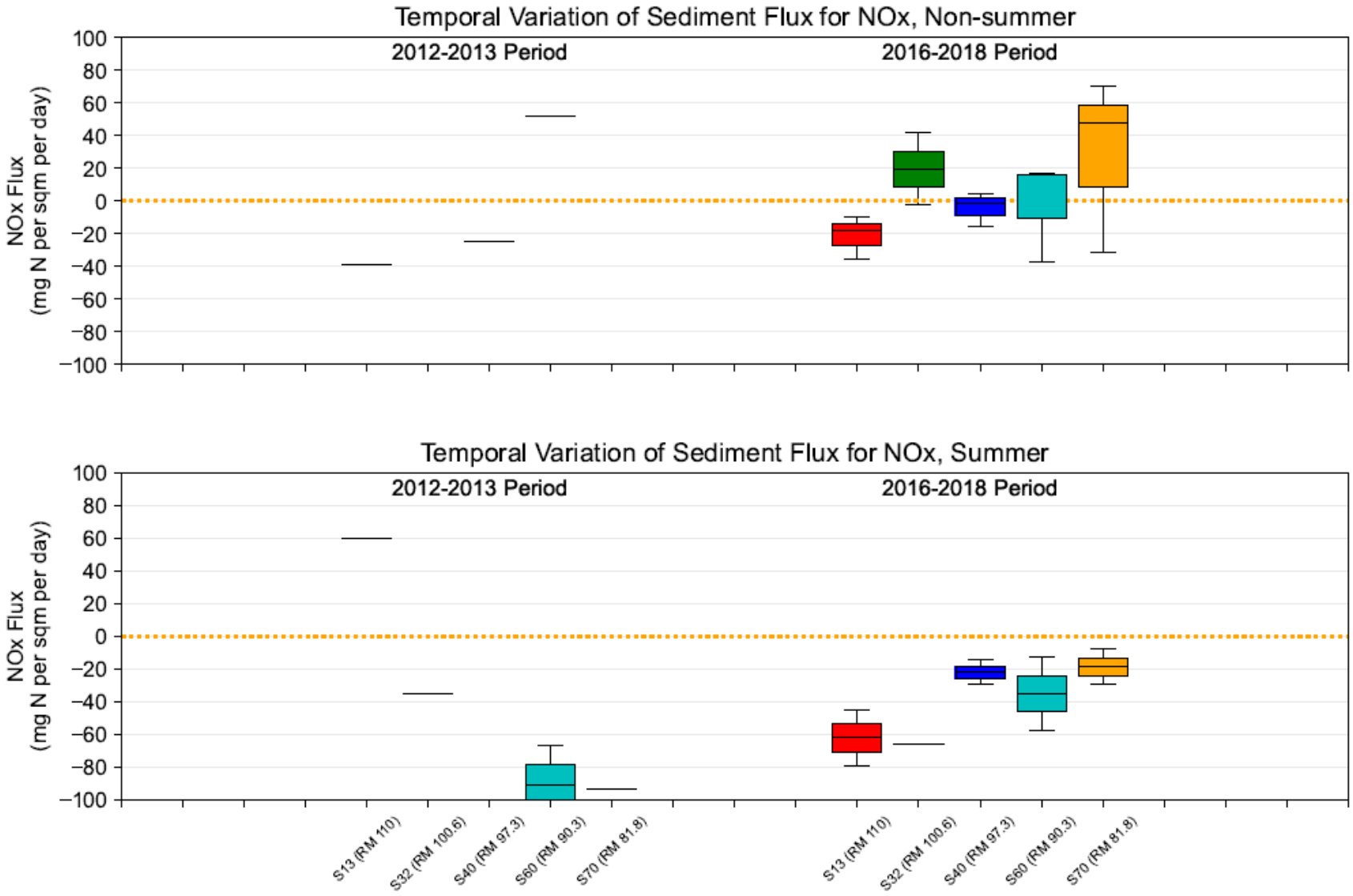

Figure 3-8: Temporal variation of sediment nitrate flux, summer vs. non-summer

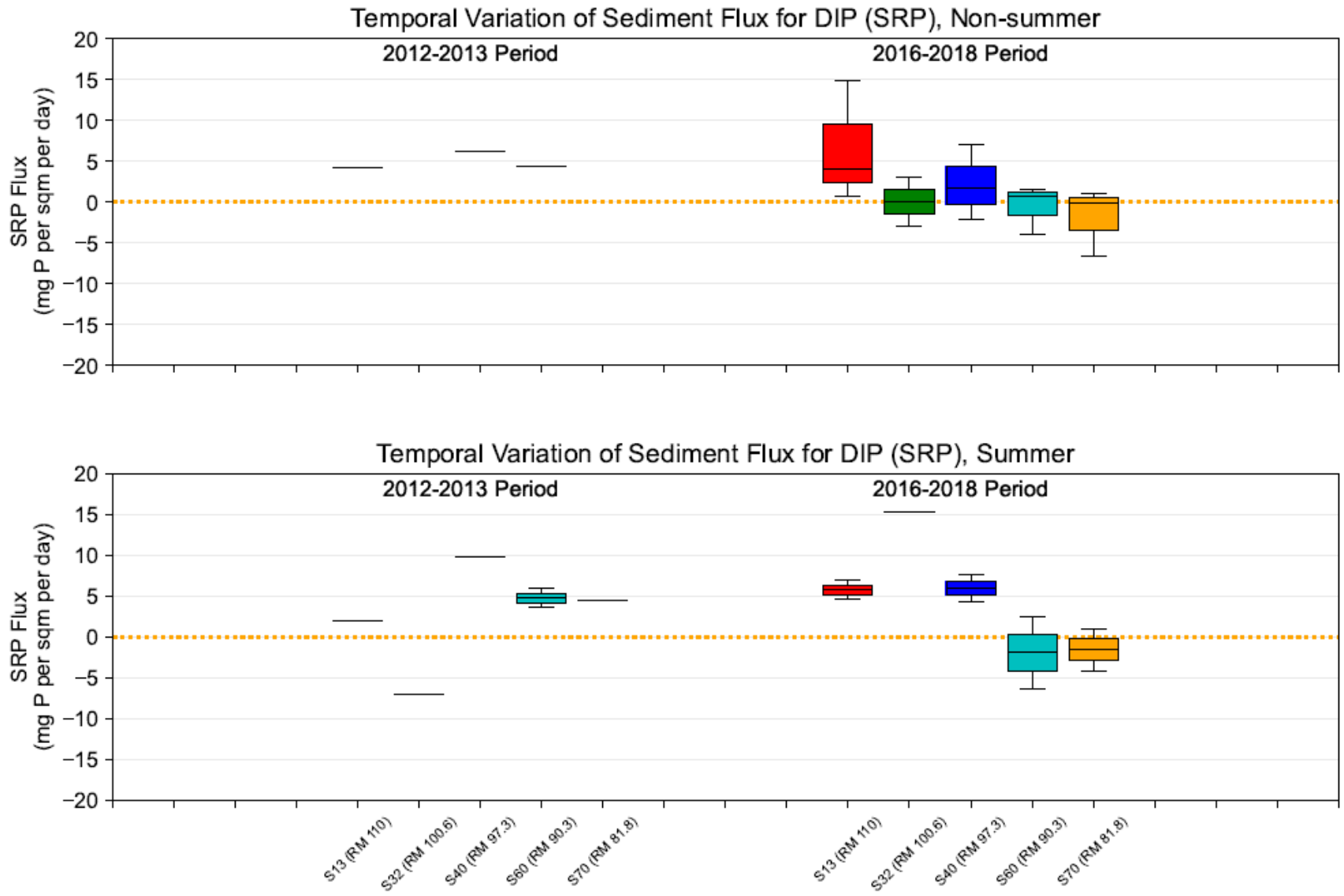

Figure 3-9: Temporal variation of sediment phosphate flux, summer vs. non-summer

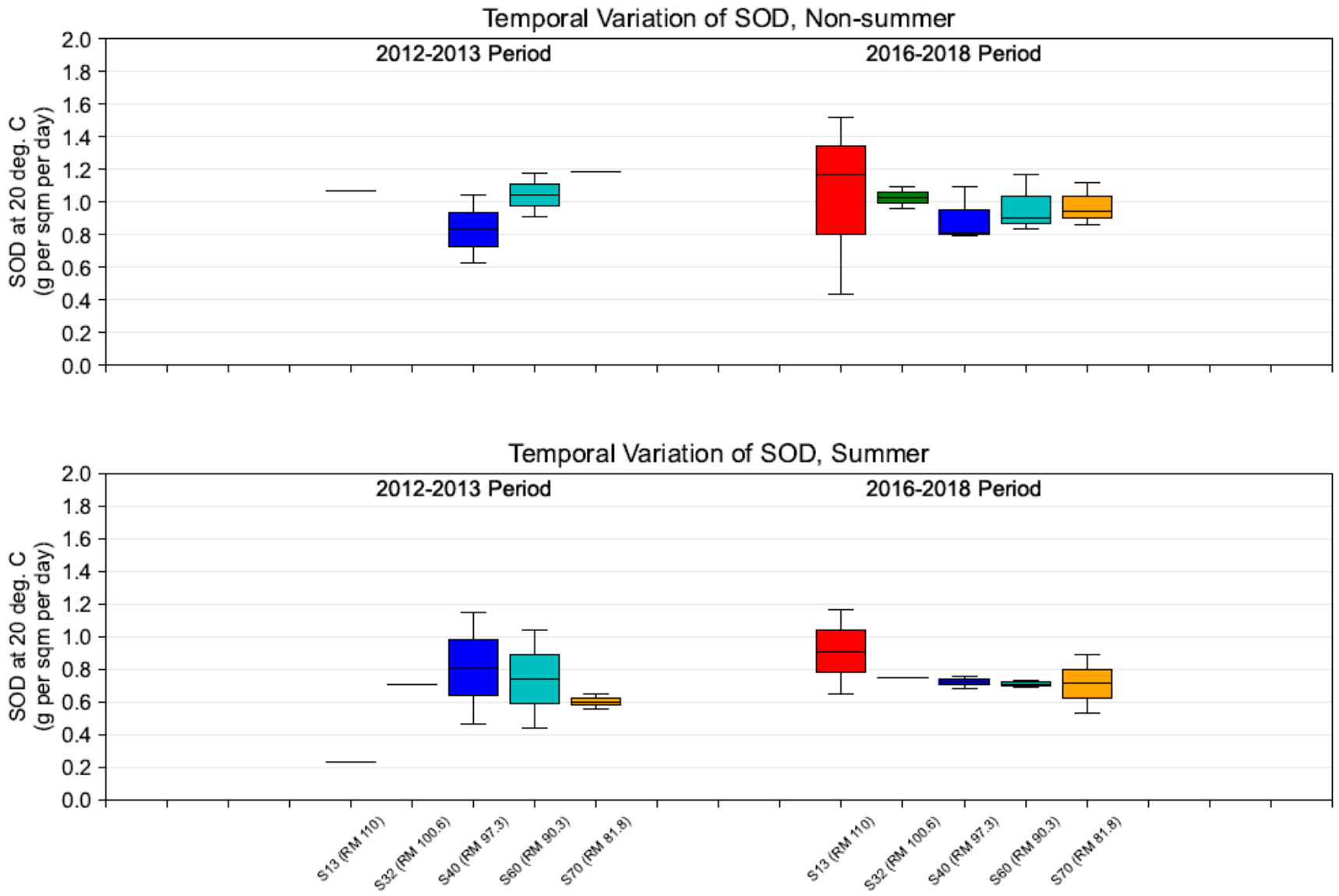

Figure 3-10: Temporal variation of SOD, summer vs. non-summer

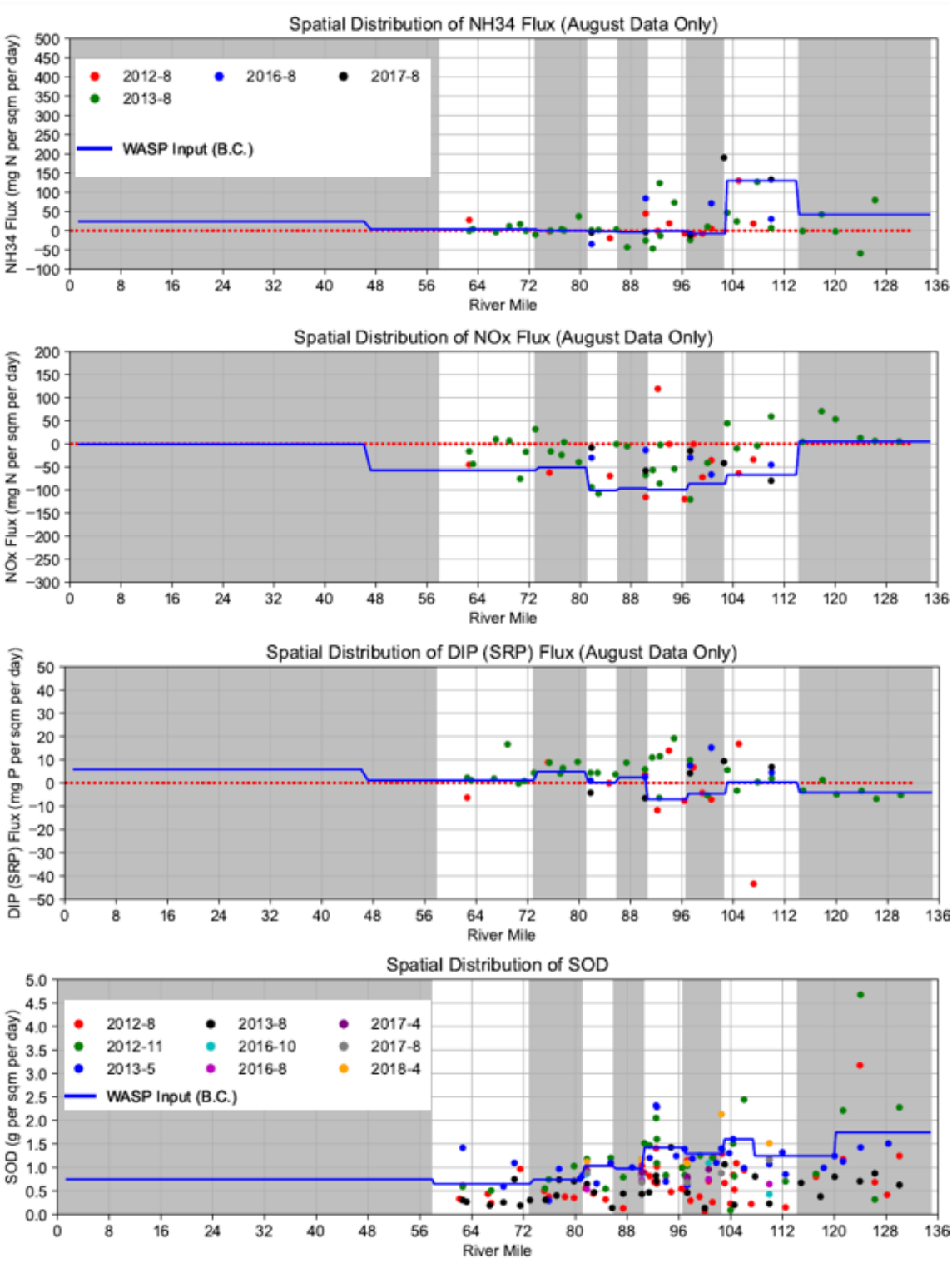

Note: data bins applied to benthic flux and SOD specifications are shown by alternate shading

Figure 3-11: Spatial distribution of benthic flux and SOD data summarized to bins

3.5.7 Initial Conditions

Initial conditions (initial concentrations for each state variable) are assigned to every active grid cell in the model domain, including salinity, water temperature, and components of flow, which are transferred through the hydrodynamic linkage files.

Initial conditions for each state variable were derived from data collected in the Estuary during the winter and early spring of 2012 and 2017–2018; values were assigned to each model grid cell using a proximity analysis. To minimize initial condition effects, the model was brought to a dynamic equilibrium by determining spin-up time and constituent behavior. Model spin-up time was determined by calculating the amount of time the model needed to reach equilibrium for a conservative tracer applied at each boundary. Simulations show that spin-up time within the model domain is highly variable; at and near significant tributary inflows in the upper portion of the tidal river spin-up time is relatively quick (2 to 4 days); farther downstream in the Estuary, the spin-up period increases and can range from 2 to 10 weeks, with the longest spin-up times coinciding with areas of greatest water age or residence time. Multiple, recursive 10-week runs were made with the fully loaded model for the 2018 and 2012 simulation periods, with output for each state variable subsequently reinitialized for the next run. The process was repeated until a quasi-steady state was achieved for concentrations of nitrogen, phosphorus, carbon, silica, and DO constituents. The resulting state variable concentrations were then applied as initial water column conditions. For the 2019 simulation year, state variable output from the 2018 simulation was used.

3.5.8 Hydrologic Conditions

The model calibration period was established for 2018-2019 based on the intensive data collection efforts performed to characterize model input concentrations and to establish model calibration targets in ambient waters for that period. The two largest inflows into the Delaware River Estuary are the Delaware River at Trenton, New Jersey (USGS 01463500), and the Schuylkill River at Philadelphia, Pennsylvania (USGS 01474500)., They contribute over 65% of the combined freshwater inflows in the Estuary, and annual statistics of their daily discharges over the past two decades are shown in Figure 3-12 and Figure 3-13. The two-year model calibration period of 2018-2019 is relatively wet. Due to this reason, the project team determined to corroborate the model for year 2012 which has relatively lower flow conditions especially in the summer season. These flow patterns are generally consistent with the precipitation pattern shown in Figure 3-14. Detailed information on the hydrologic conditions for 2012 and 2018-2019, such as time series of flow rates, is provided in the hydrodynamic model calibration report (Chen et al., 2024).

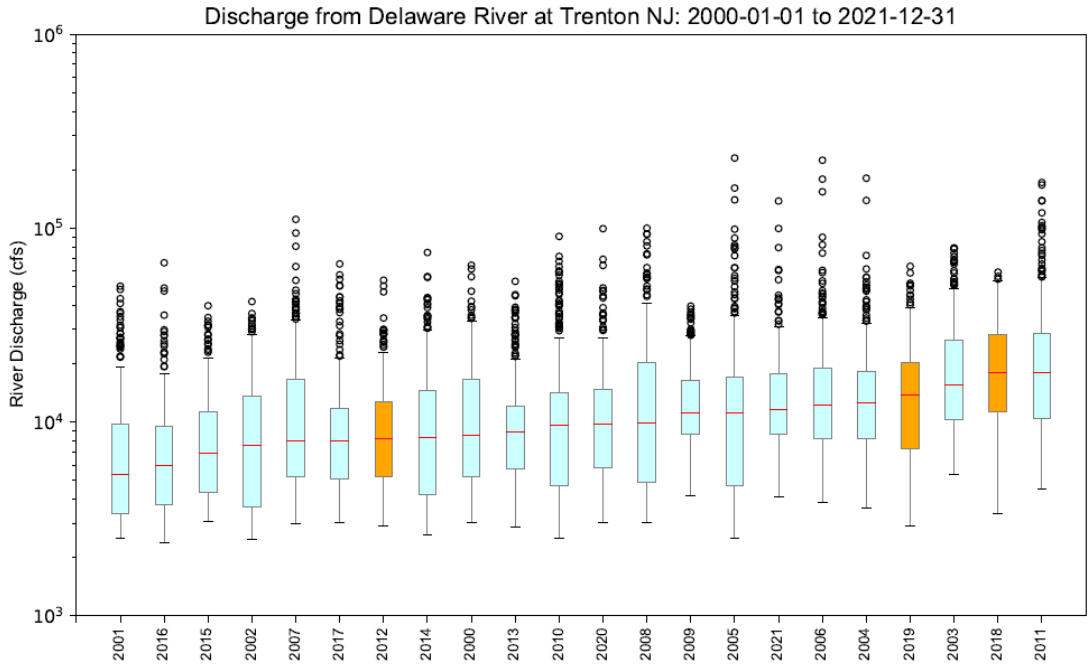

Figure 3-12: Daily flow by year at Delaware River at Trenton, New Jersey

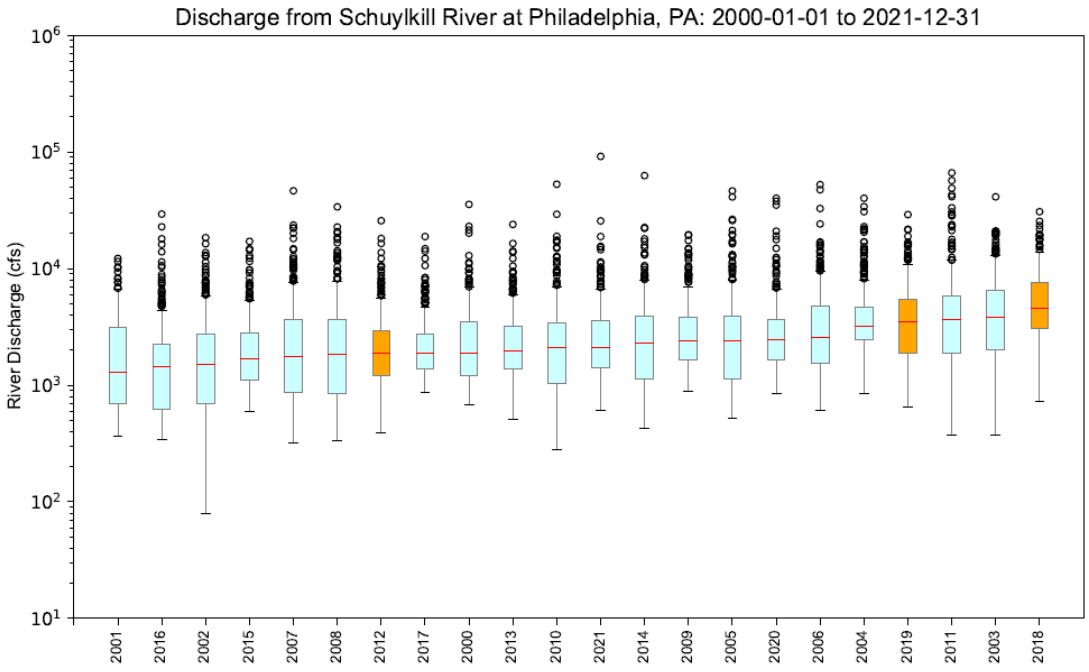

Figure 3-13: Daily flow by year at Schuylkill River at Philadelphia, Pennsylvania

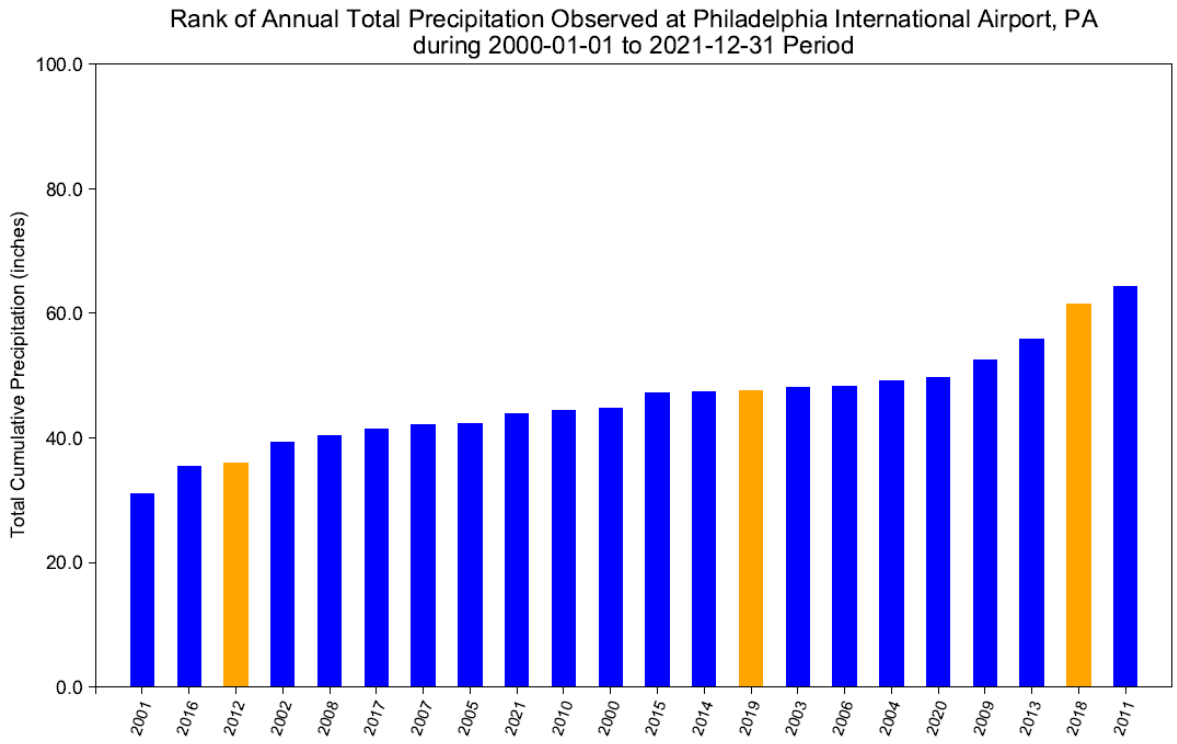

Figure 3-14: Annual Precipitation at Philadelphia, Pennsylvania

4. WATER QUALITY MODEL CALIBRATION

After the data inputs were developed to define the model initial conditions, boundary conditions, and inflows for the 20 state variables, Estuary-specific coefficients for the model's physical and kinetic equations were determined through comparisons of the observed and the simulated results for each state variable, information derived from sensitivity simulations, published values and ranges in the literature for similar systems, and professional judgement based on current science. This process is called model calibration. The primary focus of the model calibration was the period of April through October in Zones 2 through 5, representing the location and time period during which low dissolved oxygen conditions usually occur.

The utility of the model for making realistic predictions of future conditions rests on its ability to represent the physical, chemical, and biological processes that control the dynamics of the state variables. The ability of the model to simulate these processes was assessed by evaluating the performance of the model relative to measured water quality constituents.

Model calibration was conducted for the intensive monitoring period of 2018–2019. Next, the model was corroborated for 2012 using the same coefficients used for the 2018-2019 calibration. Year 2012 was selected for corroboration because it represented a "dry" summer with low DO concentrations, as compared to the relatively wetter conditions of 2018-2019. Also, 2012 had sufficient flow and nutrient data to characterize the point source discharges. However, less data for defining boundary conditions and comparing model results to ambient data were collected during 2012 as compared to the 2018–2019 calibration period. Therefore, the less extensive 2012 measured data were compared to the 2012 predicted model results to corroborate the model; however, the model coefficients were not adjusted to calibrate the model results from 2012 against measured data.

4.1 CALIBRATION DATA

Model-to-data comparison locations are shown in Figure 4-1, which include: DRBC Boat Run sampling stations, USGS continuous *in-situ* monitoring locations, and two additional continuous *in-situ* buoys deployed by the PWD during the 2018-2019 calibration period.

Multiple parameters collected by the DRBC Boat Run (depicted in Section 2.1.1.1) were selected to calibrate and corroborate the model, including: dissolved organic carbon (DOC), ammonia nitrogen (NH34), nitrite and nitrate nitrogen (NO3O2), total nitrogen (TN), orthophosphate (D-DIP), total phosphorus (TP), chlorophyll-a (PHYTO), inorganic suspended solids (SOLID), dissolved oxygen (DISOX), and dissolved oxygen percent saturation (DOSAT). There are about 21 monitoring events for each parameter at a given station during the calibration years of 2018–2019 and 7 monitoring events during the corroboration year of 2012. All data were collected at the water surface at a monthly interval.

Continuous dissolved oxygen and chlorophyll-a data collected by the USGS (Section 2.1.1.2) were also used to assess model performance. These data were reported at a 15-minute interval. Chlorophyll-a data were available only at the Ben Franklin Bridge station for the calibration period 2018–2019. Dissolved oxygen observations at the Pennypack Woods station started in October 2018. USGS sondes are typically deployed at two to three feet below water surface during low tide (personal communication with USGS staff).

The buoy survey program conducted by PWD and Woods Hole Group included collection of continuous dissolved oxygen, chlorophyll-a, and other parameters along the Delaware River Estuary (Section 2.1.1.2). These parameters were measured at about one meter below the water surface and reported at a 12-minute interval. Data from Buoys B and P (Figure 4-1) covered the model calibration period of 2018–2019 and were used to help calibrate the model.

Transect profile surveys have been conducted by USGS at selected locations adjacent to USGS stations, where dissolved oxygen and other parameters were measured along the transects and at different depths. Five surveys were included during the period of model calibration and corroboration (Table 4-1). Dissolved oxygen data from these surveys were used to evaluate model performance.

Table 4-1: USGS transect surveys conducted during 2012, 2018, and 2019

Date	Location	River Mile
July 24, 2019	Pennypack Woods	110.5
December 4, 2019	Ben Franklin Bridge	100.0
October 11, 2012	Ben Franklin Bridge	100.0
July 19, 2018	Delaware Memorial Bridge	68.9
June 7, 2019	Reedy Island	54.0

Figure 4-1: Calibration data locations

4.2 CALIBRATION APPROACH

In accordance with the established Quality Assurance Project Plan (DRBC, 2019) for this project, a "weight of evidence" approach was used in close coordination with the Model Expert Panel and DRBC's modeling consultants in order to judge the acceptability of the model for its intended purpose. Model calibration was managed through the processes below:

- Initial model testing was performed to examine whether the nutrient loads into the system were specified correctly. This was accomplished by disabling kinetics and settling velocities, but leaving all the boundary conditions, thereby testing the model with nutrients as conservative substances. The goal of this testing was to ensure more than sufficient predicted dissolved organic carbon, total nitrogen, and total phosphorous concentrations were present throughout the system in comparison to observations. This testing was essentially used to flag and correct possible issues with boundary mass loadings being underestimated.
- A faster, two-dimensional (2D) depth-averaged water quality model was used as a surrogate to guide three-dimensional (3D) calibration testing, considering: (1) the urban area of the Estuary is well-mixed, and (2) there is a significant difference in computation time between the two models, i.e., 1.5-hr per simulation year for the 2D model, compared to 32-hr per simulation year for the 3D model.
- A series of initial sensitivity analyses were conducted with the 2D model to understand the responses of key parameters and processes and to identify the calibration parameters to which the model responses would be most sensitive.
- An iterative process of incremental calibration of the coefficients (rate constants) for the physical and kinetic equations was carried out, starting with preliminary calibration of dissolved organic carbon, nitrogen, phosphorus, and dissolved oxygen without phytoplankton. Next the calibration incorporated phytoplankton, and then spatial variation of sediment oxygen demand and benthic nutrient fluxes was introduced.
- Dissolved oxygen component analyses were used to understand the model behavior and identify the relative importance of dissolved oxygen-impacting processes over space and time within the entire Estuary.
- Phytoplankton outputs were grouped to the growth seasons of the three modeled algal communities and compared with *in-situ* data and long-term trends.
- Model-to-data comparisons were comprehensively evaluated, using: (1) spatial and longitudinal plots for individual Boat Run sampling events; (2) time series plots, 1-to-1 plots, cumulative frequency distributions, target diagrams, and statistical metrics for individual stations; and (3) lateral and vertical profiles of dissolved oxygen for individual surveys. The judgment of model calibration fit used both qualitative and quantitative methods.
- Model calibration coefficients were adjusted based on site-specific field and laboratory data, published literature, results from model applications to other similar sites, and guidance from the Model Expert Panel, based on their many decades of collective experience with water quality model development and application. Thus, the final set of model parameters resulted in a model that is consistent with scientific understanding of the underlying processes, field and laboratory studies of these processes, and the particular conditions of the Delaware River Estuary.

4.3 Calibration Parameters

Coefficient values for model physical and kinetic processes were adjusted within logical ranges to improve the ability of the model-predicted results to agree with the measured data. See details in Section 4.4.1. A complete description of the model parameters and their final calibration values are listed in Appendix F (specifically F-1). Key parameters are shown in Table 4-2.

Table 4-2: Key calibration coefficients used in water quality model

Coefficient	Value
Nitrification Rate Constant @20°C (1/day)	0.6
Nitrification Temperature Coefficient (dimensionless)	1.1
CBOD Decay Rate Constant @20°C (1/day)*	0.033 / 0.087 / 0.001
CBOD Decay Rate Temperature Correction Coefficient (dimensionless)*	1.065 / 1.065 / 1.065
Phytoplankton Maximum Growth Rate Constant @20°C (1/day)**	4 / 3.75 / 4
Phytoplankton Carbon to Chlorophyll Ratio (mg C/mg Chl)**	40 / 30 / 40
Phytoplankton Respiration Rate Constant @20°C (1/day)**	0.03 / 0.05 / 0.03
Phytoplankton Death Rate Constant (Non-Zoo Predation) (1/day)**	0.02 / 0.08 / 0.05
Phytoplankton Settling Velocity (m/day)**	0.1 / 0.1 / 0.2
POM Settling Velocity (m/day)	0.2
Solid Settling Velocity (m/day)	1
SOD and Benthic Fluxes of Ammonia and Phosphate	Spatially variable (see Table 3-5)

* Three types of CBODU (stream/ point source/ refractory) are simulated.
** Three classes of phytoplankton assemblages (spring marine / summer freshwater/ summer marine diatom community) were calibrated independently. See the justification for algae representation in Appendix K.

4.4 Calibration Results

Overall model performance should be evaluated both qualitatively and quantitatively, and model acceptance is a decision that involves both approaches. For efficient post-processing, model results were extracted every two hours and compared to measured data. Longer intervals (e.g., daily or seasonal) were used when comparing phytoplankton concentrations, given the associated uncertainty (e.g., transient light attenuation and water clarity).

4.4.1 COMPARISONS TO DRBC BOAT RUN DATA

Model simulation results from the surface layer at the locations of Boat Run monitoring stations were extracted and compared to the observed Boat Run data. Spatial and temporal comparisons for key state variables are presented in this section.

For spatial comparisons (see Figure 4-2, for example), each Boat Run event from the summer months (i.e., June to August) for the calibration years 2018–2019 and corroboration year 2012 are graphically presented. The complete set of comparisons for the three-year period are available in Appendix F (specifically F-2). Each panel in the plots represents a single survey event, with the observed Boat Run data displayed as red solid circles, and the computed daily ranges and medians on the survey dates shown as shaded areas and dashed lines, respectively. The plots provide a snapshot of spatial comparisons of the state variables. Overall, the absolute magnitudes and spatial patterns of the state variables/parameters are reproduced reasonably well by the model.

For temporal comparisons (see Figure 4-3, for example), model simulation results for each state variable were also compared to the observed Boat Run data for the two-year calibration period. Considering the large number of plots required (22 stations for each of 20 state variables, or 440 plots) to show all of the data in this format, comparisons from one station (the Navy Yard at RM 93.2) are discussed in this report in the ensuing sections. The Navy Yard station was selected because the minimum dissolved oxygen sag is typically located near this station. Comparisons at three additional station locations (Ben Franklin Bridge at RM 100.2, Paulsboro at RM 87.9, and Marcus Hook at RM 78.1) within the urban area of the Delaware River Estuary are also presented in Appendix F (specifically F-3). In these temporal comparison plots, the top left panel illustrates time series of model predictions with the observed data overlain as individual points. The top right panel displays scatter plots (also known as 1-to-1 or 1:1 plots) comparing the paired model predictions and observed data points with a best-fitting linear regression line (dashed red line) and 1:1 line (blue line). In a perfect match between model and data, all points would lay on the 45 degree 1:1 line, and the red dashed line would overlay the blue line. The bottom left panel shows the cumulative frequency distribution curves for the paired model predictions (black line) and observed data (red line). A cumulative frequency distribution reveals how good the model predictions are compared with data at the low end, mid-range, and high end, respectively. The bottom right panel reports several common summary and goodness of fit statistics, as well as maps showing the station locations. Model results shown in the 1:1 plots, cumulative frequency distributions, and statistics are interpolated values at the exact time the monitoring data were collected. Overall, the absolute magnitudes of the state variables/parameters, their seasonal patterns, and their cumulative frequency distributions are adequately reproduced by the model.

A series of statistical metrics summarized by EPA Region 4 (Appendix B of Davis, 2019) were applied to provide a statistical assessment in this study. An overview of selected metrics is provided below.

- Coefficient of determination (R^2) – Assesses the strength of the linear relationship between observed and simulated data. Describes the proportion of variation in the observed data that is

explained by a simple linear regression relating observed and simulated data. Values of R^2 range from 0 to 1, with better fitting models possessing higher R^2 values.

$$R^2 = \left[\frac{\sum_{i=1}^{N}(O_i - \overline{O})(S_i - \overline{S})}{\sqrt{\sum_{i=1}^{N}(O_i - \overline{O})^2} \times \sqrt{\sum_{i=1}^{N}(S_i - \overline{S})^2}}\right]^2 \quad (4\text{-}1)$$

where *O* and S represent "Observation" (i.e., data) and "Simulation", respectively.

- Mean Absolute Error (MAE) – Measures the average magnitude of the difference (i.e., error) between observed and simulated data. It does not consider the direction of those differences (i.e., whether the model is over or underpredicting) or natural variability in the observed data. Calculated similarly to Mean Error, but the absolute value of the difference is taken.

$$\text{MAE} = \frac{1}{N}\sum_{i=1}^{N}|S_i - O_i| \quad (4\text{-}2)$$

- Nash–Sutcliffe Coefficient (NSE) – This metric is closely related to mean square error and root mean square error. Using the mean of the observed data as a baseline, it assesses the magnitude of the difference in observed and simulated data relative to the residual variance (i.e., natural variation) of the observed data. This unitless metric indicates how well the linear fit of observed versus simulated data fits a 1:1 line. Values range from -Infinity to 1, whereby NSE = 1 represents a perfect match of simulated and observed data, NSE = 0 indicates that model predictions are as accurate as the mean of observed data, while NSE = –Infinity indicates that the mean of observed values is a better predictor than simulated data.

$$\text{NSE} = 1 - \frac{\sum_{i=1}^{N}(S_i - O_i)^2}{\sum_{i=1}^{N}(O_i - \bar{O})^2} \quad (4\text{-}3)$$

- Root Mean Square Error (RMSE) – Measures the difference (i.e., error) between observed and simulated data. This metric provides assurance that the model is matching the frequency, magnitude, and duration of water quality changes. However, it does not account for natural variability in observed data. Values of RMSE range from 0 to infinity, with RMSE = 0 indicating a perfect match between observed and simulated data.

$$\text{RMSE} = \sqrt{\frac{1}{N}\sum_{i=1}^{N}(S_i - O_i)^2} \quad (4\text{-}4)$$

- Index of Agreement, or Skill Factor (d) – Provides a measure of model error relative to natural variability (i.e., error). Values range from 0 to 1, with an index of agreement = 1 indicating a perfect fit of simulated and observed data, and a value of 0 indicating no agreement between them.

$$d = 1 - \frac{\sum_{i=1}^{N}(S_i - O_i)^2}{\sum_{i=1}^{N}(|S_i - \bar{O}| + |O_i - \bar{O}|)^2} \quad (4\text{-}5)$$

Table 4-3 lists the average values of statistical metrics over all 22 Boat Run stations for each state variable during the calibration period 2018–2019. Definitions for all statistical metrics are provided in Appendix F-4, while the complete statistical metrics for all parameters at each Boat Run station are available in Appendix F-5. Note that the number of observations for each state variable from the Boat Run survey are limited, since the surveys are conducted on a monthly basis. More weight should be given to the continuous data comparisons in Section 4.4.2 when evaluating model statistics.

These statistical metrics were computed for all paired model-data values at each Boat Run survey station. The values of the statistical metrics varied noticeably by location, the state variable/parameter, and the metric itself. Of all state variables/parameters, dissolved oxygen has the highest values of R^2 (0.94), Nash-Sutcliffe Coefficient (0.90), and index of agreement (0.98). A value of 1 in these metrics indicates a perfect fit between model predictions and observed data (Davis, 2019, Appendix B). Conversely, phytoplankton had the lowest values of R^2 (0.21), Nash-Sutcliffe Coefficient (-0.25), and index of agreement (0.59). Note that a value of 0 in the Nash–Sutcliffe Coefficient indicates that the model predictions are as accurate as the mean of the observed data, and a value of 0 in the index of agreement indicates no agreement between the predictions and observations (Appendix B of Davis, 2019). Chlorophyll-a levels in the Delaware River Estuary are highly variable in general as phytoplankton populations respond to light, nutrient, water temperature, and hydrodynamic flow patterns. Further investigation of phytoplankton dynamics and growth limitations is discussed in Section 4.5. For the dissolved organic carbon (DOC), nitrogen (NH34, NO3O2, and TN), and phosphorus (D-DIP and TP), the R^2 ranged from 0.35 to 0.64; the Nash-Sutcliffe Coefficient ranged from -0.02 to 0.56; and the index of agreement ranged from 0.67 to 0.85, indicating reasonably good agreement between the model predicted and observed values. In a tidal environment, model predictions lead or lag by a relatively short time (e.g., a few hours), and the resulting values of R^2, Nash-Sutcliffe Coefficient, and index of agreement can be highly affected. Moreover, the model captures reasonably well the absolute concentrations, as well as the spatial and temporal trends, of these state variables/parameters indicating that the model adequately reflects inter-annual changes of carbon, nitrogen, and phosphorus in the system.

In the following sections, spatial and temporal comparisons between the computed and the observed data are presented graphically for each of the key state variables (DOC, NH34, NO23, TN, D-DIP, TP, solids, phytoplankton, DISOX, and DOSAT), together with brief descriptions of the calibration approach.

Table 4-3: Average statistical metrics at the 22 Boat Run Stations, 2018–2019

Metric	D-DIP	DISOX	DOC	DOSAT	NH34	NO3O2	PHYTO	TN	TP
Number of Observations	21	21	21	21	21	21	21	21	21
Observed Mean	0.04	8.97	3.03	91.47	0.11	1.19	10.46	1.60	0.09
Observed Variance	0.00	4.71	0.44	68.84	0.01	0.18	114.59	0.16	0.00
Simulation Mean	0.05	8.83	3.00	89.18	0.06	1.22	6.81	1.71	0.09
Simulation Variance	0.00	5.21	0.36	80.70	0.00	0.12	38.16	0.14	0.00
Mean Error	0.01	-0.15	-0.04	-2.29	-0.05	0.03	-3.66	0.10	0.00
Mean Absolute Error	0.01	0.48	0.37	4.93	0.06	0.17	6.36	0.20	0.02
RMSE	0.02	0.60	0.50	6.22	0.08	0.24	9.77	0.26	0.03
NRMSE %	26.43	9.05	23.75	23.40	26.87	16.99	27.91	19.36	26.20
R2	0.59	0.94	0.46	0.60	0.56	0.63	0.21	0.64	0.35
Spearman Coeff.	0.73	0.95	0.62	0.69	0.58	0.77	0.59	0.77	0.48
PBias	12.39	-1.66	-1.55	-2.60	-46.01	2.81	-35.44	6.93	1.59
Nash	0.13	0.90	0.08	0.08	0.03	0.56	-0.25	0.43	-0.02
Index of Agreement	0.81	0.98	0.76	0.81	0.67	0.85	0.59	0.85	0.68
Kling-Gupta Effic. Modified	0.64	0.89	0.60	0.63	0.27	0.67	0.22	0.72	0.40
Kling-Gupta Pear. Coeff.	0.76	0.97	0.64	0.73	0.66	0.77	0.42	0.79	0.49
Kling-Gupta Beta (Ratio Means)	1.12	0.98	0.98	0.97	0.54	1.03	0.65	1.07	1.02
Kling-Gupta Gamma (Ratio CV)	0.96	1.07	0.99	1.14	0.99	0.83	1.00	0.89	0.82

4.4.1.1 DISSOLVED ORGANIC CARBON (DOC)

Calibration approach: The WASP model employed ultimate CBOD (or CBODU) as a state variable, and DOC was computed internally. Three types of CBOD were simulated to represent ultimate CBOD from streams, point sources, and a refractory component. The assignment of CBOD decay rates at 20^{o} C were based on a 90-day BOD experiment, with 0.033/day and 0.087/day used for the CBOD originating from streams and point sources, respectively. A smaller decay rate of 0.001/day was used for the refractory CBOD. Temperature correction coefficients for CBOD decay rates were selected to achieve optimum agreement between predicted and observed dissolved organic carbon. A final temperature correction coefficient of 1.065 was used for all three CBOD types. Zion et al. (1978), Bowie et al. (1985), and Chapra (1997) have reported a range of 1.02 to 1.09 for temperature correction coefficients for numerous rivers around the country.

Spatial comparisons: DOC predicted by the model matched the measured data reasonably well, both in absolute concentrations and spatial patterns, e.g., relatively high levels in the tidal river and relatively low levels in the Bay. Figure 4-2 shows spatial comparisons of DOC for the model predicted versus measured Boat Run data from June through August during each of the calibration and corroboration years.

Temporal comparisons: Figure 4-3 shows temporal comparisons of DOC for the model predicted versus measured Boat Run data at the Navy Yard station for the 2018-2019 calibration period. This figure also shows linear regression results, a cumulative frequency distribution, and statistical measures for the data comparison at this station. Discounting a few apparent outliers, the model captures DOC concentrations at Navy Yard reasonably well.

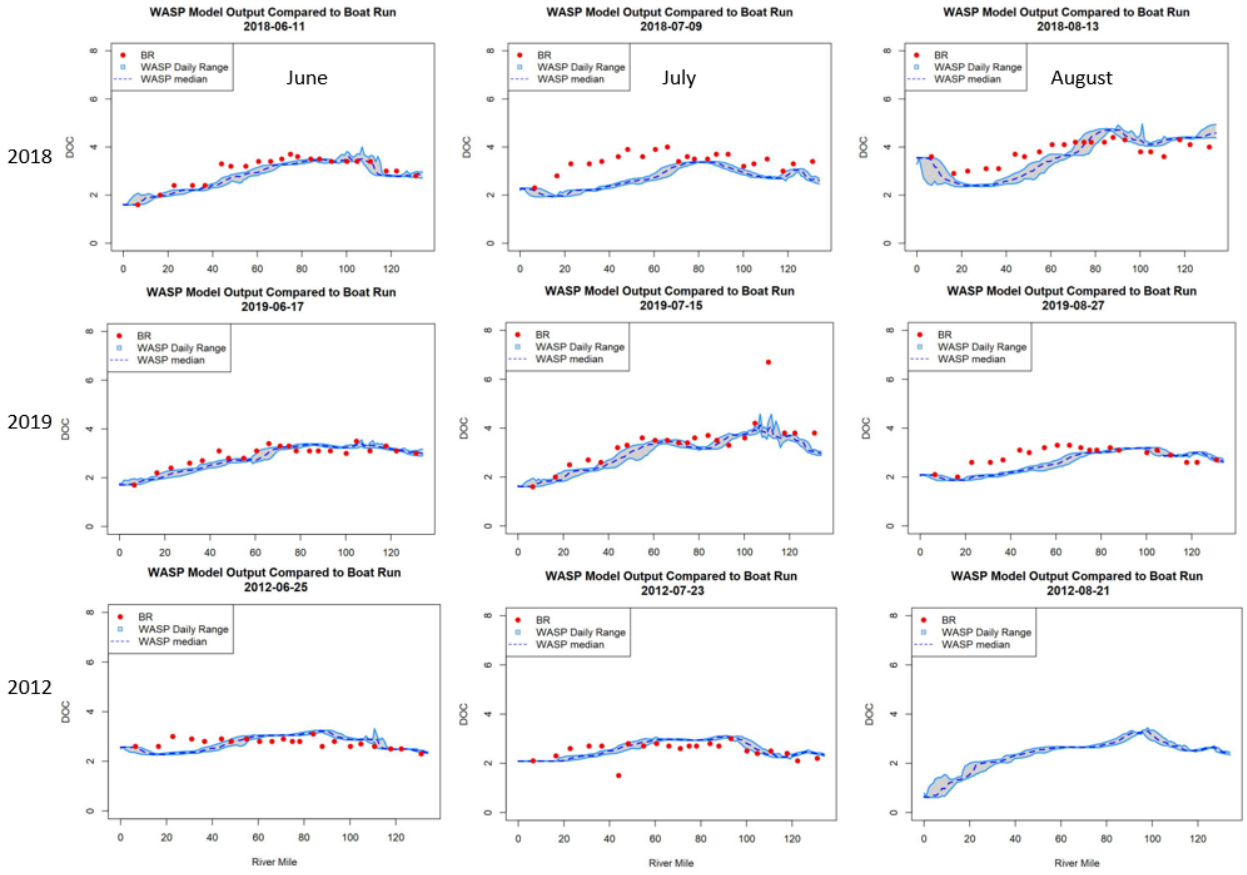

Figure 4-2: Model to Boat Run data spatial comparisons – DOC during summer

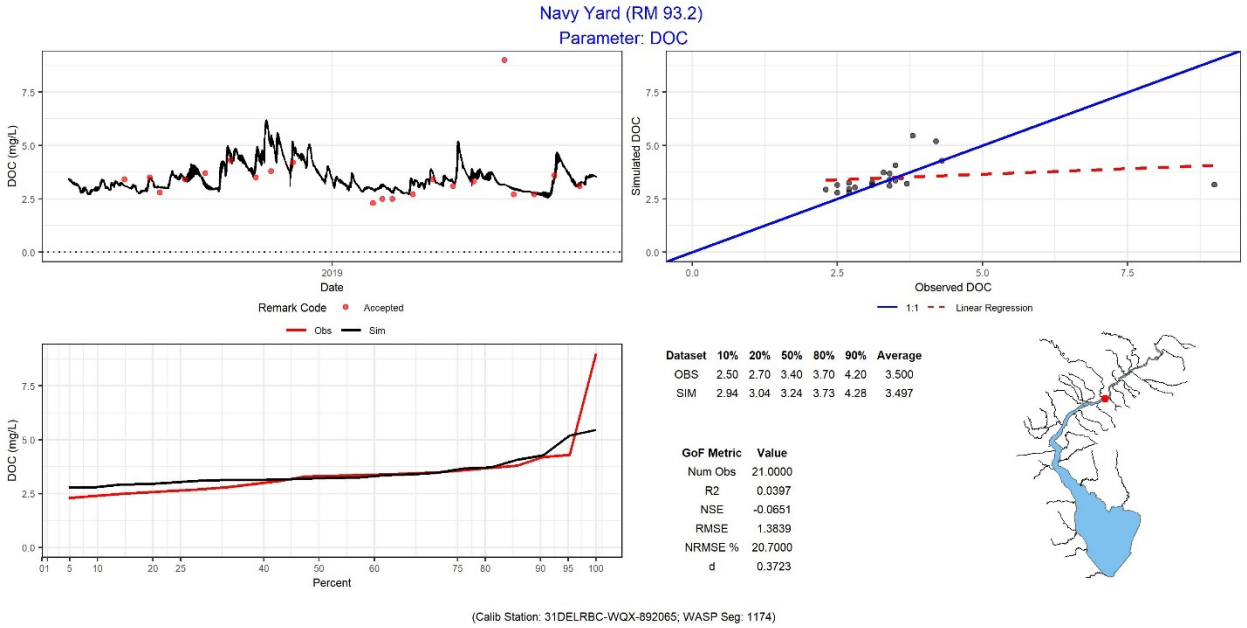

Figure 4-3: Model to Boat Run data temporal comparison – DOC at Navy Yard, 2018–2019

4.4.1.2 NITROGEN (NH34, NO3O2, AND TN)

Calibration Approach: The nitrification rate, together with a water temperature correction coefficient, was determined within a range of uncertainty to best match the observed ammonia nitrogen (NH34) and nitrite + nitrate (NO3O2, hereinafter nitrate) levels for the entire model domain and throughout the year. However, the selection of the nitrification rate and temperature correction coefficient were biased to best calibrate the model in the urban area of the Estuary during the summer period that is critical to fish propagation. A final nitrification rate of 0.6/day at 20° C, and a corresponding temperature coefficient of 1.1, were used. The current WASP model code does not support the option of varying the nitrification rate spatially within the domain. The final nitrification rate of 0.6/day is around the 40th percentile of observed nitrification rates for the Delaware River, ranging from 0.01 to 2.20/day, as measured by the Philadelphia Water Department (PWD) in August 2013 (Figure 4-4). Zion et al. (1978) and Bowie et al. (1985) have reported a range of 0.02 to 3.00/day for the nitrification rate at 20° C, and 1.02 to 1.10 for temperature coefficient, for numerous rivers around the country.

Spatial comparisons: Figures 4-5, 4-7, and 4-9 show spatial comparisons of ammonia, nitrate, and TN concentrations, respectively, for the model predicted versus measured Boat Run data from June through August during each of the calibration and corroboration years. The simulated concentrations compared generally well with the measured data during summer. The observed and predicted concentrations of ammonia were elevated in the urban area (e.g., RM 80–110). However, a single nitrification rate with water temperature correction coefficient, rather than spatial varying nitrification rates, was employed in WASP. As a result, the model over-predicts nitrification around RM 20–80 during spring (see relevant figures in Appendix F-2). The model generally captured the absolute concentrations and spatial patterns of nitrate and TN during multiple surveys across three years. Both the model results and the measured data demonstrated that the peak concentrations of nitrate and TN occurred in the urban area of the Estuary around RM 70–110. The model slightly over-predicted the TN concentrations in the middle of the Estuary in 2012; the uncertainty in point source nutrient concentrations in 2012 due to limited data availability seemed to be a major contributor.

Temporal comparisons: Figures 4-6, 4-8, and 4-10 show temporal comparisons of ammonia, nitrate, and TN, respectively, for the model predicted versus measured Boat Run data at the Navy Yard station for the 2018-2019 calibration. The observed and predicted ammonia concentrations and seasonal patterns were similar – elevated in spring and winter and depressed in summer due to temperature impacts on the nitrification rate. The model under-predicted ammonia at higher concentrations, perhaps due to the single nitrification rate employed in the WASP model or/and due to the simplified representation of temperature effects on nitrification (a biologically mediated reaction). These differences in ammonia magnitude are not significant but are driven by exactly how quickly at any point in space and time nitrification occurs. In general, the model reproduced the nitrate and TN concentrations, seasonal patterns, and cumulative frequency distributions quite well. Both observed and predicted concentrations reach peak values in summer or early fall.

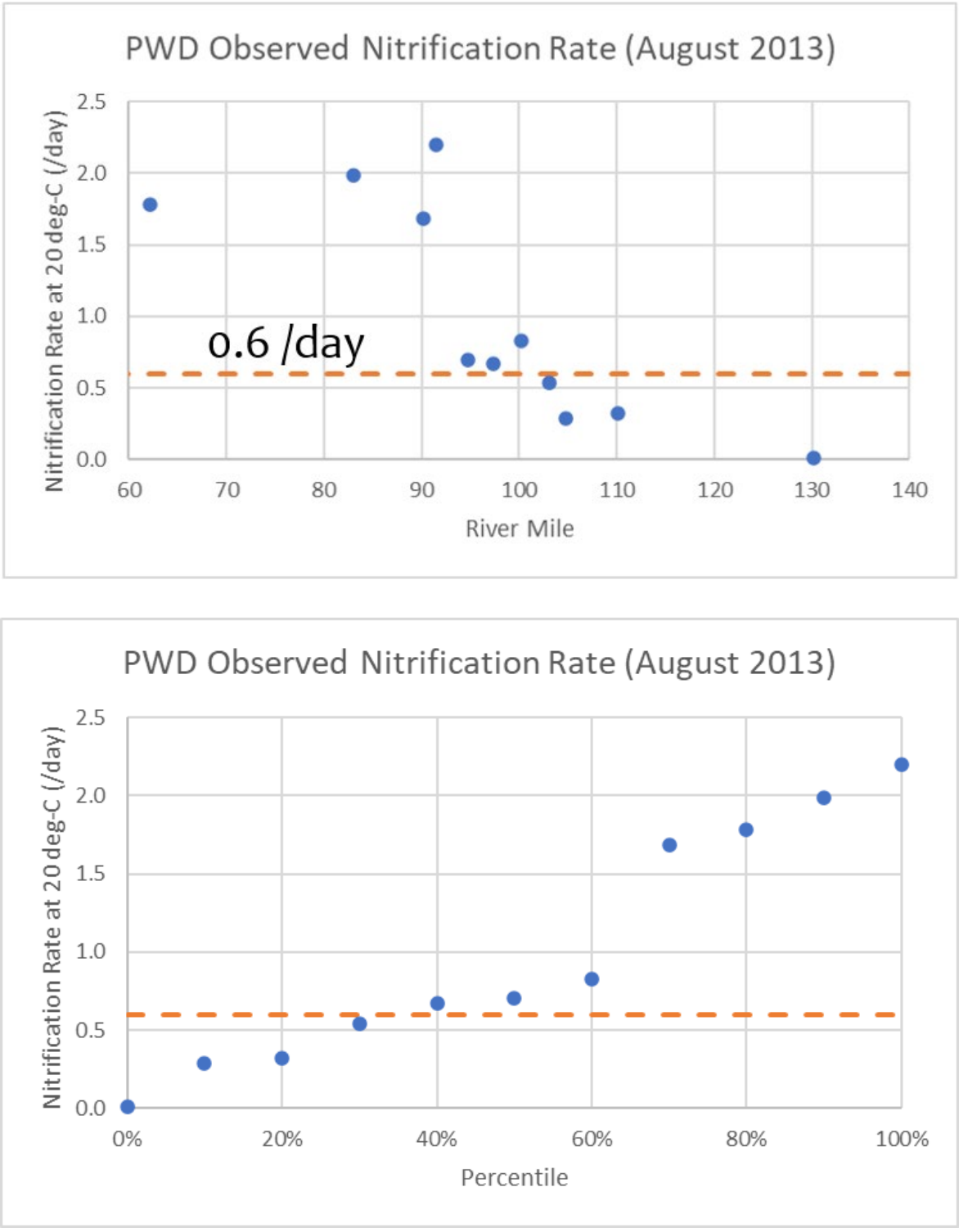

Figure 4-4: Observed Nitrification Rates at 20°C by PWD in August 2013 (PWD 2015)

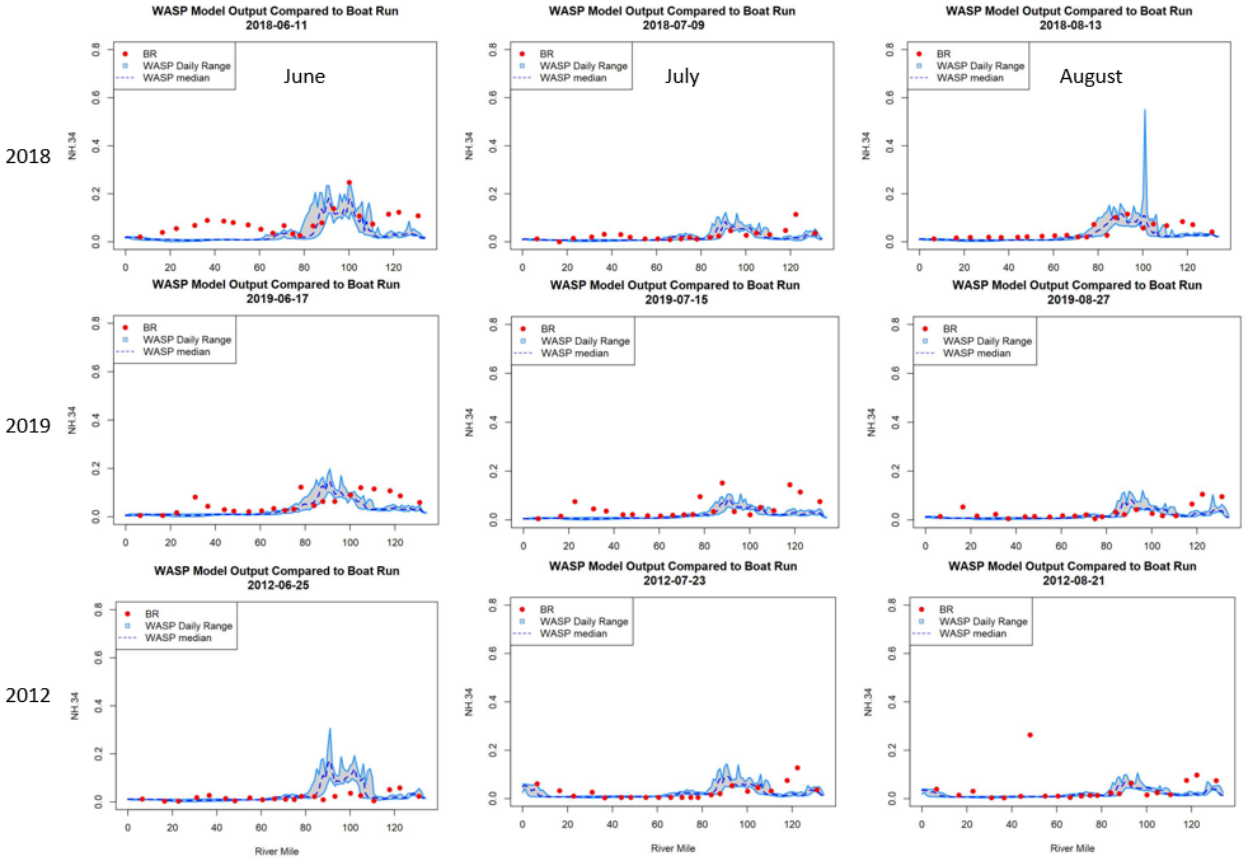

Figure 4-5: Model to Boat Run data spatial comparisons – ammonia during summer

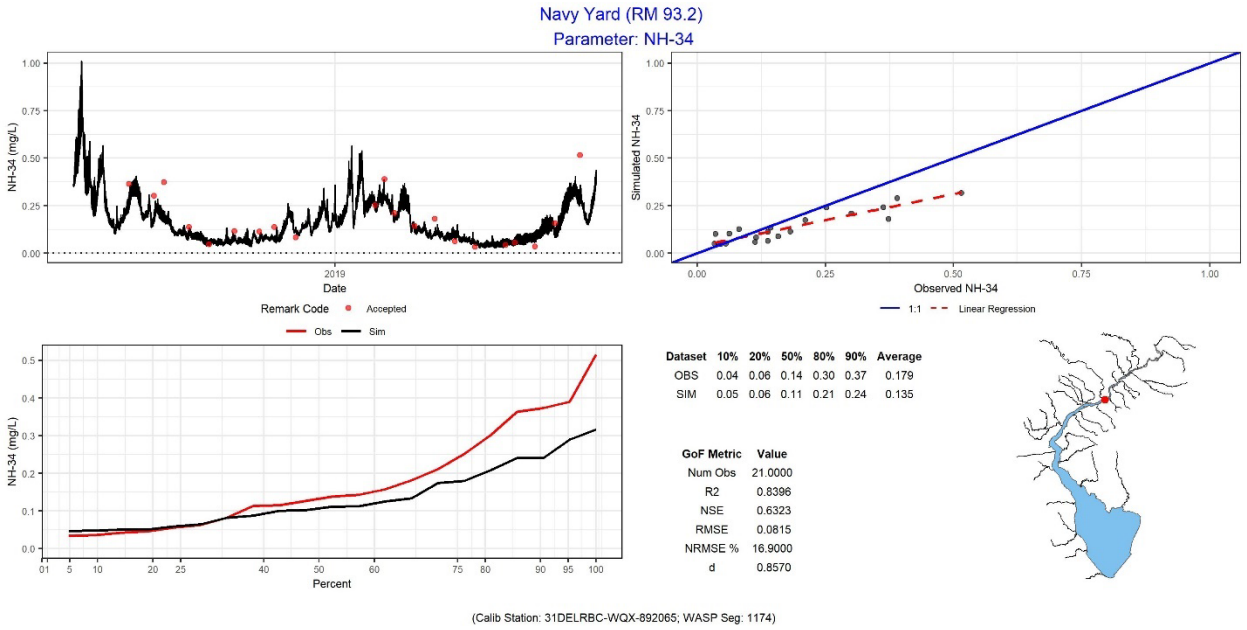

Figure 4-6: Model to Boat Run data temporal comparison – ammonia at Navy Yard, 2018–2019

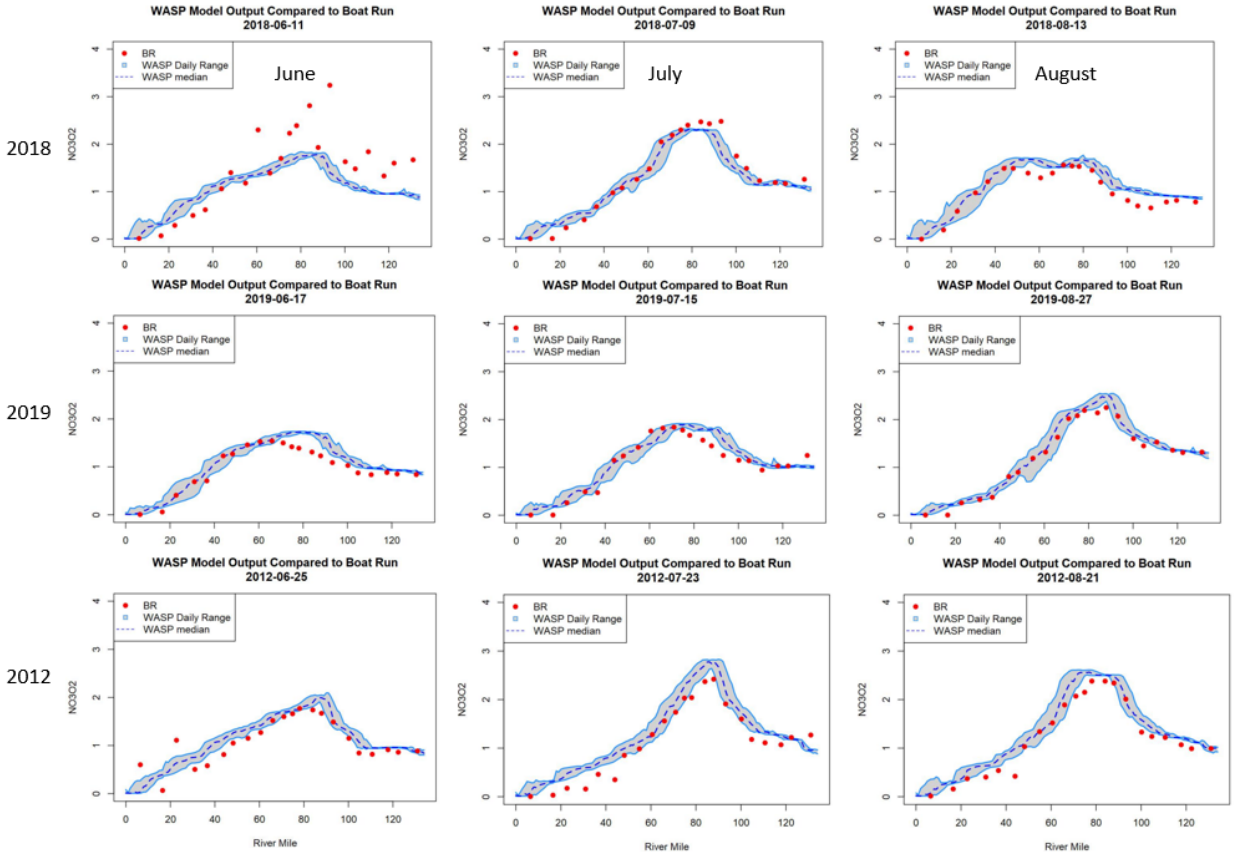

Figure 4-7: Model to Boat Run data spatial comparisons – nitrate during summer

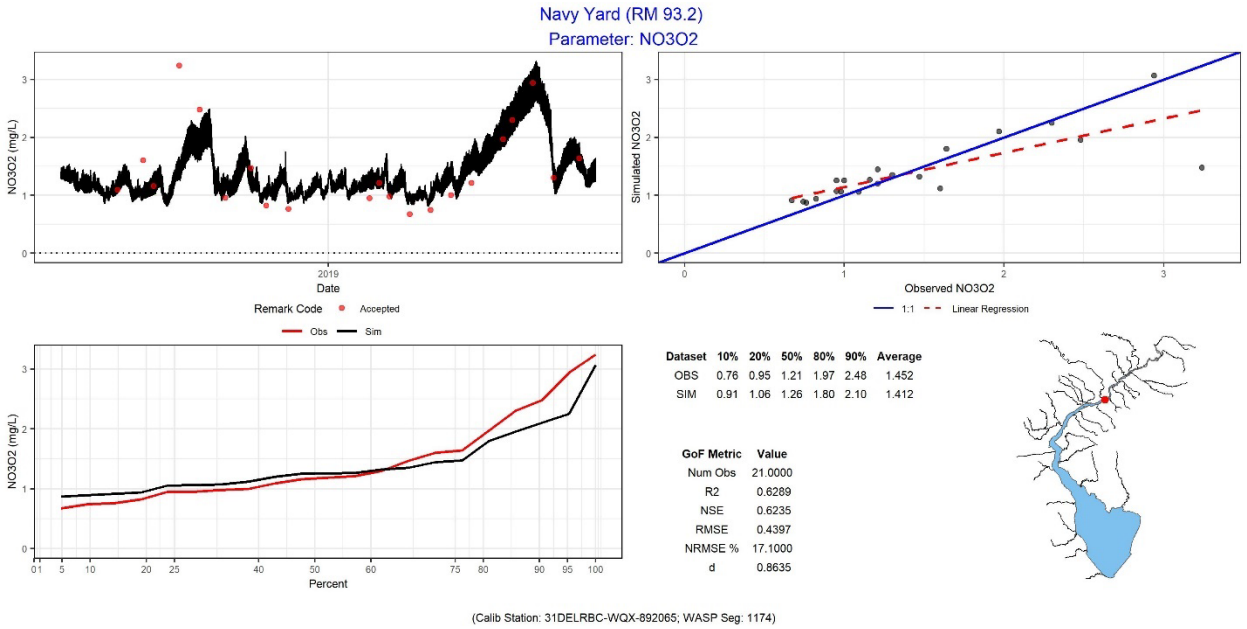

Figure 4-8: Model to Boat Run data temporal comparison – nitrate at Navy Yard, 2018–2019

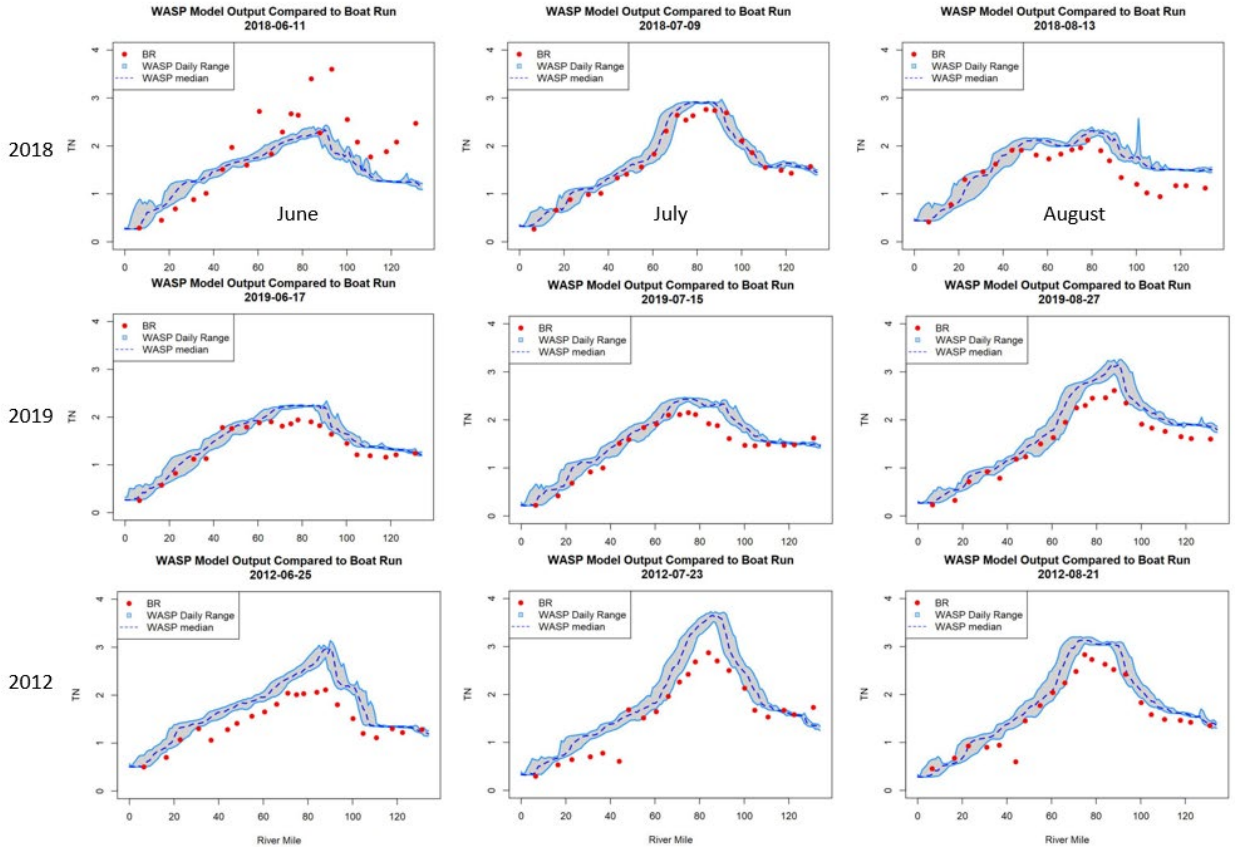

Figure 4-9: Model to Boat Run data spatial comparisons – TN during summer

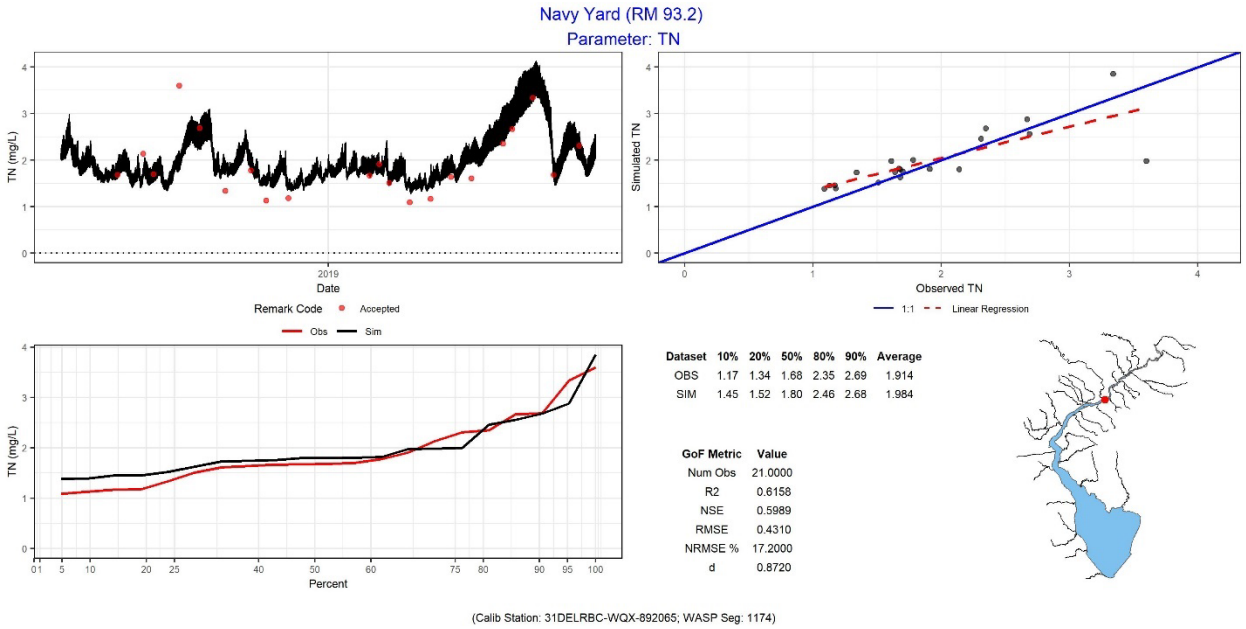

Figure 4-10: Model to Boat Run data temporal comparison – TN at Navy Yard, 2018–2019

4.4.1.3 PHOSPHORUS (D-DIP AND TP)

Calibration approach: The partition coefficient of phosphate to solid in the water column, settling speed of solids, phosphorus uptake rate by phytoplankton, and phytoplankton mortality rate all contribute to phosphorus dynamics. Additionally, the benthic flux rate of phosphate from the sediment layer (assigned per Table 3-5) also affects phosphorus dynamics.

Spatial comparisons: Figure 4-11 and Figure 4-13 show spatial comparisons of phosphate (D-DIP) and total phosphorus (TP) concentrations, respectively, for the model predicted versus measured Boat Run data from June through August during each of the calibration and corroboration years. The observed and modeled concentrations of phosphate were elevated in the tidal river. The model simulation over-estimated the peak concentrations of phosphate in the urban area during some summer surveys but showed a better match for the spring and winter seasons (see relevant figures in Appendix F-2). Phosphate is more readily sorbed to solid particles compared to nitrogen, and a fully functional sediment transport model is not included in this study. This could in part cause some mismatch between the predicted and measured phosphorus data. However, this mismatch is not critical to the overall model simulation because algae growth in the Delaware River Estuary is not phosphorus limited (see Section 4.5.2). The concentrations and spatial patterns of TP were reproduced by the model reasonably well for most of the surveys, indicating phosphorous loads into the system were reasonably accounted for. Both the observed and computed concentrations of TP were elevated at the urban area around RM 60-110.

Temporal comparisons: Figure 4-12 and Figure 4-14 show temporal comparisons of phosphate and TP, respectively, for the model predicted versus measured Boat Run data at the Navy Yard station for the 2018-2019 calibration. The concentrations, seasonal patterns, and cumulative frequency distributions of phosphate and TP were reproduced by the model reasonably well. Both observed and computed phosphate and TP concentrations were elevated in the summer and early fall. Phosphate concentrations are over-estimated at higher concentrations, perhaps due to the sorption process not being fully captured as discussed in the following Section 4.4.1.4 on solids.

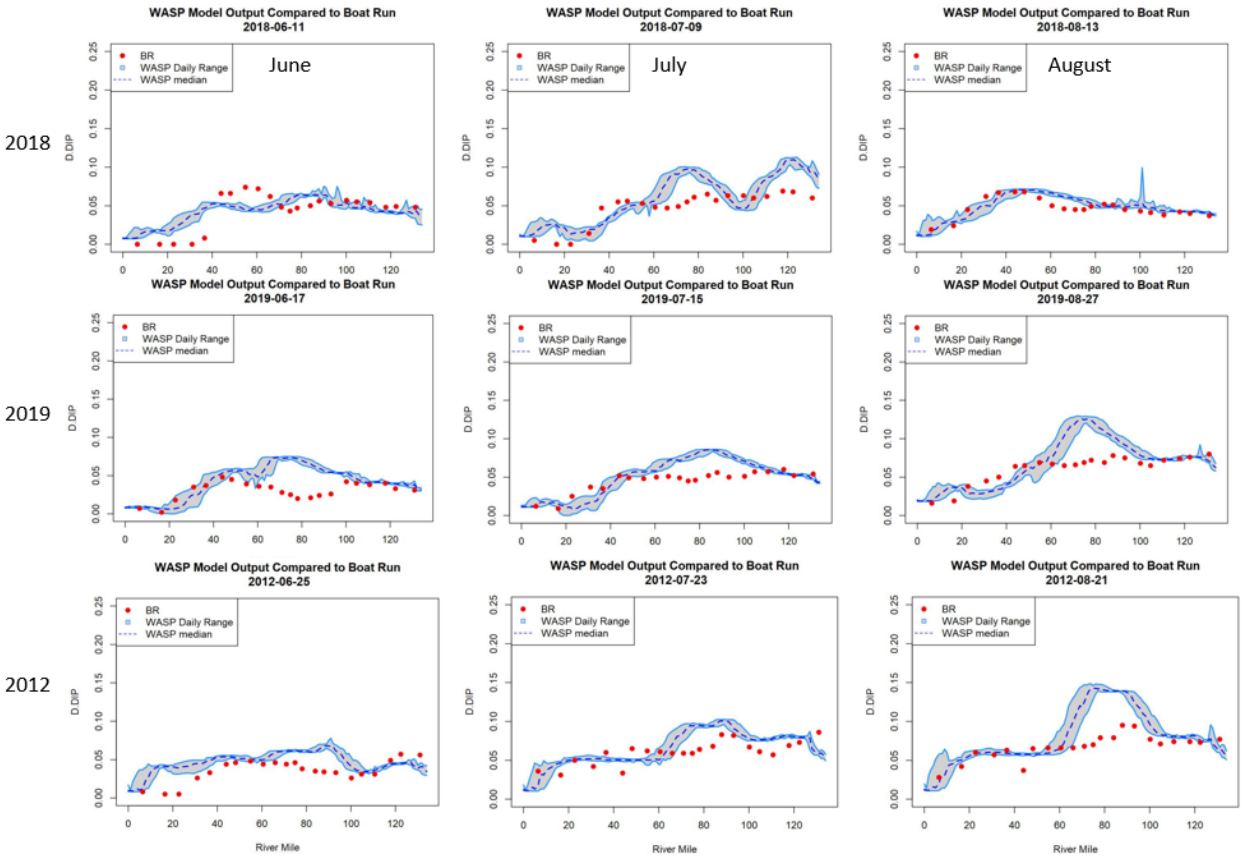

Figure 4-11: Model to Boat Run data spatial comparisons – phosphate during summer

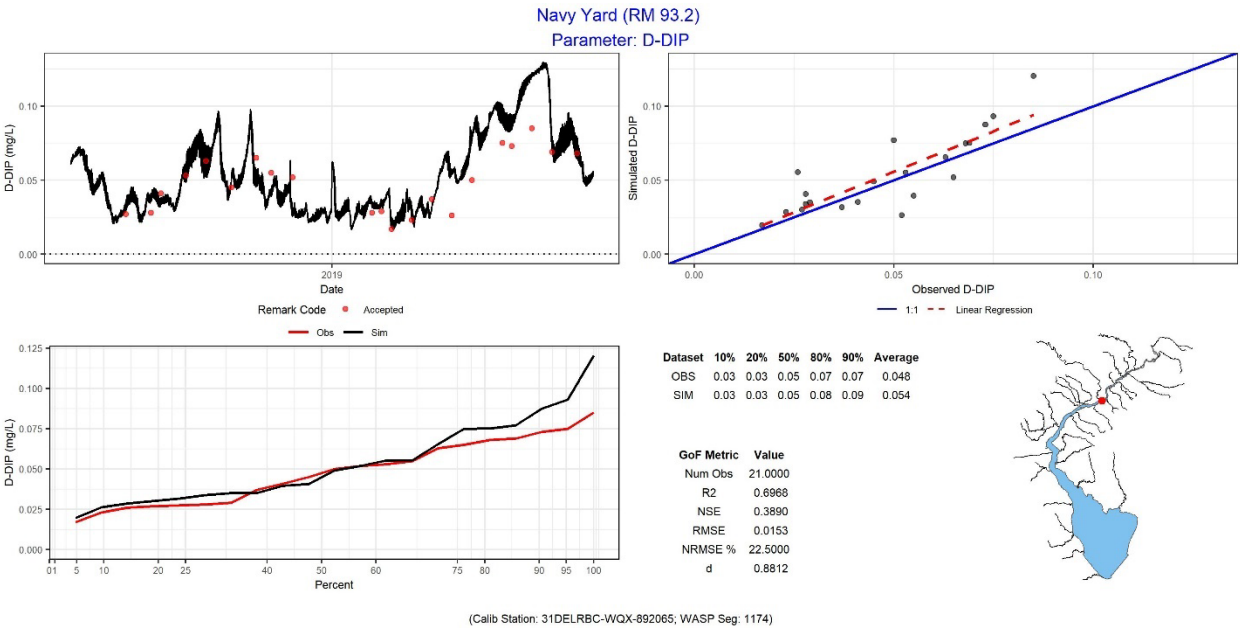

Figure 4-12: Model to Boat Run data temporal comparison – phosphate at Navy Yard, 2018–2019

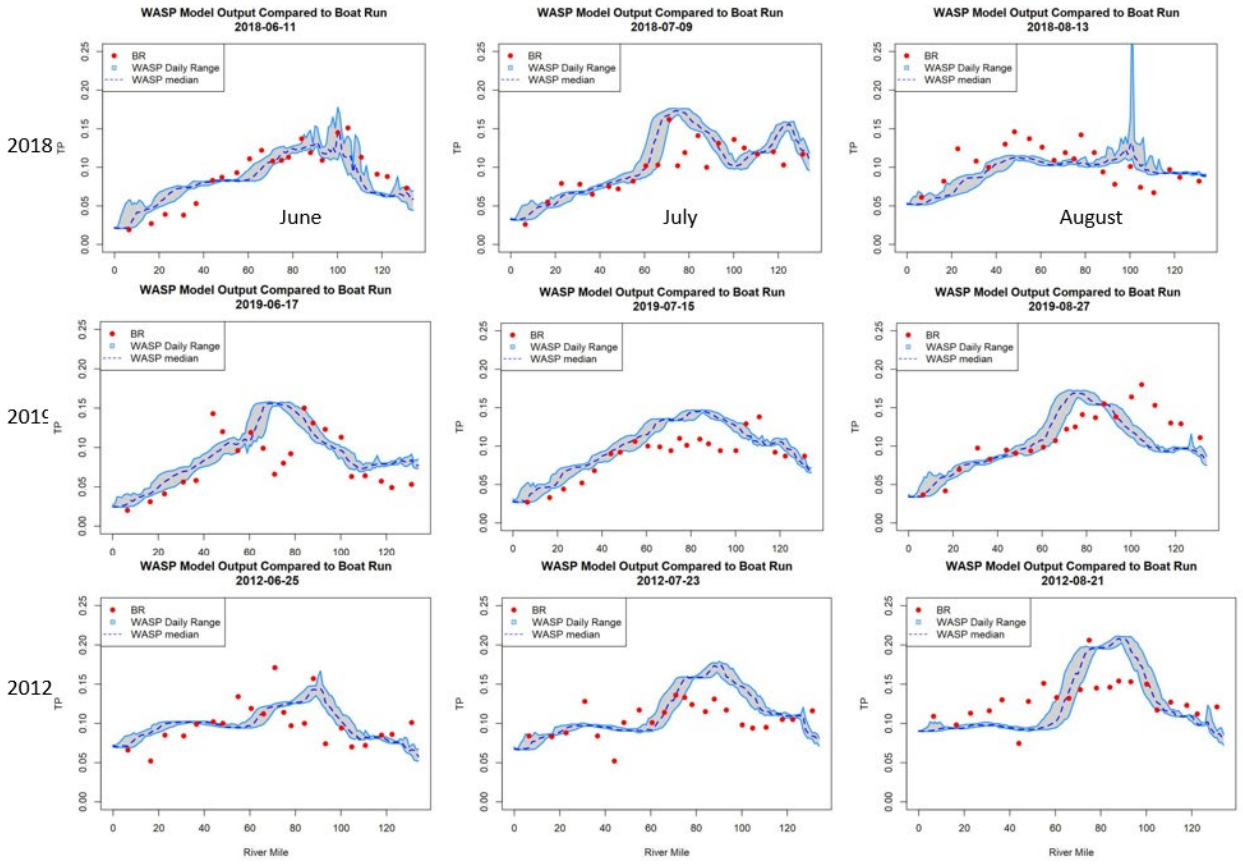

Figure 4-13: Model to Boat Run data spatial comparisons – TP during summer

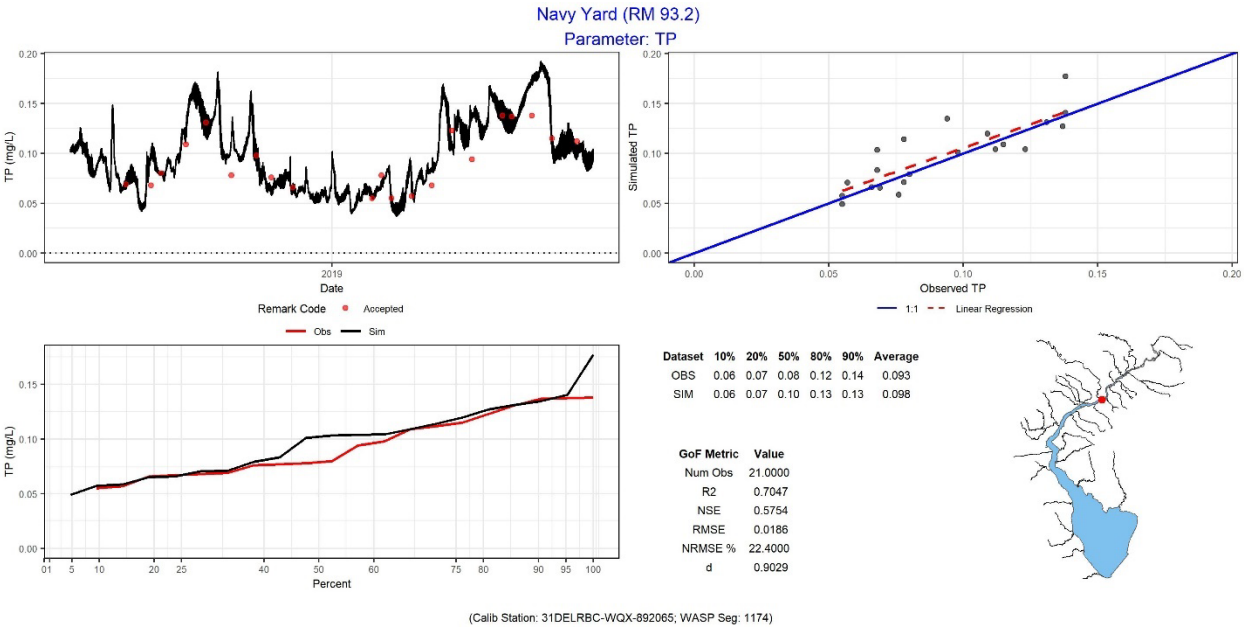

Figure 4-14: Model to Boat Run data temporal comparison – TP at Navy Yard, 2018–2019

4.4.1.4 SOLIDS

Calibration approach: A fully functional sediment transport model with resuspension processes is not included in this study due to limited data and resultant uncertainty in accounting for all of the sediment loads, the complexity of sediment transport models, and the computational time required relative to the time frame of the study. However, inorganic solids are included in the model because the simulation of sorption and settling of phosphate (D-DIP) is needed to capture important geochemical processes that retain phosphorus, especially in the Estuarine Turbidity Maximum (ETM) zone (Lebo and Sharp, 1992). In the water quality model, the solid particles are treated in a way similar to a dissolved tracer but with a settling velocity. A consequence of this modeling approach is that predicted suspended solids concentrations are much lower than observed concentrations, especially in the ETM area. This causes over-prediction of phosphate in the water column. To overcome this issue, inorganic suspended solids loads from major tributaries and selected point source discharges were adjusted such that predicted and observed suspended solids concentrations matched reasonably well and sorption kinetics could function adequately. This was done solely to provide an operational framework for the suspended solids concentrations required for the phosphorus sorption-desorption processes in the model.

Spatial comparisons: Figure 4-15 shows spatial comparisons of suspended solids concentrations for the model predicted versus measured Boat Run data from June through August during each of the calibration and corroboration years. The model reasonably computes the solids concentration.

Temporal comparisons: Figure 4-16 shows temporal comparisons of suspended solids concentrations for the model predicted versus measured Boat Run data at the Navy Yard station for the 2018-2019 calibration. The predicted solids concentrations match the observed levels reasonably well.

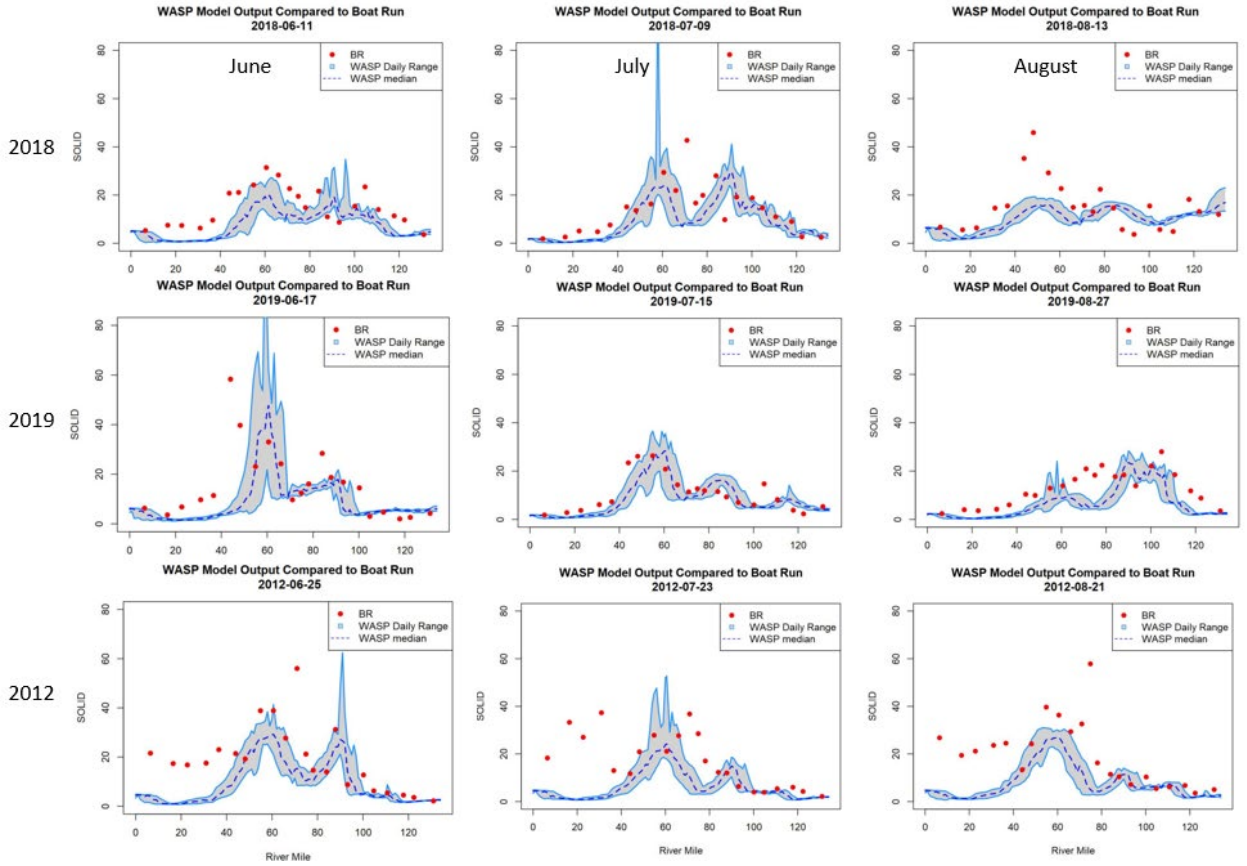

Figure 4-15: Model to Boat Run data spatial comparisons – solids during summer

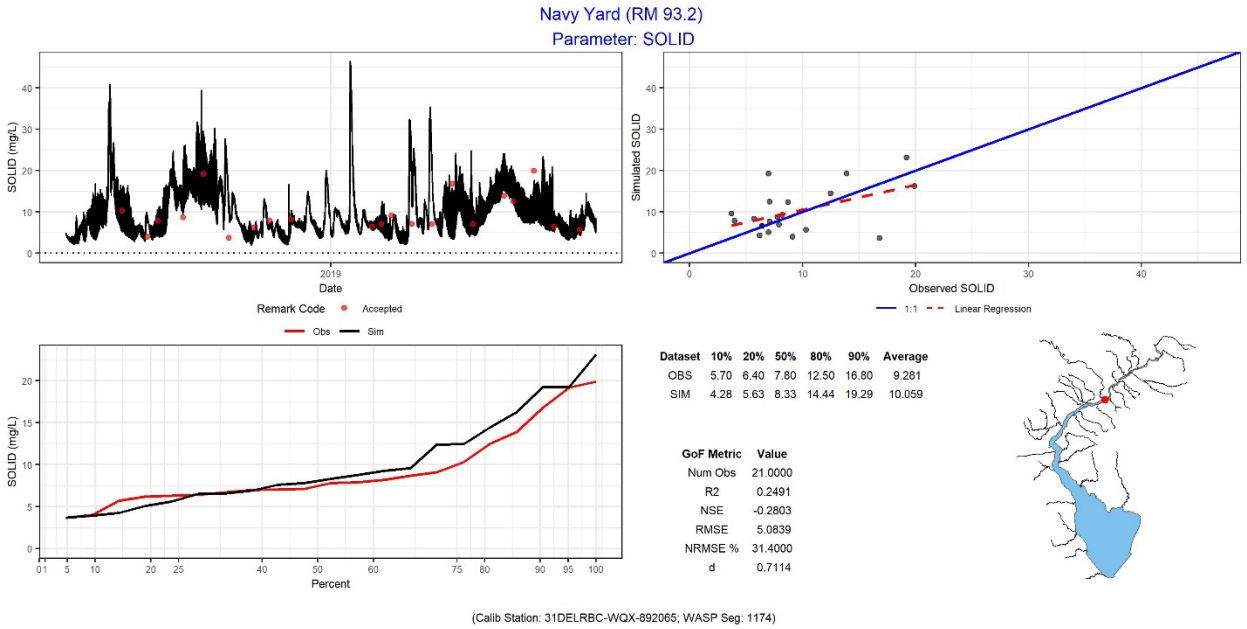

Figure 4-16: Model to Boat Run data temporal comparison – solids at Navy Yard, 2018–2019

4.4.1.5 PHYTOPLANKTON

Calibration approach: Three classes of phytoplankton assemblages are simulated in the water quality model, one each representing spring marine, summer freshwater, and summer marine diatom communities (Appendix K). Phytoplankton maximum growth rates, carbon to chlorophyll-a ratios, respiration rates, mortality rates, optimal light saturation, and half-saturation constants for nutrient uptake (Table 4-2 and Appendix F-1), were set to match observed seasonal patterns in chlorophyll-a levels in the Bay and tidal river. These parameter values are within ranges of published literature (Zion et al., 1978; Bowie et al., 1985; Chapra, 1997; Sathyendranath et al., 2009; Jakobsen and Markager, 2016; Cerco and Noel, 2019). Optimal temperature and shape parameters for phytoplankton growth were adjusted to represent the timing of the algal blooms.

Spatial comparisons: Figure 4-17 shows spatial comparisons of the summed concentrations of all three phytoplankton assemblages for the model predicted versus measured Boat Run data from June through August during each of the calibration and corroboration years. The model captures reasonably well the algal blooms in the Bay but is not able to fully predict the observed blooms in the tidal river during the summer of 2018–2019. The focus of the model at this stage is on dissolved oxygen, especially during low-DO episodes in the urban estuary. While phytoplankton obviously causes significant short-term increases in DO due to photosynthesis, the effect on depletion is less pronounced and somewhat mitigated by reaeration in the Estuary as discussed in Section 4.5.1. The inability of the model to fully capture the summer blooms is further investigated in subsequent Sections 4.4.2 and 4.5 of this report.

Temporal comparisons: Figure 4-18 shows temporal comparisons of the summed concentrations of all three phytoplankton assemblages for the model predicted versus measured Boat Run data at the Navy Yard station for the 2018-2019 calibration. The model under-predicted the measured data during some of the bloom periods. These discrepancies are further investigated in Section 4.5.

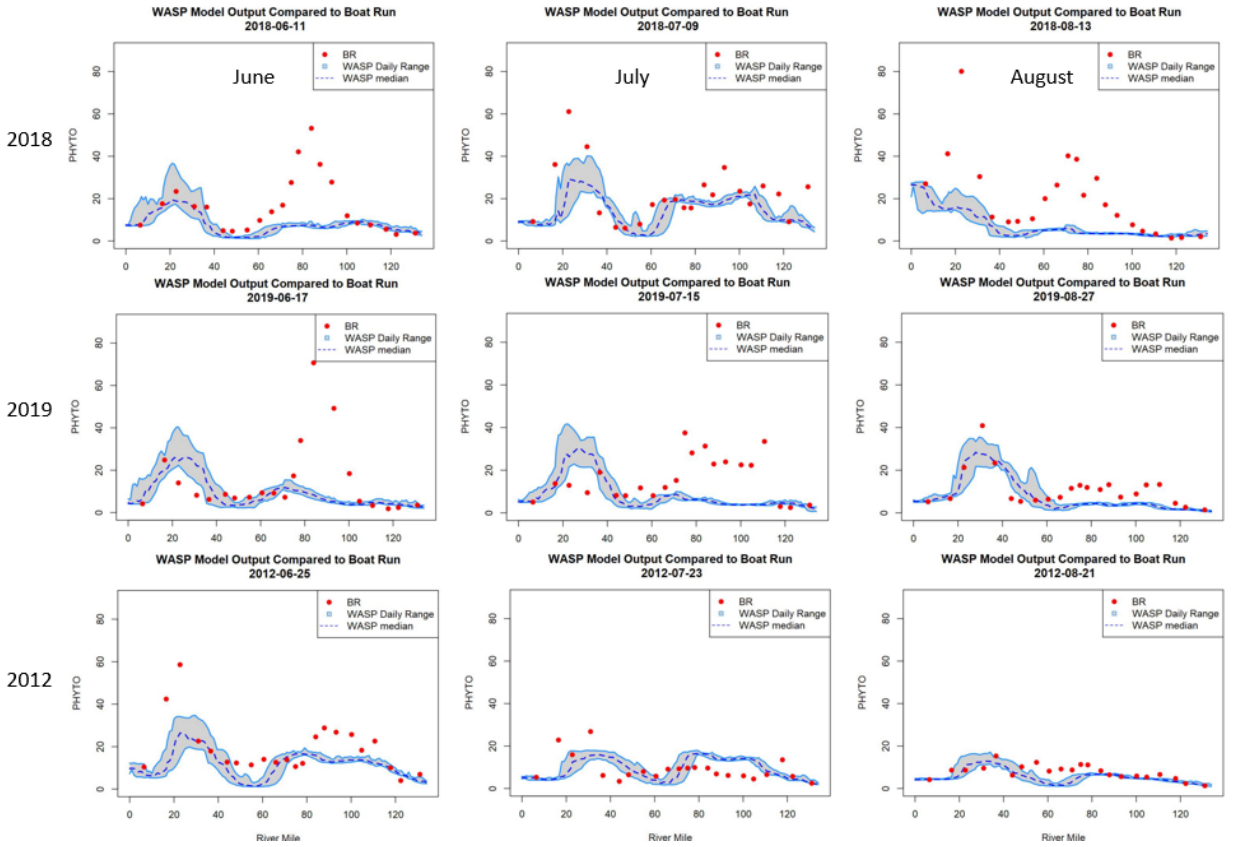

Figure 4-17: Model to Boat Run data spatial comparisons – phytoplankton during summer

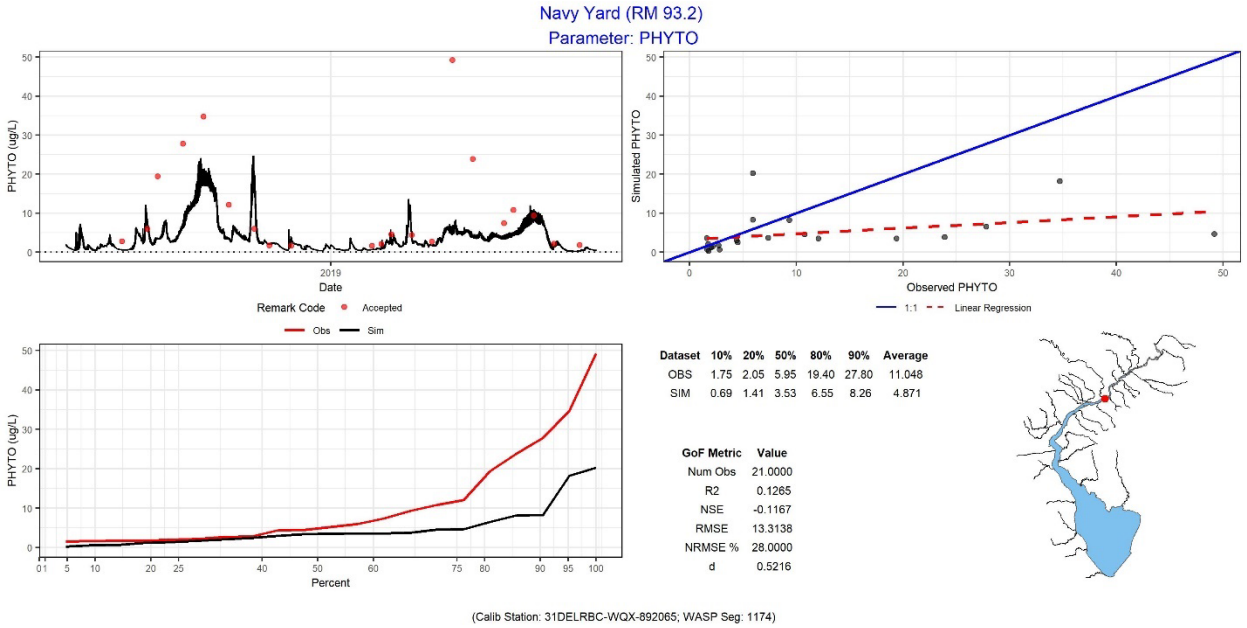

Figure 4-18: Model to Boat Run data temporal comparison – phytoplankton at Navy Yard, 2018–2019

As noted above, both spatial and temporal model-to-data comparisons of phytoplankton indicate that the model under-predicts the algal blooms in the tidal river during summer 2018—2019. One hypothesis for this is that the model may not be simulating the light attenuation accurately. Phytoplankton growth in the Delaware River Estuary is extremely sensitive to light attenuation due to its turbid environment (Pennock, 1985; McSweeney et al., 2017). In the discussion below, the model predictions of the light extinction coefficient, *Ke,* are compared to "observed" *Ke* values, which were calculated from light intensity collected at the surface and at a 1-meter depth during the DRBC Boat Run survey (see Section 3.4.3).

Figure 4-19 shows the model-to-data comparisons of the light extinction coefficient, *Ke,* in the surface layer by river mile during the June Boat Run survey in 2018, 2019, and 2012. The complete comparison plots for *Ke* from all surveys during the calibration years 2018–2019 and corroboration year 2012 are provided in Appendix F-6. The red lines and gray-shaded areas in the spatial plots represent the means and daily ranges, respectively, of the predicted *Ke* on the indicated survey dates. The yellow vertical dashed lines corresponded to the station locations of Reedy Island (RD) and Ben Franklin Bridge (BF). If light intensity data were not available for a given survey, PAR-derived *Ke* values were supplemented using simple regressions (overall R^2=0.78) with Secchi depth measurements (shown as open circles) at each Boat Run location. Secchi depth measurements were not used to derive Ke estimates directly, though subsequent work by DRBC will seek to improve the model by utilizing Secchi depth measurements from the Boat Run surveys to further improve the light extinction submodel. As described in Section 3.4.3, minimum light penetrates at *Ke* > 3.5 m^{-1}. In other words, it is most important for the model to predict a representative *Ke* over the range of 0 to ~3.5 m^{-1}. Figure 4-19 and relevant plots in Appendix F-6 demonstrate that the model generally does a good job predicting *Ke* in this practical range.

Predicted phytoplankton concentrations were also grouped as follows to investigate their seasonal variations against recent 10-year data trend:

- Season 1: February 1 to April 15 for the late winter and early spring, which is a growing season for the marine diatom (i.e., phytoplankton group 1).
- Season 2: April 15 to August 31 for the late spring and summer, which is a growing season for both freshwater and marine diatoms (phytoplankton groups 2 and 3).
- Season 3: September 1 to October 31 for the fall period, which represents periods of decline for marine and freshwater summer diatom communities (phytoplankton groups 2 and 3)
- Season 4: November 1 to January 31 for the winter period, during which some growth of winter marine phytoplankton is expected but little data exists to corroborate (phytoplankton group 1).

Figure 4-20 and Figure 4-21 display spatial comparisons of predicted and measured phytoplankton concentrations during the indicated seasons for the calibration and corroboration periods, respectively. The complete set of comparisons for all four seasons are provided in Appendix F-7. The shaded area in the figures represent seasonal model results between the predicted 25th and 75th percentiles; the box and whiskers depict the recent 10-year Boat Run data trends; and the symbols next to the boxes corresponded

to data from 2018–2019 or 2012. Note that Boat Run surveys during 2012 started on April 23 and ended October 22. As a result, there are no 2012 data displayed on the top panel in Figure 4-21. In general, the model reproduced reasonably well the seasonal variation in trends of the recent 10-year measured data.

The underprediction of phytoplankton in late spring and summer 2018-2019 impacts the DO predictions, as discussed in Sections 4.4.1.6 and 4.5.3. Based on test simulations performed in which algal blooms are predicted, they result in short-term increases in DO due to photosynthesis followed by relatively minor decreases in DO following each bloom due to oxidation of organic carbon. Algal production results in detrital carbon, some of which settles to the sediment and results in a secondary impact on sediment oxygen demand. This water quality model does not dynamically simulate sediment diagenesis and, therefore, does not capture the secondary impacts of algal production. However, since algal productivity is mostly light limited in the Estuary and relatively insensitive to nutrient loads, the current model with this limitation was deemed acceptable for its intended purpose by the DRBC and its Model Expert Panel.[18] Future enhancements to the model are expected to incorporate dynamic simulation of sediment diagenesis.

In order to better understand the factors that are preventing the model from better predicting the observed algal blooms in summer 2018 and 2019, additional diagnostic tests were conducted to: (1) increase boundary loads of phytoplankton, and (2) introduce random variations to the existing light extinction values for reflecting transient variation of light intensity. Based on the diagnostic simulation results, it is unlikely that these factors caused the model to under-predict the algal blooms in the tidal river. Further comparisons to continuous data (Section 4.4.2) and additional diagnostic analyses (Section 4.5) were performed to explore why the model did not predict the algal blooms in the tidal river during the summer 2018–2019. As light availability is one of the key factors controlling phytoplankton growth in the tidal river, further enhancements to the *Ke* prediction submodel are expected to be the subject of future model enhancements consistent with agency resources and goals.

[18] Water Quality Advisory Committee on April 27, 2022

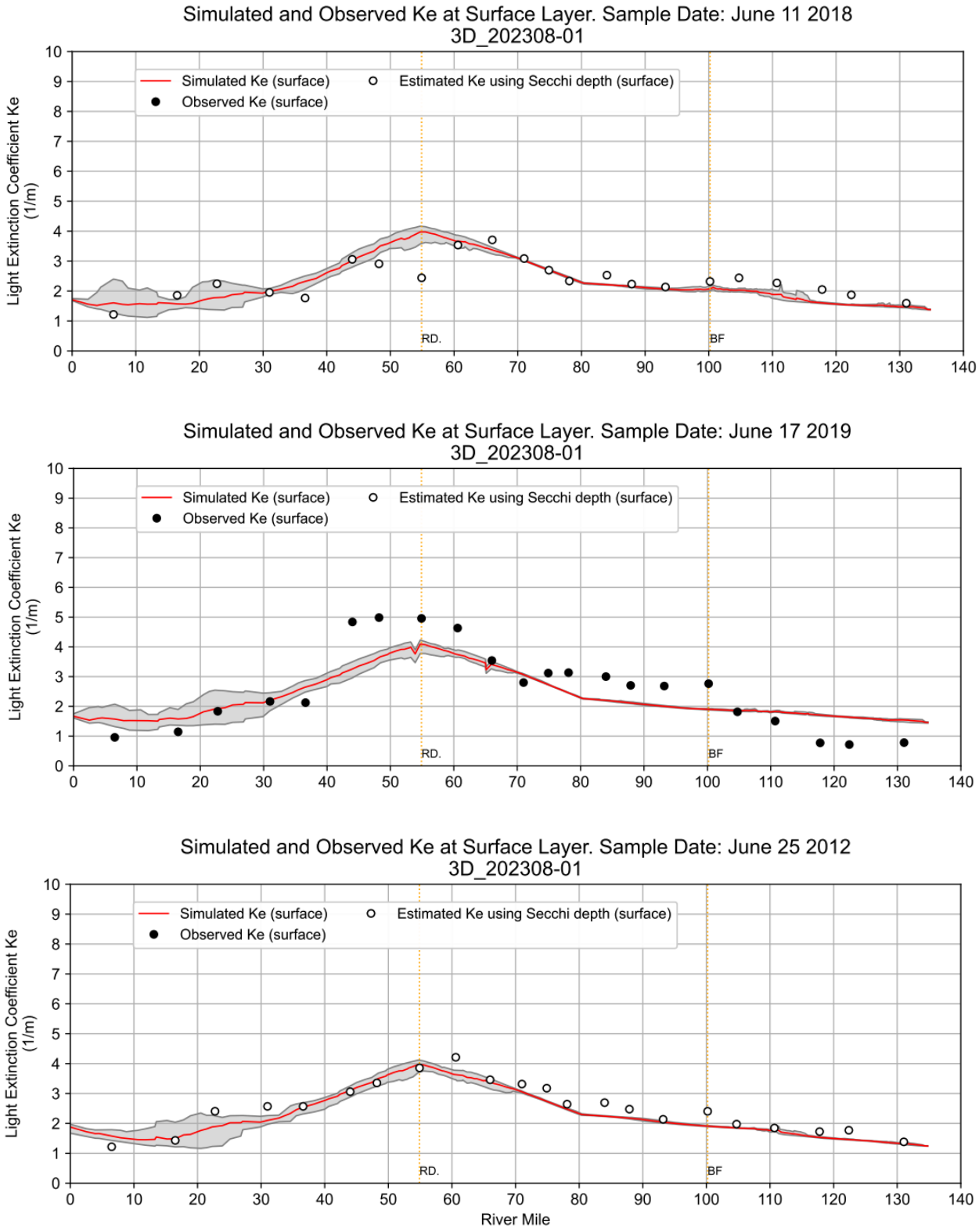

red lines and gray-shaded areas represent the means and daily ranges of the predicted Ke

Figure 4-19: Spatial comparisons of simulated and observed light extinction – June 2018, 2019, and 2012

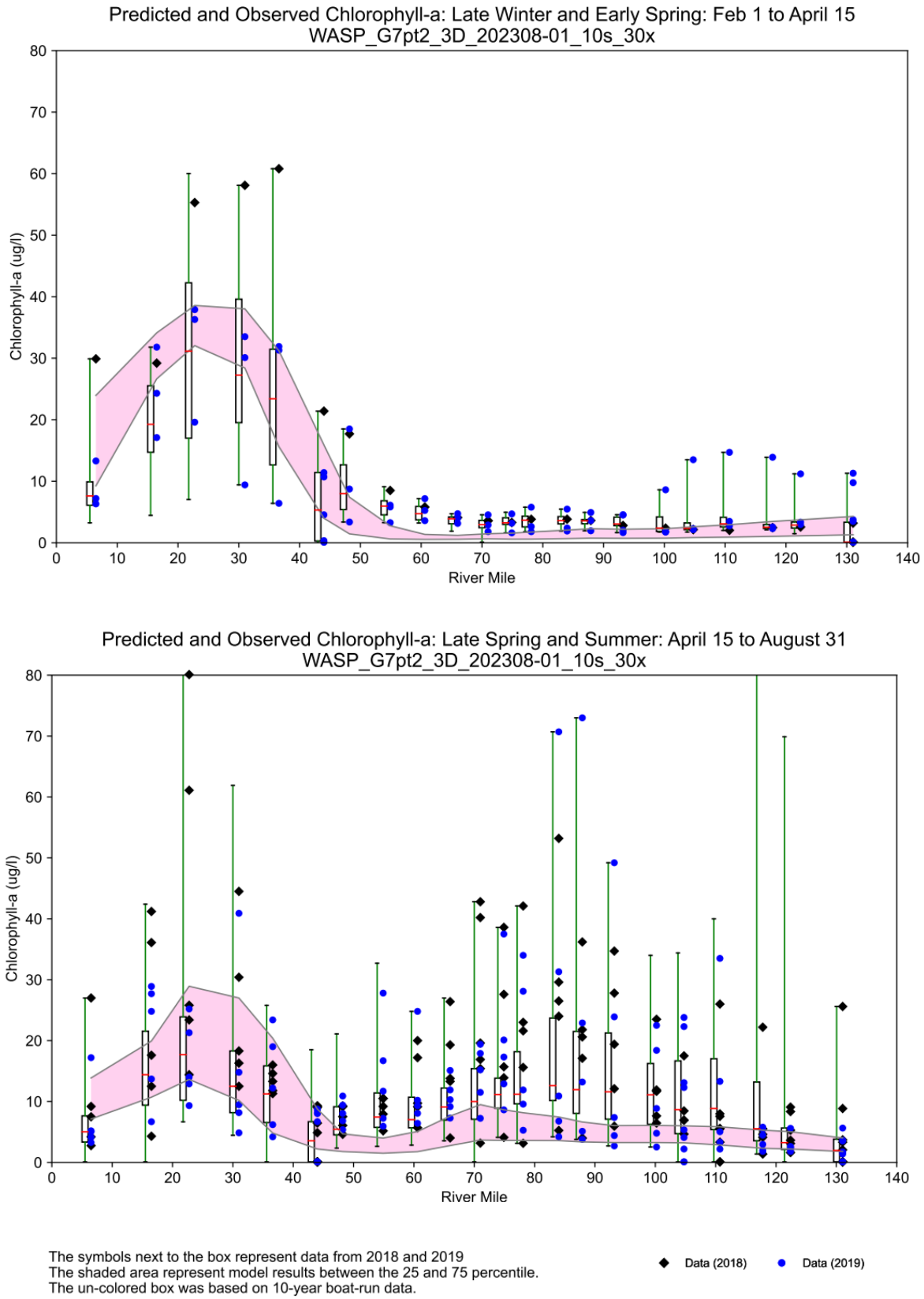

Figure 4-20: Spatial phytoplankton comparisons by season, 2018–2019

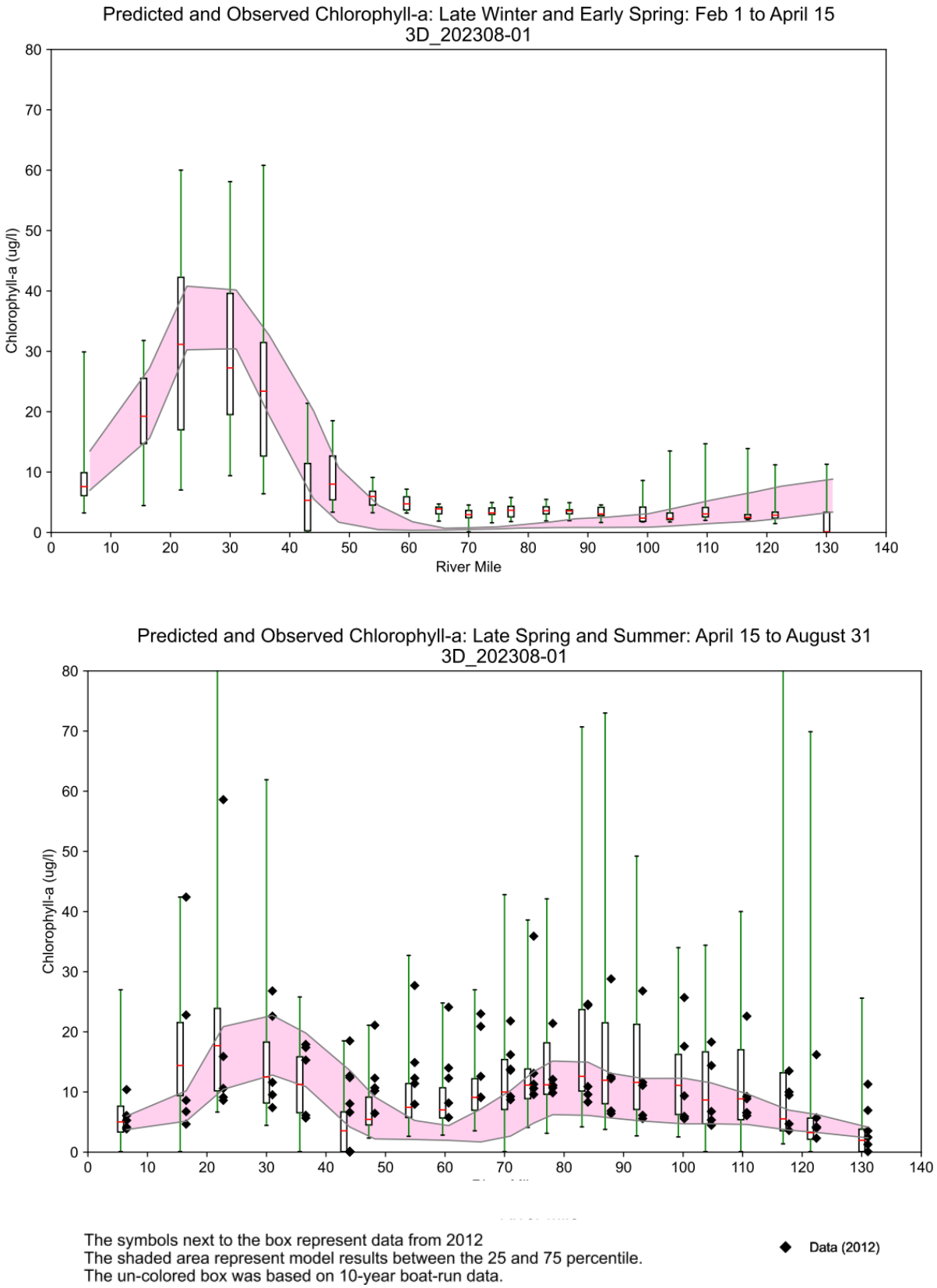

Figure 4-21: Spatial phytoplankton comparisons by season, 2012

4.4.1.6 DISSOLVED OXYGEN (DISOX)

Calibration approach: Phytoplankton growth (photosynthesis) and reaeration at the air-water interface are sources of dissolved oxygen, while phytoplankton respiration, CBOD oxidation, nitrification, and SOD are sinks. The calibration parameters of SOD and benthic nutrient fluxes were determined based on the best fit of the model predicted dissolved oxygen (DISOX) with the measured dissolved oxygen data, after evaluating the impacts of other parameters and processes, such as nitrification, CBOD oxidation, phytoplankton production and decay, and reaeration.

Spatial comparisons: Figure 4-22 shows spatial comparisons of model predicted dissolved oxygen (DISOX) versus measured Boat Run data from June through August during each of the calibration and corroboration years. The model results matched the absolute concentrations and spatial patterns of dissolved oxygen reasonably well, including the dissolved oxygen sags around RM 90. The model sometimes under-predicts dissolved oxygen in the urban area (e.g., the surveys in June), likely due to under-prediction of phytoplankton production. This issue is further explored in Section 4.4.2 and Section 4.5.3

Temporal comparisons: Figure 4-23 shows temporal comparisons of model predicted dissolved oxygen (DISOX) versus measured Boat Run data at the Navy Yard station for the 2018-2019 calibration. The model matched the absolute concentrations, seasonal patterns, and cumulative frequency distributions of dissolved oxygen very well. Both observed and computed DISOX concentrations reach minimum values around July-August.

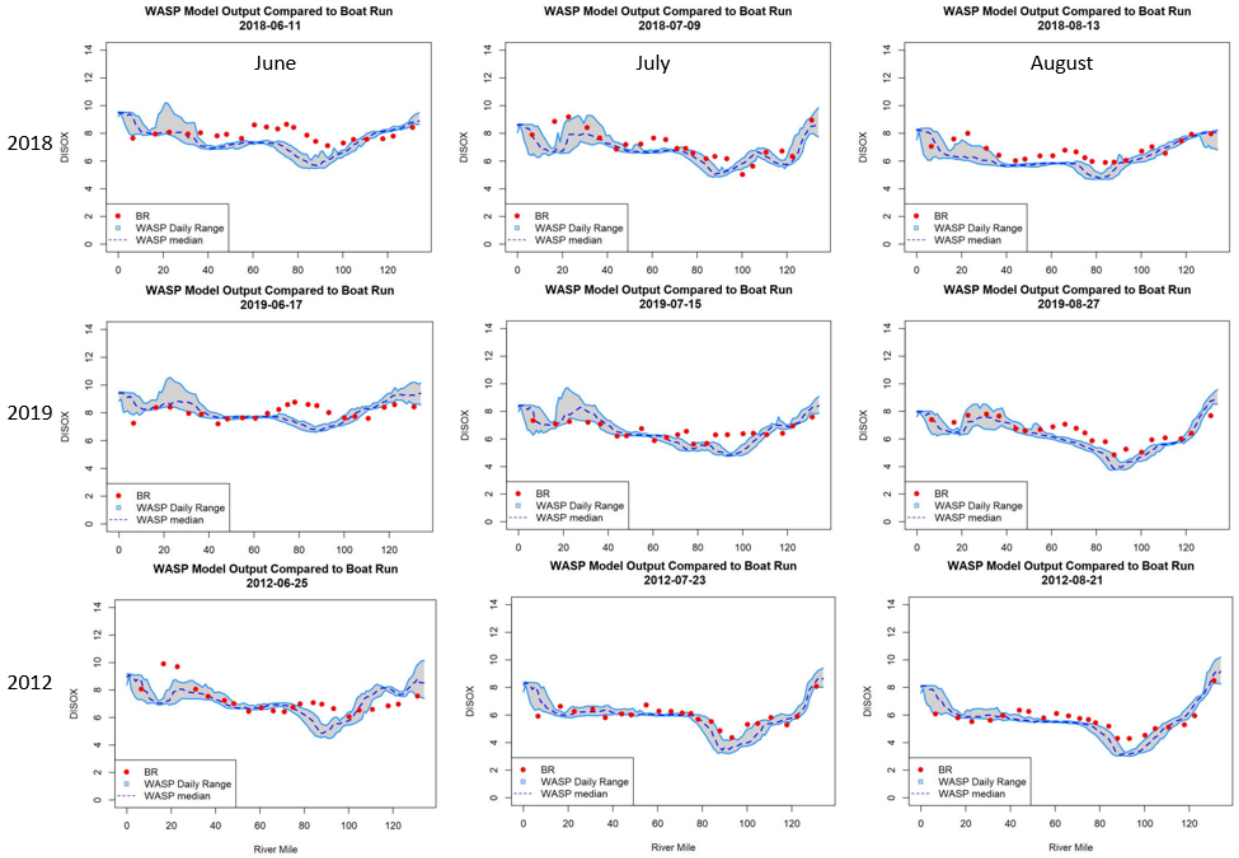

Figure 4-22: Model to Boat Run data spatial comparisons – DISOX during summer

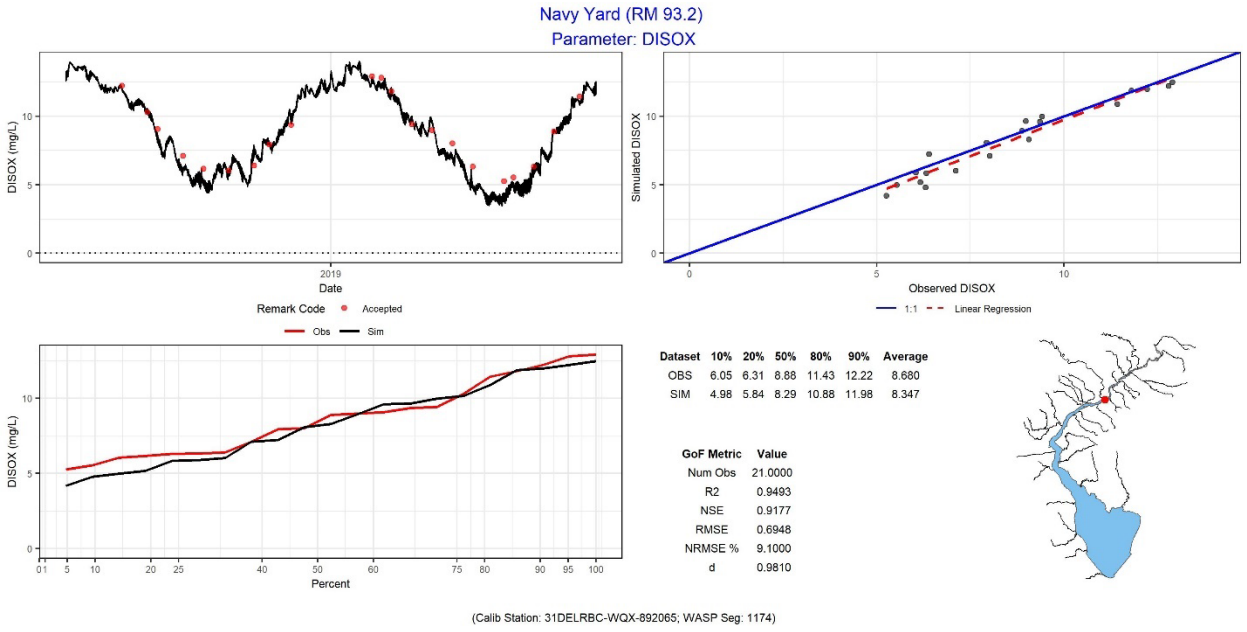

Figure 4-23: Model to Boat Run data temporal comparison – DISOX at Navy Yard, 2018–2019

4.4.1.7 DISSOLVED OXYGEN PERCENT SATURATION (DOSAT)

Calibration approach: While dissolved oxygen percent saturation (DOSAT) is not an independent model state variable, DOSAT is an important WASP model output parameter that can be compared with field observations to evaluate its performance. DOSAT varies with DO concentration (a water quality state variable) as well as with water temperature and salinity (both of which are hydrodynamic model state variables passed to WASP in the linkage file).

Spatial comparisons: Figure 4-24 shows spatial comparisons of model predicted DOSAT versus measured Boat Run data from June through August during each of the calibration and corroboration years. Model-to-data comparisons of DOSAT were generally good. Since the prediction of DOSAT varies with the predicted salinity and water temperature in the linked hydrodynamic EFDC model, the accuracy to which salinity and water temperature are simulated affects the model-to-data comparisons of DOSAT. Similar to dissolved oxygen, the WASP water quality model sometimes under-predicts DOSAT in the urban area during the summer, likely due to the model under-predicting phytoplankton production. This issue is further explored in Section 4.4.2 and Section 4.5.3.

Temporal comparisons: Figure 4-25 shows temporal comparisons of model predicted DOSAT versus measured Boat Run data at the Navy Yard station for the 2018-2019 calibration. Model-to-data comparisons of DOSAT are reasonable, with the model slightly under-predicting the DOSAT concentrations, perhaps due to slightly over-predicting the water temperature in the EFDC hydrodynamic model (Chen et al., 2024).

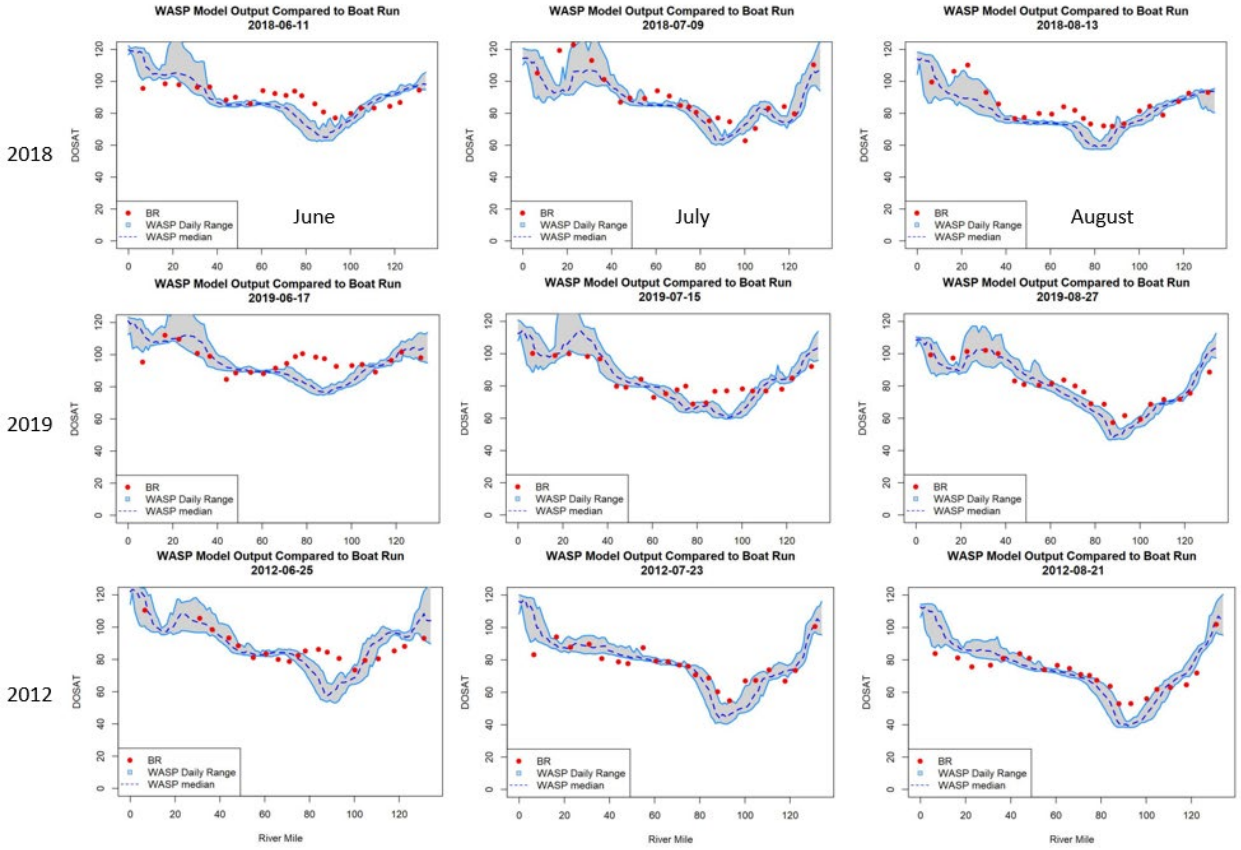

Figure 4-24: Model to Boat Run data spatial comparisons – DOSAT during summer

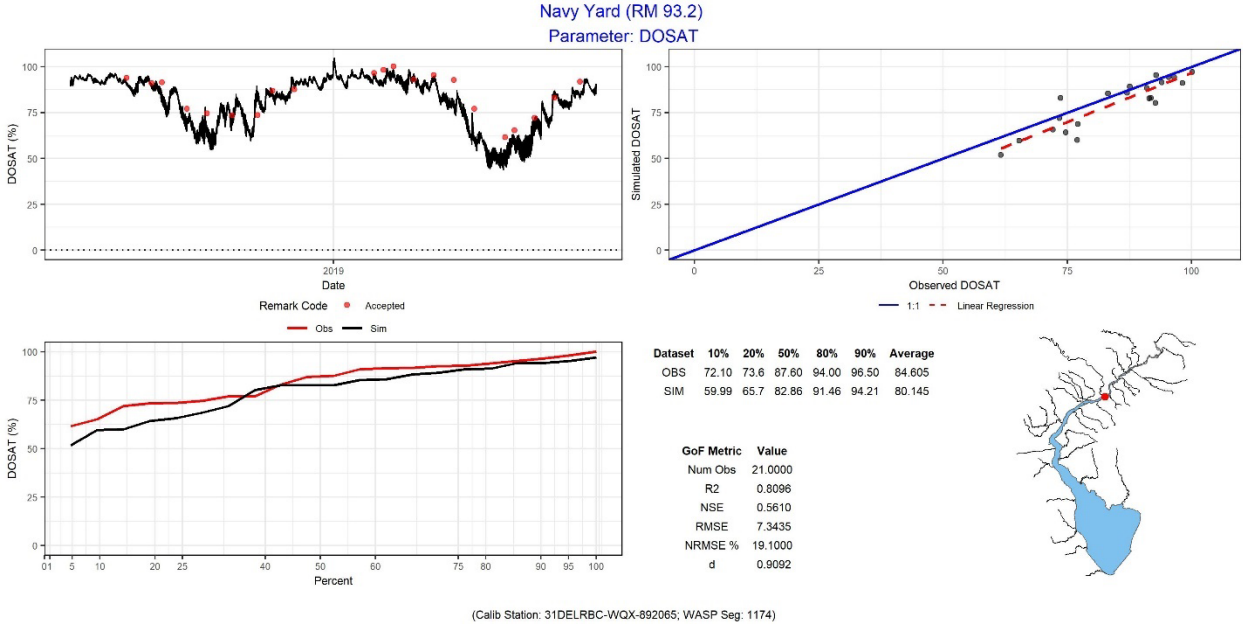

Figure 4-25: Model to Boat Run data temporal comparison – DOSAT at Navy Yard, 2018–2019

4.4.2 Comparisons to the Continuous Data at Discrete Locations

4.4.2.1 Comparisons over the Calibration and Corroboration Periods

Predicted dissolved oxygen concentration, percent oxygen saturation, and phytoplankton (as chlorophyll-a) were compared with continuous data collected at four USGS stations and two PWD buoy stations (Figure 4-1) for both the 2018–2019 two-year model calibration period and the 2012 corroboration year. PWD buoy data were not available for 2012. Sensors at the USGS stations were installed at fixed locations (i.e., approximately two to three feet below the water surface during low tide), approximately corresponding to the second model vertical layer below the water surface (model vertical layer thickness is about 1.5 m/4.9 feet), whereas floating sensors at the PWD buoy stations were positioned about one meter below water surface at all times, corresponding to the model surface layer. In the model-to-data comparisons of dissolved oxygen and percent DO saturation, model predictions of instantaneous values were extracted at two-hour intervals; accordingly, the continuously measured USGS and PWD data (typically recorded every 12 minutes for PWD meters and 15 minutes for USGS meters) were sampled on a two-hour interval to match the model output. In the model-to-data comparisons of chlorophyll-a, daily averaged values were used for both the model predictions and the measured data. Comparisons to these temporally high-resolution data are invaluable in assessing model performance.

Figure 4-26 to Figure 4-31 present the predicted and measured (near-) surface dissolved oxygen concentrations for the 2018-2019 calibration period, in the sequence of upstream to downstream stations. Similar figures for the 2012 corroboration period are available in Appendix F (specifically F-8). The top panel in the figures shows the time series comparisons of model predictions and continuously measured near-surface DO concentrations at two-hour intervals. DRBC Boat Run grab sample data are also displayed as green circles for additional information. The bottom left panel shows comparisons of the cumulative frequency distributions of the model predicted and continuously measured data, while the bottom right panel shows 1-to-1 comparisons with key statistical metrics displayed. Over the 2018-2019 model calibration period, the concentrations, seasonal variations, and cumulative frequency distributions of dissolved oxygen are reproduced well by the model at all stations. Model predictions sometimes do not capture the magnitude of the fluctuations of the observations, e.g., at Buoy-B and Chester during June – July 2019. This is likely caused by the under-prediction of phytoplankton production during the summer. This issue is further explored in the following comparison of chlorophyll-a results and in the discussion of Zone 2 light attenuation in Section 4.5.3. Lower dissolved oxygen in the Delaware River Estuary occurs around July-August, as a result of the lower solubility of oxygen in the water column, and elevated nitrification, CBODU oxidation, and sediment oxygen demand, caused by higher summer water temperatures. During the calibration period of 2018–2019, the model predictions match well with the observations at lower dissolved oxygen concentrations (i.e., at the 1st percentile) for most of the monitoring stations, with the differences between model predictions and measured data of about 0.1 to 0.3 mg/L. The largest differences (about 0.7 mg/L at 0.01 percentile) between the model predictions and observations for lower dissolved oxygen concentrations occurs at the Reedy Island station around RM 54;

however, the difference is relatively small (about 0.1 mg/L) at the 1st percentile. Spatially, both the model predictions and measured data indicate the summer dissolved oxygen sag occurs around Buoy B (RM 93.5), near the Schuylkill River confluence. During the model corroboration period of 2012, the model-to-data comparisons for lower dissolved oxygen concentrations, spatially and temporally, are not as good as those during the calibration period. This is likely due to the less frequent data available in 2012 for specifying boundary conditions, including loadings from point source dischargers. Overall, the model performs well in predicting the observed lower dissolved oxygen concentrations, dissolved oxygen sag locations, temporal trends, and variations over all three calibration and corroboration years, indicating that the model captures well the principal processes affecting dissolved oxygen in the Delaware River Estuary.

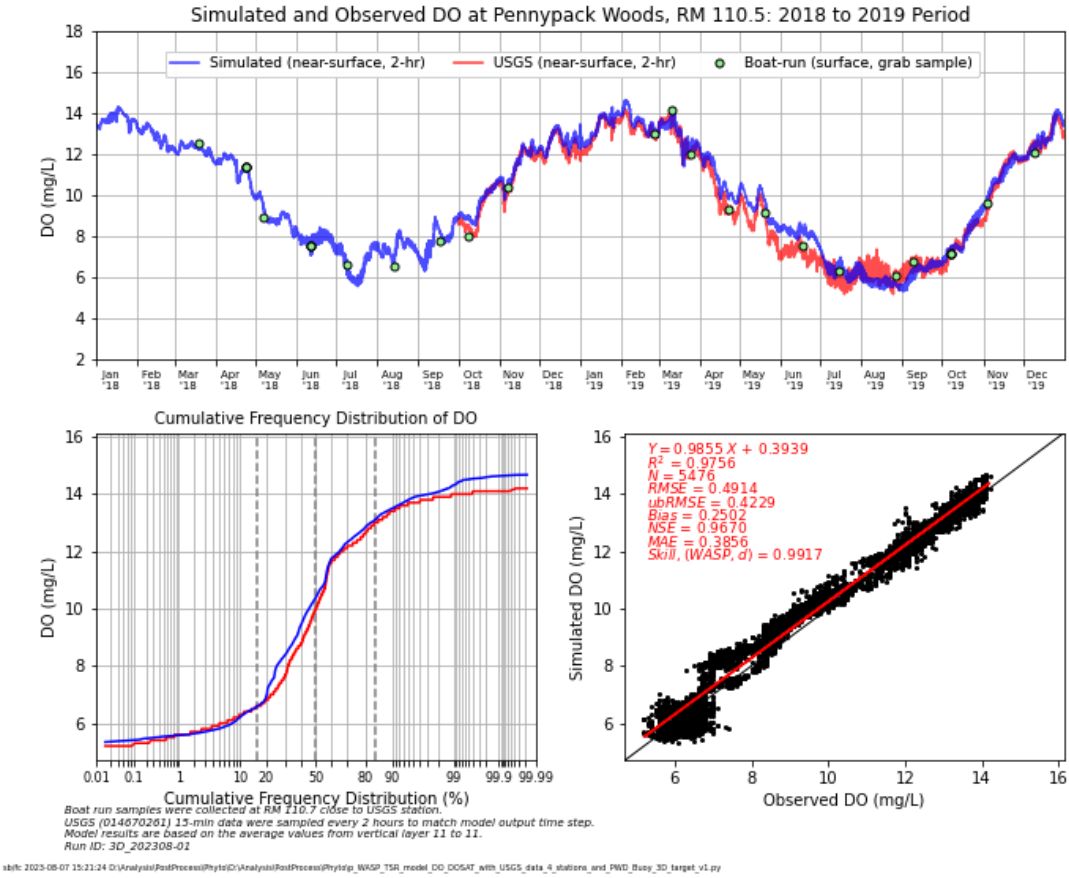

Figure 4-26: Model to Continuous Data Comparison – DO at Pennypack Woods during 2018–2019

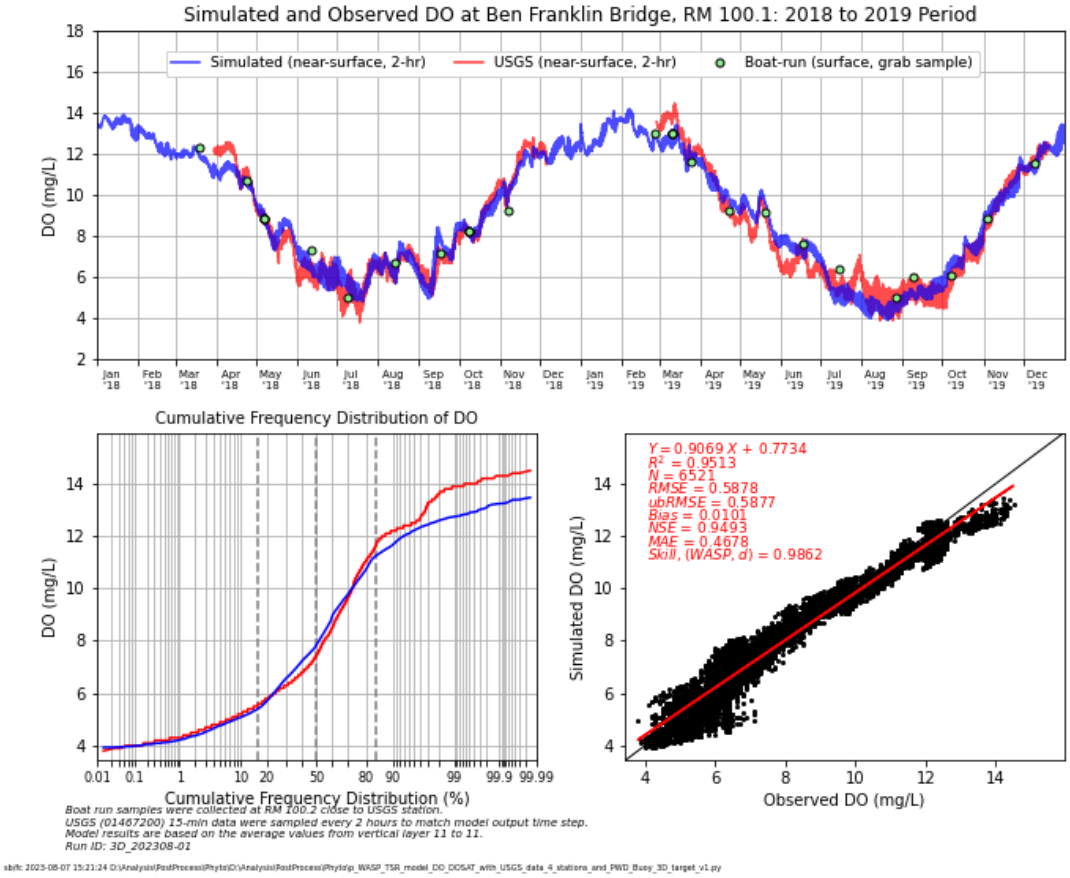

Figure 4-27: Model to Continuous Data Comparison – DO at Ben Franklin Bridge during 2018–2019

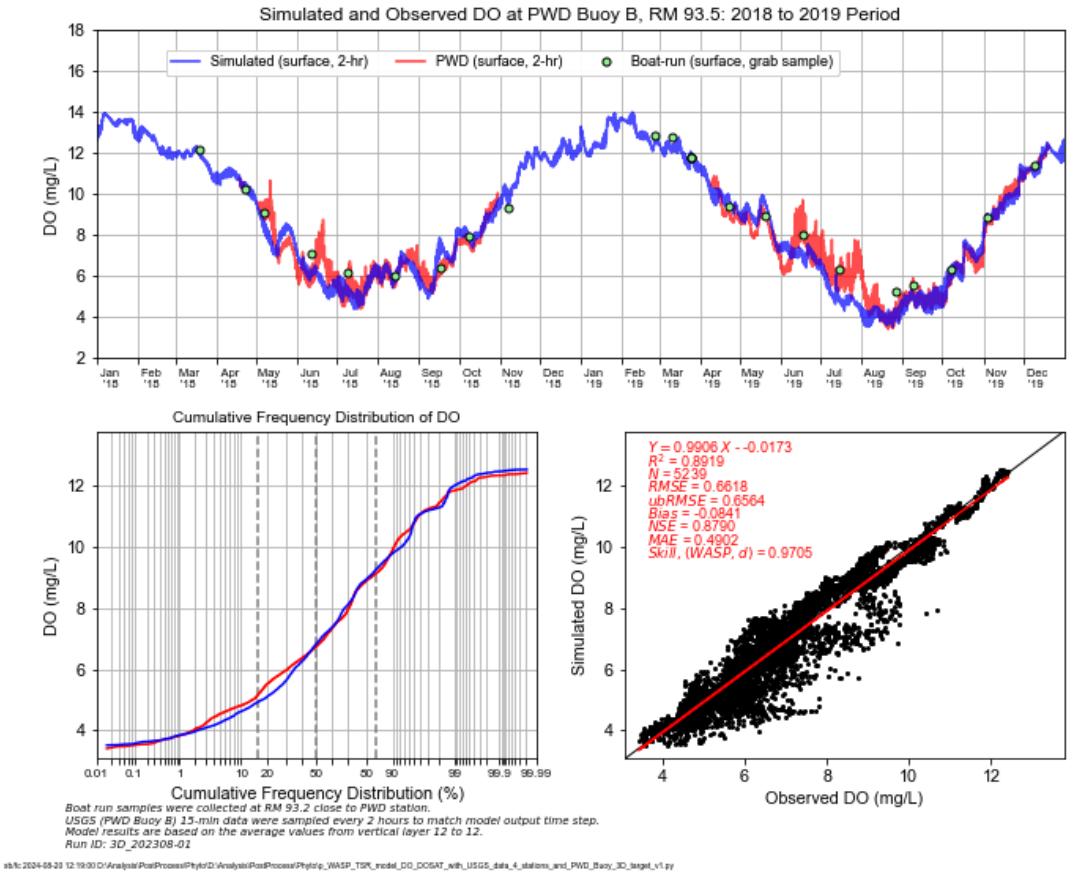

Figure 4-28: Model to Continuous Data Comparison – DO at Buoy B during 2018–2019

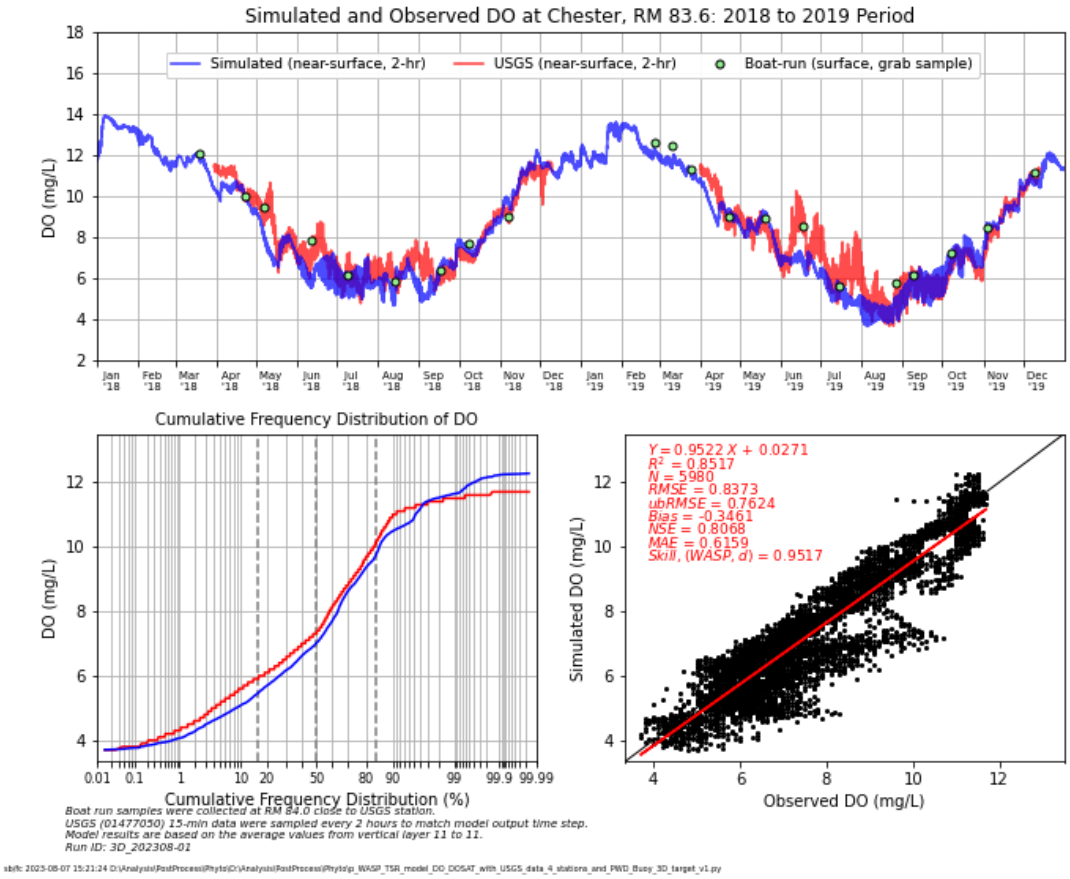

Figure 4-29: Model to Continuous Data Comparison – DO at Chester during 2018–2019

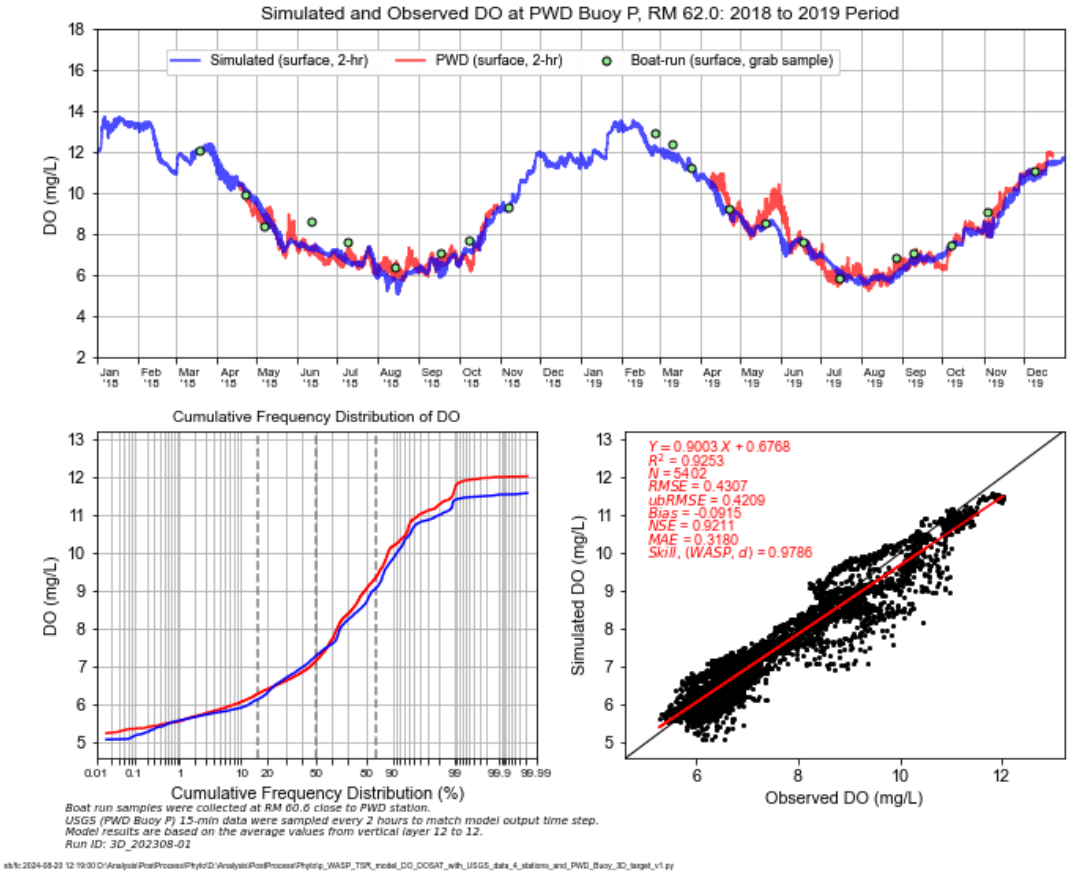

Figure 4-30: Model to Continuous Data Comparison – DO at Buoy P during 2018–2019

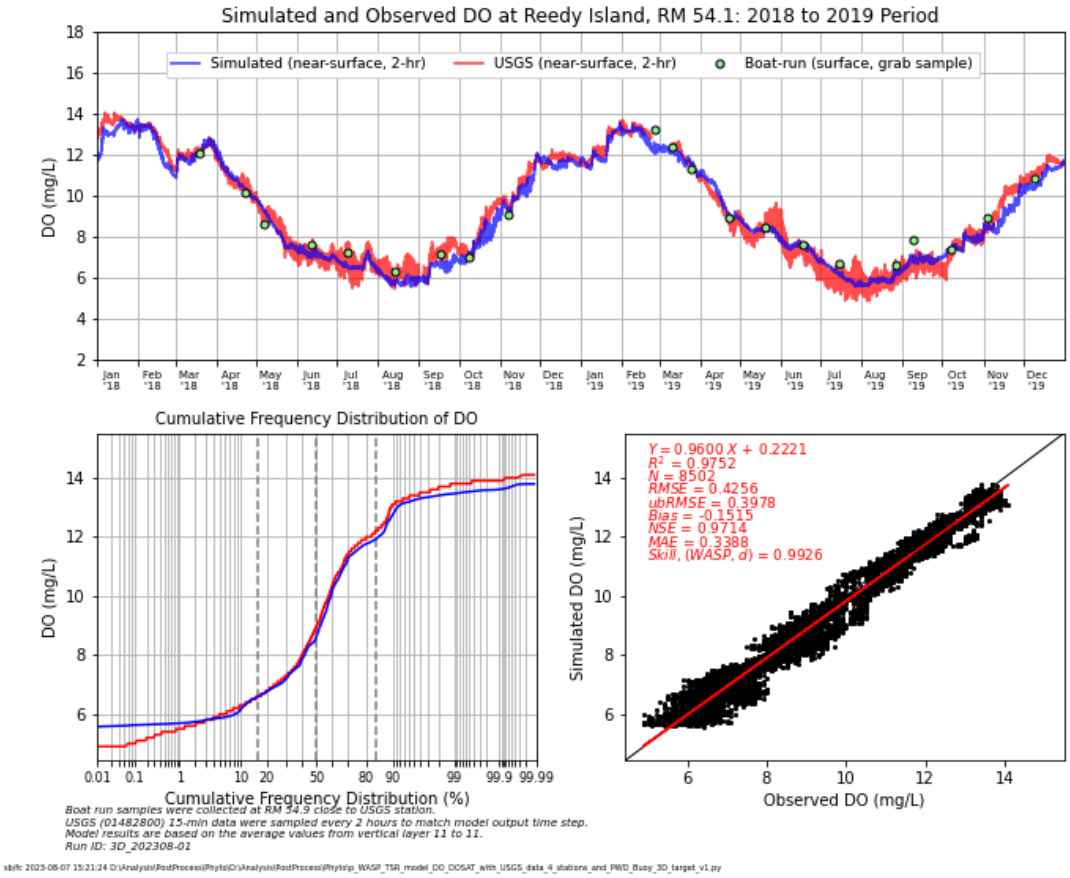

Figure 4-31: Model to Continuous Data Comparison – DO at Reedy Island during 2018–2019

Figure 4-32 to Figure 4-37 present the predicted and observed (near-) surface dissolved oxygen percent saturations (DOSAT) for the 2018-2019 calibration period, again in the sequence of upstream to downstream stations. These comparisons further illustrate the model's ability to reproduce production and consumption of oxygen due to metabolic processes. The figure formats are the same as those in the previous dissolved oxygen comparisons. Similar figures for the 2012 corroboration period are available in Appendix F-8. Both the model predictions and observed data represent instantaneous values paired at two-hour intervals. The model predictions match adequately with the observations of seasonal trends and dissolved oxygen percent saturations at lower values (i.e., at the 1st percentile) for most of the monitoring stations, with the differences between model predictions and measured data of about 3% or less. The largest differences (about 5% at the 0.01 percentile) between the model predictions and observations for lower dissolved oxygen percent saturation values occur at the Buoy P station around RM 62; however, the difference is relatively small (less than 1%) at the 1st percentile. At the Chester station, the model under-predicts the dissolved oxygen percent saturation during most of the calibration period. Model predictions sometimes do not capture the magnitude of the fluctuations of the observations, e.g., June – July 2019. This is likely caused by the under-prediction of algal blooms (i.e., phytoplankton production) in the summer (see the following comparison of chlorophyll-a results and the discussion of Zone 2 light

attenuation in Section 4.5). In addition to the impact of algae blooms on dissolved oxygen percent saturation, it is calculated based on both the predicted salinity and water temperature from the EFDC hydrodynamic model (Chen et al., 2024) and, thus, also impacted by the accuracy to which those parameters are predicted.

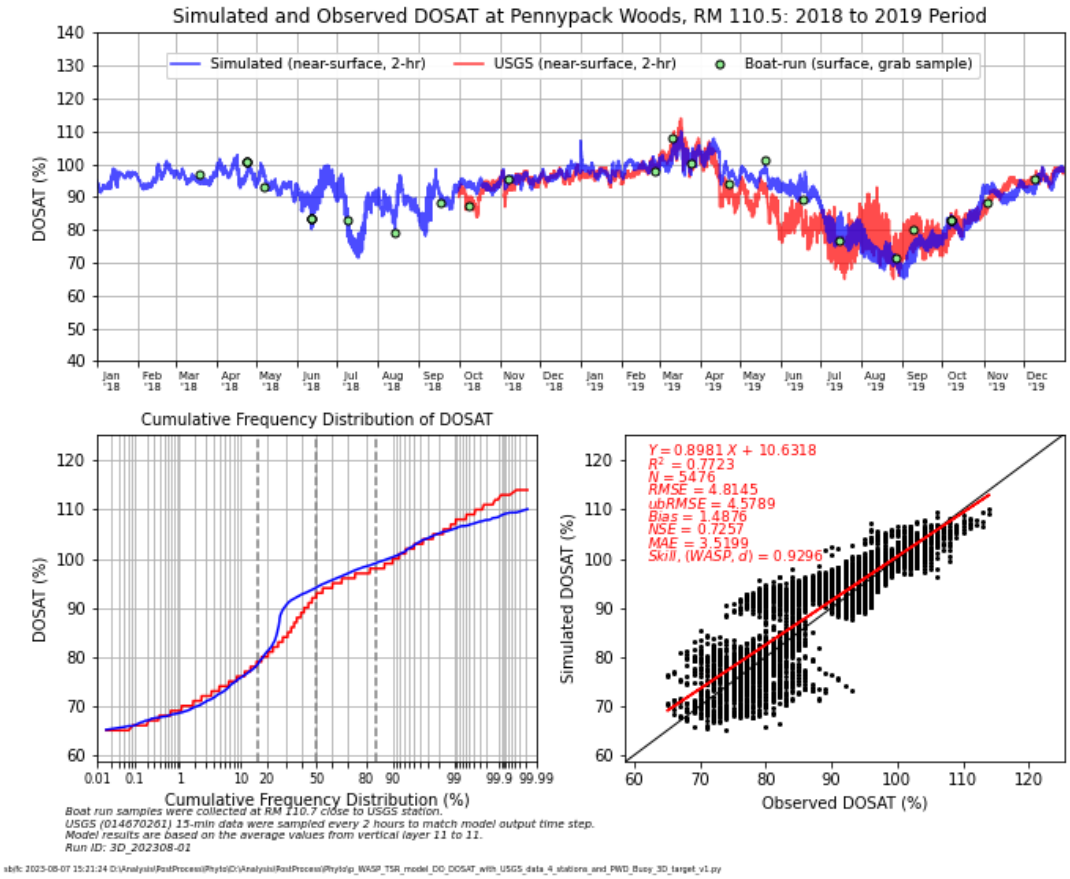

Figure 4-32: Model to Continuous Data Comparison – DOSAT at Pennypack Woods during 2018–2019

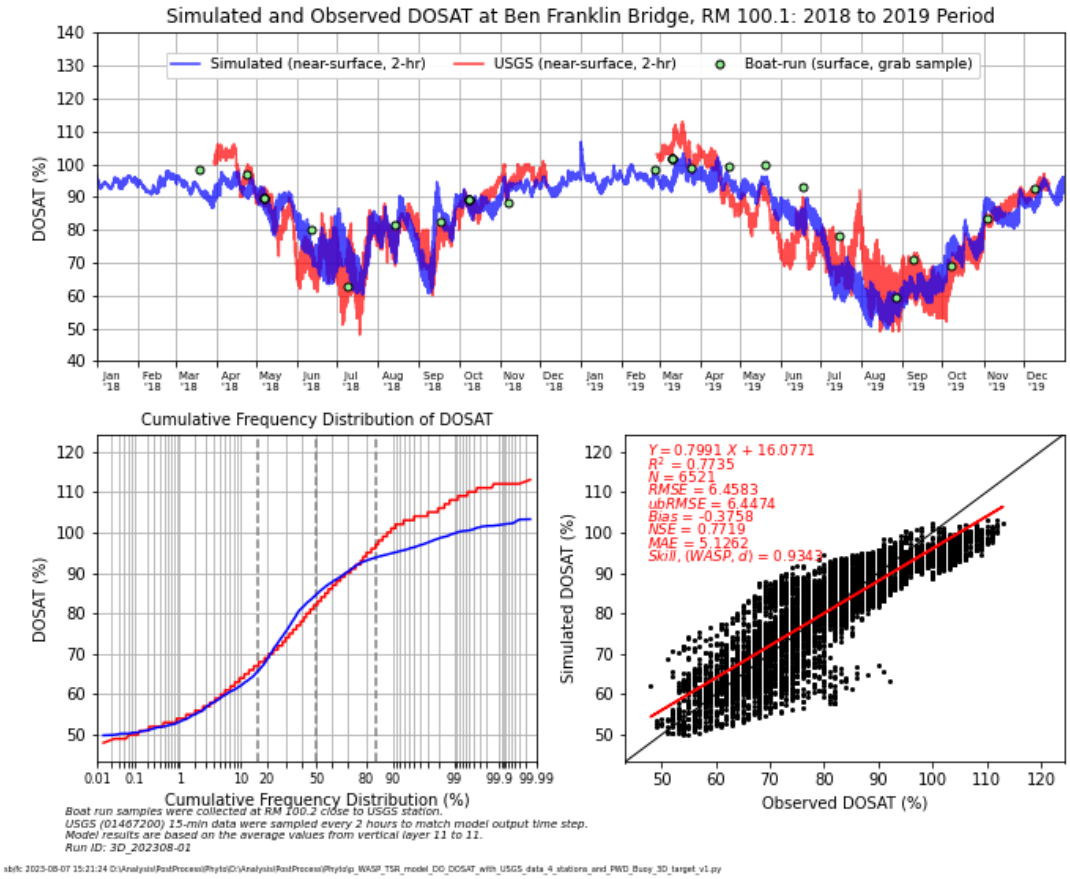

Figure 4-33: Model to Continuous Data Comparison – DOSAT at Ben Franklin Bridge during 2018–2019

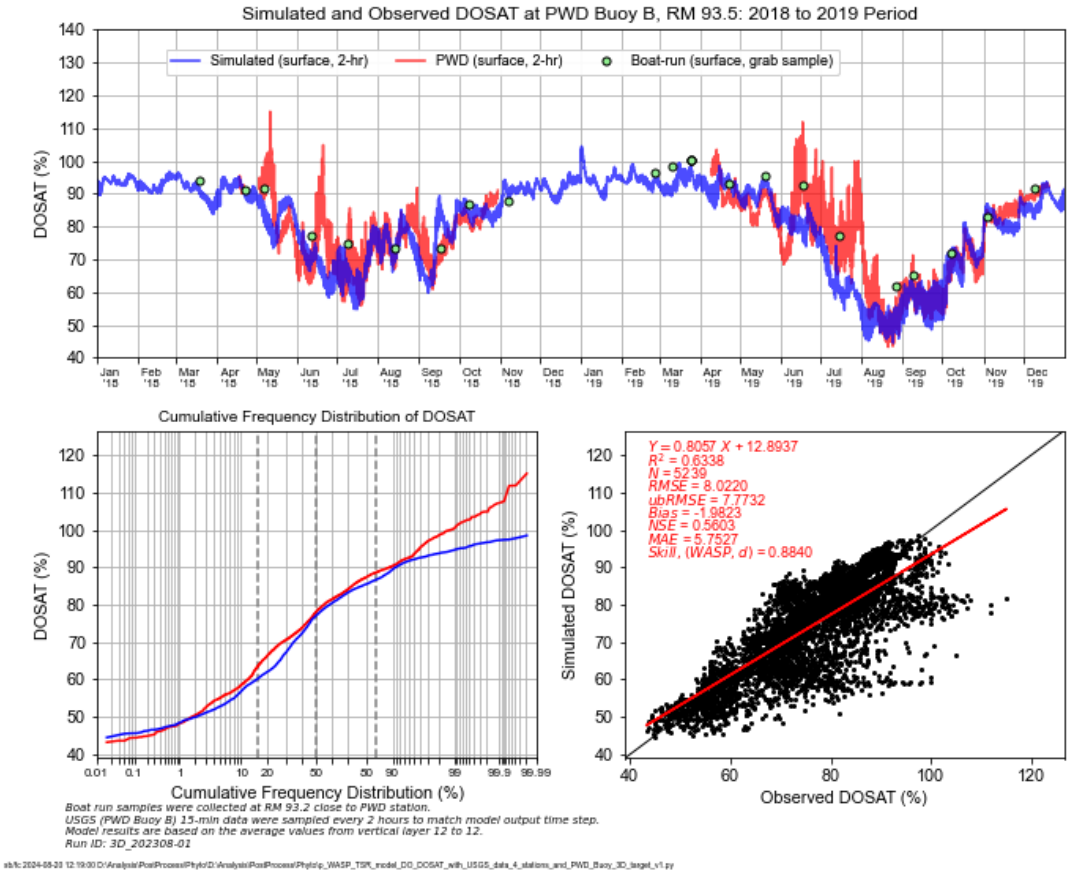

Figure 4-34: Model to Continuous Data Comparison – DOSAT at Buoy B during 2018–2019

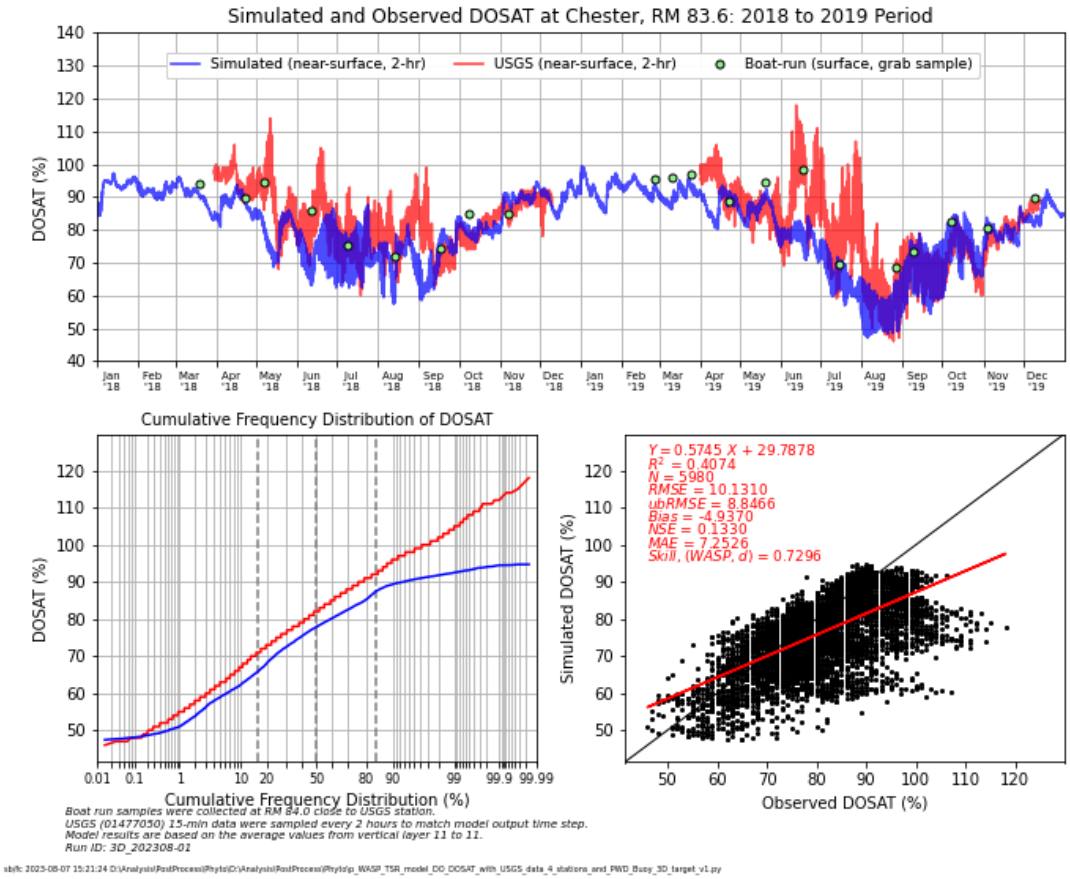

Figure 4-35: Model to Continuous Data Comparison – DOSAT at Chester during 2018–2019

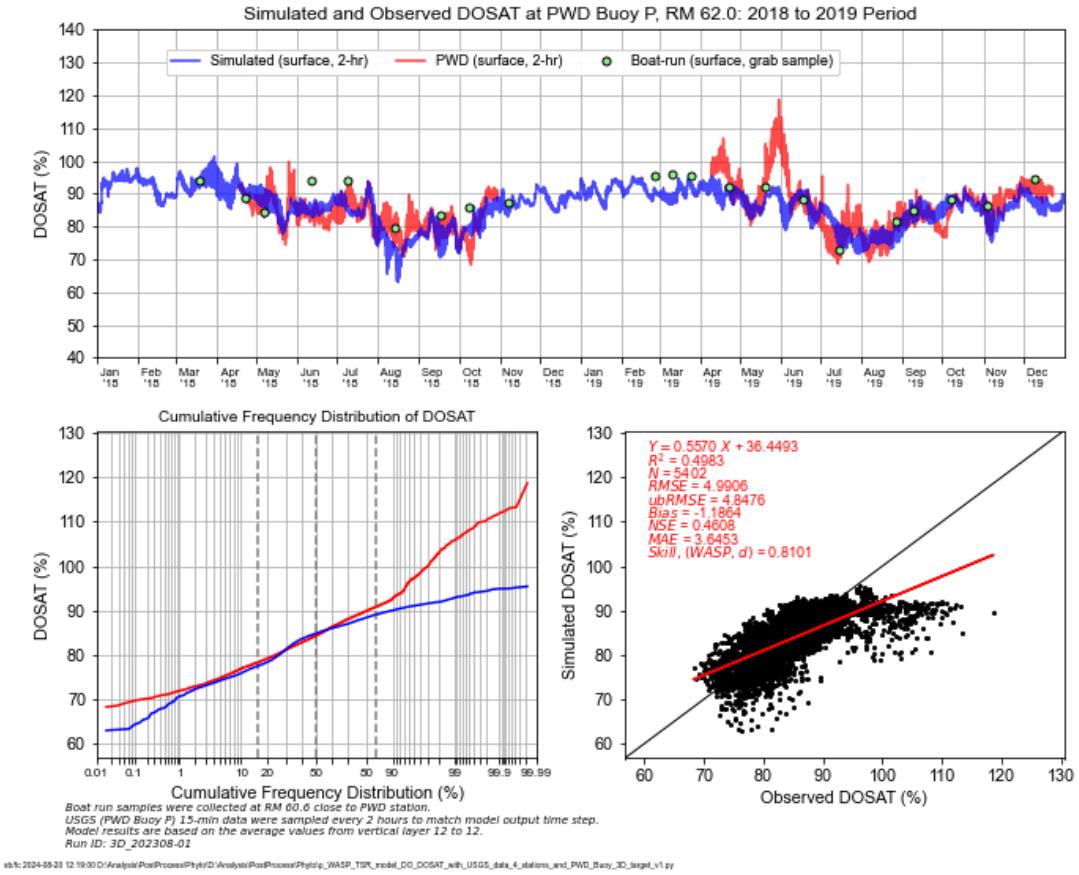

Figure 4-36: Model to Continuous Data Comparison – DOSAT at Buoy P during 2018–2019

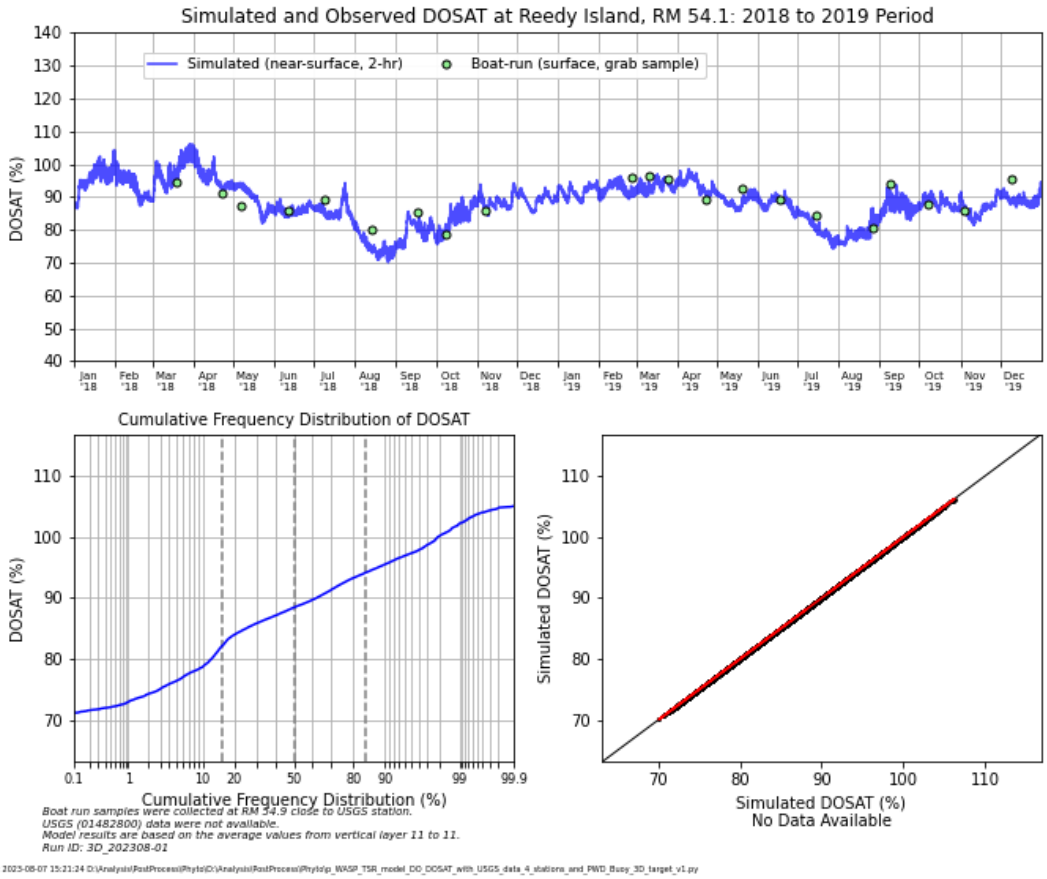

Figure 4-37: Model to Continuous Data Comparison – DOSAT at Reedy Island during 2018–2019

Figure 4-38 to Figure 4-40 illustrate the comparisons of predicted and measured (near-) surface phytoplankton concentrations during the calibration period 2018–2019. The figure formats are the same as those in the dissolved oxygen comparisons. Similar figures for the corroboration period 2012 are available in Appendix F. Daily averaged values were used for both model and data. Continuous phytoplankton data were available only for the USGS station at Ben Franklin Bridge and PWD Buoys B and P during 2018–2019. The pink lines in the top panel of figures represent water age (right y-axis), one of the WASP model output variables, where high values correspond to low flow conditions. The Delaware River Estuary does not normally experience persistent high algal bloom events, but there have been times with minor active phytoplankton events. In this document, whenever there is an uprising peak of phytoplankton concentrations we refer to it as an algal bloom. During the calibration period, the model did reasonably well predicting an algal bloom that occurred in the tidal river during June–July 2018, with the maximum observed chlorophyll-a (Chl-a) concentration being slightly underestimated and the timing of bloom shifting by about a half-month relative to the data. However, the model simulation was unable to reflect an observed algal bloom that occurred in the tidal river around June–July 2019, as also indicated in the comparisons to Boat Run data. Additionally, at Ben Franklin Bridge and Buoy B, the model simulation under-predicts an observed algal bloom in May 2018 and over-predicts a bloom in September 2018. During the 2012 corroboration period, the model does a reasonable job in predicting the observed phytoplankton concentrations, considering the less frequent data available to describe boundary conditions for input to the model. The impact of phytoplankton on dissolved oxygen is shown well in the observed data for June-July of 2019 at Buoy B. As the observed phytoplankton concentration increased to approximately 20 µg/L (Figure 4-39), the observed dissolved oxygen concentrations and percent saturations followed similar trends as shown in Figure 4-28 and Figure 4-34. Under prediction of dissolved oxygen in June-July 2019 at Buoy B can be explained by the under-prediction of phytoplankton. At the same time, the observed data at the Ben Franklin Station did not show the phytoplankton impact on dissolved oxygen for the same time period. Further diagnoses were conducted and presented in Section 4.5 to investigate potential factors (e.g., nutrient and light limiting factors) that may lead to under-prediction of algal blooms in the tidal river, especially during June–July 2019.

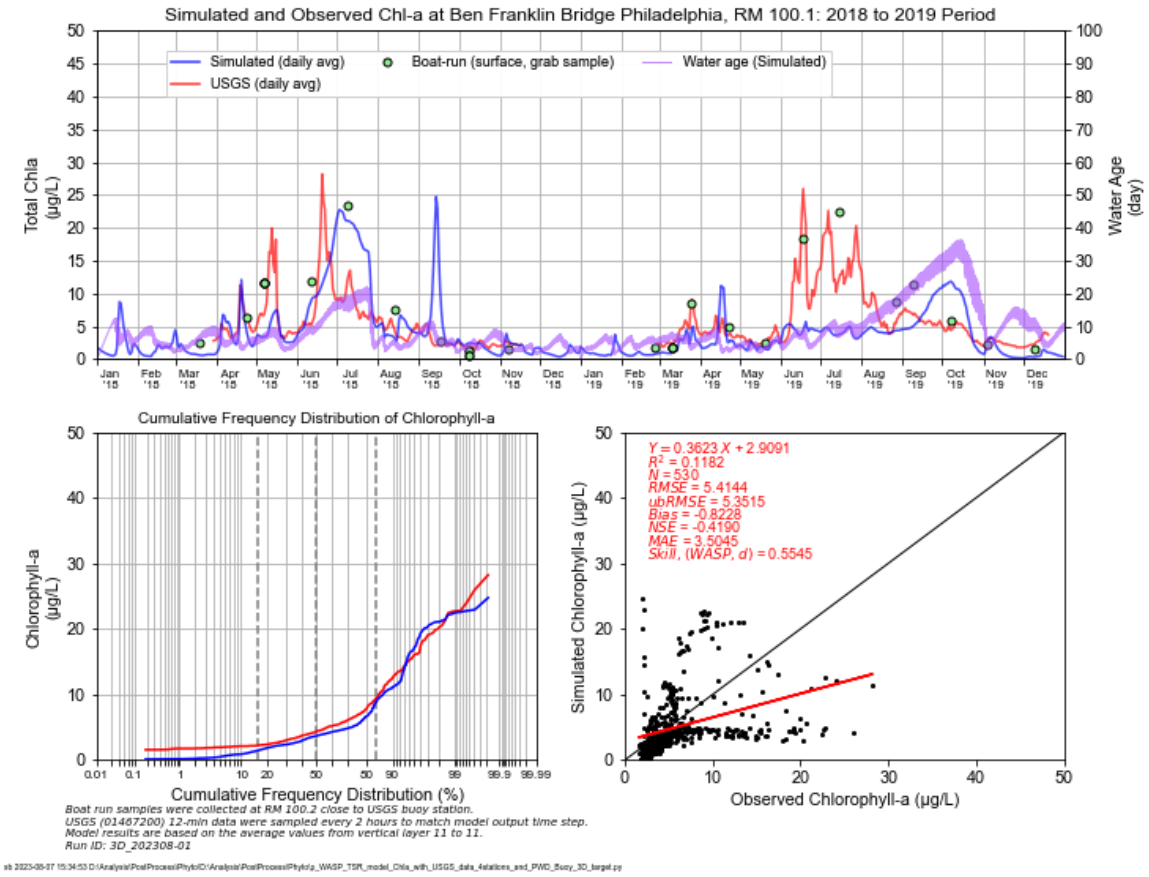

Figure 4-38: Phytoplankton at Ben Franklin Bridge during 2018–2019

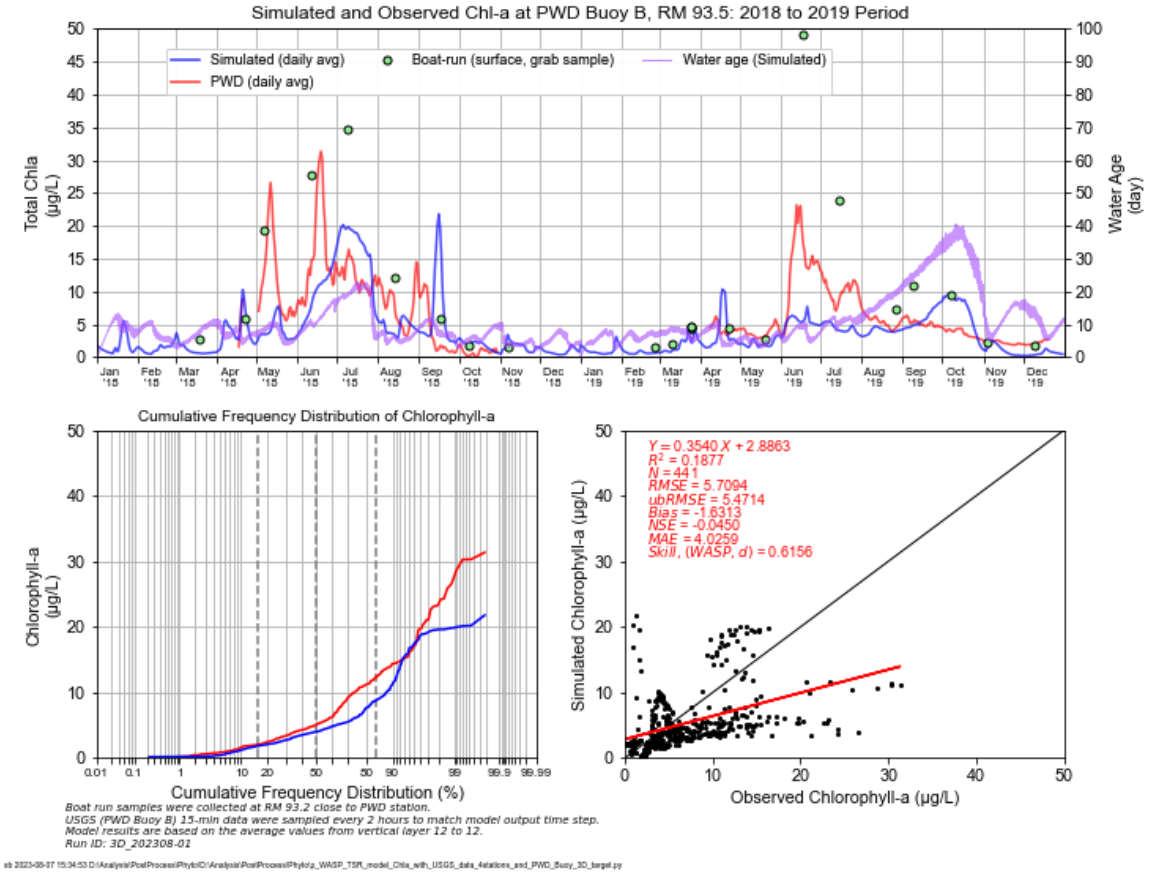

Figure 4-39: Phytoplankton DO at Buoy B during 2018–2019

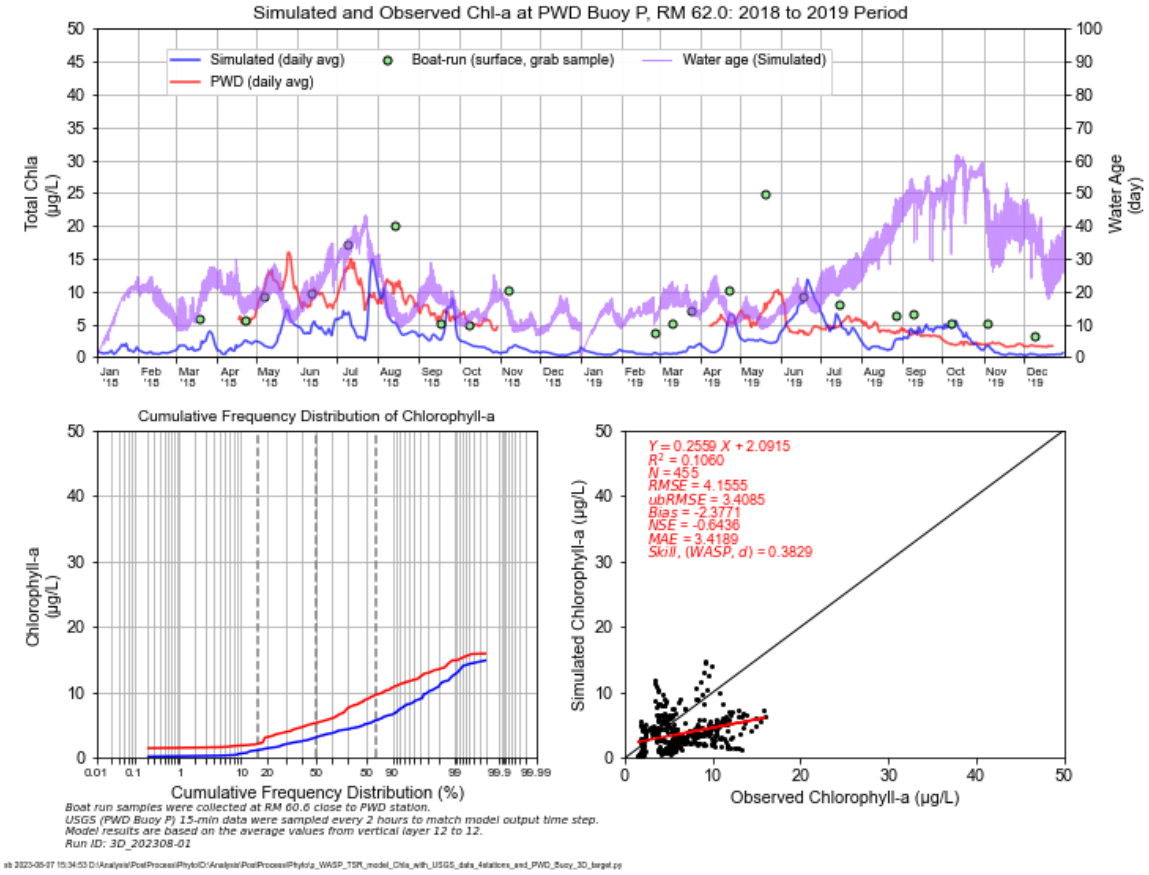

Figure 4-40: Phytoplankton at Buoy P during 2018–2019

The model calibration statistical metrics are summarized in Table 4-4 to Table 4-6 for dissolved oxygen concentrations, percent oxygen saturation, and chlorophyll-a, respectively. Definitions of the metrics can be found in Equations (4-1) to (4-7) and Appendix F. In general, the statistical metrics demonstrate that the model captures the main features of the dissolved oxygen observations exceptionally well. For example, in Table 4-4 the skill factors (or index of agreement) are 0.95 or above at all stations. Additionally, the R^2 and Nash-Sutcliffe coefficients (NSE) at four out of six stations are greater than 0.92. Values of 1 for skill factor, R^2, and NSE represent a perfect match between model predictions and observed data (Davis, 2019, Appendix B). The statistical metrics for dissolved oxygen percent saturation are provided in Table 4-5, and are not as good as those for dissolved oxygen. The skill factors range from 0.73 to 0.93, R^2 ranges from 0.41 to 0.77, and NSE values vary from 0.13 to 0.77. Percent oxygen saturation comparisons are impacted by the combination of temperature and dissolved oxygen uncertainties, so it is not a surprise that the statistical metrics are not as strong. The statistical comparisons for chlorophyll-a (Table 4-6) shows that skill factors, R^2, and NSE range from 0.38 to 0.62, 0.12 to 0.19, and -0.64 to -0.05, respectively. A NSE value of 0 indicates that model predictions are only able to accurately represent the mean of observed data (Davis, 2019, Appendix B). The nature and causes of the weaker model-to-data comparison with regard to chlorophyll-a, as well as its relevance to dissolved oxygen, is explored in Section 4.5.

Table 4-4: Statistical Metrics of Dissolved Oxygen at USGS Stations and PWD-Buoys, 2018–2019

Metrics	USGS-Pennypack Woods	USGS-Ben Franklin Bridge	USGS-Chester	USGS-Reedy Island	PWD Buoy B	PWD Buoy P
N	5476	6521	5980	8502	5239	5402
R^2	0.98	0.95	0.85	0.98	0.89	0.93
RMSE	0.49	0.59	0.84	0.43	0.66	0.43
ubRMSE	0.42	0.59	0.76	0.40	0.66	0.42
Bias	0.25	0.01	-0.35	-0.15	-0.08	-0.09
NSE	0.97	0.95	0.81	0.97	0.88	0.92
MAE	0.39	0.47	0.62	0.34	0.49	0.32
Skill Factor	0.99	0.99	0.95	0.99	0.97	0.98

Note: N stands for Number of observations.

Table 4-5: Statistical Metrics of DO Percent Saturation at USGS Stations and PWD-Buoys, 2018–2019

Metrics	USGS-Pennypack Woods	USGS-Ben Franklin Bridge	USGS-Chester	USGS-Reedy Island	PWD Buoy B	PWD Buoy P
N	5476	6521	5980	N/A	5239	5402
R^2	0.77	0.77	0.41	N/A	0.63	0.50
RMSE	4.81	6.46	10.13	N/A	8.02	4.99
ubRMSE	4.58	6.45	8.85	N/A	7.77	4.85
Bias	1.49	-0.38	-4.94	N/A	-1.98	-1.19
NSE	0.73	0.77	0.13	N/A	0.56	0.46
MAE	3.52	5.13	7,25	N/A	5.75	3.65
Skill Factor	0.93	0.93	0.73	N/A	0.88	0.81

Note: DO percent saturation data are available only at USGS-Reedy Island station.

Table 4-6: Statistical Metrics of Chlorophyll-a at USGS Stations and PWD-Buoys, 2018–2019.

Metrics	USGS-Pennypack Woods	USGS-Ben Franklin Bridge	USGS-Chester	USGS-Reedy Island	PWD Buoy B	PWD Buoy P
N	N/A	530	N/A	N/A	441	455
R^2	N/A	0.12	N/A	N/A	0.19	0.11
RMSE	N/A	5.41	N/A	N/A	5.71	4.16
ubRMSE	N/A	5.35	N/A	N/A	5.47	3.41
Bias	N/A	-0.82	N/A	N/A	-1.63	-2.38
NSE	N/A	-0.42	N/A	N/A	-0.05	-0.64
MAE	N/A	3.50	N/A	N/A	4.03	3.42
Skill Factor	N/A	0.55	N/A	N/A	0.62	0.38

Note: Continuous chlorophyll-a data are available only at USGS-Ben Franklin Bridge station and PWD Buoys B and P.

To better understand model fitness, the model-to-data comparisons of dissolved oxygen, percent saturation, and chlorophyll-a concentrations during 2018–2019 were evaluated using target diagrams (Figure 4-41 to Figure 4-43), which provides a summary of model performance at multiple stations and during multiple years. Jolliff et al. (2009) and MacWilliams et al. (2015) provided a detailed description of target diagrams and their use in model skill assessment. In short, the bias and the unbiased Root Mean

Square Difference (ubRMSD) described in Equations (4-6) and (4-7) are normalized by the observed standard deviation, so the values are comparable among different variables (i.e., to compare model accuracy among groups of stations, and/or among different periods, etc.). On the target diagram, the normalized bias is plotted on the Y-axis and the normalized ubRMSD is plotted on the X-axis.

The bias of model estimates is calculated as

$$bias = \frac{1}{N}\sum_{n=1}^{N} X_{Mi} - \frac{1}{N}\sum_{n=1}^{N} X_{Oi} \quad (4\text{-}6)$$

where subscripts “M” and “O” stand for model and observation values.

Negative bias indicates that the model underpredicts relative to data; positive bias indicates that the model overpredicts relative to data.

The ubRMSD is calculated as

$$ubRMSD = \left[\frac{1}{N}\sum_{n=1}^{N}\left[\left(X_{Mi} - \overline{X}_M\right) - \left(X_{Oi} - \overline{X}_O\right)\right]^2\right]^{0.5} \quad (4\text{-}7)$$

The ubRMSD metric quantifies the model-to-data differences with the bias removed. It is similar to a root-mean-square error, but the effects of bias are removed from the calculation. As ubRMSD increases, the difference between oscillations in the predicted and observed variable becomes larger. To indicate whether the modeled variability is greater than or less than the observed variability, the ubRMSD is multiplied by the sign of the difference between the modeled and observed standard deviations in the target diagram.

An ideal model-to-data comparison would lie on the origin of the target diagram. Jolliff et al. (2009) and MacWilliams et al. (2015) recommend that (1) predictions falling inside a radius of 0.5 are classified as indicating accurate agreement between the model predictions and the observed data, (2) agreement is acceptable if predictions fall inside a radius of 1, and (3) agreement is poor if predictions fall outside a radius of 1. They considered this threshold independent of variables (e.g., chlorophyll a, hydrodynamic parameters, and DO). The target diagram is used as an additional skill assessment tool for evaluating the model performance.

In Figure 4-41, all symbols representing the normalized values of dissolved oxygen comparisons fall within the 0.5-radius. The distribution of the symbols indicates: (1) two-hour instantaneous and daily averaged outputs have almost identical patterns and thus share similar degree of performance (i.e., symbol

positions with respect to the origin where perfect results lie on); (2) model results slightly underestimate dissolved oxygen concentrations, since the count of positive-y symbols is a little less than the negative-y ones; and (3) model results slightly overestimate the variability in dissolved oxygen concentrations, considering the count of positive-x symbols is a little more than the negative-x ones. Overall, the target diagram demonstrates that the model performs well in predicting observed dissolved oxygen concentrations at multiple locations throughout the estuary during the calibration period.

In Figure 4-42, comparisons of dissolved oxygen percent saturation fall within the 1.0-radius except for Chester station, which falls slightly outside the 1.0-radius. This suggests that model predictions of dissolved oxygen percent saturation are acceptable. The distribution of the symbols indicates: (1) two-hour instantaneous and daily averaged outputs have similar patterns and thus share a similar degree of performance; (2) model results slightly underestimate dissolved oxygen percent saturation, since the count of positive-y symbols is less than the negative-y ones; and (3) model results underestimate the variability in dissolved oxygen percent saturation, considering the count of positive-x symbols is less than the negative-x ones.

In Figure 4-43, chlorophyll-a comparisons at PWD Buoy B during 2018–2019 and USGS station at Ben Franklin Bridge during 2019 are located approximately at the 1.0-radius; comparisons at the remaining stations fall beyond the 1.0-radius. The two-hour instantaneous and daily averaged outputs demonstrate a similar degree of performance. The model systematically underestimates chlorophyll-a concentrations since most symbols have negative-y values. In addition, symbols located in the negative-x axis are a little more than those in the positive-x axis, which suggests that the model slightly underestimates the variability in chlorophyll-a. Diagnostic analyses presented in Section 4.5 further address possible reasons for why the model simulation underestimated algal blooms in the tidal river during summer 2018-2019.

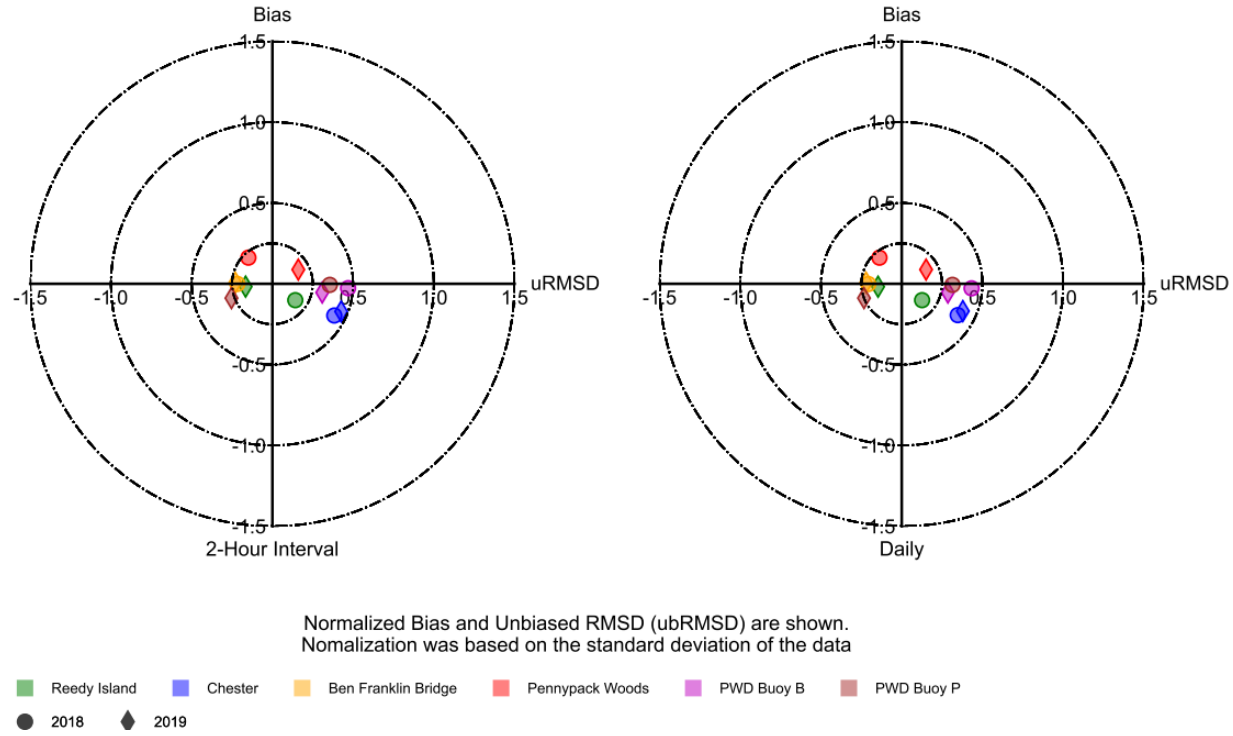

Figure 4-41: Target Diagram for Predicted DO at Continuous Stations, 2018–2019

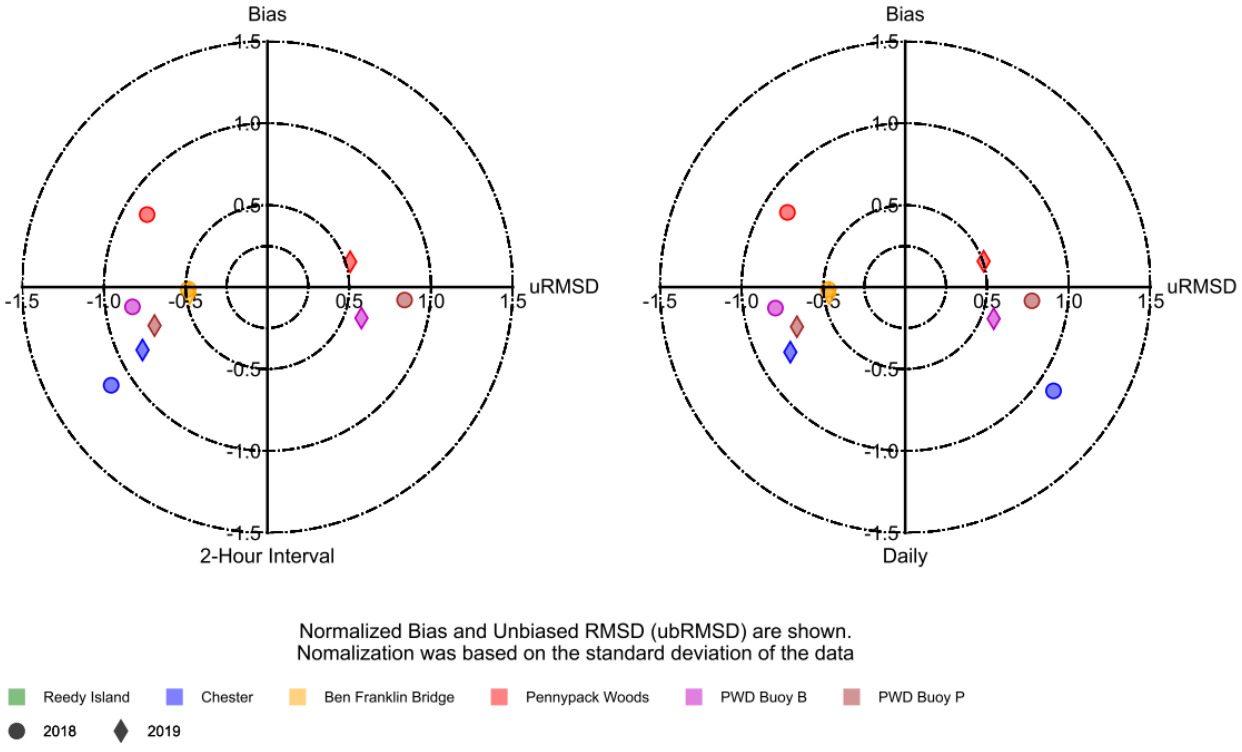

Figure 4-42: Target Diagram for Predicted DOSAT at Continuous Stations, 2018–2019

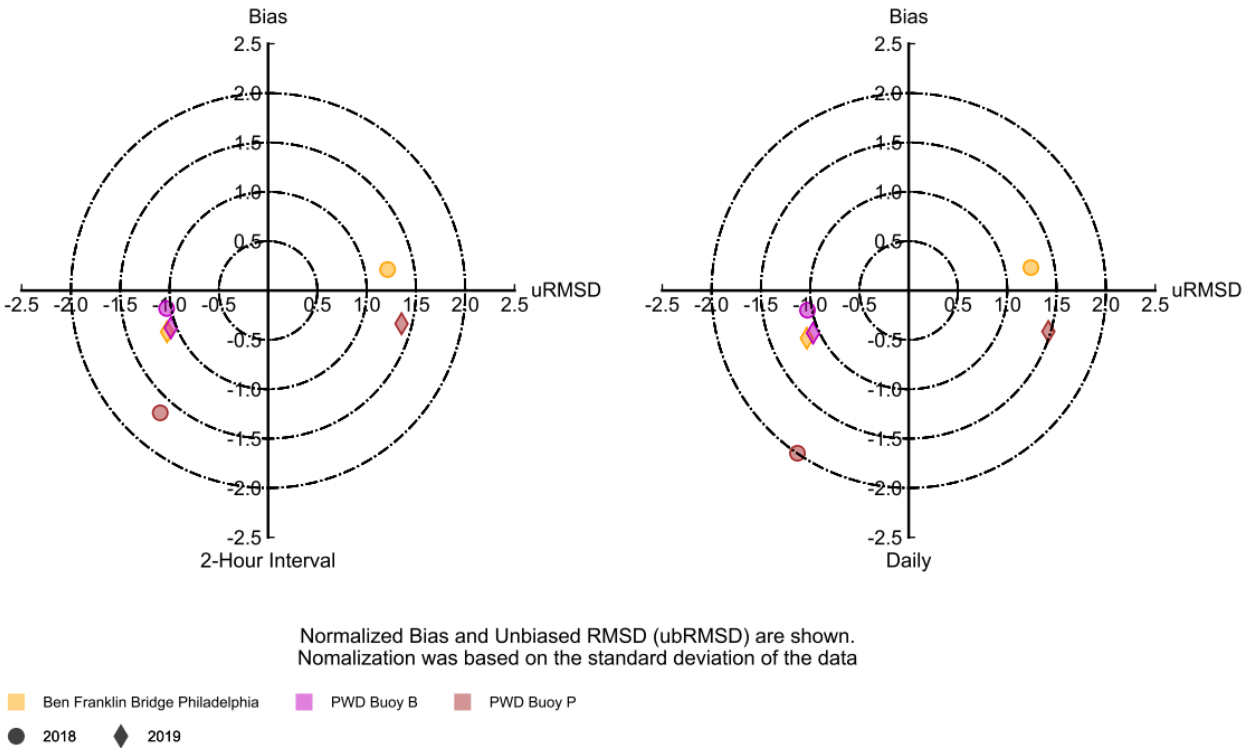

Figure 4-43: Target Diagram for Predicted Chlorophyll-a at Continuous Stations, 2018–2019

4.4.2.2 Dissolved Oxygen Comparisons focused on the Critical Propagation Season

In this section, model predictions of dissolved oxygen are evaluated over a short-term summer period, with an emphasis on the critical fish propagation season from May 1 to October 15. The model statistical metrics for dissolved oxygen during the critical propagation season in 2018-2019 are summarized in Table 4-7. The skill factors (or index of agreement) are equal or larger than 0.92 at all stations, except for Chester with a value of 0.83. A value of 1 for skill factor represents a perfect match between model predictions and observed data (Davis, 2019, Appendix B). Additionally, the R^2 values range from 0.59 to 0.86, and Nash-Sutcliffe coefficients (NSE) values range from 0.42 to 0.80. As mentioned in the previous section, overall model performance should be evaluated both qualitatively and quantitatively.

Cumulative frequency distributions of predicted and measured dissolved oxygen at four USGS stations and two PWD buoy stations during the critical propagation season in 2018-2019 are presented in Figure 4-44, in which the percentile values of model-to-data comparisons are displayed. For example, the 1st percentile dissolved oxygen is the value for which 1% of modeled or measured dissolved oxygen values are lower and 99% are higher. The 1st percentile dissolved oxygen generally characterizes the minimum or acute value at a particular station, while the 50th percentile dissolved oxygen reflects the median or chronic condition. The model generally matches the lower end of dissolved oxygen data well. The absolute differences between model and data at the 1st percentile are about 0.1 to 0.2 mg/L or less at all

stations, except for Reedy Island around RM 54 with a difference about 0.4 mg/L. The larger discrepancy at the Reedy Island station is likely due to the lack of available sediment oxygen demand (SOD) data downstream of RM 60. The differences at the 50th percentile range from 0.0 to 0.4 mg/L. At the Chester station, the model under-predicts the dissolved oxygen during most of the critical propagation period. The model-to-data comparisons at the higher end of dissolved oxygen values are not as good as at the lower end ones, which is in part attributable to the model did not capturing well the phytoplankton production during the critical propagation season.

Figure 4-45 depicts the model-to-data comparisons in the target diagrams for dissolved oxygen during the critical propagation season in 2018-2019. All symbols of dissolved oxygen comparisons fall within the 1.0-radius, and the majority of them are at or within the 0.5-radius. Note that that predictions falling inside a radius of 0.5 are classified as indicating accurate agreement between the model predictions and the observed data, and agreement is acceptable if predictions are inside a radius of 1 (Jolliff et al., 2009 and MacWilliams et al., 2015).

In summary, the statistical metrics results, cumulative frequency distributions, and target diagrams demonstrate that the model captures the main features of the dissolved oxygen observations adequately at multiple locations throughout the estuary over the critical propagation season, especially at the lower end of dissolved oxygen values that are critical from a management perspective.

Table 4-7: Statistical Metrics of Dissolved Oxygen at USGS Stations and PWD-Buoys over critical propagation season in 2018–2019

Metrics	USGS-Pennypack Woods	USGS-Ben Franklin Bridge	USGS-Chester	USGS-Reedy Island	PWD Buoy B	PWD Buoy P
N	2171	3989	3947	3953	3963	3981
R^2	0.86	0.85	0.59	0.81	0.76	0.79
RMSE	0.63	0.61	0.95	0.43	0.73	0.43
ubRMSE	0.55	0.58	0.83	0.42	0.72	0.43
Bias	0.31	0.18	-0.46	-0.06	-0.13	-0.04
NSE	0.67	0.77	0.42	0.80	0.71	0.79
MAE	0.53	0.48	0.72	0.34	0.55	0.31
Skill Factor	0.93	0.95	0.83	0.95	0.93	0.94

Note: N stands for Number of observations.

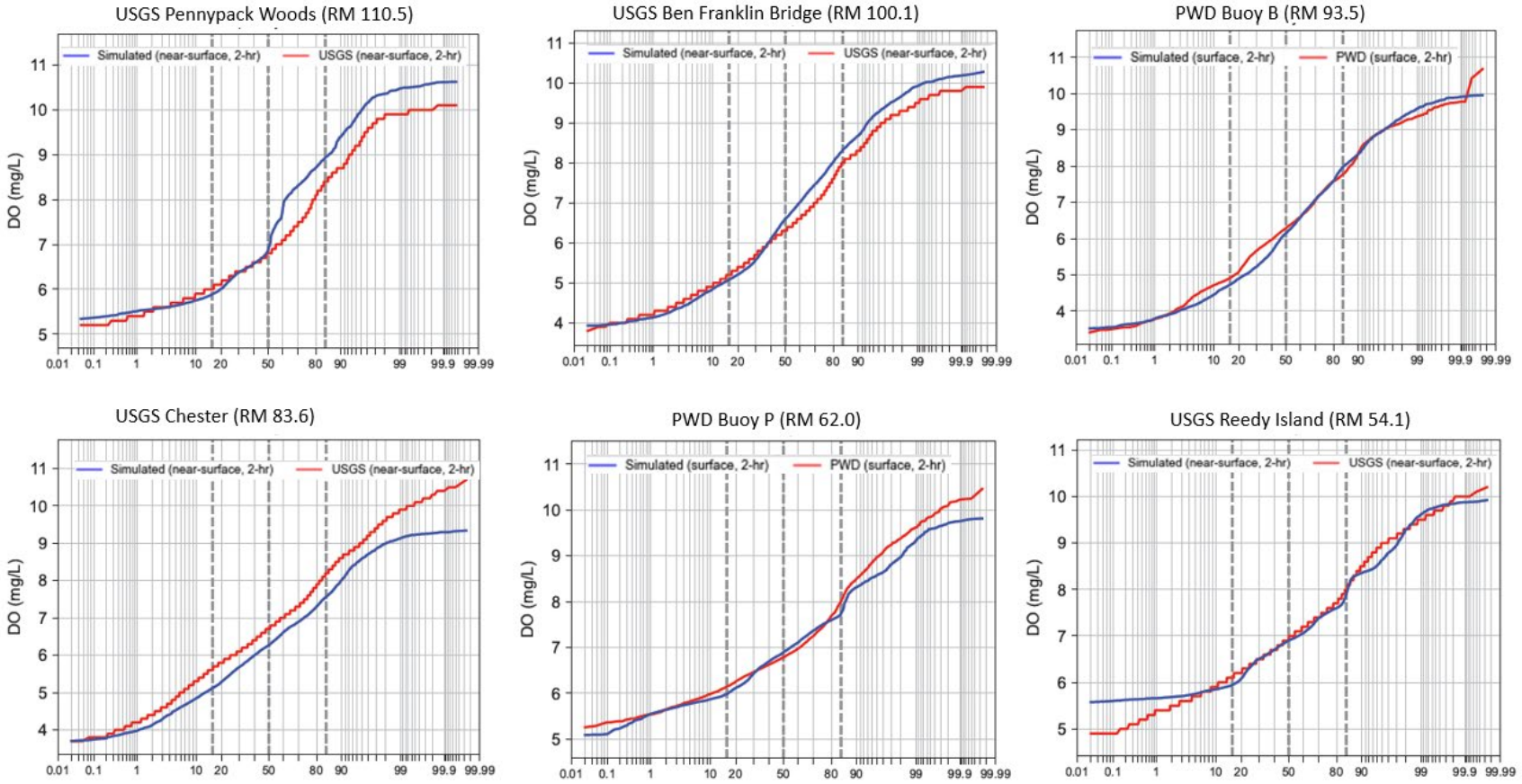

Figure 4-44: Model to Data Comparisons of Dissolved Oxygen at USGS Stations and PWD Buoys over the Critical Propagation Season

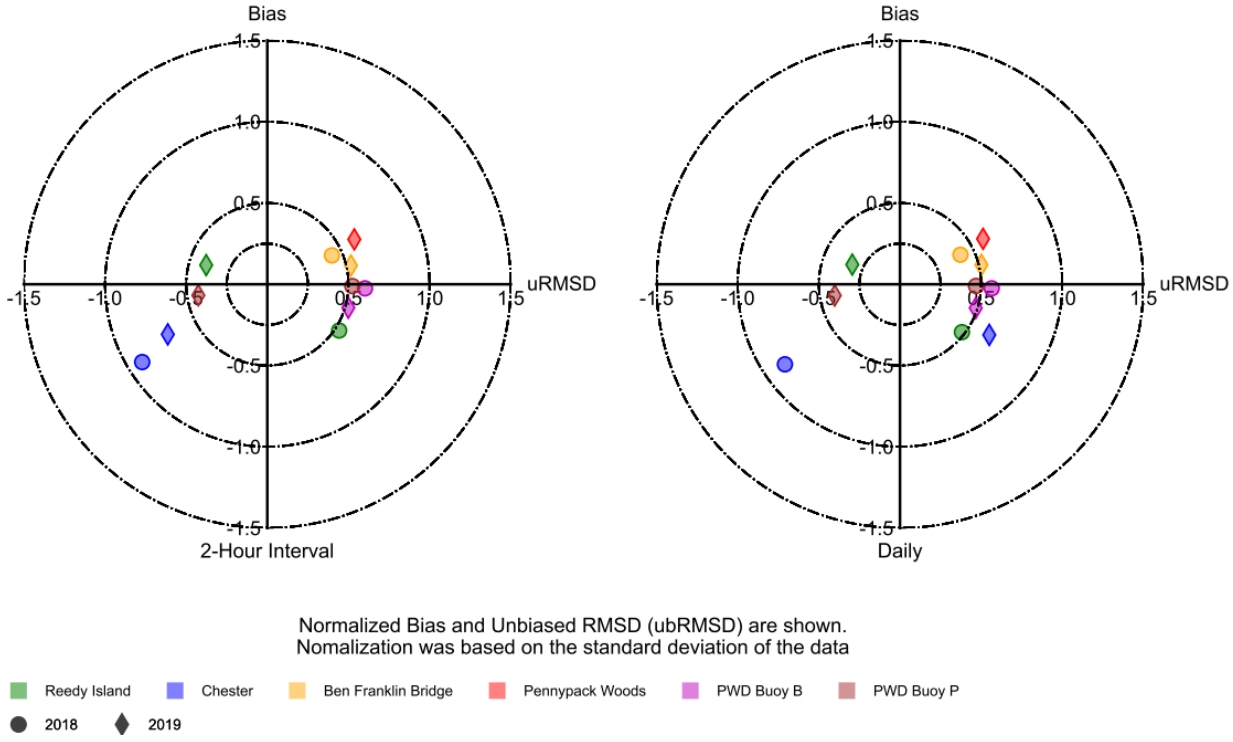

Figure 4-45: Target Diagram for Predicted DO at Continuous Stations over the Critical Propagation Season in 2018–2019

4.4.3 Comparisons to Transect Data

Figure 4-46 through Figure 4-48 illustrate vertical profiles of predicted and measured dissolved oxygen concentrations across five transects near USGS stations during surveys conducted in 2018–2019 and 2012 (Table 4-1). The observed dissolved oxygen concentrations for different vertical profiles are shown as dots and grouped into model grid cells, with different colors (e.g., red, orange, and magenta) representing different measurement profiles (casting of sensors). The values of 'Mod I' represent the model cell IDs across the transects from the Pennsylvania shore (the smaller values) to the New Jersey shore (the larger ones). These vertical profile data reflect the common understanding that the Delaware River Estuary is weakly stratified, especially in the urban area, e.g., up to about 0.5 mg/L difference in dissolved oxygen concentrations from the surface to bottom. Lateral variations show similar ranges of differences in dissolved oxygen concentrations, with New Jersey shore dissolved oxygen concentrations sometimes being slightly higher than those near the Pennsylvania shoreline.

A typical transect survey was performed over a few hours. Model results closest to the middle of the survey span were extracted and are shown as lines in the figures. The model simulations produced similar vertical and lateral structures to the measured dissolved oxygen profiles, although uncertainties exist in terms of the exact timings and locations for comparing the model-predicted and measured values. Model predictions align nearly on top of measured profiles at the transects around Pennypack Woods, Ben

Franklin Bridge, and Delaware Memorial Bridge (except at one shallow cell near the New Jersey shore). The model over-predicted dissolved oxygen concentrations as much as about 0.5 mg/L at the downstream transect near Reedy Island, perhaps due to insufficient or lack of SOD and benthic flux forcing data to inform the model inputs in those areas. More importantly, the vertical gradients of predicted dissolved oxygen were consistent with those of observations.

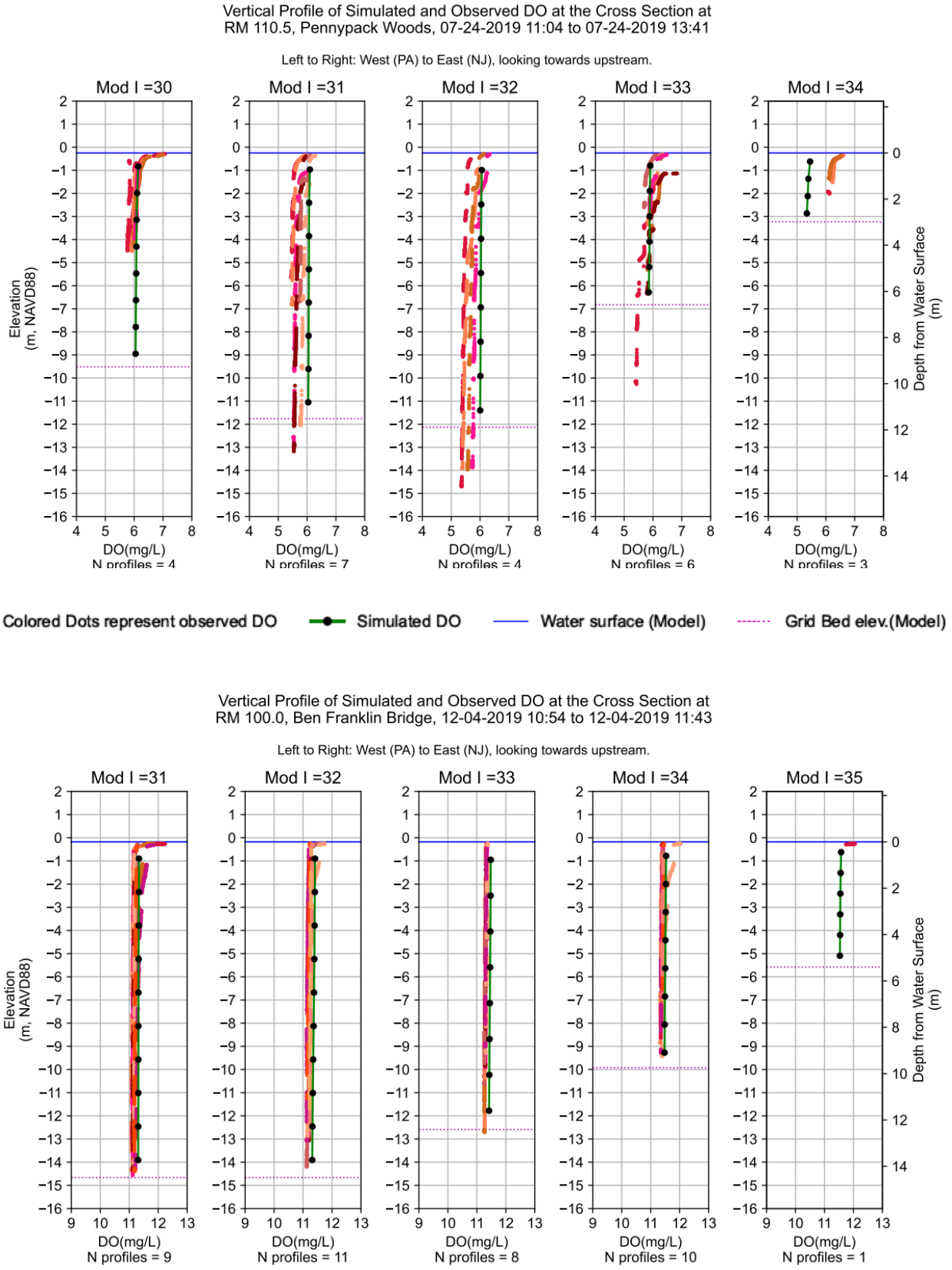

Figure 4-46: Model to Transect Data Comparisons at Pennypack Woods and Ben Franklin Bridge

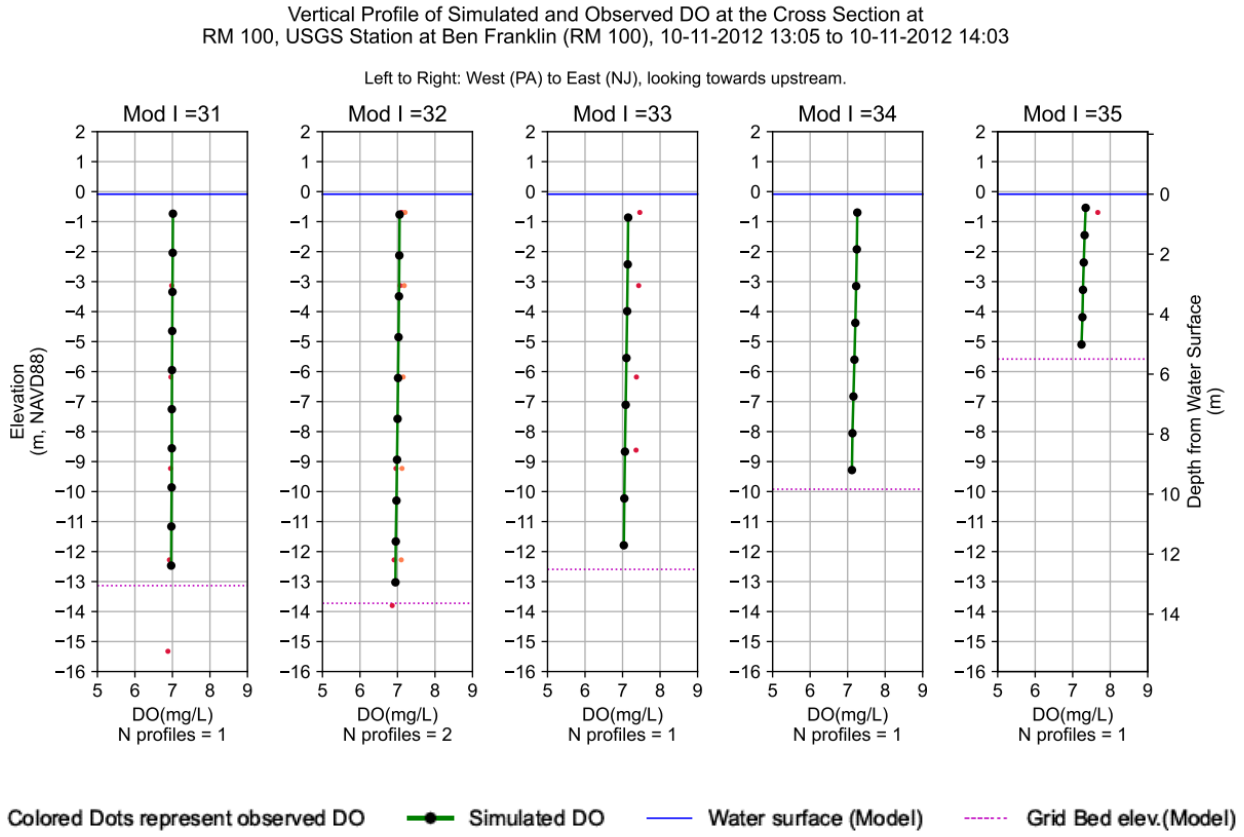

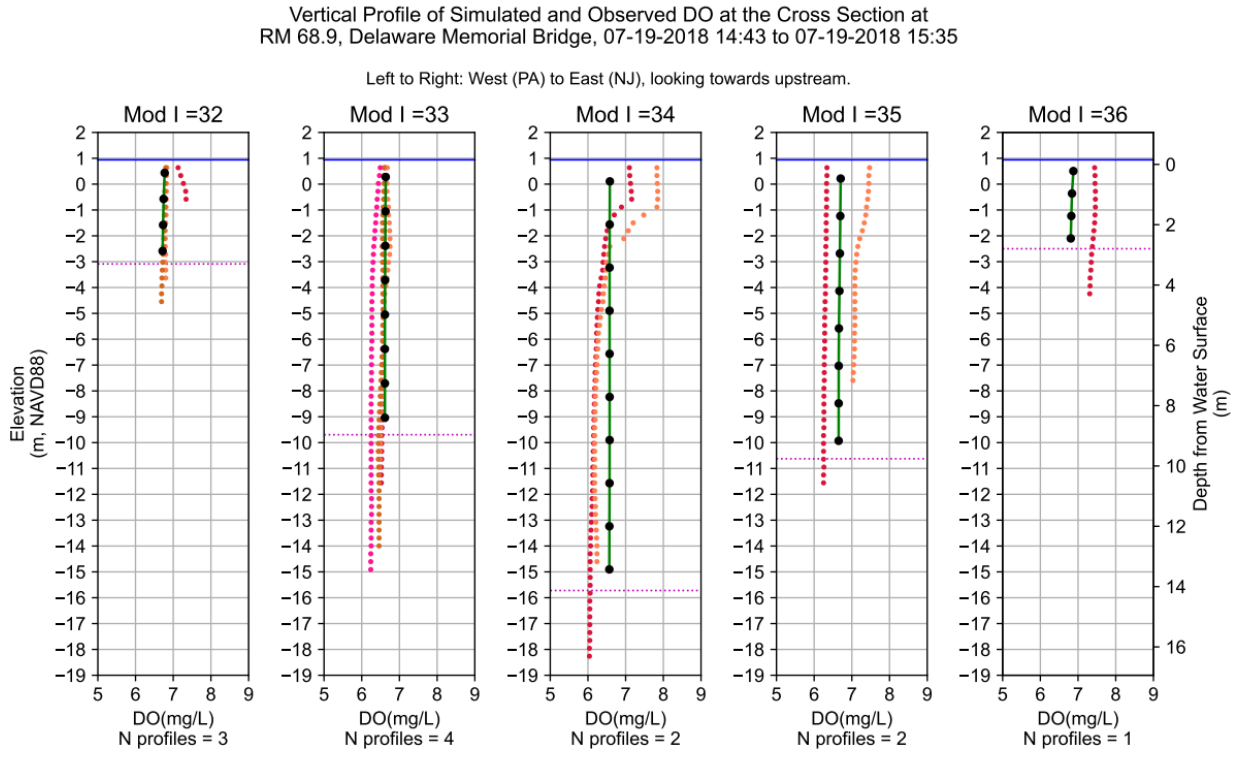

Figure 4-47: Model to Transect Data Comparisons at Ben Franklin and Delaware Memorial Bridges

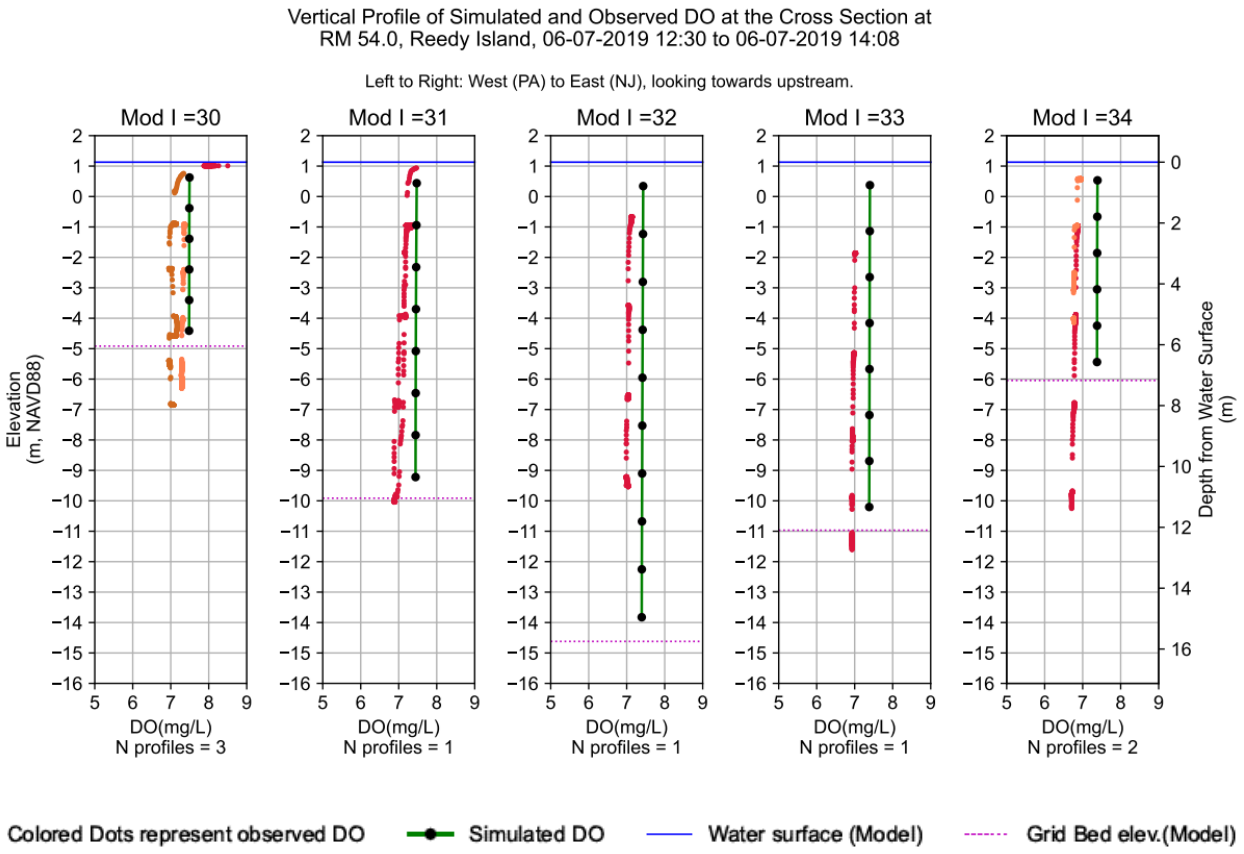

Figure 4-48: Model to Transect Data Comparisons at Reedy Island

4.5 Diagnostic Analyses

A series of diagnostic analyses were conducted to gain a better understanding of model performance and reliability and to help inform decisions about model acceptance and usability.

4.5.1 Dissolved Oxygen Component Analysis

The objective of this analysis is to understand what processes control dissolved oxygen and by how much. This was accomplished by assessing the WASP model output of dissolved oxygen components associated with different processes along the navigation channel.

Figure 4-49 presents the dissolved oxygen gain (as positive) and loss (as negative) in the water column along the navigation channel during February (top panel) and July 2018 (bottom panel). The black solid lines represent the net dissolved oxygen flux (i.e., net impact), and the yellow dash line represents the net algal production (i.e., photosynthesis minus respiration). The complete set of dissolved oxygen component analysis results for the 2018–2019 calibration and the corroboration year of 2012 are provided in Appendix G. The results presented in Figure 4-49, which are monthly-averaged and displayed in a

stacked-fashion, represent the dissolved oxygen gain/loss over the entire water column from the mouth of the Bay (RM 0) to the head of the tide (RM 134).

For the model simulation of February 2018, the predicted major contributor to dissolved oxygen gain in the Bay is algal productivity (photosynthesis), which caused supersaturation in a portion of the Bay. As a result, reaeration transferred dissolved oxygen from the water to the atmosphere. Other loss terms in the Bay are algal respiration, followed by SOD and CBOD oxidation. In the tidal river, reaeration is the major contributor to the dissolved oxygen gain in the water column. The contribution from algal production by freshwater diatoms is minimal during this wintertime month (i.e., part of the non-growing season). The major dissolved oxygen loss term is nitrification, with CBOD oxidation and SOD being the second and third largest losses.

For the model simulation of July 2018, algal productivity remains the major contributor to the dissolved oxygen gain in the Bay. Major loss terms in the Bay are algal respiration and SOD, followed by CBOD oxidation, nitrification, and reaeration. In the tidal river, reaeration and algal productivity contribute a similar amount to dissolved oxygen gain. The principal dissolved oxygen loss term in the tidal river for this summer month is dominated by nitrification, followed by SOD and CBOD oxidation.

This diagnostic analysis of dissolved oxygen components indicates that in the urban estuary, reaeration and photosynthesis are the major processes controlling dissolved oxygen production. The major processes affecting dissolved oxygen consumption within this reach of the urban estuary are nitrification, followed by SOD, CBOD oxidation, and respiration. Note that the dissolved oxygen gain from net algal production (yellow dash line) is much smaller than the dissolved oxygen loss caused by nitrification (red color zone) in the tidal river. Furthermore, reaeration, because it is driven by the gradient between DO at full saturation and water column DO, mitigates the impact of variations in photosynthesis. For both of these reasons, the practical impact of photosynthesis is less than what otherwise might be expected.

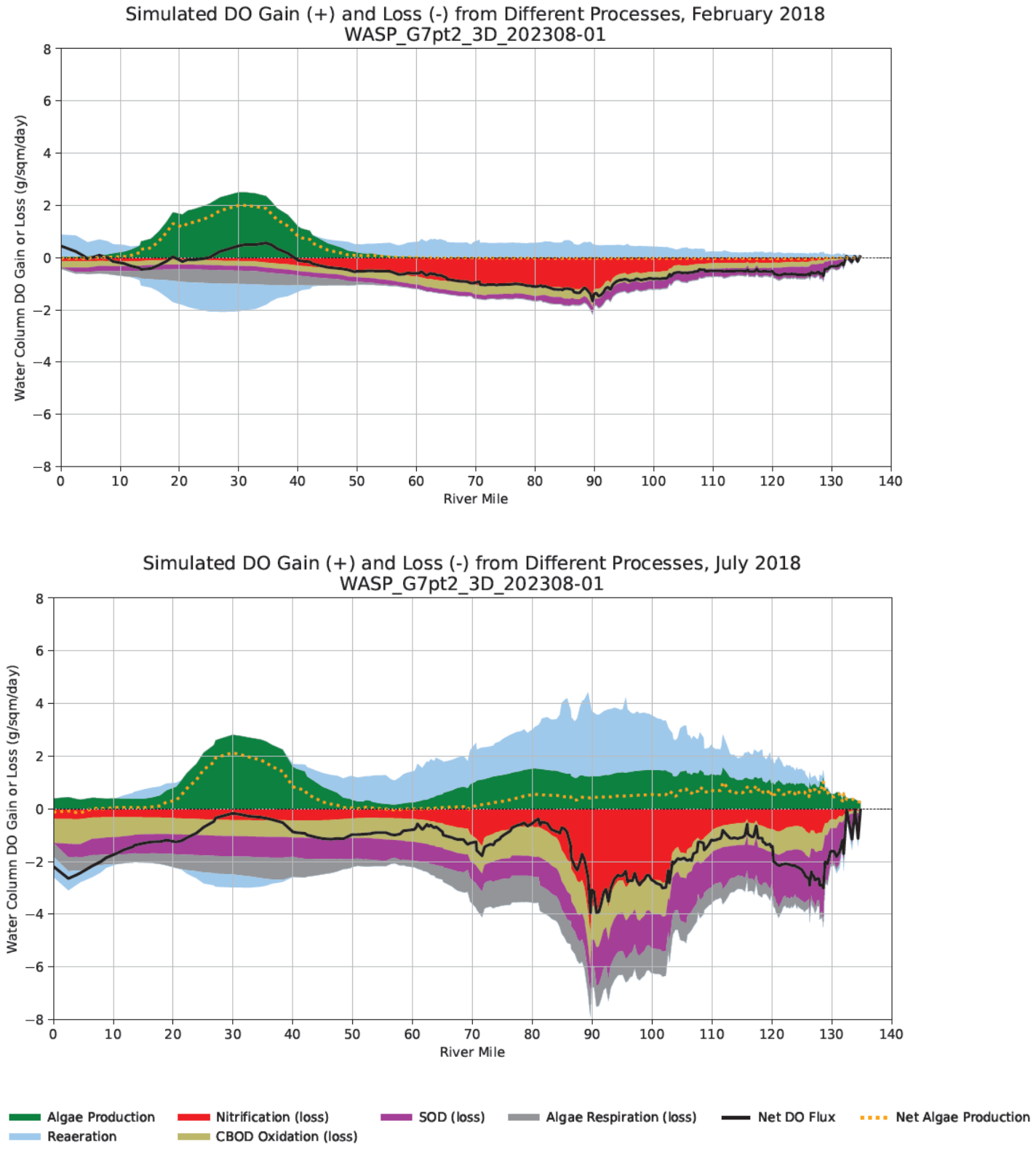

Figure 4-49: DO Component Analyses – February and July 2018

4.5.2 PHYTOPLANKTON LIMITING FACTORS

The objective of this model diagnostic was to ascertain which factors control phytoplankton growth (i.e., chlorophyll-a concentrations in the model) and their relative seasonal importance. This was done by analyzing the growth-limiting factors associated with nutrients, light, and water temperature.

Figure 4-50 and Figure 4-51 present the limiting factors of nutrients (i.e., nitrogen, phosphorus, and silica) and light at Ben Franklin Bridge during 2019 at the water surface and water column depth-averaged, respectively. Additional figures of limiting factors at other locations and years are provided in Appendix G. Light and nutrient limiting factors were calculated based on Equations (3-11) and (3-12), which are multipliers applied to the user specified maximum growth rates in Equation (3-8). In other words, the values of limiting factors reflect a fraction of maximum growth rates.

Results in Figure 4-50, Figure 4-51, and Appendix G indicate that there is infrequent growth limitation associated with nitrogen and silica (i.e., limiting factor close to 1, almost 100% of the maximum growth rates), but some occasional perceptible growth limitation for phosphorus. Strong vertical mixing in the tidal river results in nearly uniform distribution of nutrient concentrations in the vertical direction. As a result, the nutrient limiting factors at the water surface and throughout the water column (i.e., depth-averaged) are almost identical, as shown in Figure 4-50 and Figure 4-51.

Results in Figure 4-50 and Figure 4-51 also suggest that light does constrain phytoplankton growth as expected. Limiting factors are up to about 0.7 to 0. 8 (i.e., 70% to 80% of the maximum) at the water surface, while the depth-averaged values are up to about 0.1 (i.e., 10% of the maximum throughout the water column on average). The vertical variation of light limiting factor at Ben Franklin Bridge (Figure 4-52) further indicates that light limiting factors decrease dramatically with water depth. For example, the light limiting factors reduce from 0.7 to 0.8 at the surface layer to about 0.1 to 0.2 in the second layer (immediately below the surface layer), then become close to zero in the third layer, and further drop to zero in the bottom layer. This implies that only the top two layers receive enough light to permit phytoplankton growth, and the lower layers are almost completely dark. The vertical stratification in light limiting factor is caused by the highly turbid environment in the Delaware River Estuary. Longitudinally, figures in Appendix G indicate that light limiting factors at the upper portion of the estuary are a little larger (e.g., 0.8 to 0.9 during summer at Pennypack Woods) than those at the downstream portions (e.g., around 0.7 during summer at Ben Franklin Bridge, Chester, and Reedy Island). In other words, light penetrates the water column relatively easier in the upper portion.

Figure 4-53 illustrates the limiting factors associated with water temperature at Eddystone (RM 84) for three groups of phytoplankton during 2019. The patterns of temperature limiting factors at other locations and years are similar. Temperature limiting factors were calculated based on Equations (3-9) and (3-10). The maximum value of 1.0 corresponds to the optimal temperature for growth, which are defined as calibration parameters in the model (see Section 4.3) to be 4.3, 22.5, and 26.3^{o}C, for phytoplankton groups 1, 2, and 3, respectively. When water temperature is not at the optimal temperature for growth for a particular phytoplankton group then growth is constrained for that group.

In other words, temperature always defines the upper bound envelope for the phytoplankton growth rate, and light and nutrients control the specific growth rates within this envelope.

This diagnosis indicates that (1) nutrients, light, and temperature can all limit phytoplankton growth, consistent with Equation (3-8); and (2) regardless of temperature, phytoplankton is more limited by light than by nutrients in the Delaware River Estuary.

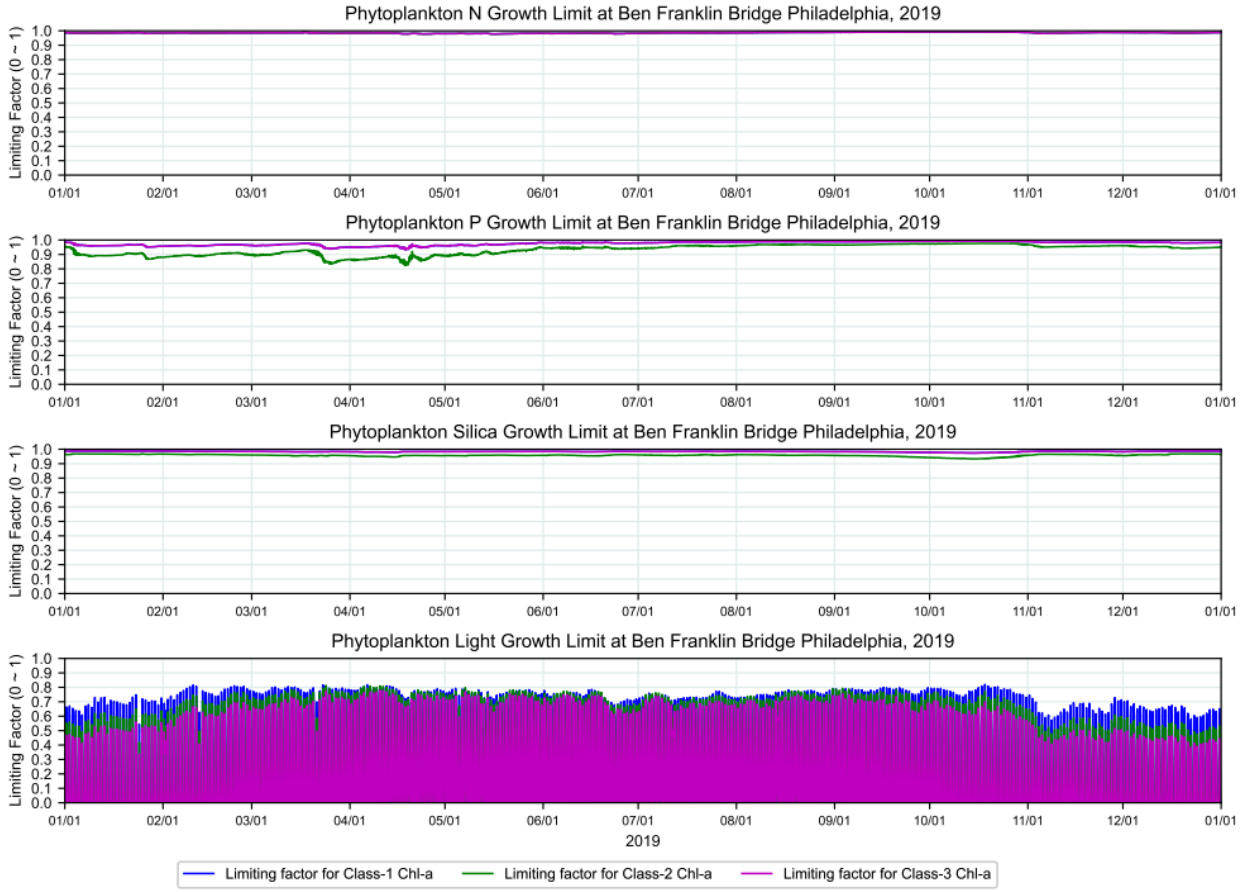

Figure 4-50: Phytoplankton Growth Limiting Factors at Ben Franklin Bridge during 2019 – Water Surface

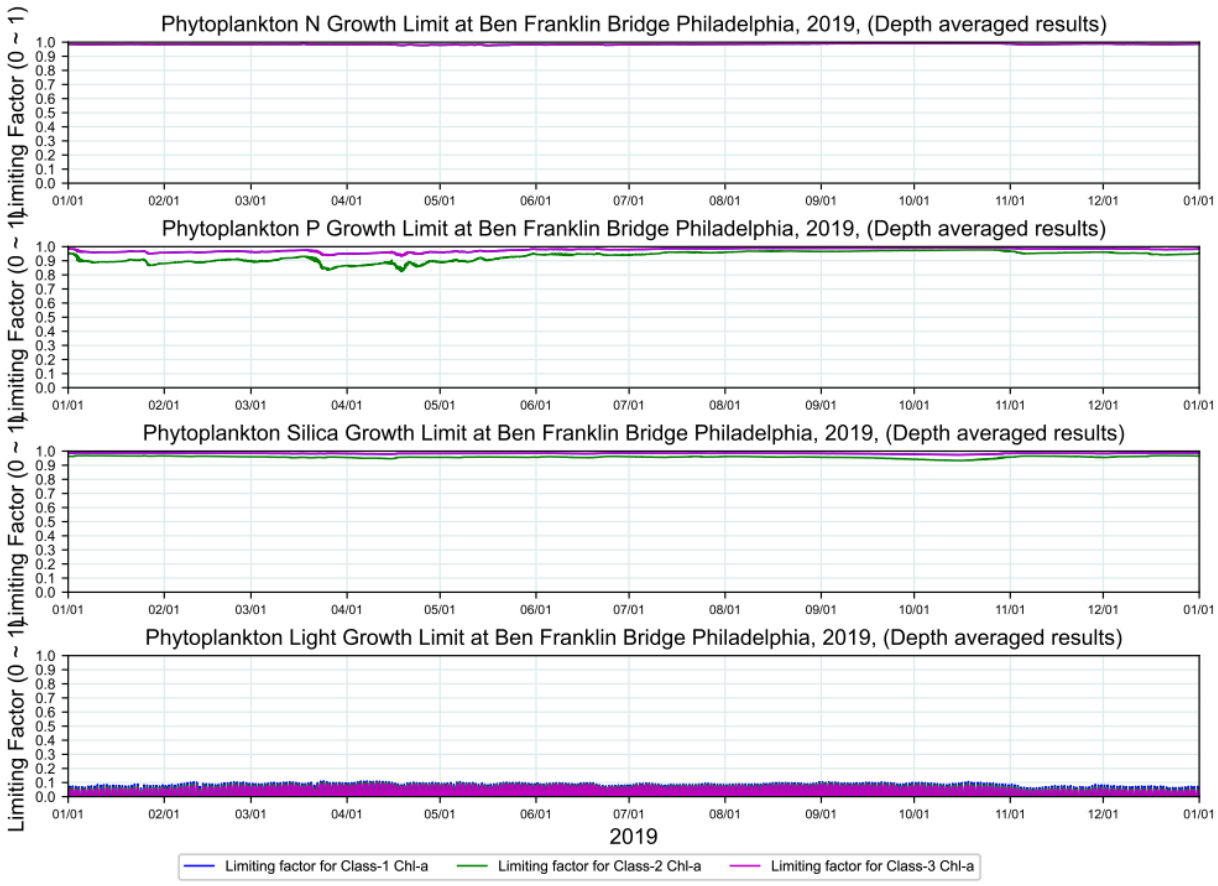

Figure 4-51: Phytoplankton Growth Limiting Factors at Ben Franklin Bridge during 2019 – Depth-averaged

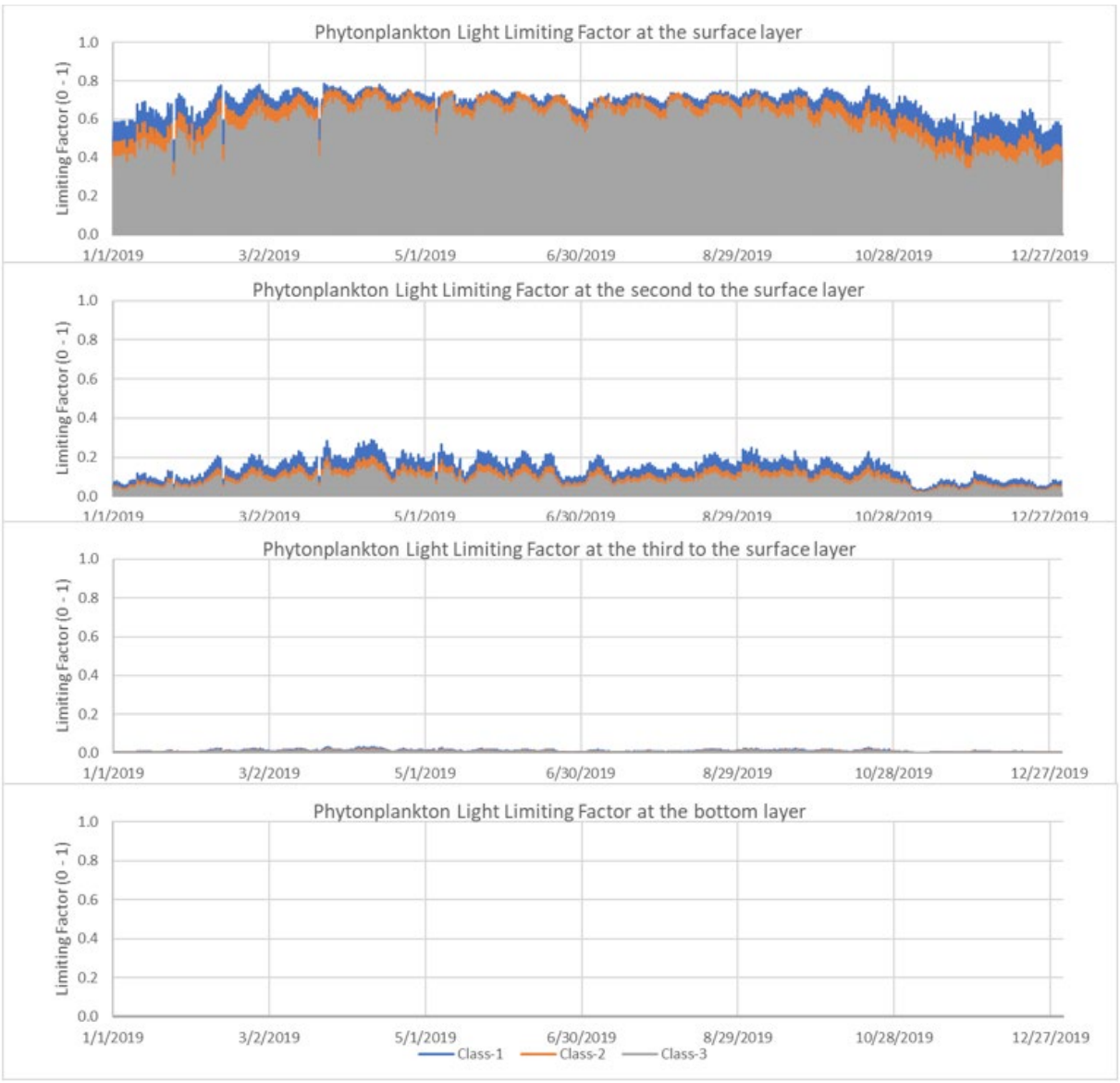

Figure 4-52: Light Limiting Factors on phytoplankton growth at Ben Franklin Bridge during 2019 – Vertical profile

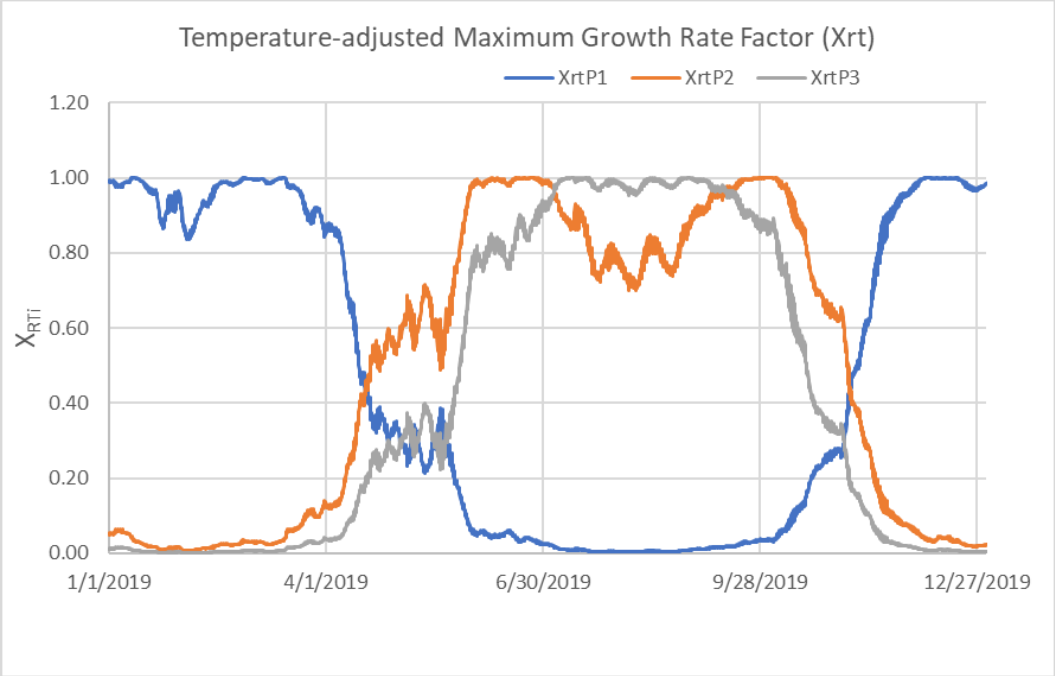

Figure 4-53: Temperature Limiting Factors on phytoplankton growth at Eddystone during 2019

4.5.3 Zone 2 Light Attenuation Diagnosis

The previously discussed model diagnostic tests were used to evaluate potential factors causing the under-prediction of algal blooms in the tidal river during June—July 2019, including temperature, boundary loads of phytoplankton (i.e., chlorophyll-a), kinetic specifications, random variations to the light extinction coefficients, nutrient limiting factors, and flow conditions. The conclusion is that these factors are unlikely to be causing the under-prediction of phytoplankton. On the other hand, the diagnosis in the previous section indicates that light availability in the water column largely controls the growth of phytoplankton in the Delaware River Estuary. One hypothesis is that the existing light extinction formulation may not capture all the necessary mechanisms governing water column light attenuation, although the model generally does a good job reproducing the derived light extinction coefficients *Ke* based on observed PAR measurements during the DRBC Boat Run surveys (Figure 4-19 and Appendix G).

Dr. Chant (one of the DRBC Model Expert Panel members) and his colleagues have extensively studied the physical and biological processes of the Delaware River Estuary. According to Dr. Chant's findings:[19]

> "It has long been recognized the primary production in Delaware Bay is light limited (Pennock, 1985). The predominant physical factor limiting light, and thus phytoplankton biomass, is suspended sediment (McSweeney et al., 2017). In tidal rivers heavy loads of sediment are supplied

[19] Personal correspondence with Dr. Chant and DRBC staff via email.

to the system during high river flow events which are temporarily stored at the bed in the upper reaches of the river. The finer sediments deposited by these events are reworked by tidal currents and remain in suspension (Ralston and Geyer, 2017) and thus persistently limit light levels and primary production. Tidal resuspension, and thus sediment concentration, is proportional to tidal current amplitude. In the Delaware River tidal currents in main channel are between 80-120 cm/s throughout much of the estuary but rapidly fall off to near zero at the head of the estuary at Trenton (Pareja-Roman et al., 2020) thus we expect water clarity to increase in the upper reaches of the river. Indeed, observations of light levels in the upper reach of the river during low flow conditions reveal that the depth penetration of the 1% light level increases from a depth of less than 5 meters at the ETM around km 100 to nearly 10 m at km 200 at Trenton (Figure 3 MsSweeney et al., 2017) [Figure 4-54]. Coincident with the elevated light levels are elevated Chlorophyll concentration (3B) and elevated oxygen levels (3D) all consistent with elevated primary production in this reach of the river. I note that in our field survey in 2011 also observed elevated Chlorophyll in the upper reaches of the river. In an ensuing river flow event these water masses, would be advected down-stream and influence water quality throughout the system.

An example of this phenomena occurred in June of 2019 when a series of high river flow events was followed by increased chlorophyll concentrations at Ben Franklin Bridge [Dr. Chant included a graph, which is reproduced as Figure 4-55]. Here, the model needed to increase water clarity in the upstream reaches of the river to produce this biomass that was produced upstream and later advected down-stream by elevated river flow events."

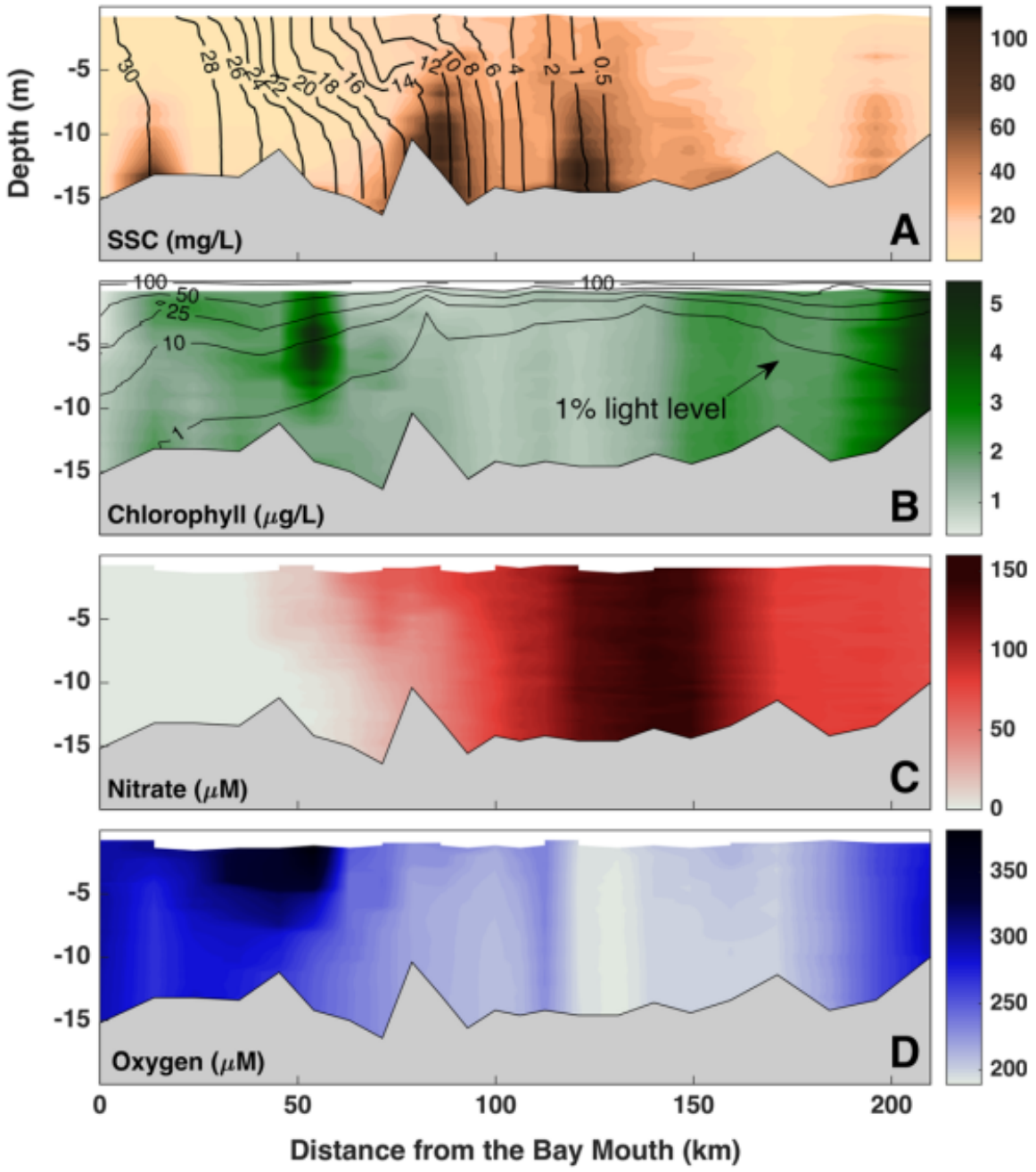

Fig. 3 June 2010 along channel distribution of sediment (mg/L), chlorophyll ($\mu g/L$), nitrate (μM), and dissolved oxygen (μM). *Black contours* in *top panel* are salinity and contours in *second panel* are PAR as a percentage of that at the surface

Figure 4-54: Figure 3 from McSweeney et al. 2017

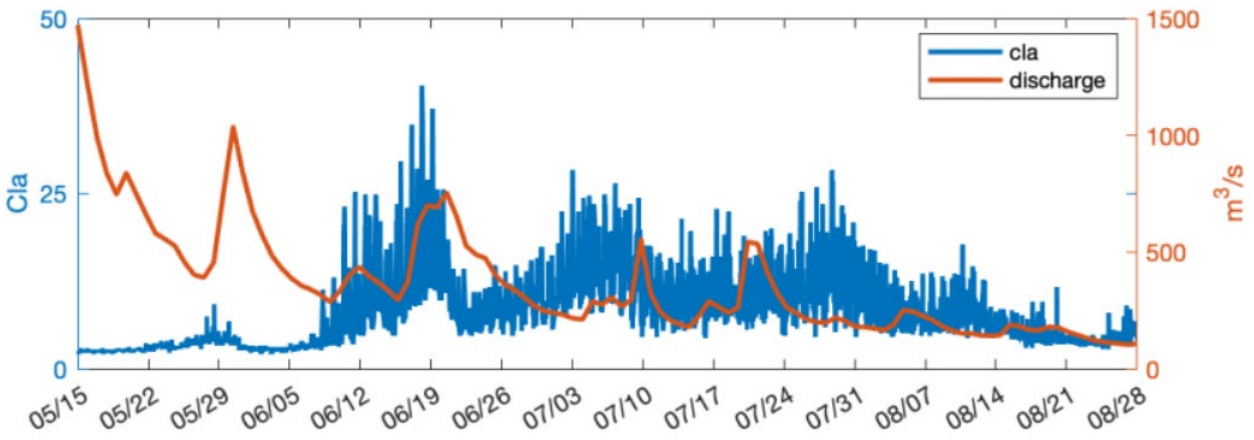

Graph prepared by Dr. Bob Chant (Rutgers University) based on USGS measured chlorophyll-a data and discharge flow data at Penns Landing and Trenton, respectively

Figure 4-55: Chlorophyll-at Ben Franklin Bridge and River Discharge Flow at Trenton, 2019

Upon closer examination, it was determined that the model simulation sometimes does over-predict the light extinction coefficient, *Ke,* in Zone 2 (RM >108.7) during the freshwater diatom growing season (i.e., April 15 to August 31), as shown in the middle panel of Figure 4-19 for June 2019 or in the top left panel of Figure 4-56 for June 2019. To test Dr. Chant's hypothesis, a seasonal adjustment was made to test to the light extinction coefficient, i.e., the existing *Ke* values were multiplied by 0.55 (i.e., artificially reducing the *Ke* or increasing available light in the water column), in Zone 2 for the period of May 1 to July 15.

The complete set of model simulation results for *Ke*, phytoplankton, and dissolved oxygen from the test are provided in Appendix G. Some key results are provided here to compare with the base case (i.e., without the *Ke* seasonal adjustment) and for exploring the effects of the adjusted *Ke* on algal blooms and associated dissolved oxygen concentrations.

Figure 4-56 presents the comparisons of *Ke* between the base case and the seasonal adjustment test for June 2019. The seasonal adjustment resulted in the predicted *Ke* better matching the data for the Boat Run survey on June 17, 2019.

As a result of the seasonal adjustment of *Ke*, the chlorophyll-a concentrations (i.e., phytoplankton) were improved in the urban area, especially for the period of June–July 2019, as illustrated by the blue lines in Figure 4-57. However, the seasonal adjustment of Ke caused the model to over-predict concentrations at Pennypack Woods during June-July 2018.

With more phytoplankton resulting from the seasonal adjustment of *Ke* during June–July in 2018–2019 in Zone 2, the predicted dissolved oxygen concentrations increased in the urban area during these two periods as well as shown in Figure 4-58. This resulted in dissolved oxygen being over-predicted at Pennypack Woods and Ben Franklin Bridge while being improved at Buoy B and Chester during the algal blooms. The effects of increased phytoplankton during the algal blooms on the dissolved oxygen

concentrations are also reflected in the 20th–60th percentiles in cumulative frequency distributions of chlorophyll-a (Figure 4-59).

However, the lower end dissolved oxygen levels (e.g., ≤ 10th percentile) during the post-bloom period (e.g., August 2019) were less noticeably affected by the blooms (see Figure 4-58 and Figure 4-59). In other words, algal productivity increases dissolved oxygen levels during the blooms, but does not significantly change the lower end dissolved oxygen magnitudes during the post-bloom period. This is also reflected in the dissolved oxygen component analyses for June-July 2019 (Figure 4-60 and Figure 4-61) versus August 2019 (Figure 4-62). This observation is in part because (1) algal blooms and lower end dissolved oxygen concentrations happened at different time, e.g., June-July for algal bloom versus July-August for lower end dissolved oxygen concentration, as indicated by data in Figure 4-63, and (2) detrital matter formed during the algal blooms did not deplete the dissolved oxygen in the post-bloom period.

In summary, the seasonal adjustment of the light limitation coefficient, Ke, confirms Dr. Chant's finding that the algal blooms in the tidal river could be caused by the growth of phytoplankton in the upper portion of the estuary (e.g., Zone 2) due to higher water clarity (i.e., lower turbidity) and the subsequent advection to downstream reaches. The results from this diagnostic evaluation also indicate that a mechanistic adjustment of *Ke* may be needed to achieve further improvement in the model representation of summer algal blooms and the associated effect of increasing dissolved oxygen magnitudes.

Base case

Seasonal adjustment: multiply light extinction coef.
By 0.55 for the period of 5/1 ~ 7/15

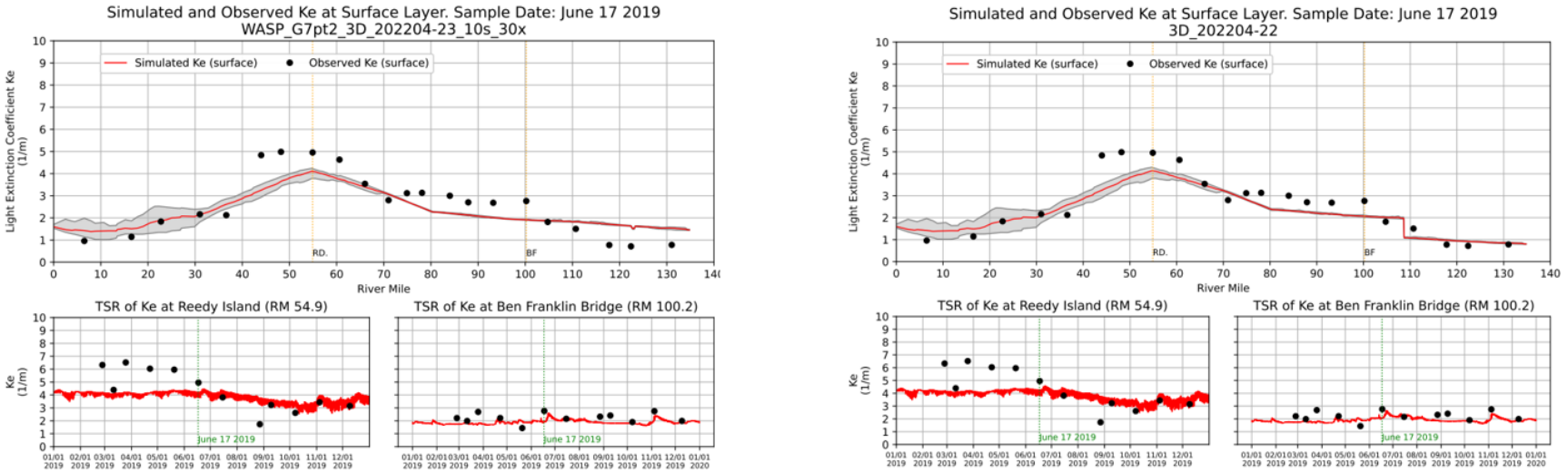

Note “TSR” stands for Time Series

Figure 4-56: Time series comparisons between Base Case and Seasonally Adjusted light extinction coefficient – Ke

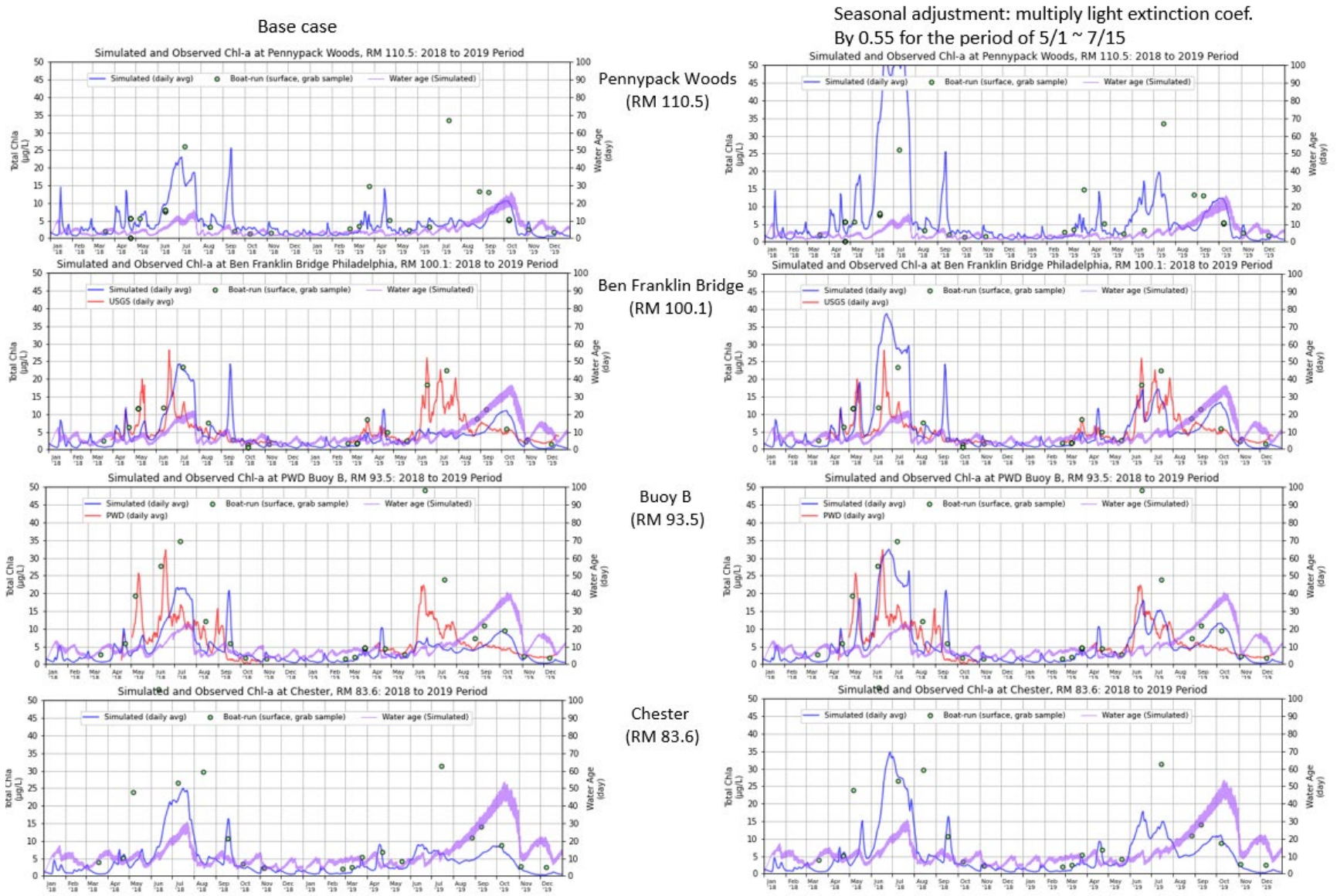

Figure 4-57: Time series comparisons between Base Case and Seasonally Adjusted Ke – Chlorophyll-a

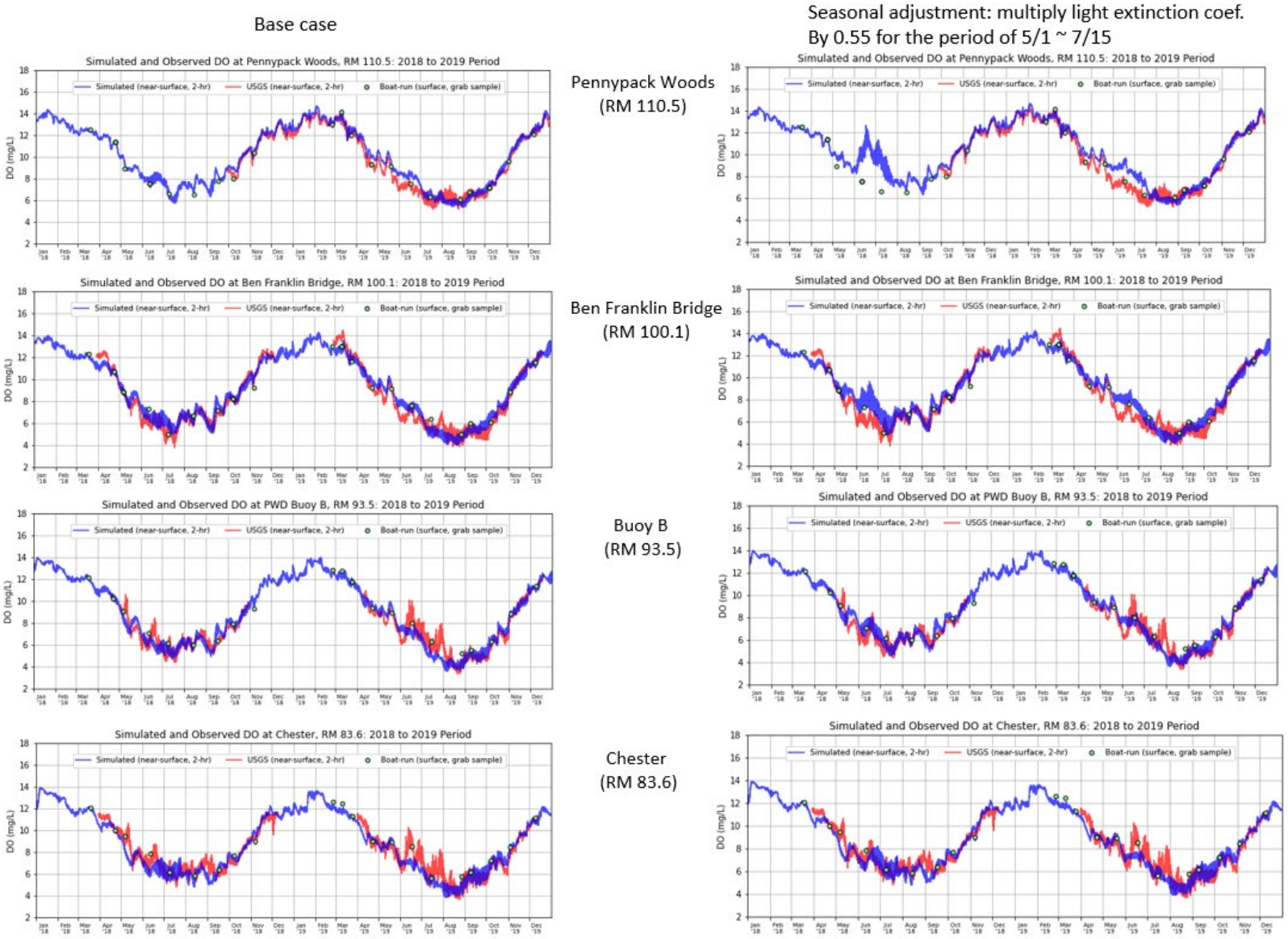

Figure 4-58: Time series comparisons between Base Case and Seasonally Adjusted Ke – DO

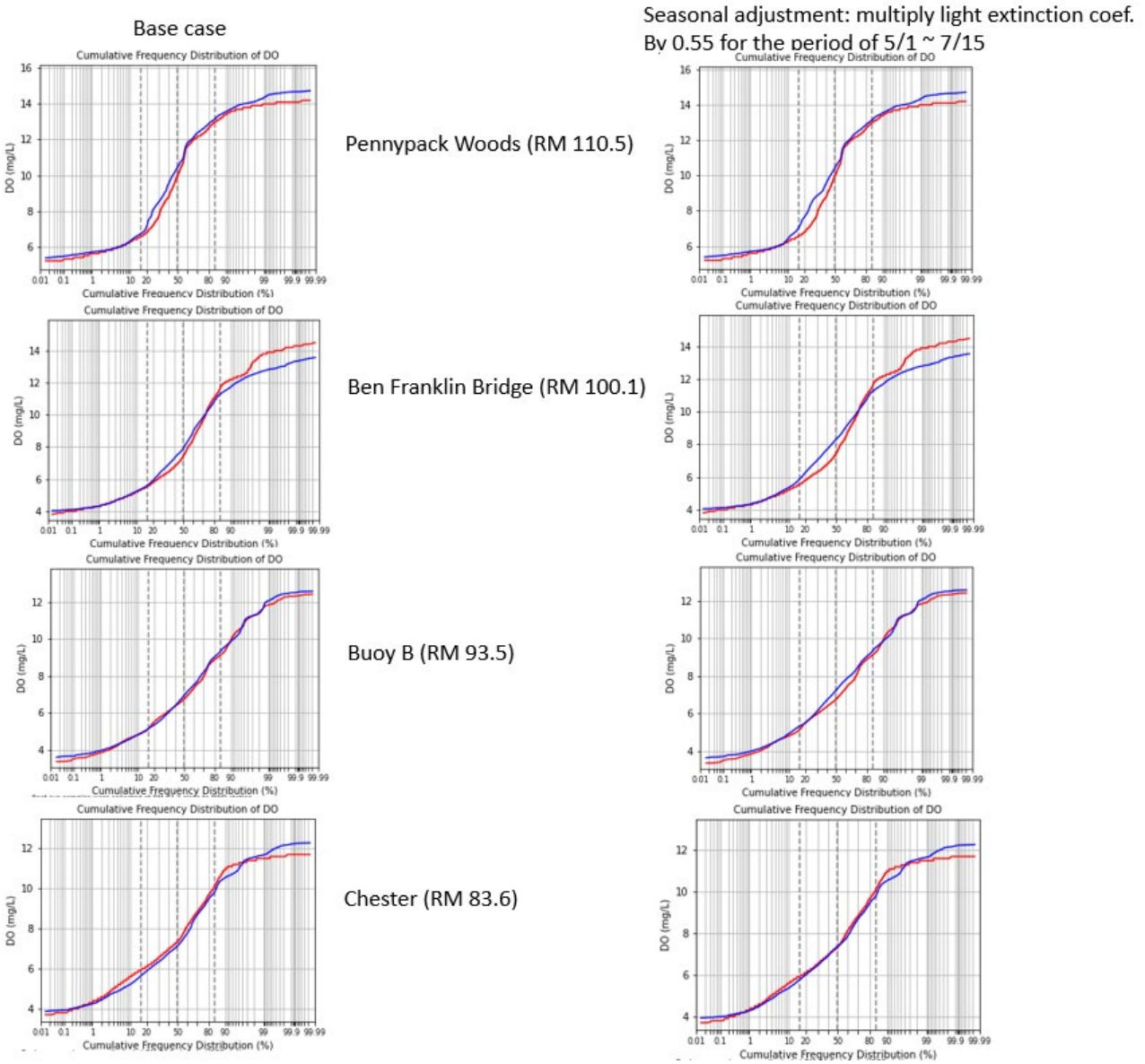

Figure 4-59: Comparisons between Base Case and Seasonally Adjusted Ke – DO Cumulative Frequency Distribution

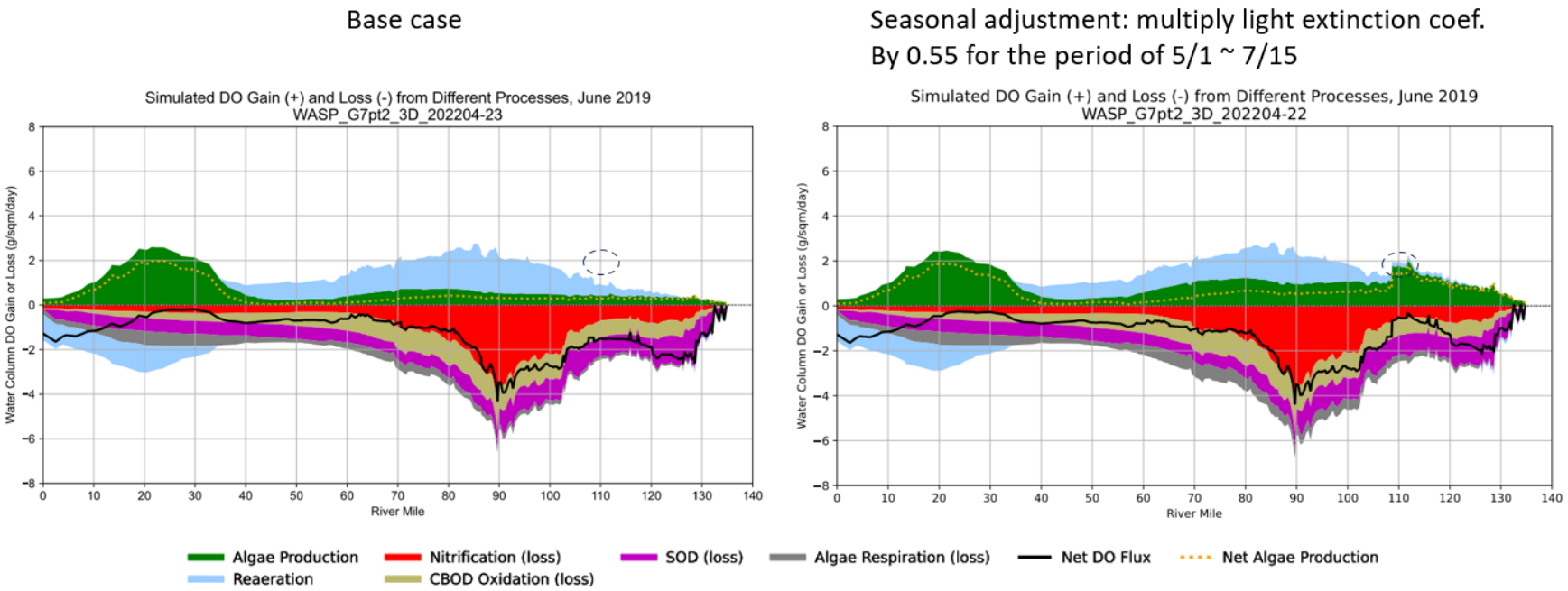

Figure 4-60: Comparisons between Base Case and Seasonally Adjusted Ke – DO Component Analyses in June 2019

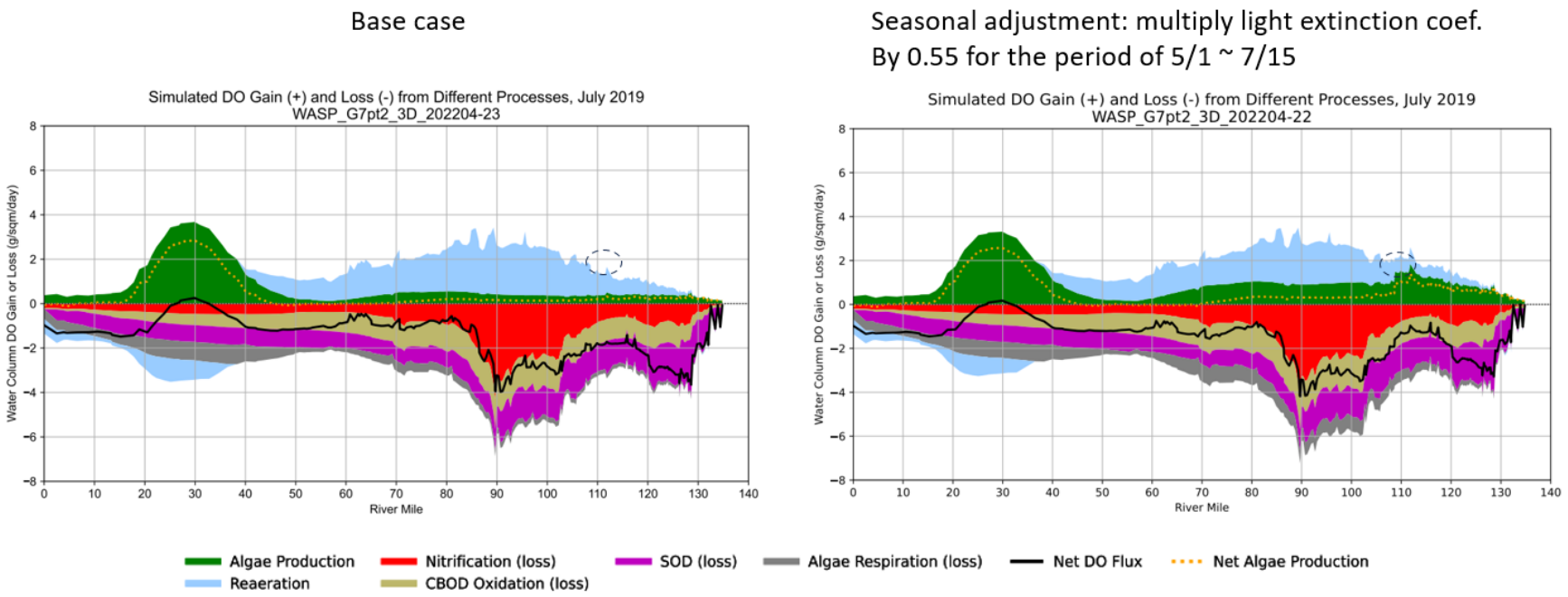

Figure 4-61: Comparison between Base Case and Seasonally Adjusted Ke – DO Component Analyses in July 2019

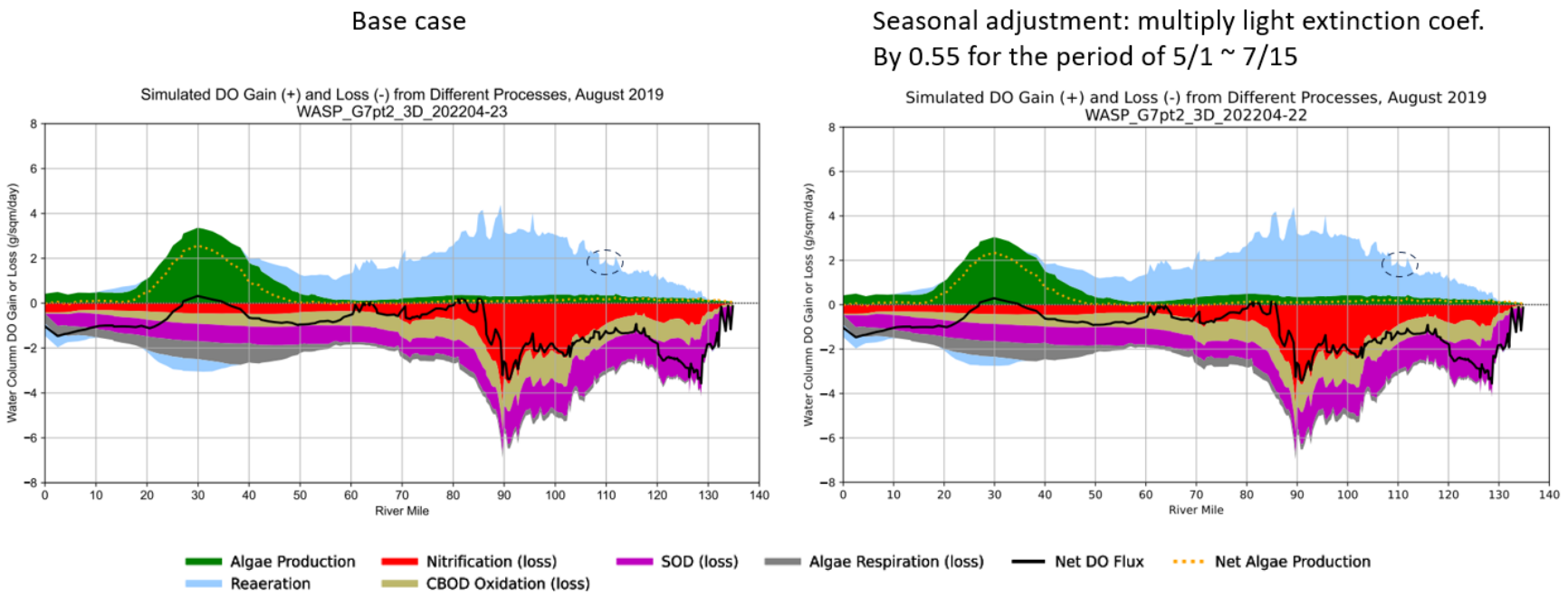

Figure 4-62: Comparison between Base Case and Seasonally Adjusted Ke – DO Component Analyses in August 2019

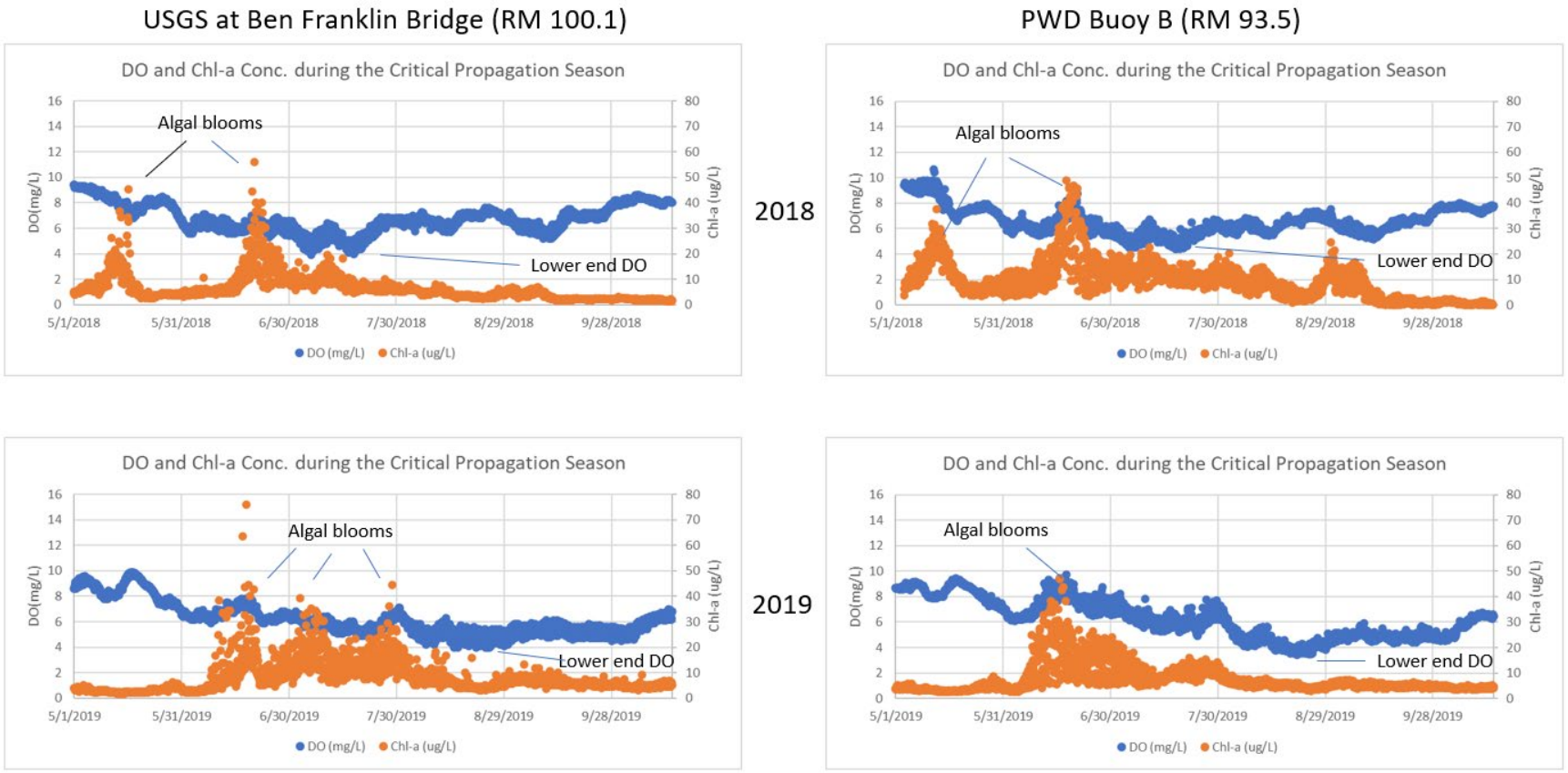

Figure 4-63: Measured DO and Chla a Concentrations during the Critical Propagation Season

4.6 Evaluation of Model Accuracy, Reliability, and Uncertainty

Following with the established Quality Assurance Project Plan (DRBC, 2019) for this project, independent data collected over a multi-year period have been used to evaluate the model accuracy and reliability. While there is no consensus on model performance criteria from the past and recent model-related literature (Walski, 2019), a variety of comparison plots, together with various statistical metrics, have been generated to evaluate model fitness for its intended use. The comparison plots are presented in the form of spatial distributions, time series, 1-to-1 comparisons, cumulative frequency distributions, and target diagrams. The model was well-calibrated to the intensive project dataset that is available for 2018–2019, with high flows in 2018 and medium flows in 2019, as well as moderately low dissolved oxygen in both years. One exception to the generally good model-to-data comparisons is that the model did not capture the observed algal bloom in the tidal river during June-July 2019. Note that this is a different period of time from the low dissolved oxygen period (i.e., August 2019), and detrital matter formed during the algal blooms did not deplete the dissolved oxygen in the post-bloom period. In other words, this model flaw does not significantly affect predicted lower end dissolved oxygen magnitudes (Section 4.5.3). The model successfully hindcasted historical conditions in 2012 with low flows and low dissolved oxygen. The model corroboration was performed using 2012 available flows, boundary conditions, and forcing functions without changing calibration coefficients. Model predictions are quantitatively consistent with observed data across a range of flow and dissolved oxygen conditions. The ability of the model to match these variations in year-to-year patterns of data provides strong support that (1) the parameterization and kinetics currently used in the model calibration are effective in representing the most important processes controlling the Delaware River Estuary water quality; and (2) the model captures the principal mechanisms affecting dissolved oxygen in the Delaware River Estuary.

As with any mathematical model of a natural system, the simulated results contain uncertainty, which stems from both incomplete information and natural variability in the data upon which they are based. Ideally, quantitative analyses to evaluate the impact of that uncertainty on model predictions would be conducted. However, an approach such as a comprehensive Monte Carlo uncertainty analysis for the Delaware River Estuary water quality model, incorporating each model parameter, is not possible because uncertainty distributions are not known for every parameter. Furthermore, the actual timeframe required for performing the necessary model simulations would be prohibitive (e.g., tens of months and perhaps multiple years of computational time using the same up-to-date computer hardware on which model the calibration was conducted). To address this, a series of sensitivity analyses were conducted to evaluate calibration uncertainty. Sensitivity analyses were conducted to identify the extent to which model predictions were affected by uncertainty in the model parameters. Parameters evaluated in the sensitivity analyses were chosen based upon professional judgment, which in turn was based upon a large number of model simulations performed in the process of model calibration. Two criteria were kept in mind: 1) the model is likely to be sensitive to variations in the value of the parameter, within the bounds of its uncertainty; and 2) parameters that are likely to affect dissolved oxygen should be the primary focus.

Twenty (20) model parameters were chosen for sensitivity analysis (Table 4-8). Each parameter/input was increased or decreased by 10%. The sensitivity of the calibrated model to this modified range of input valueswas then evaluated and quantified by repeating the 2019 simulation by modifying each parameter's value, one at a time, using the 2D model. The 2D model was selected in consideration of the computational time required to perform this level of sensitivity analysis. The resulting ranges in the model-predicted dissolved oxygen concentration changes relative to the base case are summarized in Table 4-8. The most sensitive parameters are all related to phytoplankton processes, including maximum growth rates, respiration rates, optimal temperatures for growth, and optimal light saturation. A complete set of figures from the sensitivity analysis is included in Appendix H. Analysis results for the two most sensitive parameters are presented in Figure 4-64 and Figure 4-65. The top panels depict the time series of dissolved oxygen concentration changes relative to the base case at four USGS stations and two PWD buoys due to ±10% changes for a given parameter. Although it is not easy to visually identify the results from each simulation (represented by dashed lines) in the plots, the envelopes formed by the lines demonstrate how sensitive the model is to the change of a given parameter. For instance,

- A ±10% change in the maximum growth rate constants for the three phytoplankton groups (Figure 4-64) results in dissolved oxygen variations up to 1.2 mg/L, equivalent to a 20% change in dissolved oxygen concentration (see Appendix H).
- A ±10% change in the respiration rate constants for the three groups (Figure 4-65) generates dissolved oxygen variations up to 1.0 mg/L, equivalent to a 12% change in dissolved oxygen concentration (see Appendix H).
- Changes in dissolved oxygen with respect to other modified input parameters can be found Table 4-8 and Appendix H.

Most of the changes in the dissolved oxygen concentrations caused by the modified input values occur in the period of June-October 2019; the maximum changes occur in September-October, when the model predicts a phytoplankton bloom. Although phytoplankton productivity increases dissolved oxygen concentration, it is less likely to change the low dissolved oxygen magnitude, since the low dissolved oxygen in the Delaware River Estuary occurs at a different period (e.g., August 2019) from the phytoplankton bloom (see Section 4.5.3).

The bottom panels in the sensitivity plots present the target diagrams of dissolved oxygen model-to-data comparisons at the USGS stations and PWD buoys for the base case, and the sensitivity analysis cases with the 10% decrease and 10% increase in parameter values. Overall, the patterns in the target diagrams vary insignificantly between the base and sensitivity cases, except for the cases with maximum (+10%) growth rate constants for all phytoplankton groups; for this parameter, the results are more biased with respect to the ±10% input parameter variation. Detailed information on the target diagram is available in Section 4.4.2. Note that another significant uncertainty in the model – light attenuation – was diagnosed and discussed in the previous section and therefore not included here.

It wasobservated from the results presented in this section that for equal 10 percent changes in the model calibration parameters, the average change in dissolved oxygen concentration was 5.1 percent for phytoplankton parameters, 2.8 percent for SOD parameters, and 0.7 percent for nitrification, DOC and CBOD parameters. This implies that dissolved oxygen concentrations computed by the calibrated model are less sensitive to changes in the principal oxygen consumption processes (nitrification, SOD and CBOD) than to changes in phytoplankton photosynthesis, one of the two principal sources of dissolved oxygen, the other being reaeration. From the above diagnostic analysis, it follows that a better understanding of the influence of light and temperature on photosynthesis would lead to a better understanding of the uncertainty in dissolved oxygen concentrations computed by the calibrated model.

Table 4-8: Results of the Sensitivity Analysis - range of predicted dissolved oxygen relative to Base Case

Description	Units	Base Value	Increase (+10%)	Decrease (-10%)	ΔDO Range	ΔDO Range (%)
Phytoplankton Maximum Growth Rate Constant (Group 2)	per day	3.75	4.125	3.375	0.5	8.0
Phytoplankton Maximum Growth Rate Constant (Group 1,2,3)	per day	3.92	4.308	3.525	1.2	20.0
Phytoplankton Carbon to Chlorophyll Ratio	mg C/mg Chl	40	44	36	0.3	4.1
Phytoplankton Death Rate Constant (Non-Zoo Predation; Group 2)	per day	0.08	0.088	0.072	0.1	2.0
Phytoplankton Respiration Rate Constant (Group 2)	per day	0.05	0.055	0.045	0.1	1.5
Phytoplankton Respiration Rate Constant (Group 1,2,3)	per day	0.037	0.040	0.033	1.0	12.0
Phytoplankton Respiration Temperature Coefficient (Group 2)	dimensionless	1.072	1.079	1.065	~ 0.0	0.5
Optimal Temperature for Growth (Group 2)	deg C	22.5	24.75	20.25	0.2	4.0
Optimal Temperature for Growth (Group 1,2,3)	deg C	17.7	19.47	15.93	0.4	6.0
Phytoplankton Settling Rate (Group 2)	m/day	0.100	0.110	0.090	~ 0.0	0.2
Sediment Oxygen Demand[1]	g/m2-day	1.012	1.114	0.911	0.2	4.0
Theta -- SOD Temperature Correction	dimensionless	1.065	1.072	1.059	0.1	1.5
Nitrification Rate Constant	per day	0.600	0.660	0.540	0.1	0.8
Dissolved Organic Nitrogen Mineralization Rate Constant	per day	0.010	0.011	0.009	~ 0.0	0.5
CBOD Decay Rate Constant (Watershed)	per day	0.033	0.037	0.030	0.1	1.0
CBOD Decay Rate Constant (Point Source)	per day	0.087	0.0957	0.0783	~ 0.0	0.5
Phytoplankton Optimal Light Saturation (chla 1)	watts/m2	100	110	90	0.1	0.5
Phytoplankton Optimal Light Saturation (chla 2)	watts/m2	150	165	135	0.2	3.0
Phytoplankton Optimal Light Saturation (chla 3)	watts/m2	200	220	180	0.3	4.0
Phytoplankton Optimal Light Saturation[2] (chla 1,2,3)	watts/m2	150	165	135	0.4	5.0

[1] Average rate across bottom segments

[2] Average optimal light saturation for three classes

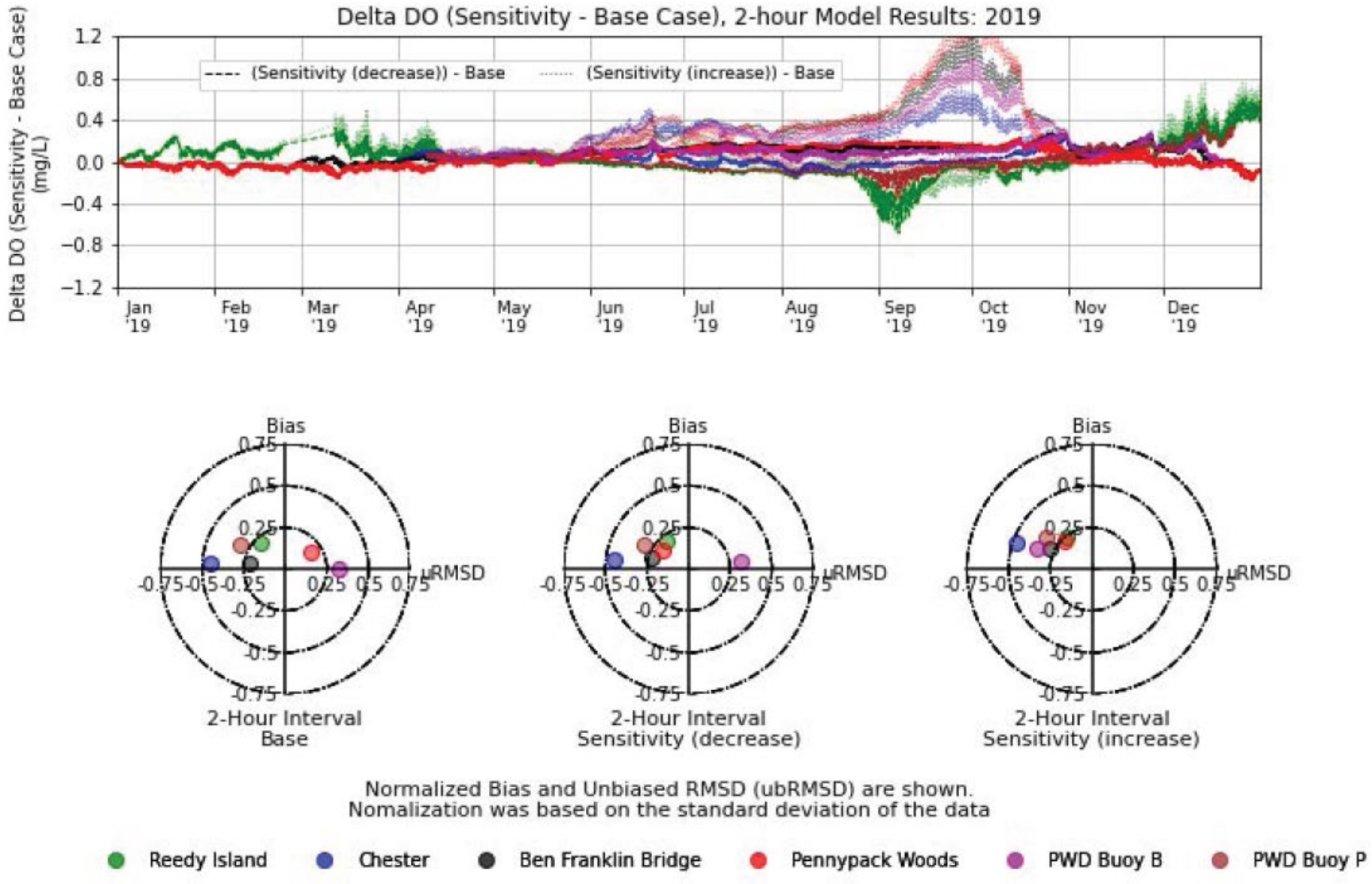

Figure 4-64: Sensitivity Test: Phytoplankton Maximum Growth Rate Constant (Group 1, 2, 3)

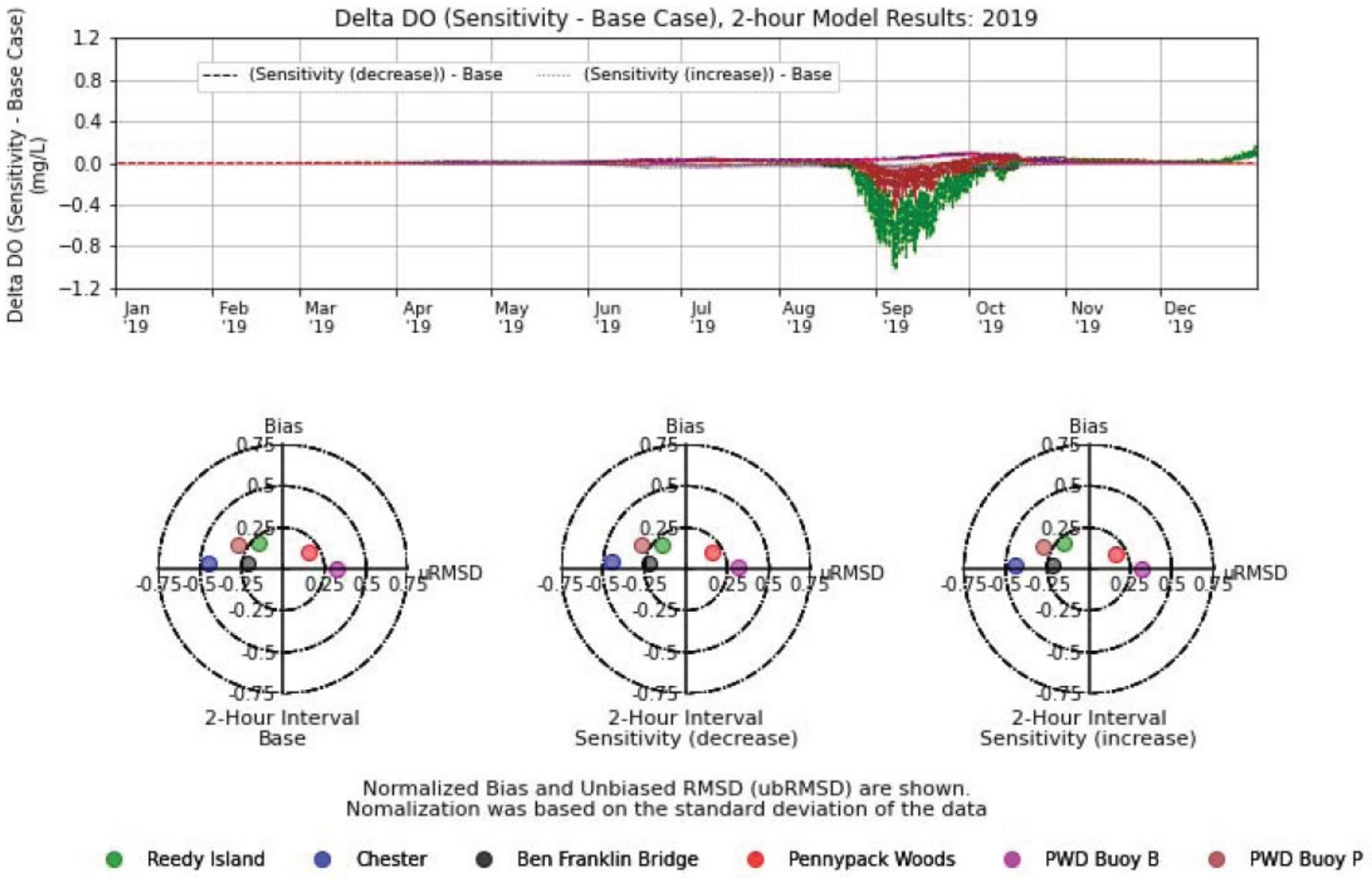

Figure 4-65: Sensitivity Test: Phytoplankton Respiration Rate Constant (Group 1, 2, 3)

4.7 Model Limitations

Numerical models are useful tools for testing and refining conceptual models of eutrophication, developing an understanding of the dynamics of the system of study, identifying potential management strategies, and guiding future monitoring efforts. Like any dynamic water quality model, the Delaware River Estuary eutrophication model has inherent limitations and uncertainties due to data availability and quality, site-specific complexities, parametric uncertainty, and global parameterization (i.e., parameters/coefficients that cannot be varied spatially and/or temporally).

A global nitrification rate constant and global temperature coefficient were used in the study, aimed at predicting the observed ammonia and nitrite + nitrate levels in the urban area during the summer period, which are the critical area and period for fish propagation. The WASP model does not support the option of a spatially-varying nitrification rate. As a result, nitrification process may be over-estimated in the non-urban areas during the non-summer period.

Model algorithms used to simulate algal communities are simplifications of actual processes and rely on the use of global and lumped parameterization values to describe complex interactions and responses to light, nutrients, flow, and vertical mixing, and they do not allow for adjustments based on spatial, temporal, or water quality variability within the Estuary. The three general classes of phytoplankton simulated in this study (as three chlorophyll-a groups) are described by composited properties, and thus the model may predict behavior that is not necessarily representative of specific algal communities. Sources of error in this model include uncertainties in growth rates, nutrient uptake rates, settling rates, and stoichiometric ratios. In addition, the effects of zooplankton grazing on phytoplankton populations in the Estuary were not well-known during model construction, and thus were excluded from the study.

Estimation of watershed inputs using statistical techniques presents its own set of limitations on model accuracy. Simple methods for regionalization and transfer of hydrologic and water quality information to unmonitored areas do not account for attenuation or transformation processes that likely occur during transport to the Estuary. Time-series inputs generated in this way may not account for episodic (higher flow) events and may not capture short-term variability in watershed processes and constituent concentrations.

SOD and nutrient releases from the sediment layer (benthic nutrient fluxes) for ammonia (NH3-N), nitrate (NO3-N), and phosphate (DIP) were externally specified as model inputs using available data, rather than dynamically simulated by sediment diagenesis (see Section 3.5.6). This modeling project benefitted from a significant amount of SOD data compared to almost any project of this scale. In one sense, prescribing SOD and benthic flux rates within the range of observed data is a more certain approach than using a predictive sediment diagenesis model. On the other hand, this prescriptive option dissociates diagenesis from water column dynamics, in particular the production of organic carbon. To the extent that organic

carbon is likely to change in the future, predicting future water quality conditions may incorporate larger uncertainties.

To help understand the potential for SOD to change in the future, repeated SOD and benthic flux observations at five locations in 2012–2013 and 2016–2018 were compared and analyzed (Section 3.5.6), revealing no apparent temporal trends for SOD or benthic fluxes from 2012 to 2018. In addition, the SOD data collected by PWD during 2012-2018 was compared with historical SOD data collected by DRBC, EPA, and the Academy of Natural Sciences in 1986 (DRBC, 1987), in which about 35 sediment cores were collected and analyzed along 13 transects in the Delaware River Estuary from RM 85 to 118. These data were converted to values at 20°C using the SOD temperature correction of 1.065 (Chapra, 1997) employed in this modeling effort and compared to the SOD data collected by PWD from RM 80 to 120 as shown on Figure 4-66 (a). The box plots display the minimum (bottom whisker), 25th percentile (bottom edge), median (middle line), mean (triangle), 75th percentile (upper edge), and maximum (upper whisker) values among data. Generally, the SOD data collected in 1986 exhibit slightly lower rates than those collected during 2012—2018. Since most sediment cores collected by PWD are in the near-shore areas, the 1986 SOD data collected in the mid-channel (i.e., mainly sand sediment) was further exlucded. The revised comparisons are shown on Figure 4-66 (b), which indicates that SOD measurements spanning three decades are comparable. This is remarkable given the fact that overall carbon loads decreased significantly during this period; this indicates that SOD rates may be quite stable in the Delaware River Estuary. Additionally, the location of the maximum measured SOD is around RM 125, upstream of the urban areas. These factors tend to mitigate the apparent limitations caused by the prescriptive (i.e., externally specified rates using available data) option.

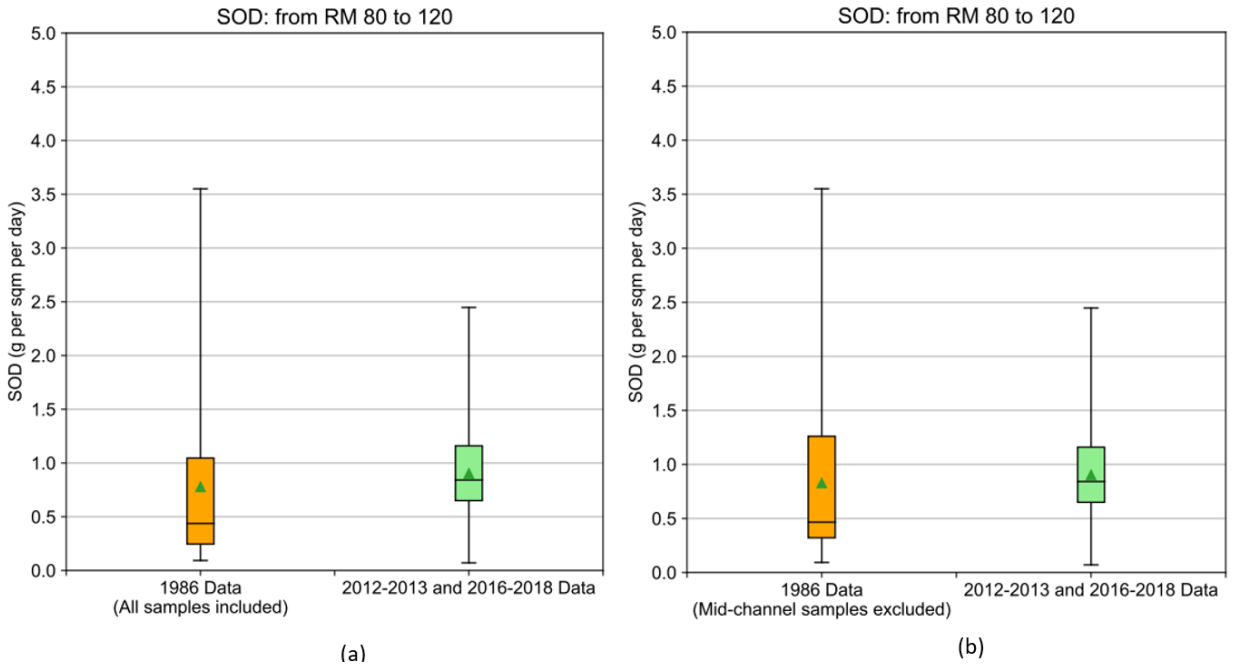

Figure 4-66: Comparisons of SOD Data Collected during 2012—2018 vs. 1986

The light extinction equation does not capture all the transient variation in water clarity, especially in the upper portion of the study area, as discussed in Section 4.5.3. This is in part due to the limitation that a full-scale sediment transport model with resuspension and deposition is not included in this study and because the effect of suspended sediment on the light extinction coefficient is not directly incorporated. A refinement to the light extinction equation may enhance the predictability of the phytoplankton dynamics. The diagnostic analyses in Section 4.5 also demonstrate that (1) algal blooms and low dissolved oxygen concentrations happen at different times; (2) algal productivity increases dissolved oxygen concentrations during the blooms but barely changes the low dissolved oxygen concentrations during the post-bloom period; and (3) dissolved oxygen gain from net algal production (i.e., photosynthesis minus respiration) is much smaller than the dissolved oxygen loss caused by nitrification. Finally, a test case in the next paragraph illustrates how dissolved oxygen is affected by algal growth in an extreme condition of zero for the phytoplankton growth rates.

A numerical test was conducted by turning off growth rates for all three phytoplankton groups to evaluate the influence of phytoplankton on the dissolved oxygen concentrations. On Figure 4-67, the left panel shows the spatial dissolved oxygen components averaged over July 2018 from a base case with all parameters turned on; the right panel presents the dissolved oxygen components averaged for the same period but from the test case with zero for growth rates for all three phytoplankton groups. On the dissolved oxygen production side, when phytoplankton growth rates are zero the contribution from photosynthesis disappears; meanwhile, the reaeration process plays a more significant role in contributing to DO levels by filling many gaps left by the lack of photosynthesis. On the dissolved oxygen loss side, when the phytoplankton growth rates are zero, (1) the contribution to the loss of DO from respiration is reduced dramatically. Note that a small amount of phytoplankton still exists in the system due to transport from boundaries; (2) the contributions to the loss of DO from nitrification and SOD remain about the same as in the base case; and (3) the contribution to the loss of DO from CBOD oxidation is reduced to some extent, e.g., between 70 < RM < 90. Figure 4-68 presents the comparisons of the cumulative frequency distributions of dissolved oxygen between the base case and the no phytoplankton growth test case at four USGS stations and two PWD buoys during 2018-2019. The differences between these two scenarios are not substantial. Most of the differences between these two scenarios occur in the 40^{th} percentile and lower portion of DO. At the lower end (e.g., 1^{st} percentile), the differences range from 0.2 to 0.8 mg/L, with an average of 0.4 mg/L. To sum up, as a result of the predicted adjustments between the mechanisms impacting dissolved oxygen, the overall effect of zero phytoplankton growth on dissolved oxygen concentrations tends to be tempered.

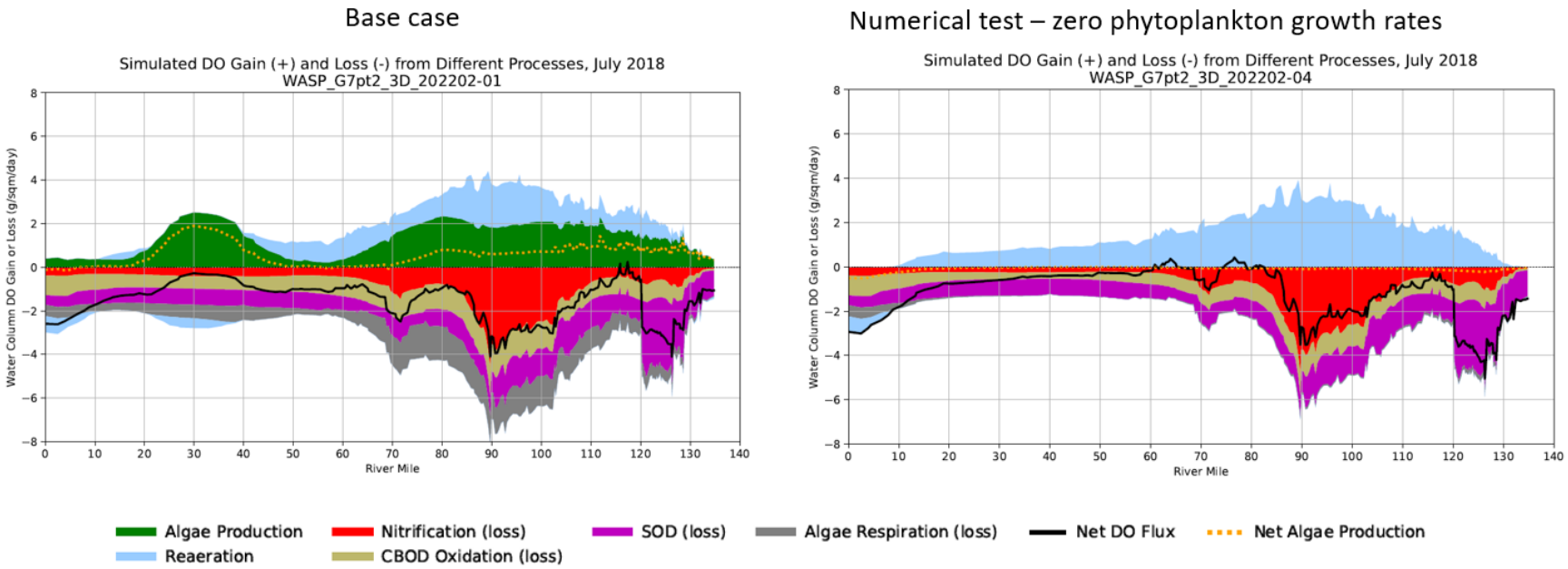

Figure 4-67: Comparison between Base Case and No Phytoplankton Growth – DO Component Analysis for July 2018

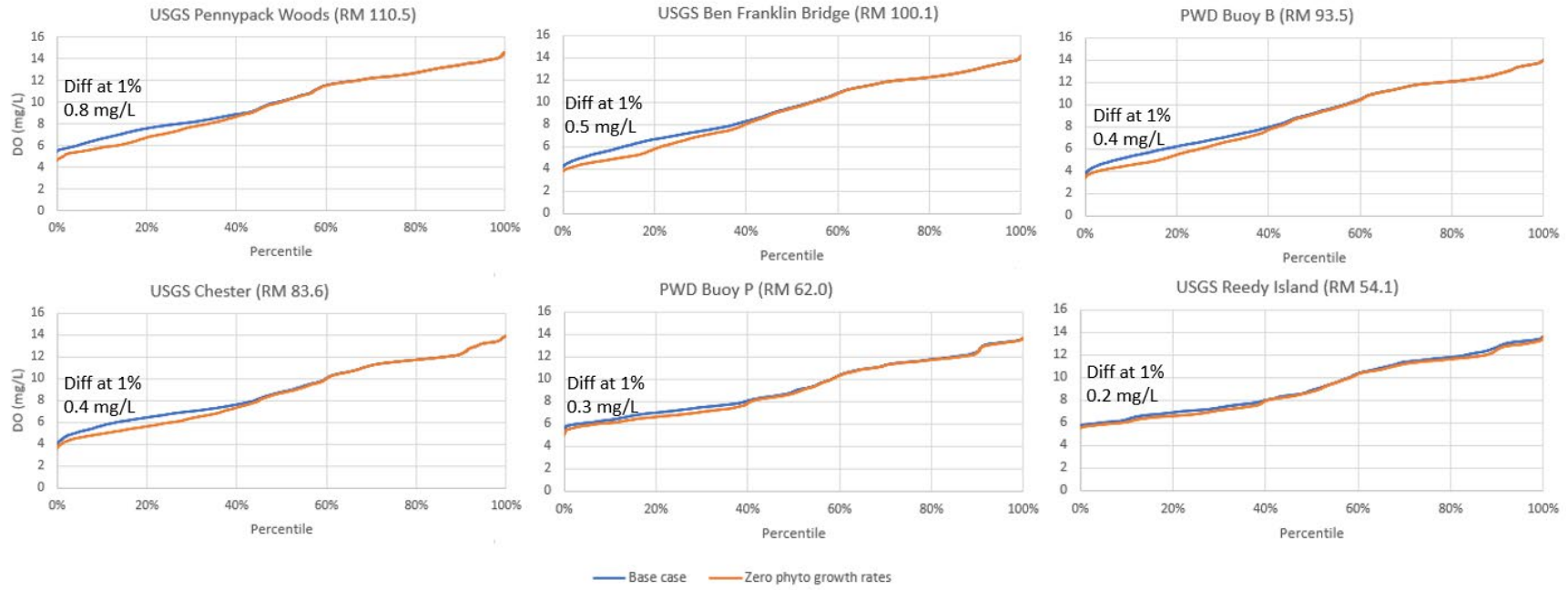

Figure 4-68: DO Cumulative Frequency Distribution during 2018-2019 – Base Case vs. No Phytoplankton Growth

5. MODEL SUMMARY

The Delaware River Estuary water quality model was developed and calibrated to an intensive project dataset obtained for 2018-2019, with the intent to capture a wide range of hydrologic and climatic conditions over a two-year period. This goal was generally met, with high flows in 2018 and more typical flows in 2019. In order to further demonstrate model performance during an unusually dry year, the model was also corroborated for 2012 using the more limited data available for that period, without changing calibration coefficients. This report documents the water quality model framework, dissolved oxygen and eutrophication processes, summary of data used to drive the model, and calibration approaches. Calibration results were provided by comparing the observed and simulated results for various key state variables and through visualizations such as the DO component evaluation. Uncertainty evaluations were performed on key model parameters, limiting factors on phytoplankton growth were analyzed, and numerical testing of light extinction on phytoplankton growth and associated impact on DO were performed. Incorporation of a mechanistic reaeration algorithm and the development of a Delaware River Estuary specific light extinction sub-model are two notable achievements by this project.

Multiple lines of evidence were used to evaluate the reliability of the model during the calibration and corroboration process, since model fitness is impacted not just by the quality of the calibration but also by the quality of boundary and field data and code limitations such as the model having global parameterization for certain processes. The model was able to reproduce temporal and spatial trends and variabilities well for both nitrogen (NH34, NO3O2, TN) and phosphorus (D-DIP, TP) species and dissolved organic carbon. The model simulated phytoplankton concentrations with a lesser degree of accuracy in terms of magnitude and timing, likely due to overestimation of the light extinction coefficients in sections of the estuary and a simplified representation of the phytoplankton communities into three groups as discussed in the report. However, as shown in the diagnostic simulation with zero phytoplankton growth rates, the impacts of phytoplankton on dissolved oxygen levels is not substantial. Although uncertainties and limitations exist, the water quality model predictions are overall quantitatively consistent with observed data across a range of flow and DO conditions, especially in the urban area during critical low DO conditions.

The DRBC modeling team and the Model Expert Panel that informed and consulted with DRBC throughout the course of this modeling study concluded[20] that: 1) the Delaware River Estuary water quality model is scientifically defensible over a wide range of environmental conditions; and 2) the model is appropriate for its intended use, namely to determine the improvement in dissolved oxygen condition that would result from specific reductions to point and nonpoint source loadings.

[20] The Model Expert Panel formalized these conclusions in a presentation to the Water Quality Advisory Committee meeting on April 27, 2022: https://www.nj.gov/drbc/library/documents/WQAC/042722/suk-amidon-bierman_modeling-update.pdf

Major processes controlling dissolved oxygen were identified through modeling as: reaeration and photosynthesis for production; and nitrification, followed by SOD, CBOD oxidation, and respiration for consumption. The extensive modeling study demonstrates that: 1) nitrification is the most important low dissolved oxygen driver and is centered in the urban estuary; 2) low flows and high temperatures, as expected, exacerbate low dissolved oxygen; and 3) photosynthesis from phytoplankton tempers low dissolved oxygen events. The diagnostic analyses suggest that light and temperature control phytoplankton under current Estuary conditions and that phytoplankton growth during summer periods of higher clarity in Zone 2 can impact the entire estuary.

The DRBC is continuing to develop modifications to improve model accuracy and reduce uncertainties, consistent with its goals and resources. Specific areas identified for further study include better representation of sediment interactions, CSOs, and carbon inputs and transformations.

REFERENCES

Agrawal, Y.C., Terray, E.A., Donelan, M.A., Hwang, P.A., Williams III, A.J., Drennan, W.M., Kaham, K.K., & Kitaigorodskii, S.A. (1992). Enhanced dissipation of kinetic energy beneath surface waves. *Nature, 359*, 219 – 220. https://www.nature.com/articles/359219a0#citeas

Ambrose, R.B., Wool, T.A., & Barnwell, Jr., T.O. (2009). Development of water quality modeling in the United States. *Environ. Engineering Res., 14*(4), 200-210. https://doi.org/10.4491/eer.2009.14.4.200

Bowie, G.L., Mills, W.B., Porcella, D.B., Campbell, C.L., Pagenkopf, J.R., Rupp, G.L., Johnson, K.M., Chan, P.W.H., Gherini, S.A., & Chamberlin, C.E. (1985). *Rates, Constants, and Kinetic Formulations in Surface Water Quality Modeling (Second Edition)*. (EPA/600/3-85-040). United States Environmental Protection Agency. https://nepis.epa.gov/Exe/ZyNET.exe/9100R3IW.TXT

Brumer, S.E., Zappa, C.J., Anderson, S.P., & Dugan, J.P. (2016). Riverine skin temperature response to subsurface processes in low wind speeds. *J. Geophys. Res.: Oceans, 121*(3), 1-15. https://doi.org/10.1002/2015JC010746

Burchard, H. (2001). On the q^2l Equation by Mellor and Yamada (1982). *J. Physical Oceanography, 31*, 1377-1387. https://doi.org/10.1175/1520-0485(2001)031%3C1377:OTQLEB%3E2.0.CO;2

Burchard, H., Petersen, O., & Rippeth, T.P. (1998). Comparing the performance of the Mellor-Yamada and the *k-ε* two-equation turbulence models. *J. Geophys. Res. 103*(C5), 10543-10554. https://doi.org/10.1029/98JC00261

Camacho, R.A., Zhang, Z., & Chao, X. (2019). Receiving Water Quality Models for TMDL Development and Implementation. *J. Hydrologic Engineering, 24*(2). https://doi.org/10.1061/(ASCE)HE.1943-5584.0001723

Cerco, C., & Cole, T. (1994). *Three-dimensional eutrophication model of Chesapeake Bay*. (Technical Report EL-94-4). US Army Corps of Engineers Waterways Experiment Station. https://apps.dtic.mil/sti/citations/ADA280760

Cerco, C.F, & Noel, M.R. (2013). Twenty-one-year simulation of Chesapeake Bay water quality using the CE-QUAL-ICM eutrophication model. *J. American Water Resources Association, 49*(5), 1119-1133. https://doi.org/10.1111/jawr.12107

Cerco, C.F, & Noel, M.R. (2019). *2017 Chesapeake Bay Water Quality and Sediment Transport Model: A Report to the US Environmental Protection Agency Chesapeake Bay Program Office*. US Army Engineer Research and Development Center. https://d18lev1ok5leia.cloudfront.net/chesapeakebay/2017_chesapeake_bay_water_quality_and_sediment_transport_model.pdf

Chapra, S.C. (1997). *Surface Water-Quality Modeling*. Waveland Press, Inc. https://www.researchgate.net/publication/48447645_Surface_Water-Quality_Modeling

Chapra, S.C. (2022). *Applied Numerical Methods with MATLAB for Engineers and Scientists* (5th ed.). McGraw-Hill. https://dokumen.pub/applied-numerical-methods-with-matlab-for-engineers-and-scientists-5th-edition-9781265148225-1265148228.html

Chapra, S.C., Pelletier, G., & Tao, H. (2012). *QUAL2K: A Modeling Framework for Simulating River and Stream Water Quality (Version 2.12): Documentation and User Manual*. Civil and Environmental Engineering Dept., Tufts University. https://qual2k.com/downloads/Q2Kv2_12b1.zip

Chen, F., Zheng, L., Amidon, T., Suk, N., & Kavanagh K.B. (2024). *Modeling Eutrophication Processes in the Delaware River Estuary: Three-Dimensional Hydrodynamic Model*. (DRBC Report No. 2024-4). Delaware River Basin Commission.

Churchill, M.A., Elmore, H.L., & Buckingham, R.A. (1962). The prediction of stream reaeration rates. *J. San. Engr. Div., 86*(4), 1-46. https://doi.org/10.1061/JSEDAI.0000390

Cohn, T.A., DeLong, L.L., Gilroy, E.J., Hirsch, R.M., & Wells, D.K. (1989). Estimating constituent loads. *Water Resources. Res., 25*(5), 937–942. https://doi.org/10.1029/WR025i005p00937

Connolly, J.P., & Winfield, R. (1984). *A User's Guide for WASTOX, a Framework for Modeling the Fate of Toxic Chemicals in Aquatic Environments, Part 1: Exposure Concentration*. (EPA-600/3-84-077). United States Environmental Protection Agency.

Covar, A.P. (1976). *Selecting the proper reaeration coefficient for use in water quality models.* Presented at U.S. EPA Conference on Environmental Simulation and Modeling, April 19-22, 1976, Cincinnati, OH.

Davis, J.M. (2019). *Instruction manual for R-calibration scripts*. USEPA Region 4, Model Calibration Webinar Series. Updated on September 24, 2019.

Defne, Z., Spitz, F.J., DePaul, V., & Wool, T.A. (2017). Toward a comprehensive water-quality modeling of Barnegat Bay: Development of ROMS to WASP coupler. *J. Coastal Research, 78*(sp1), 34-45. https://doi.org/10.2112/SI78-004.1

Di Toro, D.M., J.J. Fitzpatrick, & Thomann, R.V. (1983). *Documentation for water quality analysis simulation program (WASP) and model verification program (MVP)*. (EPA-600-3-81-044). United States Environmental Protection Agency. https://www.researchgate.net/publication/26991058_Documentation_for_Water_Quality_Analysis_Simulation_Program_WASP_and_Model_Verification_Program_MVP

Di Toro, D.M. (2001). *Sediment flux modeling*, Wiley-Interscience. https://www.wiley.com/en-us/Sediment+Flux+Modeling-p-9780471135357

DRBC. (1987). *Sediment oxygen demand study*. Delaware River Basin Commission.

DRBC. (2019). *Modeling eutrophication processes in the Delaware Estuary: quality assurance project plan (Rev2)*. Delaware River Basin Commission.

DRBC. (2023). *2022 Delaware River and Bay Water Quality Assessment*. (DRBC Report No. 2023-1). Delaware River Basin Commission. https://www.nj.gov/drbc/library/documents/WQAssessmentReport2022.pdf

Dijkstra, Y.M., Chant, R.J., & Reinfelder, J.R. (2019). Factors Controlling Seasonal Phytoplankton Dynamics in the Delaware River Estuary: an Idealized Model Study. *Estuaries and Coasts, 42*, 1839–1857. https://doi.org/10.1007/s12237-019-00612-3

Fisher, T.R., & Gustafson, A.B. (2015). Report to DRBC on concentrations of nutrients and chlorophyll a and rates of respiration and primary production in samples from Delaware Bay collected in May and July 2014. Revised January 25, 2019. University of Maryland Center for Environmental Science. https://www.nj.gov/drbc/library/documents/nutrients/nutrients-chlor-a_DelawareBay_UMd2015_rev012519.pdf

Fisher, T.R, & Gustafson, A.B. (2019). Report to DRBC on concentrations of nutrients and chlorophyll a and rates of respiration and primary production in samples from Delaware Bay collected in May and July 2018. Revised February 6, 2019. University of Maryland Center for Environmental Science. https://www.nj.gov/drbc/library/documents/nutrients/nutrients-chlor-a_DelawareEstuary_UMd_feb2019.pdf

Fisher, T.R, & Gustafson, A.B. (2020). Report to DRBC on concentrations of nutrients and chlorophyll a and rates of respiration and primary production in samples from Delaware Bay collected in May and July 2019. Revised September 2, 2020. University of Maryland Center for Environmental Science. https://www.nj.gov/drbc/library/documents/nutrients/nutrients-chlor-a_DelawareEstuary_UMd_sept2020.pdf

Garcia, H.E., Weathers, K.W., Paver, C.R., Smolyar, I., Boyer, T.P., Locarnini, R.A., Zweng, M.M., Mishonov, A.V., Baranova, O.K., Seidov, D., & Reagan, J.R. (2019). *World Ocean Atlas 2018, Vol. 4: Dissolved Inorganic Nutrients (phosphate, nitrate and nitrate+nitrite, silicate)*. In A. Mishonov (Technical Editor), NOAA Atlas NESDIS 84. https://www.ncei.noaa.gov/sites/default/files/2020-04/woa18_vol4.pdf

Harding Jr, L.W., Meeson, B.W., & Fisher Jr, T.R. (1986). Phytoplankton production in two east coast estuaries: Photosynthesis-light functions and patterns of carbon assimilation in Chesapeake and

Delaware Bays. *Estuarine, Coastal and Shelf Science, 23*(6), 773-806. https://doi.org/10.1016/0272-7714(86)90074-0

Hirsch, R.M., Moyer, D.L., Archfield, S.A. (2010). Weighted Regressions on Time, Discharge, and Season (WRTDS), with an application to Chesapeake Bay River inputs. *J. Am. Water Resour. Assoc., 46*(5), 857–880. https://doi.org/10.1111/j.1752-1688.2010.00482.x

Inoue, T., Glud, R.N., Stahl, H., & Hume, A. (2011). Comparison of three different methods for assessing in situ friction velocity: A case study from Loch Etive, Scotland. *Limnology and Oceanography: Methods, 9*(6), 275-287. https://doi.org/10.4319/lom.2011.9.275

Jakobsen, H., & Markager, S. (2016). Carbon-to chlorophyll ratio for phytoplankton in temperate coastal waters: Seasonal patterns and relationship to nutrients. *Limnology and Oceanography, 61*(5), 1853-1868. https://doi.org/10.1002/lno.10338

Jolliff, J.K., Kindle, J.C., Shulman, I., Penta, B., Friedrichs, M.A.M., Helber, R., & Arnone, R.A. (2009). Summary Diagrams for Coupled Hydrodynamic-Ecosystem Model Skill Assessment. *J. Marine Systems*, 76(1–2), 64–82. https://doi.org/10.1016/j.jmarsys.2008.05.014

Lebo, M.E., & Sharp, J.H. (1990). Modeling phosphorus cycling in a well-mixed coastal plain estuary. *Estuarine, Coastal and Shelf Science, 35*(3), 235-252. https://doi.org/10.1016/S0272-7714(05)80046-0

MacWilliams, M.L., Bever, A.J., Gross, E.S., Ketefian, G.S., & Kimmerer, W.J. (2015). Three-Dimensional Modeling of Hydrodynamics and Salinity in the San Francisco Estuary: An Evaluation of Model Accuracy, X2, and the Low–Salinity Zone. *San Francisco Estuary and Watershed Science, 13*(1). http://dx.doi.org/10.15447/sfews.2015v13iss1art2

Martin, J.L, & Wool, T.A. (2017). *WASP Sediment Diagenesis Routines: Model Theory and User's Guide (Supplement to water analysis simulation program user documentation)*. United States Environmental Protection Agency. https://www.epa.gov/sites/default/files/2018-05/documents/wasp8_sod_module_v1.pdf

McSweeney, J.M., Chant, R.J., Wilkin, J.L., & Sommerfield, C.K. (2017). Suspended-sediment impacts on light-limited productivity in the Delaware Estuary. *Estuaries and Coasts, 40*(4), 977-993. https://doi.org/10.1007/s12237-016-0200-3

Mellor, G.L., & Yamada, T. (1982) Development of a turbulence closure model for geophysical fluid problems. *Reviews of Geophysics, 20*(4), 851-875. https://doi.org/10.1029/RG020i004p00851

Moriasi, D.N., Arnold, J.G., Van Liew, M.W., Bingner, R.L., Harmel, R.D., & Veith, T.L. (2007). Model evaluation guidelines for systematic quantification of accuracy in watershed simulations. Transactions of ASABE, 50(3), 885−900. https://doi.org/10.13031/2013.23153

O'Connor, D.J. (1983). Wind effects on gas-liquid transfer coefficients. *J. Environ. Eng*., 109(3), 731–752. https://doi.org/10.1061/(ASCE)0733-9372(1983)109:3(731)

O'Connor, D.J., & Dobbins, W. (1958). Mechanism of reaeration in natural streams. *Trans. Am. Soc. Civ. Eng. 123*(1), 641–684. https://ascelibrary.org/doi/10.1061/TACEAT.0007609

Owens, M., Edwards, R.W., & Gibbs, J.W. (1964). Some reaeration studies in streams. *Air and Water Pollution, 8*, 469-486.

Pareja-Roman, L.F., Chant, R.J., Sommerfield, C.K. (2020). Impact of historical channel deepening on tidal hydraulics in the Delaware Estuary. *Journal of Geophysical Research: Oceans, 125*(12), e2020JC016256. https://doi.org/10.1029/2020JC016256

Pennock, J.R. (1985). Chlorophyll distributions in the Delaware estuary: regulation by light-limitation. *Estuarine, Coastal and Shelf Science, 21*(5), 711-725. https://doi.org/10.1016/0272-7714(85)90068-X

Pennock, J.R., & Sharp, J.H. (1986). Phytoplankton Production in the Delaware Estuary: Temporal and Spatial Variability. *Marine Ecology Progress Series, 34*(1), 143–155. https://www.int-res.com/articles/meps/34/m034p143.pdf

PWD. (2015). *Green City, Clean Waters: Tidal Waters Water Quality Model – Bacterial and Dissolved Oxygen*. Consent Order & Agreement Deliverable IX and X, City of Philadelphia Combined Sewer Overflow Long Term Control Plan Update. Submitted by the Philadelphia Water Department to the Commonwealth of Pennsylvania Department of Environmental Protection. https://water.phila.gov/wp-content/uploads/WQ_Model_Complete_Report_FinalDigital_WITHAPPENDICES_WithAddendumpage_2016_09_19.pdf

Ralston, D.K., & Geyer, W.R. (2017). Sediment transport time scales and trapping efficiency in a tidal river. *Journal of Geophysical Research: Earth Surface, 122*(11), 2042-2063. https://doi.org/10.1002/2017JF004337

Runkel, R.L., Crawford, C.G., & Cohn, T.A. (2004). *Load Estimator (LOADEST): A FORTRAN Program for Estimating Constituent Loads in Streams and Rivers*. (Techniques and Methods 4-A5). United States Geological Survey. https://doi.org/10.3133/tm4A5

Sathyendranath, S., Stuart, V., Nair, A., Oka, K., Nakane, T., Bouman, H., Forget, M.H., Maass, H., & Platt, T. (2009). Carbon-to-chlorophyll ratio and growth rate of phytoplankton in the sea. *Mar Ecol Prog Ser,* 383, 73-84. https://doi.org/10.3354/meps07998

Sharp, J.H., Yoshiyama, K., Parker, A.E., Schwartz, M.C., Curless, S.E., Beauregard, A.Y., Ossolinski, J.E., & Davis, A.R. (2009). A Biogeochemical View of Estuarine Eutrophication: Seasonal and Spatial Trends

and Correlations in the Delaware Estuary. *Estuaries and Coasts 32*, 1023–1043 (2009). https://doi.org/10.1007/s12237-009-9210-8

Schopp R.D., & Firda G.D. (2008). Flood magnitude and frequency of the Delaware River in New Jersey, New York, and Pennsylvania. (Open-File Report 2008–1203). United States Geological Survey. https://pubs.usgs.gov/of/2008/1203/.

Schwede, D.B., & Lear, G.G. (2014). A novel hybrid approach for estimating total deposition in the United States. *Atmos. Environ., 92*, 207-220. https://doi.org/10.1016/j.atmosenv.2014.04.008

Sun, J., Feng, Y., Zhang, Y., & Hutchins, D.A. (2007). Fast microzooplankton grazing on fast-growing, low-biomass phytoplankton: a case study in spring in Chesapeake Bay, Delaware Inland Bays and Delaware Bay. *Hydrobiologia, 589*, 127–139. https://doi.org/10.1007/s10750-007-0730-6

Terray, E.A., Donelan, M.A., Agrawal, Y.C., Drennan, W.M., Kahma, K.K., Williams, A.J., Hwang, P.A., & Kitaigorodskii, S.A. (1996) Estimates of kinetic energy dissipation under breaking waves. *J. Phys. Oceanogr., 26*(5), 792-807. https://doi.org/10.1175/1520-0485(1996)026%3C0792:EOKEDU%3E2.0.CO;2

Tetra Tech, Inc. (2007). *The Environmental Fluid Dynamics Code, Theory and Computation, Volume 1: Hydrodynamics and Mass Transport*. https://www.epa.gov/sites/default/files/2016-01/documents/efdc_hydrodynamics_mass_transport_manual.pdf

Tetra Tech, Inc. (2015). *Hydrodynamic and Water Quality Modeling Report for the Savannah Harbor, Georgia (Final Report)*. Prepared for the Corps of Engineers Savannah District, Contract 100-ATL-T32468.

Tetra Tech, Inc. (2016). *High Rock Lake Hydrodynamic and Nutrient Response Models (Draft Report)*. Prepared under EPA Contract (September 2012). Report Finalized by the North Carolina Division of Water Resources.

Tsivoglou, E.C., & Wallace, R.J. (1972). *Characterization of stream reaeration capacity*. (EPA-R3-72-012). United States Environmental Protection Agency, Research Reporting Series.

Ullman, W.J., Scudlark, J.R., & Volk, J.A. (2010). *Standard Operating Procedure for the Calculation of N and P Deposition from the Atmosphere to Waters of Delaware's Inland Bays*. Report to the Delaware Center for the Inland Bays.

Walski, T. (2019). Why global standards for calibration of water distribution models won't work. *J. Am. Water Works Assoc., 111*(5), 31-34. https://doi.org/10.1002/awwa.1287

Wool, T.A., Ambrose, R.B., & Martin, J.L. (2004). *WASP8 Multiple Algae – Model Theory and User's Guide*. Supplement to Water Quality Analysis Simulation Program (WASP) User Documentation.

United States Environmental Protection Agency. https://epawasp.twool.com/resources/MPM-User-Guide.pdf

Wool, T.A., Ambrose, R.B., & Martin, J.L. (2018). *Water Quality Analysis Simulation Program (WASP 8.2)*. Water Quality Modeling Workshop Documents, June 11 – 15, 2018, Atlanta, GA. https://www.epa.gov/sites/default/files/2018-05/documents/wasp-course-announcement-2018.pdf

Wool, T.A., Ambrose, R.B., Martin, J.L., & Comer, A. (2020). WASP8: The next generation in the 50-year evolution of USEPA's water quality model. *Water, 12*(5), 1398. https://doi.org/10.3390/w12051398

Wool, T.A., Ambrose, R.B., Martin, J.L., & Comer, E.A. (2006). *Water Quality Analysis Simulation Program (WASP), Version 6.0 Draft: User's Manual*. United States Environmental Protection Agency.

Wool, T.A., Davie, S.R., & Rodriguez, H.N. (2003). Development of three-dimensional hydrodynamic and water quality models to support total maximum daily load decision process for the Neuse River Estuary, North Carolina. *J. Water Resources Planning and Management, 129*(4). https://doi.org/10.1061/(ASCE)0733-9496(2003)129:4(295)

Zambrano-Bigiarini, M. (2017). *hydroGOF: Goodness-of-fit functions for comparison of simulated and observed hydrological time series*. R package version 0.3-10. http://hzambran.github.io/hydroGOF/

Zappa, C.J., McGillis, W.R., Raymond, P.A., Edson, J.B., Hintsa E.J., Zemmelink, H.J., Dacey, J.W.H., & Ho, D.T. (2007). Environmental turbulent mixing controls on air-water gas exchange in marine and aquatic system. *Geophysical Research Letters, 34*(10), 1-6. https://doi.org/10.1029/2006GL028790

Zison, S.W., Mills, W.B., Diemer, D., & Chen, C.W. (1978). *Rates, Constants, and Kinetic Formulations in Surface Water Quality Modeling*. (EPA/600/3-78-105). United States Environmental Protection Agency. https://www.researchgate.net/publication/230887945_Rates_Constants_and_Kinetics_Formulations_in_Surface_Water_Quality_Modeling

Please Note:

The listing of Appendices A-K appears in this report after the References section, but due to their size, Appendices A-K are available for download in a separate zip file:

https://www.nj.gov/drbc/library/documents/ALDU_RestorationPathway/WQModel_CalRpt_Appendices_A-K.zip

Appendix A: Monitoring Results and Boundary Conditions

- Flow rates, concentrations, and loads from tributaries, point dischargers, CSOs, NPSs, and MS4s during the period of 2018 – 2019.

Please Note:

The listing of Appendices A-K appears in this report after the References section, but due to their size, Appendices A-K are available for download in a separate zip file:

https://www.nj.gov/drbc/library/documents/ALDU_RestorationPathway/WQModel_CalRpt_Appendices_A-K.zip

Appendix B: Transect Profile Data

Please Note:

The listing of Appendices A-K appears in this report after the References section, but due to their size, Appendices A-K are available for download in a separate zip file:

https://www.nj.gov/drbc/library/documents/ALDU_RestorationPathway/WQModel_CalRpt_Appendices_A-K.zip

Appendix C: Verification of Transport Fidelity

- Conservative tracer simulations
- Mass balance check
- DO comparisons
- Summary

Please Note:

The listing of Appendices A-K appears in this report after the References section, but due to their size, Appendices A-K are available for download in a separate zip file:

https://www.nj.gov/drbc/library/documents/ALDU_RestorationPathway/WQModel_CalRpt_Appendices_A-K.zip

Appendix D: Enhancement in Reaeration Simulation

1. Impact of Vertical Segmentation on Ammonia and Oxygen Profiles in Estuaries
2. Calculate Mass Transfer Coefficient with Turbulence Dissipation Rate
3. Comparisons of dissolved oxygen results between Zappa's approach and conventional approaches

---

Please Note:

The listing of Appendices A-K appears in this report after the References section, but due to their size, Appendices A-K are available for download in a separate zip file:

https://www.nj.gov/drbc/library/documents/ALDU_RestorationPathway/WQModel_CalRpt_Appendices_A-K.zip

Appendix E: State Variable Calculation

1. Nitrogen
2. Phosphorous
3. Carbon
4. Silica
5. Suspended solids

Please Note:

The listing of Appendices A-K appears in this report after the References section, but due to their size, Appendices A-K are available for download in a separate zip file:

https://www.nj.gov/drbc/library/documents/ALDU_RestorationPathway/WQModel_CalRpt_Appendices_A-K.zip

Appendix F: Model to Data Comparisons

- WASP calibration parameters
- Boat-run data (Spatial)
- Boat-run data (Time Series, 1-to-1, and CFD)
- Statistical metrics definition
- Boat-run statistical metric summary
- Light extinction (Ke)
- Phytoplankton seasonal variation
- Continuous data comparisons – 2012 DO and DOSAT
- Continuous data comparisons – 2012 Phytoplankton

Please Note:

The listing of Appendices A-K appears in this report after the References section, but due to their size, Appendices A-K are available for download in a separate zip file:

https://www.nj.gov/drbc/library/documents/ALDU_RestorationPathway/WQModel_CalRpt_Appendices_A-K.zip

Appendix G: Diagnostic Analyses

- DO component analysis
- Phytoplankton limiting factors
- Zone-2 light attenuation diagnosis – Ke
- Zone-2 light attenuation diagnosis - DO
- Zone-2 light attenuation diagnosis – Phytoplankton

Please Note:

The listing of Appendices A-K appears in this report after the References section, but due to their size, Appendices A-K are available for download in a separate zip file:

https://www.nj.gov/drbc/library/documents/ALDU_RestorationPathway/WQModel_CalRpt_Appendices_A-K.zip

Appendix H: Sensitivity Analysis

Please Note:

The listing of Appendices A-K appears in this report after the References section, but due to their size, Appendices A-K are available for download in a separate zip file:

https://www.nj.gov/drbc/library/documents/ALDU_RestorationPathway/WQModel_CalRpt_Appendices_A-K.zip

Appendix I: Constituent Load Development

Please Note:

The listing of Appendices A-K appears in this report after the References section, but due to their size, Appendices A-K are available for download in a separate zip file:

https://www.nj.gov/drbc/library/documents/ALDU_RestorationPathway/WQModel_CalRpt_Appendices_A-K.zip

Appendix J: Light Extinction Methodology

Please Note:

The listing of Appendices A-K appears in this report after the References section, but due to their size, Appendices A-K are available for download in a separate zip file:

https://www.nj.gov/drbc/library/documents/ALDU_RestorationPathway/WQModel_CalRpt_Appendices_A-K.zip

Appendix K: Algae Representation

Please Note:

The listing of Appendices A-K appears in this report after the References section, but due to their size, Appendices A-K are available for download in a separate zip file:

https://www.nj.gov/drbc/library/documents/ALDU_RestorationPathway/WQModel_CalRpt_Appendices_A-K.zip

End of Document

End of Document